

THESE

Présentée

pour l'obtention du grade de

DOCTEUR DE L'UNIVERSITE DE POITIERS

(Faculté des Sciences Fondamentales et Appliquées)

(Diplôme National – Arrêté du 7 août 2006)

École Doctorale : **Ingénierie Chimique, Biologique et Géologique (ICBG) n° 362**

Secteur de recherche : **Terre solide et enveloppe superficielle**

par

Hamid POURPAK

Sujet de la thèse:

Méthodologie de déformation graduelle de modèles de réservoir hétérogène fracturé contraints par des mesures d'écoulement aux puits

MM. F. DELAY

Directeur de thèse

B. BOURBLIAUX

Promoteur

JURY

MM. P. ACKERER

Rapporteur

R. GUERIN

Rapporteur

H. AURADOU

Examineur

V. ARTUS

Examineur

F. DELAY

Directeur de thèse

B. BOURBLIAUX

Promoteur

Abstract

This thesis proposes a sequential inversion methodology for calibrating highly-heterogeneous reservoir models on well test data. The design and the application of that methodology are performed on an Experimental Hydrogeological Site settled on a karstic and fractured limestone aquifer located near to Poitiers – France. The flow model is based on a geostatistical distribution of facies. Conditioning information on flow is made of well pumping and interference data. The methodology involves two successive steps that are : - first, the inversion of facies petrophysical properties; - second, the gradual deformation of the facies distribution. By proceeding this way, the gradual deformation method, applied both globally and locally, improves the distribution of facies while keeping the previously-optimized petrophysical properties. The fairly-good capability of the resulting model to predict well responses allows to consider the gradual deformation as an efficient and robust method to find a facies geostatistical realization matching at best flow data constraints.

Alternative implementation of the sequence above are studied, by simply changing the schedule of the calibration steps. A single calibration step combining both petrophysical inversion and gradual deformation reveals as much efficient as the sequence discussed above. On the other hand, a reverse calibration sequence starting with gradual deformation and ending with petrophysical inversion does not yield a satisfactory calibration. Efficiency and numerical performances of the methodology are also assessed by changing the number of gradual deformation parameters, and by analyzing the sensitivity and evolution of the objective function during the entire optimization process.

Finally, it is investigated on the possibility to improve calibration by means of alternative flow modelling approaches. Whereas the adoption of a dual-medium model does not change significantly the simulated pressures, a more accurate modelling of conductive bodies by using a refined grid improves the prediction of short-time well responses. Further works could tentatively address the gradual deformation of object-based models that are reputed relevant for mimicking flow features of karstic and/or fractured heterogeneous reservoirs.

Résumé

Cette thèse propose une méthodologie d'inversion séquentielle pour calibrer des modèles de réservoirs très hétérogènes à partir des données de tests de puits. La conception et la démonstration de cette méthodologie sont effectuées sur le Site Expérimental Hydrogéologique d'un aquifère carbonaté karstique et fracturé situé près de Poitiers en France. Le modèle d'écoulement de cet aquifère s'appuie sur une distribution géostatistique des faciès. Les contraintes de simulation des écoulements consistent en des données de tests de pompage et d'interférence. La méthodologie comprend deux étapes successives, en premier lieu l'inversion des propriétés pétrophysiques des faciès, puis la déformation graduelle de la distribution de faciès. La méthode de déformation graduelle, appliquée globalement puis localement, améliore ainsi la distribution des faciès en conservant leurs propriétés pétrophysiques précédemment calibrées. La capacité du modèle résultant à prédire les réponses des puits nous amène à considérer la déformation graduelle comme une méthode efficace et robuste pour trouver une réalisation géostatistique de faciès qui permette d'ajuster au mieux les données d'écoulement.

Des variantes de mise en oeuvre de la méthodologie décrite ci-dessus ont été étudiées, en modifiant l'ordre de la séquence de calibration. Alors qu'une étape de calibration unique, combinant inversion pétrophysique et déformation graduelle, s'avère aussi efficace que la séquence précédente, une séquence inversée commençant par la déformation graduelle et suivie de l'inversion pétrophysique ne conduit pas à un calage satisfaisant. L'efficacité et la performance numérique de la méthodologie sont également évaluées en changeant le nombre de paramètres de déformation graduelle, et en analysant la sensibilité et l'évolution de la fonction objectif au cours de l'ensemble du processus d'optimisation.

Finalement, la possibilité d'améliorer encore l'ajustement aux données de champ est explorée au moyen d'approches alternatives de modélisation des écoulements. Alors que l'adoption d'un modèle double milieu ne modifie pas beaucoup les pressions simulées, une modélisation plus précise des corps conducteurs au moyen d'une grille raffinée améliore la prévision des réponses des puits aux temps courts. Finalement, la déformation graduelle d'un modèle objet de corps conducteurs aux propriétés d'écoulement pré-estimées serait également adaptée à ces cas de réservoir hétérogène karstique et/ou fracturé.

LIST OF FIGURES	IV
------------------------------	-----------

LIST OF TABLES	X
-----------------------------	----------

INTRODUCTION	1
---------------------------	----------

CHAPTER 1. INTRODUCTION TO MULTI-MEDIUM FRACTURED/HETEROGENEOUS KARSTIC RESERVOIRS : THE EXPERIMENTAL HYDROGEOLOGICAL SITE (EHS) ...7

1.1. Introduction	9
1.2. Karstic/Heterogeneous aquifers	9
1.3. Origin of fractures and their impact on flow	11
1.4. Construction of a geological model of a heterogeneous/fractured reservoir	12
1.4.1. Discrete models	12
1.4.2. Equivalent homogenous models	13
1.5. Presentation of heterogeneity parameters in the geostatistical models of reservoirs	13
1.6. The Experimental Hydrogeological Site (EHS) : a heterogeneous fractured reservoir	14
1.6.1. (Hydro-)geological frame work	16
1.6.2. Stratigraphy and depositional sequences	17
1.6.3. Structural features - tectonic history - fracturing features	19
1.6.4. Diagenetic fingerprints- Evidence of the karstic nature of the aquifer	23
1.6.5. Previous studies and analysis using pumping data at EHS	27
1.7. Conclusion	32

CHAPTER 2. APPROACHES AND TOOLS FOR MODELLING, SIMULATING AND CALIBRATING THE HYDODYNAMICS OF AN UNDERGROUND RESERVOIR..... 35

2.1. Introduction	37
2.2. The reservoir modelling workflow	38
2.2.1. Geostatistical and Geological modelling	38
2.2.2. Flow modelling	40
2.2.3. History matching	41
2.2.4. Optimization methods	42
2.2.5. Parameterization techniques	48

2.3.	Workflow tools and methodologies	55
2.3.1.	Geostatistical modelling using HERESIM methodology	55
2.3.2.	Flow modelling using SIMTESTW simulator	56
2.3.3.	Petrophysical inversion using WELGEM methodology	57
2.3.4.	Gradual deformation using CONDOR software package.....	59

CHAPTER 3. PRELIMINARY STUDIES AND GEOSTATISTICAL MODELLING OF THE SITE 63

3.1.	Introduction	65
3.1.1.	Preliminary pumping data analysis	65
3.1.2.	Flowmeter data analysis and interpretation.....	69
3.1.3.	Imaging data	69
3.1.4.	Core derived petrophysical parameters	69
3.2.	Building a geostatistical model of the site	71
3.2.1.	Reference 3D grid	71
3.2.2.	Modelling features	72
3.2.3.	Variogram of model.....	76
3.2.4.	The petrophysical modelling.....	77
3.2.5.	Resulting Geostatistical model of the EHS.....	78
3.3.	Conclusion.....	82

CHAPTER 4. DESIGN AND APPLICATION OF A SEQUENTIAL METHODOLOGY FOR CALIBRATING THE HYDRODYNAMIC MODEL OF A HIGHLY-HETEROGENEOUS RESERVOIR..... 85

4.1.	Introduction	87
4.2.	Preliminary tests	87
4.3.	Design of a sequential calibration methodology	89
4.4.	Flow model: application to the EHS.....	90
4.5.	Selected well data for model calibration.....	94
4.6.	Preliminary calibration of the flow boundary conditions	96
4.7.	Petrophysical inversion.....	96
4.8.	Gradual deformation of facies	98

4.9.	Local gradual deformation of facies	101
4.10.	Predictability of the resulting model.....	104
4.11.	CONCLUSION.....	106
CHAPTER 5. ANALYSIS AND DISCUSSION		109
5.1.	Introduction	111
5.2.	Analysis of inversion as regard the schedule of steps in the sequential calibration	112
5.2.1.	Gradual deformation followed by petrophysical inversion.....	112
5.2.2.	Combining (global) gradual deformation and petrophysical inversion in a single calibration phase 115	
5.3.	Impact of the parameterization on the calibration performance	118
5.4.	Optimization efficiency and computation times	122
5.4.1.	Optimization parameters	122
5.4.2.	Performance analysis of the first sequential calibration method.....	124
5.4.3.	Performance analysis of gradual deformation followed by petrophysical inversion	130
5.4.4.	Performance analysis of combined (global) gradual deformation and petrophysical inversion	130
5.4.5.	Sensitivity of the objective function to calibration parameters.....	133
5.5.	Testing other flow models to better capture flow paths	134
5.5.1.	Testing a dual-porosity representation.....	134
5.5.2.	Refined model.....	137
5.6.	Conclusion.....	140
CHAPTER 6. CONCLUSION AND PERSPECTIVES		143
6.1.	Summary of results	144
6.2.	Perspectives of future developments and research.....	147
APPENDIX 1		155
APPENDIX 2		201

List of Figures

Figure 1.1: Components of a karst aquifer (Manda <i>et al.</i> , 2006)	11
Figure 1.2: Main Paleogeographic domains with location of the studied area (EHS).	15
Figure 1.3: Experimental Hydrogeological Site – Location of wells	16
Figure 1.4: Stratigraphic chart for the Jurassic	19
Figure 1.5: Simplified geological cross section at the EHS location	19
Figure 1.6: Transversal geological cross-section crossing the Poitou threshold(modified after Gabilly <i>et al.</i> , 1997) A means anticline, S means syncline. Note the change in subsidence of paleohigh margins with time (NE margin during Liassic, SW margin during Upper Jurassic).....	21
Figure 1.7: EHS analogue outcrops study - Passelourdin site: (left) the rose diagram of fracture azimuths and poles shows three main clusters, with the corresponding poles shown in red, blue and green colors; (right) cyclographic traces of the mean orientations of the	22
Figure 1.8: Cores from C2 well at about 97m depth: clay material is filling the upper "damaged" zone (karst residue) ; a vertical fracture is observed between two marly (dark) layers in the lower core.	23
Figure 1.9: Bore-hole images as evidences of the paleo-karstic origin of the EHS heterogeneities (Bourbiaux <i>et al.</i> , 2007).....	25
Figure 1.10: Wells set up in nested five-spots in the experimental site in Poitiers. Solid dots: wells tested in 2004, empty dots: wells tested in 2005.....	28
Figure 1.11: Representation of 3 typical shapes of drawdown curves from the pumping test of 2004 campaign (from Bernard, 2005).	31
Figure 2.1: Truncated plurigaussian simulations (Chilès and Delfiner, 1999).....	40
Figure 2.2: The Powell method and the trust region technique (Fornel, 2006)	47
Figure 2.3: Iterative search process involving the gradual deformation of two realizations (one parameter of gradual deformation)	52
Figure 2.4: Iterative search process involving the gradual deformation of $N+1$ realizations (Fornel, 2006).....	53
Figure 2.5: Vertical proportion curve computed from the well data (Doligez <i>et al.</i> , 2007)....	56
Figure 2.6: Optimization path with numerical gradient computation	59

Figure 2.7: The optimization settings window. The optimization algorithm and important control parameters for the optimization are selected from this window	61
Figure 2.8: Flow chart summing up the main steps of a gradual deformation-based optimization including the main features depicted in this chapter	62
Figure 3.1: Schematic and general illustration of wells for the permeability estimations.....	66
Figure 3.2: Permeability map of the EHS: a thick black line delimits the drilled zone of interest within the Site; wells are shown as white circles; well permeabilities range from around 100 millidarcys to nearly 11 Darcys	67
Figure 3.3: Construction of reference grid in HERESIM Software	72
Figure 3.4: Vertical Proportion Curves (VPC) of lithotypes for all wells used for the geostatistical model.....	75
Figure 3.5: Qualitative distribution of facies in the present geostatistical model (left, mono-Gaussian) and in the more advanced model (right, bi-Gaussian/not used here).....	76
Figure 3.6: Experimental vertical variograms.....	77
Figure 3.7: 3D geostatistical facies model of the Site (HERESIM software)	78
Figure 3.8: West-East facies cross-section of the Site: a poor vertical connectivity of the conductive facies is expected.....	79
Figure 3.9: North-South facies cross-section of the Site: the conductive lithotype looks here more areally-continuous than in the West-East direction, but no vertical connection is observed between the 50m and 85m productive levels within that section	79
Figure 3.10: West-East permeability cross-section of the Site	80
Figure 3.11: North-South permeability cross-section of the Site	80
Figure 3.12: West-East connectivity section including 3 groups of connected water facies bodies	81
Figure 3.13: North-South connectivity section including 3 groups of connected water facies bodies.....	81
Figure 4.1: Left: Gridded model of the drilled Site area with well locations. Right: Gridded model with surrounding fluid-source cells.....	91
Figure 4.2: The 3D model generated by SIMVIEW IFP software, with the large volume source facies surrounding the Site	91
Figure 4.3: Initial detailed facies model (left) converted to an equivalent lumped facies model (right)	93

Figure 4.4: Preliminary flow inversion tests: the resulting calibrated lumped model is seemed to match measured pressure responses as accurately as the detailed model. Simulated pressures after petrophysical properties inversion are compared to measured data at the Site: pressure drop (dP , bar) evolution with time (h) for pumped well M7 and 3 selected observation wells during the first 24 hours.	93
Figure 4.5: Selected data: location (Top) and pressure responses (Bottom) of the selected pumped well, M7, and of the observation wells showing significant pressure interference with M7	95
Figure 4.6: Simulated pressures after petrophysical properties inversion are compared to measured data at the Site: pressure drop (dP , bar) evolution with time (h) for pumped well M7 and 3 selected observation wells during the first 24 hours.	98
Figure 4.7: Top-left graph (on the top, right): Objective function evolution for the lumped facies model using the gradual deformation method: calibration is done on pumped well M7 and observation wells together. Other plots: Objective function evolution for wells M7, M5 and M9 pressure data. Note that the whole optimization process includes several steps, each step involving the deformation of a given set of geostatistical realizations. A temporary abrupt rise in the objective function may occur during the iterative deformations of such a step. This is due to the highly non-linear relationship between fluid flow results and geostatistical deformation: in that case, the iteration is re-started with a reduced variation of the deformation parameters.	100
Figure 4.8: Comparison of simulated pressures after petrophysical inversion or gradual deformation of facies, with the field data: evolution of the pressure drop dP (bar) versus time (h) for the pumped well M7 and selected observation wells during the first 24 hours.	101
Figure 4.9: Gradual deformation of the EHS model with pumped well M7 and some observation wells as calibration constraints: 2D section of model at the depth of 68 meter (from the initial realization on top on the left, to the optimal one on bottom the right).....	102
Figure 4.10: Gradual deformation of the EHS model with pumped well M7 and some observation wells as calibration constraints: lateral vertical sections (from the initial realization on top on the left, to the optimal one on bottom the right).....	102
Figure 4.11: Local gradual deformation of the EHS model in a region including wells M7 and M9: horizontal section at the depth of 68m. Only the region of interest is affected by the gradual deformation process (from the initial realization on top on the left, to the	

optimal one on bottom the right). Note that the bottom images are quite close, because at that stage, the optimization process had nearly converged to the optimal facies distribution.....	103
Figure 4.12: Comparison of simulated pressures after petrophysical inversion, global gradual deformation of facies and local gradual deformation of facies, with the field data: evolution of the pressure drop dP (bar) versus time (h) for the pumped well M7 and observation well M9 during the first 24 hours.	103
Figure 4.13: Forward/predictive simulation of pumped well M6 and its interferences. Comparison with field data: evolution of well pressure drop dP (bar) with time (h) for pumped well M6 and selected observation wells during the first 24 hours.....	105
Figure 5.1: Comparison of simulated pressures after petrophysical inversion or gradual deformation of facies, with field data: gradual deformation method has been performed before petrophysical property inversion. Evolution of the pressure drop dP (bar) versus time (h) for the pumped well M7 and selected observation wells during the first 24 hours	113
Figure 5.2: Comparison of the second sequential calibration (GDM before Petrophysical inversion) to the previous sequential calibration (Petrophysical inversion before GDM). Wells showing the largest difference in calibration results between the two sequences have been selected here.	114
Figure 5.3: Comparison of simulated pressures after petrophysical inversion or gradual deformation of facies, with field data: gradual deformation method and petrophysical property inversion have been performed in a combined calibration process (single-phase calibration). Evolution of the pressure drop dP (bar) versus time (h) for the pumped well M7 and selected observation wells during the first 24 hours	117
Figure 5.4: Comparison of results of combined (single-phase) calibration (GDM and Petrophysical inversion in a single phase) to the results of firstly-designed calibration method (dual step <i>i.e</i> , Petrophysical inversion and then GDM). Evolution of the pressure drop dP (bar) versus time (h) for the pumped well M7 and selected observation wells during the first 24 hours	118
Figure 5.5: Comparison of simulated pressures after petrophysical inversion or gradual deformation of facies, with field data: Global and local gradual deformation are performed with only one parameter. Evolution of the pressure drop dP (bar) versus time (h) for the pumped well M7 and selected observation wells during the first 24 hours.....	120

Figure 5.6: Comparison between the results of global gradual deformation with one parameter and that with four parameters. Evolution of the pressure drop dP (bar) versus time (h) for the pumped well M7 and selected observation wells during the first 24 hours.	121
Figure 5.7: Comparison between the results of local gradual deformation with one parameter and that with four parameters. Evolution of the pressure drop dP (bar) versus time (h) for the pumped well M7 and observation well M9 during the first 24 hours.	122
Figure 5.8: Optimization settings for WELGEM petrophysical inversion	123
Figure 5.9: Optimization settings for gradual deformation (CONDOR platform).	123
Figure 5.10: Objective function evolution for petrophysical property inversions: Objective function for detailed facies model inversion to the left and objective function for lumped facies model inversion to the right.	124
Figure 5.11: Evolution of the objective function for the lumped-facies model during global gradual deformation. Comparison between optimizations with one and four 4 parameter(s) of gradual deformation. Evolution of the objective function with the iteration number for all wells together and for selected observation wells.	127
Figure 5.12: Relative contribution of well data series in the objective function evolution for global gradual deformation with 4 parameters.	128
Figure 5.13: Relative contribution of well data series in the objective function evolution for local gradual deformation with 4 parameters.	128
Figure 5.14: Evolution of the objective function for the lumped-facies model during local gradual deformation. Comparison between optimizations with one and four 4 parameter(s) of gradual deformation. Evolution of the objective function with the iteration number for all wells together and for the wells in the deformation area.	129
Figure 5.15: Evolution of the objective function when gradual deformation (with 4 parameters) is performed before petrophysical inversion. Evolution of the objective function with the iteration number for all wells together and for selected observation wells.	131
Figure 5.16: Evolution of the objective function for the lumped facies model by using the gradual deformation method and petrophysical inversion mixed together.	132
Figure 5.17: Gradient of the objective function with respect to calibration parameters for different steps. The numbers 1 to 20 state for the different calibration parameters. The	

related parameters are given on the bottom of each number. The p1 to p4 represent the 4 parameters of gradual deformation.	133
Figure 5.18: Comparison between the inversions of the dual-porosity and the single-porosity models of the Site. Variation of pressure drop (ΔP) versus time (hour) for well M7 and some interference wells; model calibrated to pumped well M7 and some interference wells for short term period (24 hours).	137
Figure 5.19: Comparison of the simulated pressures from both coarse and refined grids with field data. The fine-grid model is derived from the previously-inversed-deformed coarse model. Evolution of the pressure drop dP (bar) versus time (h) for the pumped well M7 and selected observation wells.	139

List of Tables

Table 3.1: Determination of the permeability at different wells by using drawdowns of quasi-steady state radial flow around pumped wells.	68
Table 3.2: Petrophysical parameters calculated from cored-well C1 using the Miniplug method.....	70
Table 3.3: Facies coding used in well data files in HERESIM.....	73
Table 3.4: Classification of the facies into the different lithological groups (lithotypes).	74
Table 4.1: The initial petrophysical parameters assigned to the geostatistical model: porosity-permeability values derived from the core data of well C1; estimated pore compressibility values (from overall pre-calibration) consistently with other dynamic studies.	92
Table 4.2: Detailed facies (left) converted to lumped facies (right).	92
Table 4.3: Inversion parameters, denoted "?". Porosity value (0.15) for tight facies No. 1 is derived from core data.....	97
Table 4.4: Inverted values of lumped facies 1 and 2 using the short-term (24 hours) flow data from pumped well M7 and its observation wells as constraints.	97
Table 5.1: Inverted petrophysical parameters, Top: Results of petrophysical property inversion performed after gradual deformation of facies, Bottom: Results of petrophysical property inversion performed before gradual deformation of facies...	115
Table 5.2: Inverted petrophysical parameters, Top: Results of the single-step calibration of detailed-facies model, Bottom: Results of dual-step calibration with inversion of petrophysical properties inversion before gradual deformation.....	116
Table 5.3: Summary of performance for all optimization techniques. "Petro. Inv." stands for petrophysical inversion and "GD" stands for gradual deformation	132
Table 5.4: Initialization of the dual-porosity model parameters from the calibrated single-porosity model results.	136
Table 5.5: Results of the petrophysical property inversion of the dual-porosity model.....	136

Introduction

Problem description and Motivation

During the past twenty years, the technique of mathematical modelling has been extensively used for the study of groundwater resources, their management and aquifer remediation (Sun, 1994). Both forward-problem and inverse solutions have been developed during the last years. However, due to the poorly-defined or unknown parameters that exist in the reservoirs, especially in the case of heterogeneous or fractured reservoirs, it is very difficult to perform a forward simulation and obtain the satisfactory results. Therefore, inverse solutions are widely used in the domain of reservoir engineering.

Generally, forecasts from a heterogeneous fractured reservoir require a model that is able to describe in a reliable way the large-scale transfers between wells and the interactions between the constitutive media (multi-scale fractures and/or complex matrix media).

Very often from wells alone, few direct observations of underground reservoir heterogeneities and fractures are available. In the presence of fractures or of geological objects similar to fractures (thin super-permeable beds), geostatistical, *i.e.* space-dependent models are built. These models may be either pixel-based or object-based. The generation of such models is based on both parameters with a geostatistical meaning (distribution of facies, of fracture orientations and densities) and also on discrete (deterministic) information available at wellbores. However, these models reveal themselves as unreliable for flow predictions. This statement, revealed by production data is not consequence of simplifications of geological models (through homogenization techniques) at reservoir scale only. Indeed, it is also linked to the poor knowledge of multiple parameters involved in the generation of models. This discrepancy is amplified in the case of highly-heterogeneous reservoirs. It is then necessary to design and validate a methodology accounting for the existence of multiple unknown or poorly-defined parameters involved in the stochastic model generation, and the deterministic information (available at wellbores) about the generated objects.

When constraining the reservoir model to dynamic data, reservoir engineers were used to manually tune these parameters in order to obtain a suitable reservoir model. However, this approach is not feasible in the case of large reservoirs. During the past two decades considerable progress has been made in inverse problem theory to incorporate dynamic data into reservoir models, and triggering the development of assisted history-matching procedures.

In the case of heterogeneous media, it should be possible to perturb simultaneously all gridblock properties until the reservoir model reproduces the observed dynamic behaviour. This naïve approach would become however problematic for very large numbers of grid blocks involved in the perturbations. The number of parameters (*i.e.*, the number of unknowns) is at least identical to the number of grid blocks. Furthermore, numerous sets of parameters can produce the same dynamic data. Some of these sets may then generate erroneous fluid displacement forecasts. A better estimate requires either the number of parameters to be decreased or supplementary information about these parameters to be incorporated. Parameterization techniques are then a key to the problem. Several, mainly geostatistical, parameterization techniques have been proposed to reduce the number of parameters. In our approach we use the gradual deformation method. This technique allows with few parameters for the perturbation of reservoir model, irrespective of the number of gridblocks it contains. It also preserves the spatial variability model. This method has been developed for pixel-based models also for object-based models.

A research study focusing on a heterogeneous /karstic aquifer

This research has been performed to validate a model of aquifer using actual geological, geophysical and flow data collected on an Experimental Hydrogeological Site (EHS) located near Poitiers. We deal with a water-bearing reservoir of Middle Jurassic age, between 20 m and 130 m depths, made of heterogeneous, vuggy (karstic) and fractured limestones. Some thirty wells drilled in this reservoir however numerous flow data - pumping tests with interferences recorded in other wells, transient tests, quasi steady-state flow measurements along the wellbore - which constitute a valuable set of constraints to calibrate the flow models of the Site. Matrix properties and porous structure were characterized from permeability measurements on core sample fragments and from NMR (Nuclear Magnetic Resonance) measurement. The preliminary analysis of wellbore responses confirmed the heterogeneity of reservoir, which justified to undertake a multi-scale characterization of the reservoir.

The main goal of this PhD thesis is the design and implementation of a flow-model calibration methodology that is applicable to heterogeneous fractured/karstic reservoirs with well flow data as matching constraints. History matching techniques preserving the ascertained data and observations are combined into a sequential methodology, including petrophysical-property inversion and facies gradual deformation methods.

Content summary and contributions

The existing know-how and our inputs in terms of modelling and calibration are presented through different chapters of this dissertation as follows:

Chapter 1 presents a literature review on fractured and heterogeneous reservoirs in terms of characterization and modelling aspects. Then, the reservoir under consideration *i.e.*, Experimental Hydrogeological Site (EHS) is introduced in details by describing the geological and hydrogeological origin and characteristics of this aquifer. The main origins of heterogeneity and fracturing of this karstic aquifer are analysed and their impact on water flow is discussed. The previous studies are described, especially those carried out by a small research team of the University of Poitiers and aimed at the estimation of reservoir parameters with different modelling approaches.

In *chapter 2*, the main steps of integrated reservoir modelling workflows including geostatistical modelling and dynamic flow modelling are reviewed. Particular attention is awarded to history matching methodologies including parameterization techniques and inversion methodologies. All the simulation/inversion techniques and software packages that were implemented for this study are described within this Chapter.

In *chapter 3*, the preliminary studies resting on pumping tests held over EHS are presented and analysed. Then, the new data that were used for updating a pre-existing geostatistical model of the reservoir are reviewed. This Chapter ends with the description of the resulting *i.e.* updated, geostatistical model of the EHS. This updated geostatistical model is the starting point for the main subsequent step of this PhD work, that is the design of methodology of model calibration to well dynamic data.

Chapter 4 proposes a sequential calibration methodology which can be applied to flow models of highly-heterogeneous reservoirs as the karstic and fractured aquifer under consideration. This practical methodology consists of well tests history matching techniques, involving petrophysical inversion and more specifically, gradual deformation of facies. All calibrations were performed using only one selected pumped well and its observation wells within the Site area. Finally, the pumping test of another well was simulated on the previously-calibrated model to check the

prediction capability of the model. Possible ways to further improve that modelling methodology are examined at the end of this chapter.

Chapter 5 discusses and analyses the proposed methodology in terms of practical applications and modelling features. The performance of the proposed methodology and other possible sequential methodologies are examined in terms of reliability/accuracy, of computation costs, and also in terms of optimal parameterization of the problem (*i.e.* optimal number of matching parameters). An advanced modelling approach is proposed and examined to further improve the modelling methodology.

Chapter 6 summarizes the results and contributions of the 3-year PhD study. The advantages and drawbacks of our methodologies are discussed, with the hope of opening ways for both actual and future research developments.

Publications

The results of this thesis are published partially in IFP journal OGST (*Oil & Gas Science and technology*). Another paper focused on our calibration methodology is submitted for publication in a journal of the *Society of petroleum Engineers (SPE)*, either *SPE Reservoir Evaluation & Engineering* or *SPE Formation Evaluation*. These two publications are reproduced in Appendix 1. These results have also been presented at two international Conferences organized by the European Association of Geoscientists and Engineers (EAGE) and the SPE.

CHAPTER 1. Introduction to multi-medium fractured/heterogeneous karstic reservoirs : the Experimental Hydrogeological Site (EHS)

1.1. Introduction

Over the last decade, research in hydrodynamics and transport in underground reservoirs has been greatly developed, probably owing to a few strategic stakes such as the safety assessment of underground repositories, the prospecting of oil and water resources or the managing of existing reservoirs. Among topics related to this research, the simulation of synthetic (numerical) reservoirs has come up as a crux since it allows the mimicking at low cost of prospective exploitation scenarios. Whatever the method used for simulating numerical reservoirs, the conditioning on available data is needed because it dedicates a generic tool to the specificity of the handled problem. This is why, despite the increasing place taken by numerical simulations in the toolbox of reservoir engineering, field studies and experiments remain a necessity (Delay *et al*, 2007).

Several experimental sites have been developed in recent years to characterize the hydrodynamic properties of fractured or heterogeneous reservoirs. As an example, the Äspö site in Sweden develops strategies of medium characterization with the aim of providing analytical and numerical tools evaluated by their capabilities of prediction. The first step of characterization of this site lasted for five years (1996-2000) and for instance, authors like Winberge and coworkers (1996, 2003) proposed various interpretations of the geometry and the connectivity of conductive fractures. Another example is Waste Isolation Pilot Plant (WIPP) which has become recently an official underground repository site of nuclear and highly hazardous wastes managed by the Ministry of Defence in the US. The hydrogeological characteristics of this site have been studied in the framework of this project. This site has been labelled as a fractured medium with a dual porosity behaviour (Davies *et al.*, 1991). There exist many other sites with different objectives like the Yucca Mountain nuclear waste site in USA considered as a repository for nuclear waste, and also the Soultz-sous-Forêt site in the Rhine Graben-France developed for geothermal energy production.

1.2. Karstic/Heterogeneous aquifers

Karst aquifers are important sources of groundwater in many parts of the world, but up to now their management and protection is exceptionally difficult due to their complex internal structure and flow patterns. The primary reason for this complexity is the abundant dissolution features that develop due to circulations of slightly acidized groundwater in contact with the calcareous host

rock. Cavitations may range in scale from dissolved fossils to enormous caverns, and may deeply influence the hydrologic properties of a formation by increasing their porosity and their macroscopic connectivity. Owing to the geologic factors that control their formation (e.g., depositional fabric, mineralogy, fractures, groundwater chemistry), the spatial distribution of dissolution features in limestone is highly heterogeneous. Characterizing the distribution and dimensions of these karstic features may therefore contribute to the successful management of these complex water resources.

Voids visible on eye in carbonate rocks are roughly classified into include vugs (pores considerably larger than the grain/particle size), fractures, channels (nonfabric selective, elongated pores), breccias and caverns. Although inconsistently defined in the literature, the general consensus is that conduits are pipes or channels ranging from one centimetre to several meters in diameter or aperture, and represent dissolution features of intermediate size between smaller macropores and larger caves or caverns. Conduits develop in karst formations by the dissolution and widening of planar discontinuities such as bedding planes, faults and fractures. Because of their dimensions and their eventual interconnection, conduits may convey large volumetric flow rates, often under turbulent conditions. This results in highly heterogeneous distributions of aquifer conductivity, and flow regimes that often bypass the less conductive rock matrix. The high productivity of many carbonate aquifers is a direct consequence of conduit flow. As a drawback however, these conduits may propagate contaminations very rapidly. Due to their discrete nature and sometimes their scarcity, conduits are also difficult to incorporate accurately in conventional groundwater flow models. In order to better understand the internal structure of karst aquifers, new techniques and approaches are required to characterize the geometries and distribution of dissolved conduits (Manda and Gross, 2006).

Figure 1.1. sketches the major elements of a karst system. On the one hand, the vast majority of storage is provided by tight fissures, narrow fractures and the porous rock matrix. On the other hand, the karst conduit system, developed by dissolution widening of fractures, occupies only a small void ratio but is much more permeable than the fissured system and the porous matrix. Flow in karst conduits is fast and often turbulent. Contaminants that potentially enter the conduit system, for instance, via sinkholes, therefore, spread rapidly over great distances, making then karstic aquifers highly vulnerable to pollutions.

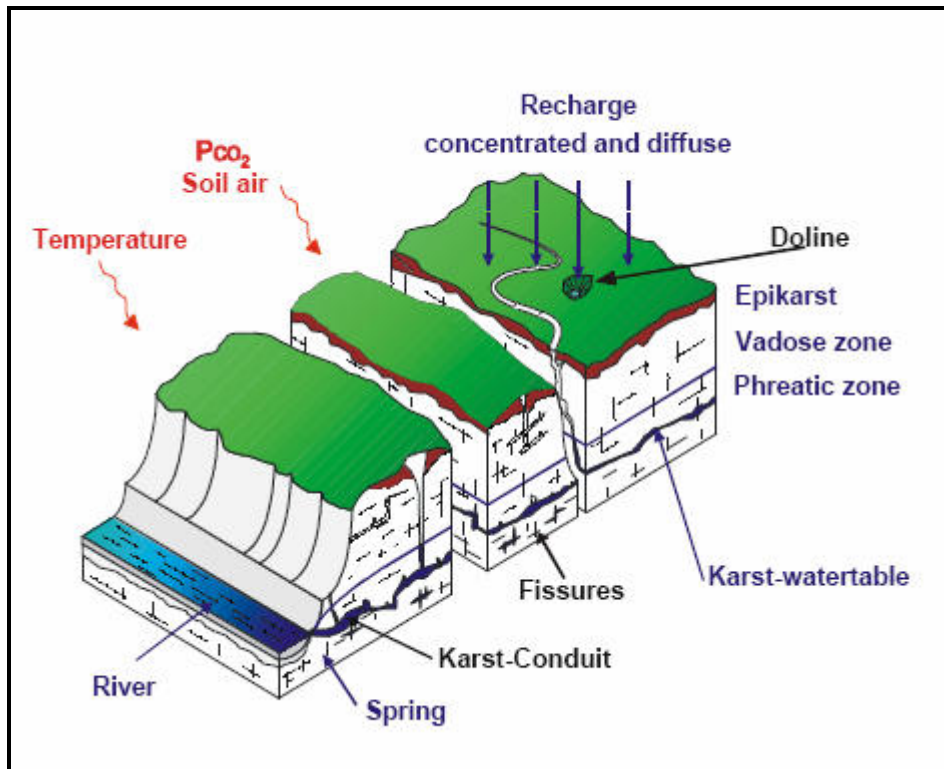


Figure 1.1: Components of a karst aquifer (Manda and Gross, 2006).

1.3. Origin of fractures and their impact on flow

A fracture is a surface of rupture in a rock. On a mechanical standpoint two categories of fractures exist: the fractures built by extension and the fractures produced by shear stress. In other words, these types of fractures have different mechanical origins and their distributions in space and the distribution of their properties (such as length, aperture, orientation, etc.) obey different laws. A fault is any planar surface or narrow zone created by shear fracturing or shear deformation (Saidi, 1987). A joint is any thin planar fracture without any parallel displacement of two fracture walls, meaning that no shear is involved during the failure. Fractures are usually characterized by the following parameters: density, length, orientation, aperture and the filling (Saidi, 1987). Fractures influence fluid flow in water and oil reservoir. They play an important role as conductive drains and also they may act as barriers when the filling material is impermeable like clay, calcite, quartz, etc (Jenni *et al*, 2004). The size and the scale over which fractures may extend are very important for the fluid dynamics in reservoirs. Faults and joints are viewed as multi-scale fracture objects.

1.4. Construction of a geological model of a heterogeneous/fractured reservoir

The fault/fracture model integrates the information about fracture position and geometry acquired both at local scale within a few wells (cores, boreholes, images, logs) and large scale from seismic surveys, with a possible additional input from the study log analogous outcrops. There are various methods to build a statistical-geological model of reservoir. The reliability of that kind of model depends on the amount of constraining data or rules including fracture orientation, length, spacing or density. In addition, the presence of fractures at the various scales affects the flow dynamics within a reservoir, thus yielding uncertainty on reservoir production forecasting. Methodology and tools are now available to construct geologically-realistic models of fracture networks and thus to turn models into simplified tools for the purpose of routine field-scale applications.

1.4.1. Discrete models

Discrete models of fractured media are based on a discrete representation of the real fractured network. Such a representation is justified for the dynamic reservoir modelling of large-scale faults or fracture swarms that cannot be homogenized. Different methods have been proposed to build a discrete model of the real fracture network. Discrete models are based on a discrete representation of the real fractured network. Different methods have been proposed to generate discrete model of fracture media. The models called DFN (discrete fracture network) models represent fracture networks as sets of simple geometric objects characterized by their main features (shape, size, etc.). Ezzedeni (1994) describes a model based on a generation of disks (Baecher, 1983) or a generation of planar surfaces (Dershowitz, *et al*, 2003). Koudina *et al* (1998) proposed a discrete general fracture network based on stacking polygons over which flow equations are solved. Delay and Bodin (2001) et Bodin *et al* (2003) proposed another approach where the flow and transport are solved by a Lagrangian approach (taking into account the advection, dispersion and diffusion of matrix) using the time of transition between two fixed point of network simulating the 2D fractures.

The advantage of discrete models is their ability to preserve the explicit representation of media for different scales. The fractures are characterized perfectly. However, their numerical procedures are time consuming, expensive.

1.4.2. Equivalent homogenous models

In one cell of the dynamic model the impact of joints and faults which are much smaller than the flow-simulation grid cell is taken into account using homogenization. Typically the equivalent permeability (Bourbiaux *et al*, 2002) and its eventual anisotropy may fully depict the single-phase flow behaviour of a fracture network homogenized by a continuous medium.

Equivalent homogenous models are used in the framework of the single medium approach or of the dual medium approach. A single-medium model takes into account both contributions of fracture and matrix media. Pseudo-parameters, especially pseudo-relative permeabilities have to be assigned to the cells of the model. The dual-medium concept named also dual-porosity was first proposed by Zheltov in 1960. This dual medium approach is based on the superposition of two equivalent media; the fracture medium characterized by a high permeability and a low porosity, and the matrix medium characterized by a low permeability but a high porosity (Kazemi *et al*, 1976). Using the dual-medium concept, Warren and Root (1963) proposed a conceptual representation of the fractured medium as parallelepiped blocks surrounded by a connected and uniform network of fractures (sugar-box model). They considered that the matrix acts only like one source of fluids feeding the conductive fractures.

1.5. Presentation of heterogeneity parameters in the geostatistical models of reservoirs

As seen before, to analyze fluid flow in underground porous media such as aquifers, a numerical model must first be built. This model is assumed to depict the spatial distribution of physical properties influencing fluid flow (such as porosity and permeability). Reservoir modelling must therefore incorporate all available data: static and dynamic data. Static data are often collected prior to any reservoir production while dynamic data is acquired during the production process.

Historically the reservoir image was considered as a set of petrophysical (such as porosity and permeability). Generally, there is not enough data available on the reservoir to map accurately porosity and permeability. Geostatistics are therefore used to build possible images of the reservoir. In other words geostatistical parameters such as correlation lengths, spatial variability model, variance, etc. are defined to build the model of reservoir.

In the case of heterogeneous reservoirs, most often the direct observation of heterogeneity is from the core data. When the objects like fractures, vugs or fissures are present, stochastic object-models may be of great interest. The generation of such models depends on the way to handle known parameters such as facies distribution, densities and orientations of fractures. They depend also on the deterministic information of discrete objects which are obtained from wells data. Nevertheless these models without calibration reveal unable to reproduce well data. The reason is not only related to the simplification of geological data but also it is strongly related to number of unknowns hardly conditioned on available data. This problem is amplified in the case of heterogeneous or fractured reservoirs.

Different stochastic models have been developed for describing reservoir heterogeneities in different depositional environments and at different scales. These models can be classified in three types: 1- the pixel-based models (e.g., Gaussian-related stochastic models), 2- the object-based models (e.g. Boolean models) and 3- the process-based (genetic) models (Hu and Le Ravalec, 2004).

The pixel models are based on the discretisation of a random function on a grid and this random function characterizes the spatial variability of properties. Pixel based models are relatively easy to constrain by quantitative data but they are unable to describe complex geological features. On the contrary, process-based models reproduce complex geological models, but they are high difficult to constrain by quantitative data. In this case where geological objects can be clearly identified (fractures, faults, channels and vugs), object-based models can be a good compromise between pixel-based and process-based models.

1.6. The Experimental Hydrogeological Site (EHS) : a heterogeneous fractured reservoir

The Experimental Hydrological Site (EHS) is located at the geological threshold between Paris Basin, and Aquitanian basin, and between the Armorican massif in the north-west and the Central Massif in the south-east (Figure 1.2.). More precisely, it lies in the department of Vienne on a plateau of average elevation between 100 to 130 m. The Experimental Hydrogeological Site belongs to the University of Poitiers and is established at 3 kilometres south east of the Poitiers city. The instrumented area is 210×210 m.

It covers two principal and regional aquifers which are the infra- and supra- Toarcian. The EHS was developed within the framework of 12th state-region contractual partnership (CPER) 2000-2006. The objective is to acquire knowledge, experience and data in the water resources and transfers in porous media.

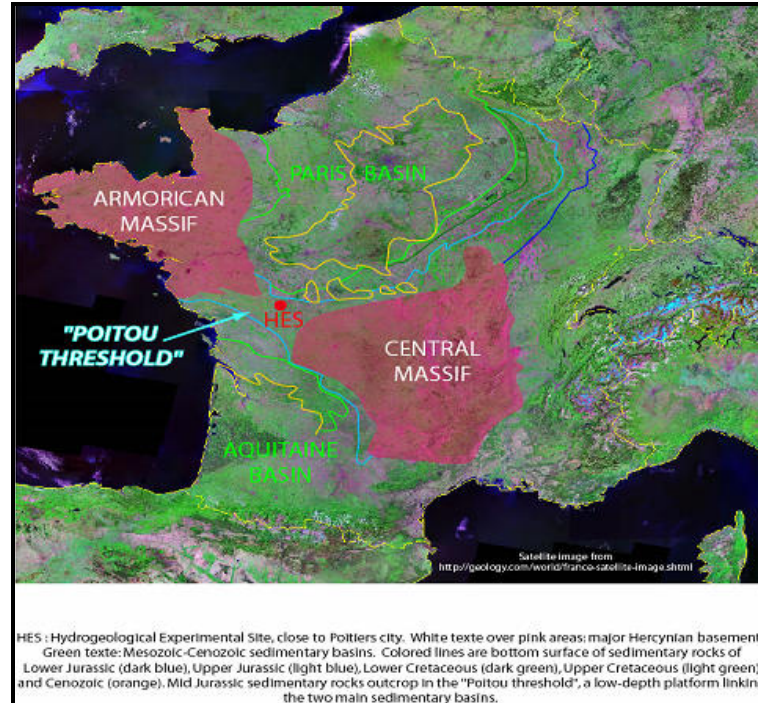


Figure 1.2: Main Paleogeographic domains with location of the studied area (EHS).

Around 30 wells have been drilled on this site, according to a NW-SE-oriented five-spot regular pattern, with an average well spacing of 70 meters. Most wells dispose of documented drilling records and logs of various nature, among which gamma-ray, temperature and acoustic velocity. In addition, two wells were entirely cored, named C1 and C2. Wellbore and surface seismic data were also acquired in the vicinity of selected wells (Figure 1.3). Regarding flow data, (wellbore) production logs and pumping tests were performed on most wells of the site with interference recording in all other wells. Vertical production profiles were also measured along wellbores.

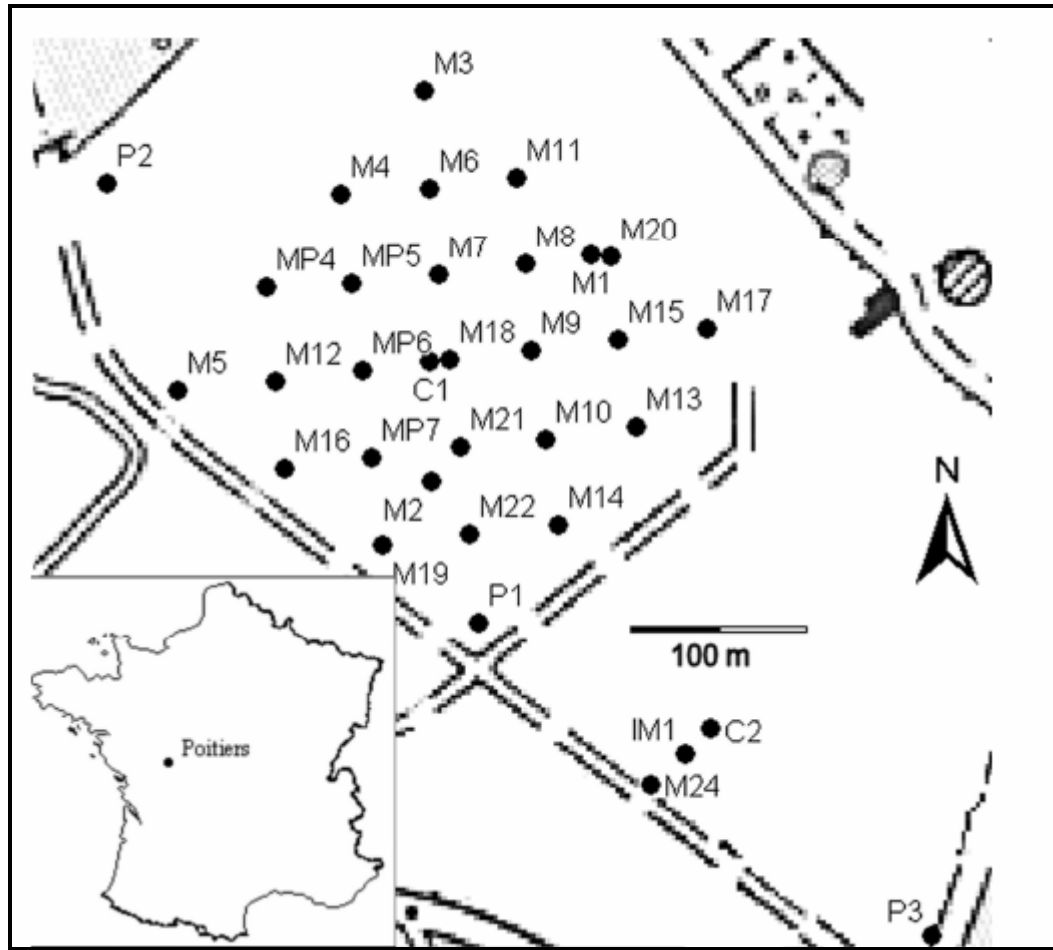


Figure 1.3: Experimental Hydrogeological Site – Location of wells.

1.6.1. (Hydro-)geological frame work

1.6.1.1. Origin of the “Poitou threshold: Jurassic Paleogeography

Jurassic sediments constitute the host rock in which the aquifer flows towards the north. This water-bearing reservoir is located on a transition area named the “Poitou threshold” and also called by geologists the “Poitou Channel”. The channel is pinched between two Meso-Cenozoic sedimentary basins: the Paris basin towards the north-east and the Aquitaine basin to the south west (Figure 1.2).

Sedimentary deposits of the “Poitou threshold” are thinner than in adjacent basins, in relation with an overall reduced subsidence at that location. They overlie, probably with an onlap pattern, a Hercynian granitic basement that was strongly eroded during several tens of millions of years at the end of the Paleozoic (Gabilly and Cariou, 1997).

Except the Armorican Massif and perhaps few domains of the Central Massif which were emerged during the Jurassic, most of France was covered by extensive seas bordering the north-western margin of the Tethys Ocean. In the Vienne area including the Site, depositional setting changed with time from deep lagoon and basin (Lower Jurassic) to low-depth platform margin (Middle Jurassic). At that time tropical conditions prevailed over shallow-marine platforms covering the Paris Basin and the north-eastern part of the “Poitou threshold” (Gaumet, 2007).

1.6.1.2. Present -time Hydrogeology of the Poitou threshold

The “Poitou threshold” is now a roughly east-west line of flow separation between the Paris Basin and the Aquitaine.

The Vienne area includes several aquifers which are the following (Renault *et al.*, 2002) :

- the metamorphized substratum at the northern border of the Vienne area, as being a confined aquifer under Toarcian marls;
- the infra-Toarcian deep confined aquifer located to the south of Poitiers city and to the west of the Vienne river;
- the supra-Toarcian unconfined karstic aquifer at the south of Poitiers city and in the south-west part of the Vienne area where the aquifer is highly productive;
- the Upper Jurassic aquifer in the north-west part of the Vienne area and at the east of the Clain river where it is in continuity with the Dogger aquifer;
- the Cenomanian sand aquifer, unconfined when cut by valleys and confined under the Turonian chalk;
- several local aquifers of small extension as being alluvial and phreatic nappes.

1.6.2. Stratigraphy and depositional sequences.

Mesozoic rocks encountered in the EHS belong to the Lower and Middle Jurassic (Figures 1.4 & 1.5). They correspond to a total time interval of deposition of about 40 millions of years. Hiatuses in deposition are possible, notably during the Lower Jurassic and also during Bathonian-Callovian times, yielding reduced thicknesses of sediments and highly variable facies in space.

Oldest Jurassic sediments overlapping the eroded substratum are regionally dated from Hettangian-Sinemurian times (Gabilly and Cariou, 1997). Lower Hettangian sediments were fluvial sand and shale passing laterally to motley shales with gypsum traces deposited in lagoonal setting (Renault *et*

al., 2002). Crystalline dolomites then deposited during the Sinemurian in a deeper but again restricted lagoon. They reach a maximum thickness of 30 meters.

The Pliensbachian, with deposits highly variable in thickness (between 2 and 20 meters), is a period of marine transgression that deposited marls and shaly limestones characterized by a high shell content.

The maximum rise of relative sea-level occurred during the Toarcian when blue marls and argillaceous limestones, full of ammonites and belemnites were deposited. Such pelagic-rich deposits are still regionally variable in thickness, between 2 and 15 meters.

After the Upper Liassic drowning episode, a shallowing upward trend established during the Dogger. It started with Aalenian deposits 20-meter thick, subdivided in two main depositional sequences. The first one recorded a climate change that modified the sediment supply from clastic dominated to carbonate-rich, reflecting the starting of the carbonate factory (Pomar, 2001). The second one started with an abrupt arrival of siliceous sponges and ended with first oncoid-rich deposits which are made of wave-induced microbial laminations encrusting pieces of shells and small grains.

The shallowing trend continued with Bajocian deposits stacking three successive depositional sequences accumulated in an outer platform setting. Bioclastic and grainy limestones with oolites, crinoids and bivalves reach a thickness of 45 meters.

Similar coarse-grained facies of platform margin accumulated during the Bathonian, but this stage is characterized by a high content of chert more or less banded horizontally, and by regional thickness variations between 20 and 40 meters.

The top of the Dogger aquifer in the EHS (Figure 1.5) belongs to the Callovian time, characterized here by finer grained chalky limestones that probably recorded a new deepening trend over the “Poitou threshold”. However, tectonic activity re-started at the end of the Dogger, and Callovian sedimentary record is highly variable at the scale of the Vienne area, with simultaneously sedimentary hiatuses, coarse-grained platform limestones or still Fe-oolite condensed limestones (Gaumet, 2007).

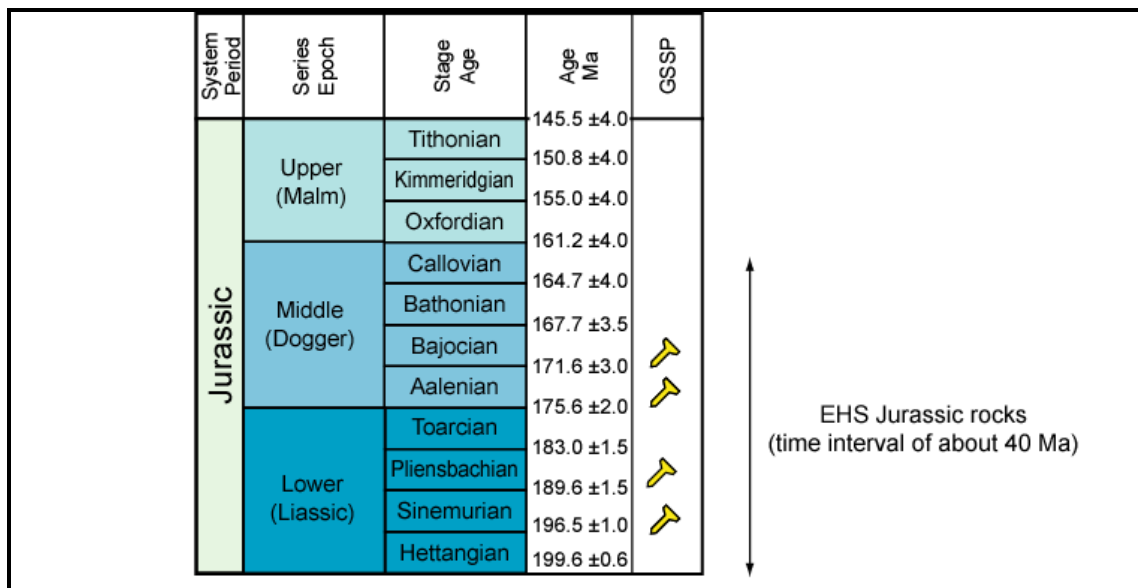


Figure 1.4: Stratigraphic chart for the jurassic (Gaumet, 2007).

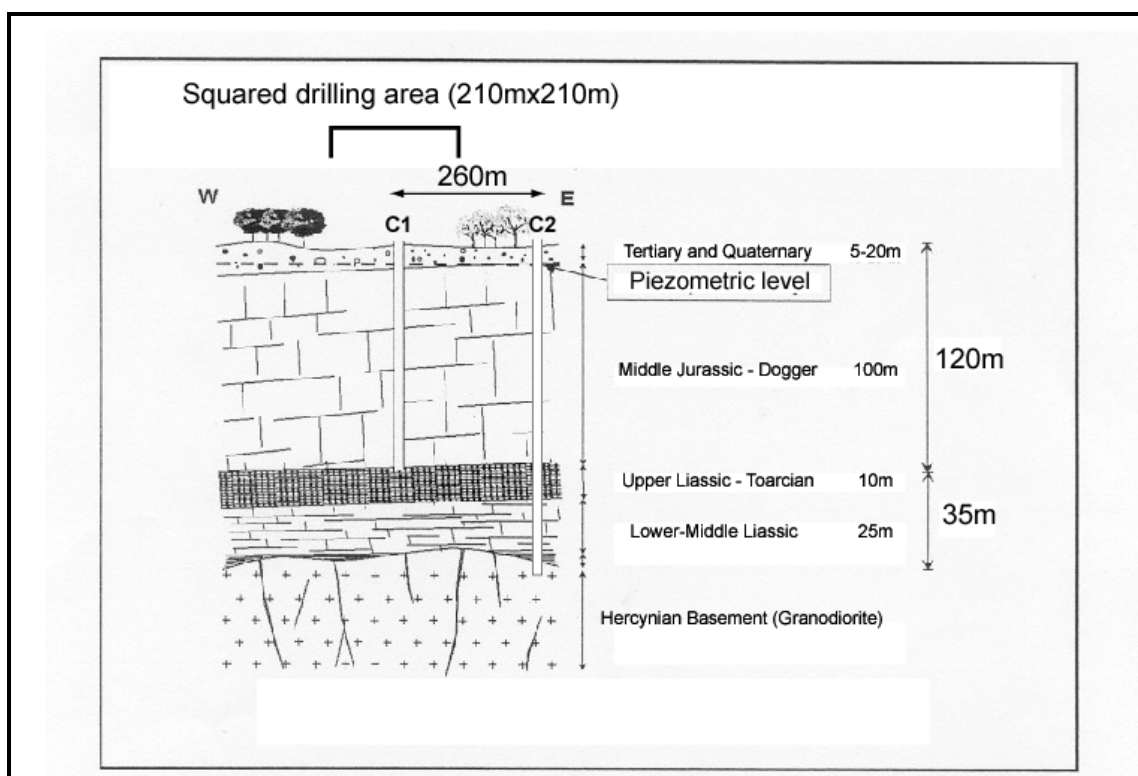


Figure 1.5. Simplified geological cross section at the EHS location (Gaumet, 2007).

1.6.3. Structural features - tectonic history - fracturing features

A geological cross-section perpendicular to the main axis of the “Poitou threshold” reveals the two main steps of structural evolution in that area (1.6): first the building of a Precambrian – Paleozoic

substratum, extensively folded and eroded during Caledonian-Hercynian orogenesis; second the deposition of Meso-Cenozoic sedimentary rocks.

The Jurassic sediments constituting the reservoir were deposited in a low-depth platform environment located at the threshold of two sedimentary basins (Poitou threshold). At that location, sedimentary deposits are thinner than in the Paris and Aquitaine Basins and they overlie a Hercynian granitic basement linking the Vendée and Limousin domains.

The structure of this basement is influenced by N120° to N140° and N060 to N070° tectonic lineaments which have been reactivated during Jurassic, as suggested by the thickness and lithology variations of sediments (Mourier and Gabilly, 1985).

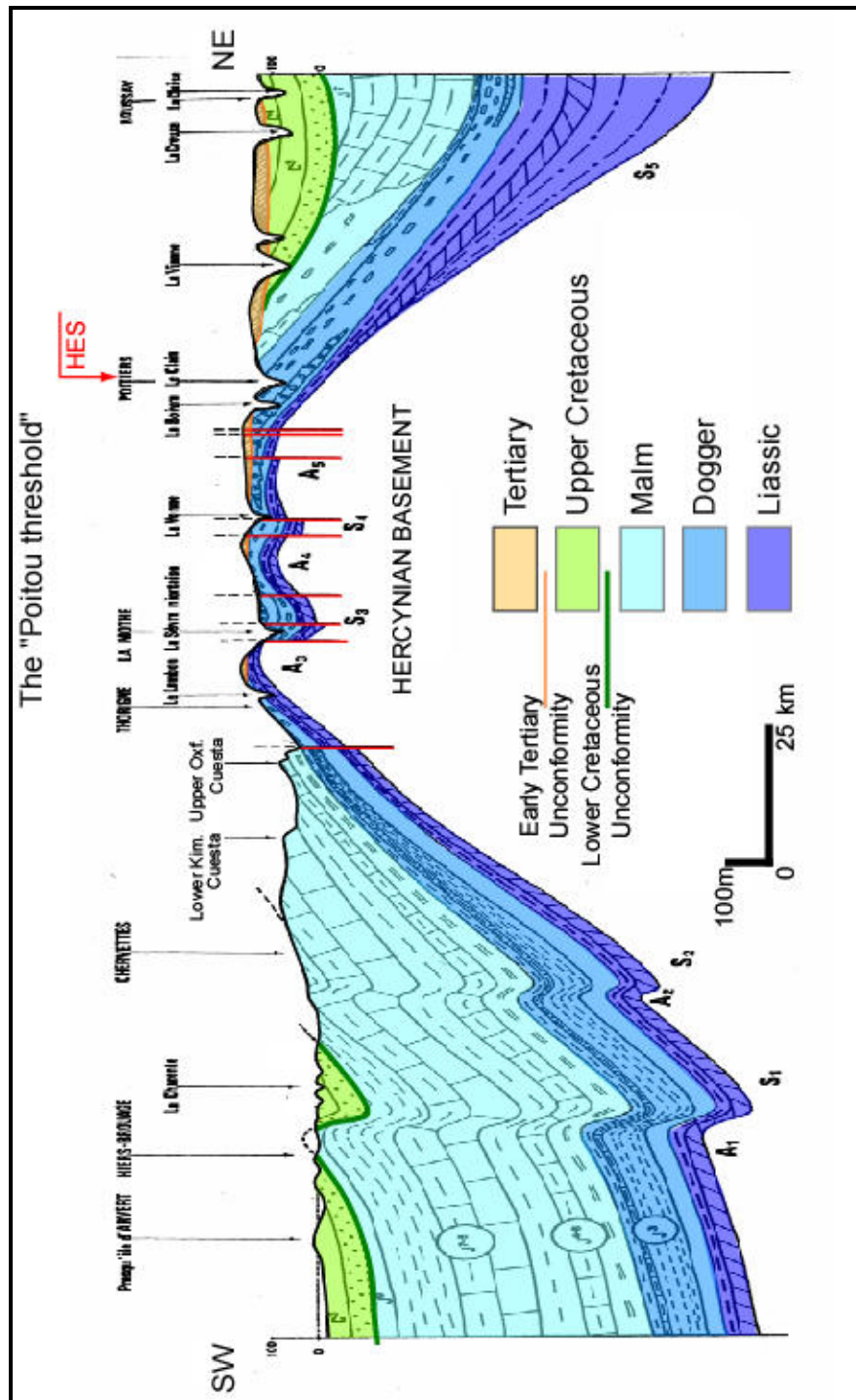


Figure 1.6: Transversal geological cross-section crossing the Poitou threshold (modified after Gabilly and Cariou, 1997). A means anticline, S means syncline. Note the change in subsidence of paleohigh margins with time (NE margin during Liassic, SW margin during Upper Jurassic).

Following the sedimentation on the post-Hercynian peneplain, several tectonic events, related to distant Pyrenean and Alpine orogenesis of Tertiary age, induced a fracturing of the carbonate deposits. Because of their possible impact on the aquifer flow behaviour, a characterization of these

fractures was undertaken on analogue outcrops located near the hydrogeological site, and from the observation of available cores from wells C1 and C2 (Bourbiaux *et al.*, 2007).

Outcrops show that Bajocian and Bathonian limestone formations are mainly crossed by sub-vertical fracture corridors with a high vertical extension rather than bed-controlled diffuse fractures. These fracture corridors are oriented in three directions, N120°, NS and N50° (Figure 1.7), with the N120° direction probably influenced by the pre-existing Hercynian lineaments. The spacing of these fracture sets is metric to decametric. The Callovian outcrops show a higher density of fractures, but with clay filling.

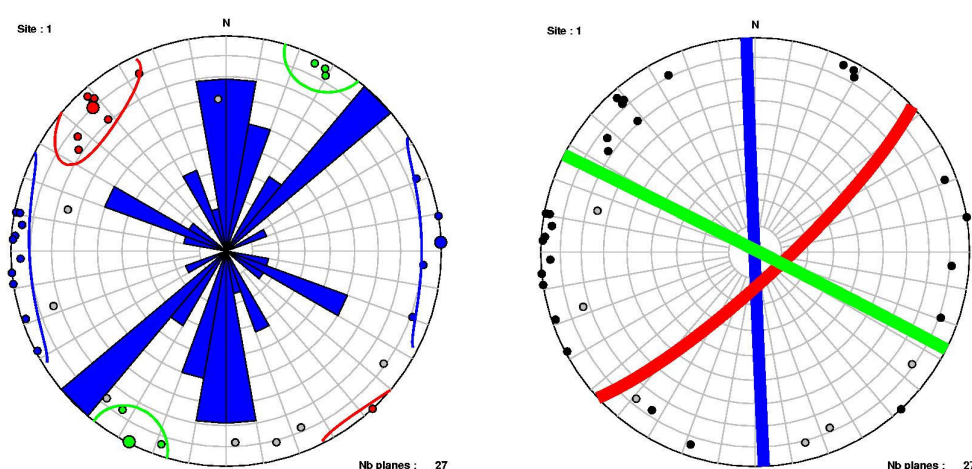


Figure 1.7: EHS analogue outcrops study - Passelourdin site: (left) the rose diagram of fracture azimuths and poles shows three main clusters, with the corresponding poles shown in red, blue and green colors; (right) cyclographic traces of the mean orientations of those three fracture sets (Bourbiaux *et al.*, 2007).

According to the core studies at the Site, fairly few fractures were observed within the Bajocian-Bathonian sections of the two vertical wells C1 and C2. More fractures were found on the Callovian upper sections, but often filled in by a clayey or organic material due to the proximity of the surface. Typical tectonic fractures, *i.e.* high-dip tension and shear fractures, are rare and most often cemented. The few observed fractures, of decimetric size, are often located at the interfaces between cherts and rock matrix or within cherts. Dominant micro-structures are sub-horizontal stylolitic surfaces and compaction bands, apparently associated with burial processes. Some of them are not cemented and may constitute flow conduits. Fluid circulation seems to have influenced the fracturing process and the evolution of fracture properties, as shown by the presence of clay smearing (Figure 1.8).

Although distant by only 200 meters, the two wells C1 and C2 revealed a high fracture density contrast: in well C1, few cemented decimetric-scale fractures are found in the host rock and cherts and are cemented; on the contrary, well C2 shows a high fracture intensity, particularly in the 85-95m and the 55-25m depth intervals, with more or less connected fractures, associated with vugs and molds. Organic matter and shale are sometimes filling the fractures.



Figure 1.8: Cores from C2 well at about 97m depth: clay material is filling the upper "damaged" zone (karst residue) ; a vertical fracture is observed between two marly (dark) layers in the lower core.

To conclude, typical diffuse tectonic fractures do not seem to constitute the main direct origin of flow heterogeneity. However, horizontal stylolite-associated discontinuities at bed boundaries may constitute preferential flow paths provided they remained open. In addition, outcrops revealed the existence of fracture corridors at a larger scale. Such discontinuities might influence the flow connectivity between wells at the reservoir scale, either as preferential flow paths or as flow barriers depending on their conductivity. They may also have played a role in the development of the diagenetic features described hereafter.

1.6.4. Diagenetic fingerprints- Evidence of the karstic nature of the aquifer

Attentive look at the cores from two wells (macroscopy analysis) allows to detect six major diagenetic phenomena that deeply modified the jurassic host rock of aquifer. Those phenomena are dolomitization, silica precipitation, compaction, fracturing-brecciation and dissolution.

In this regard, the diagenetic fingerprints, in particular the presence of silice and dolomite, were identified and characterized. Fractures are only found in the first 30 meters of well C1. Some of these fractures are filled with clays, which were identified as transported clays (El Albani *et al.*,

2005): their assumed origin would be vertisols of Tertiary age and thus, they could constitute the remaining evidence of the paleo-karstic nature of this aquifer.

A full analysis of diagenetic fingerprints on wells C1 and C2 cores revealed that diagenetic fingerprints completely modify the lithology over short distances (Bourbiaux *et al.*, 2007). Cherty limestones and fractured/karstic units may vanish or pinch out within a distance of the order of the well spacing (70 m on average). Therefore, the main origin of the contrasted well responses at the Site scale may lie in the great variability of diagenetic fingerprints that affected this limestone formation.

1.6.4.1. Borehole images

Recent borehole images from several EHS wells revealed the presence of a complex partly-collapsed cave system. The occurrence and the vertical location of this system change very much and cannot be correlated from one well to the other. Wells M3, M4, M7, M9 and M11 appear to be particularly fractured and brecciated, with clasts frequently embedded by clayey sediments. Unfilled caves and vugs, in which water should flow are often visible in these borehole images. The correspondence between flow drains determined by production logs and open vugs and caves visible by borehole optic imaging is obvious in wells M3, M4, M7, M11, M13, M17 and M21. On the contrary, the wells MP4, M8, M10 and M14 mostly cross cut weakly fractured and undisturbed host rock.

The main types of paleocave facies as described in Loucks (1999) are clearly identified on those images, as shown in Figure 1.9. Borehole images bring a direct evidence for a paleo-karst origin of the major flow network of this aquifer. The paleo-cave model (Loucks, 1999; Loucks *et al.*, 2004) is supported by the intense and local brecciation, due to the collapsing during collapsing episodes of previously-formed water tubes. The hypothesis of a simple modern near-surface cave system controlling water flows through the Dogger aquifer is abandoned, simply because such a process would not result in the so heavily fractured and locally brecciated medium as that observed in the site. We need thus to consider a more complex system like modern epigenic caves rejuvenating collapsed paleocave passages. Beside the geological understanding of the Site, borehole images point out some limitations regarding the detection of the water feeding points of a wellbore. Indeed, image logs reveal to be more reliable indicators of the productive water drains than cores, since core

sampling is often incomplete in vuggy or caved wellbore sections. Several production logs confirm the effective contribution to flow of these potentially-productive drains.

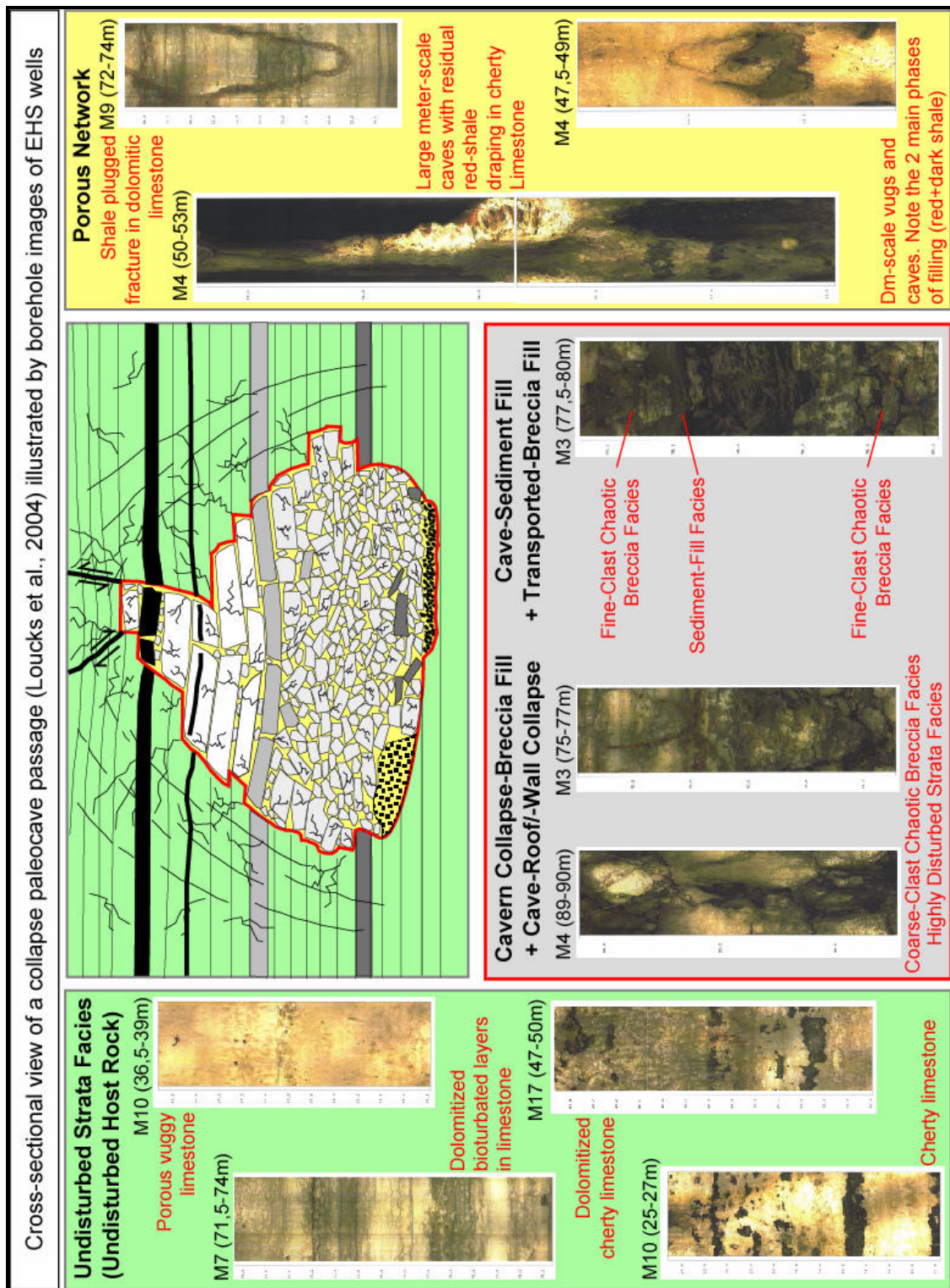


Figure 1.9: Bore-hole images as evidences of the paleo-karstic origin of the EHS heterogeneities (Bourbiaux *et al.*, 2007).

1.6.4.2. Reference well C1 data integration in relation with fluid flow behaviour

The central well in the EHS disposal (C1) provides the most complete dataset among all the Site wells, with detailed core descriptions from 129m in depth up to the surface, a large set of wireline logs including gamma-ray, resistivity, acoustic and borehole image logs, a constrained petrophysical data set and a flow profile. All these sources of information were compared between each other to derive possible indicators/drivers of lithological changes and of flow properties along the well.

Regarding fluid flow, the major water arrival observed on the production log is found at a depth of 49 to 52m and is responsible for about 75% of the well water supply. This water entry point lies at the base of a cherty limestone unit. During coring, 0.7 m of core was not recovered at that level. The presence of this drain at that depth is consistent with the full-wave acoustic log showing the disappearance of Stoneley waves in relation with the presence of a fluid-filled discontinuity. According to the recorded flow profile, an entirely-dolomitized vuggy layer at about 90m and another cherty section, 110 to 120m deep, may also contribute to fluid flow, however this contribution is not as much obvious as that found at 50m.

The matrix porosities and permeabilities were measured on 31 core fragments distributed along the wellbore. Porosity is dominated by inter-granular and intra-granular void (Zerti *et al.*, 2007), enhanced by numerous vugs, molds and dissolved micro-layers witnessing strong dissolution processes. Highest porosity and permeability data are similar to those generally measured in a good oil Dogger reservoir of the adjacent Paris basin. Porosity values are ranging from 7 to 25% with an average of 15%, and permeability values from less than 0.01md up to some 200md. Most Bajocian permeability values are comprised between 0.1 and 1md, *i.e.*, about one order of magnitude less than Bathonian-Callovian values. However, high matrix permeability contrasts, of up to three orders of magnitude, are observed locally within each unit.

The porous structure of these carbonates was characterized from Nuclear Magnetic Resonance (NMR) measurements. It varies significantly between samples, from unimodal to bimodal pore-size distributions. The bimodal structure should be the record of a mixing between micro- and macro-porosity. This dual porosity has been observed by microtomography images of mini-plugs of 6 mm in diameter (Gaumet, 2007).

1.6.4.3. Two lastly cored and deviated wells (C3 and C4)

Two lastly cored and deviated wells (C3 and C4) have been bored and cores were studied at the end of April 2007. The C3-C4 core study strongly supports the paleocave hypothesis by the recognition of typical facies well documented in the karst literature (Loucks *et al.*, 2004), like crackled to mosaic breccias or sediment fills. Coalesced collapsed paleocave systems are hemispherical brecciated areas of few meters to few tens of meters in thickness. Included host rocks are more or less fractured up to form crackled breccias. Inside collapsed paleocave structures, the old porous network is mostly filled due to breakdown processes and to several episodes of cave sediment fills. The association of dissolved structures (vugs, geodes and caves) with collapsed structures, showing several episodes of internal sediment fills, is clearly in favour of a rejuvenated paleocave system at the origin of present water flows through the EHS site (Gaumet, 2007).

1.6.5. Flow observations at EHS

As mentioned before, several wells were drilled during two campaigns 2004 and 2005 (Figure 1.10). Each well was followed by a series of large-scale interference pumping tests. Actually, after drilling, each well was pumped while measuring the pressure interferences in other wells. Such hydraulic interference tests have been widely used in hydrology and petroleum engineering to assess the hydraulic diffusivity of underground reservoirs.

All pumping tests performed during 2004 and 2005 are consistent with each other in the sense that they applied a similar hydraulic stress to the aquifer whatever the pumped well (Kaczmaryk et Delay, 2007b). Pumped flow rates varied between 30 and 70 m³.h⁻¹ and were prescribed over periods of 60 to 200 h according to water production capabilities of each well and in order to avoid pump drying out. In most cases (more than 75 % of the pumped wells), testing was performed with a constant prescribed flow rate of 60 m³.h⁻¹ over a duration of 120 h. It is important to note that there was no record of any clear-anisotropic response in all 2004 and 2005 tests.

The University of Poitiers has been working on EHS model since 2003 to better understand the flow in fractured reservoir by using different experimental modelling approaches. Since October 2006, several other modelling teams have been involved in a national research project attempting to confront different modelling approaches conditioned by the EHS data (MACH-1 project: "Modelling of Heterogeneous Carbonate Aquifers – 1. Flow Dynamics"). The tested models are

based on various conceptual/numerical approaches: 2D heterogeneous continuum (Mouche and Zakharov 2005), 2D double/triple continuum (Delay *et al.* 2007, Kaczmaryk and Delay 2007b), discrete-continuum hybrid model (Davy *et al.* 2006), fractured porous media (Bogdanov *et al.* 2003), 3D discrete fracture networks (Jourde *et al.* 2002), pipe-networks (Jeong *et al.* 2006) and the present study based on a stochastic continuum approach. The main goal of the MACH- 1 project is to analyse to which extent the variability and density of the EHS data are both relevant and sufficient to confer some predictive capabilities to these models.

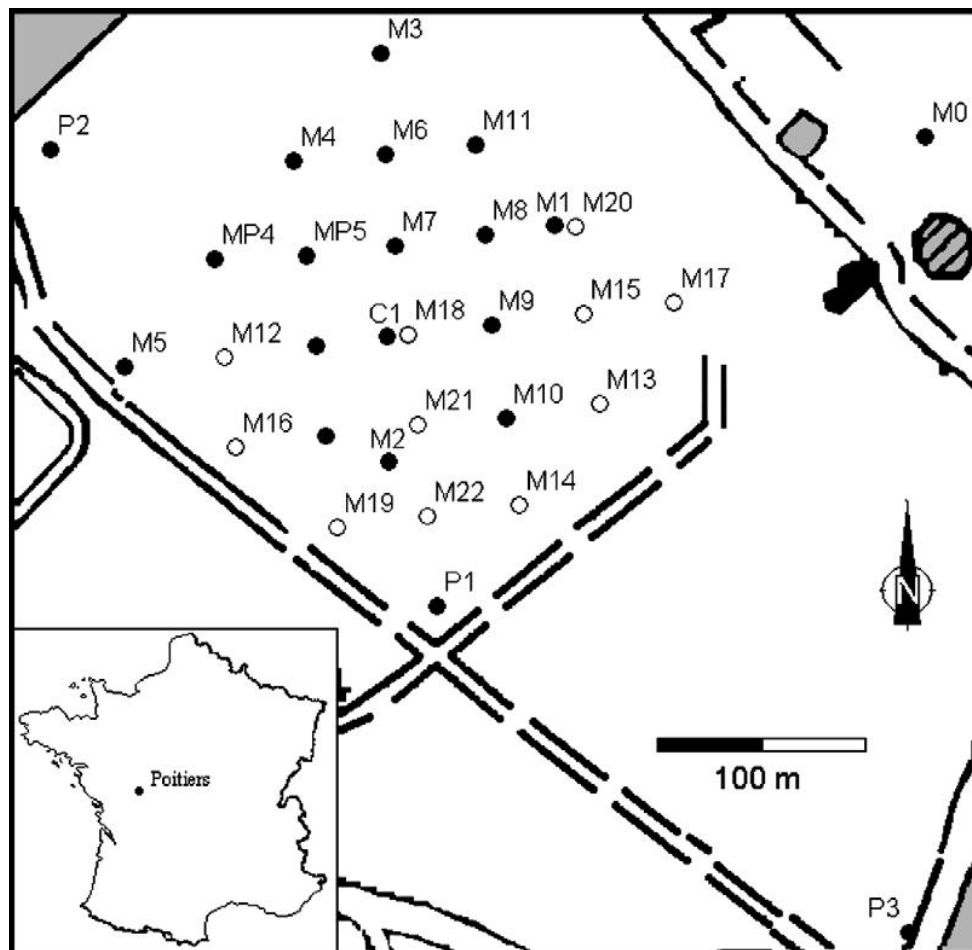


Figure 1.10: Wells set up in nested five-spots in the experimental site in Poitiers. Solid dots: wells tested in 2004, empty dots: wells tested in 2005.

Data interpretation from two campaigns of 2004 and 2005

As mentioned before, the EHS site has been built for the sole purpose of providing facilities to develop long-term monitoring and experiments for a better understanding of flow and transfers in fractured rocks. Several methods have been used by the group managing the Site to assess the

hydraulic parameters of EHS from tests performed during both campaigns of 2004 and 2005. These efforts are discussed afterwards.

The first campaign initiated in 2004 on wells M06-M11 and MP4-MP7 confirms the heterogeneity of the flow and shows drawdowns increasing more rapidly than a linear function of time. According to Bernard (2005), this behaviour could be typical of a transitional regime with hydrodynamic parameters varying in space. He stated that this could be also considered as a fractal signature of the fractured reservoirs.

Three shapes of drawdown curves are observed in distant monitored wells (Figure 1.11). Bernard (2005) concludes that the curve of type 1 could be typical of a structure with high connectivity. The curve of type 2 characterized by a very rapid increase of drawdowns at short times could correspond to wells with low productivity, while the curve of type 3 could be interpreted as the passage of a flow from 3D to 2D because of its "bayonet" shape. The interpretation with Cooper and Jacob (1946) model remains feasible but would yield several set of parameters according to the times where reference drawdowns are taken to calculate hydraulic parameters.

An alternative approximation combining analytical solution of 2D Cooper and Jacob (1946) and scaling laws for K and S_s was developed (Delay *et al.*, 2004, Bernard *et al.*, 2006). The parameters resulting from the interpretation of experimental curves depend on the shape of the curves. The resulting average hydraulic conductivity values are 3.0×10^{-5} , 5.0×10^{-6} and $2.9 \times 10^{-5} \text{ m.s}^{-1}$ for shapes 1, 2 and 3 respectively and the specific storage coefficients are 7.9×10^{-7} , 8.4×10^{-6} and $1.5 \times 10^{-6} \text{ m}^{-1}$ respectively.

The second campaign of pumping tests on wells M12-M23 in 2005 shows a change of hydraulic behaviour compared to earlier campaign. The drawdown curves from the observation wells have the same behaviour in terms of change over time, shape and the maximum drawdowns, irrespective of their distance from pumping wells. Moreover, the "bayonet" shape have been disappeared. According to Bernard (2005), this change in behaviour could be related to a succession of hydraulic tests on the EHS which would have modified the geometry of active draining channels, thereby increasing the connectivity between wells.

The interpretation based on the model by Delay *et al.* (2004) shows that the hydraulic conductivity may have homogenised at the Site scale after a few hours of pumping ($3.3 \times 10^{-5} \text{ m.s}^{-1}$ after 48

hours of pumping). The values of S_s that range from 3.9×10^{-7} to $7.1 \times 10^{-6} m^{-1}$, cannot be homogenised and show a significant decrease with respect to the distance from pumped wells.

The interference tests of the EHS were also analysed by Delay *et al.* (2007) and Kaczmaryk and Delay (2007b). In the model of Delay *et al.* (2007), the interpretation of pumping tests is based on a dual-medium approach that may be considered as homogeneous or fractal. As mentioned before, a dual-medium model assumes an exchange between a fracture system (drainage) and a matrix system (storage). As in most cases, the exchange here is parameterized by a single rate of mass (volume) transfer between the two media (Barenblatt *et al.*, 1960). The interpretation of the 2004 campaign with the homogeneous model gives a hydraulic conductivity K_f for the fracture medium ranging between 1.1 and $2.1 \times 10^{-5} m.s^{-1}$. The specific storage capacity of the fracture (S_{sf}) and matrix medium (S_{sm}) range between 2.4×10^{-7} and $4.8 \times 10^{-6} m^{-1}$ and between 1.4×10^{-6} and $3.9 \times 10^{-5} m^{-1}$ respectively.

Applying the same model on 2005 data gives a hydraulic conductivity K_f equivalent to that of 2004 but the similarity of curves in time and amplitude whatever the distance is interpreted (according to the homogeneous approach) as an effect of scale with a rapid decrease with distance of the values of specific storage capacity. S_{sf} ranges between 3.2×10^{-7} and $1.5 \times 10^{-5} m^{-1}$ and S_{sm} between 4.5×10^{-6} and $2.4 \times 10^{-4} m^{-1}$.

The fractal approach consists in ruling each hydraulic parameter P by a power-law of distance r between pumped wells and observation wells: $P(r) = P_0 r^{-\lambda}$ where P_0 is constant and λ is the power-law exponent. The interpretation of 2004 data with the fractal approach shows a homogenization of parameters P_0 at the site scale. Using data from the 2005 campaign, Kaczmaryk and Delay (2007b) conclude that the fractal dual-medium approach does not reproduce preferential flow paths transmitting very quickly the pressure wave between the wells. The drawdown curves of 2005 data were reinterpreted by introducing an equation of wave propagation into the dual medium model (Kaczmaryk and Delay 2007a). With this new model, the homogeneous approach provides the relatively constant values of K_f , S_{sf} and S_{sm} ($K_f = 2.7 - 2.8 \times 10^{-4} m.s^{-1}$, $S_{sf} = 9.2 \times 10^{-7} - 4.8 \times 10^{-6} m^{-1}$, $S_{sm} = 8.6 \times 10^{-6} - 1.3 \times 10^{-5} m^{-1}$). The values of storage coefficients are similar to those obtained by the dual homogeneous approach applied to 2004 data.

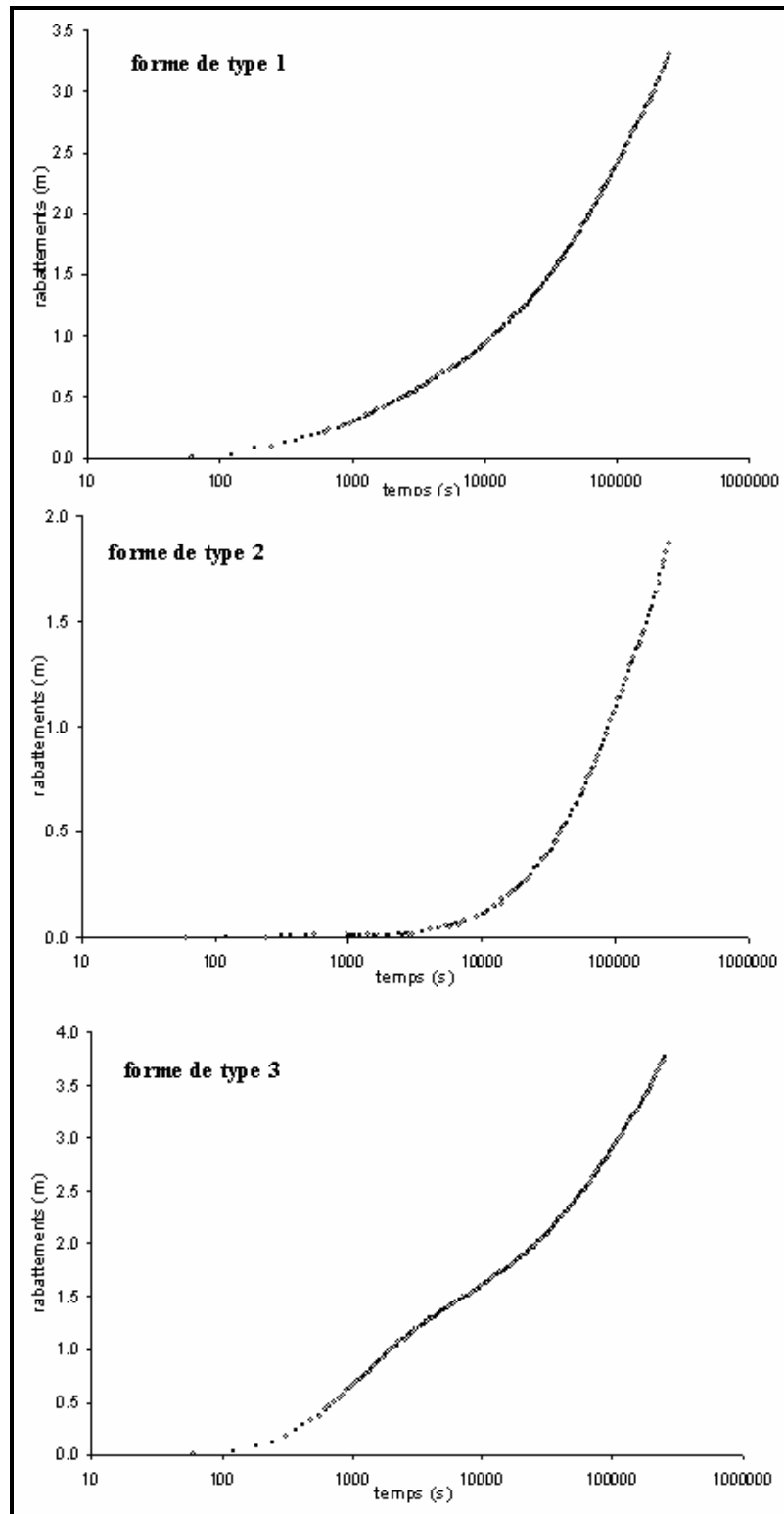


Figure 1.11: Representation of 3 typical shapes of drawdown curves from the pumping test of 2004 campaign (from Bernard, 2005).

The fractal approach shows homogenized power exponents λ (with or without wave equation) that are compatible with a fractal dimension for a 2D flow. The application of the fractal approach coupled with wave propagation is thus able to homogenise the constant values of P_0 . Note also that adding a wave propagation to a dual-medium approach is able to mimic without artifacts the similarity in time and amplitude of drawdown curves from 2005 data.

As the rock compressibility has a first-order impact on the well responses, both on early- and late-time responses, preliminary simulation and inversion tests will be performed at the beginning of our study to set facies compressibility at a value yielding a coarse overall restitution of the pressure responses of pumped wells.

1.7. Conclusion

Several underground aquifers were developed as experimental sites during the last twenty years. The scientists were always interested in flows in the heterogeneous reservoir. The Experimental Hydrogeological Site (EHS) under consideration is developed by the University of Poitiers as a research laboratory aimed at investigating and understanding flow and transport in highly-heterogeneous, *i.e.* fractured and/or karstic, aquifers. This Site is located on the border, named “the Poitou threshold”, between the Paris and the Aquitaine sedimentary basins. Around 30 wells have been drilled on the EHS, with available documented drilling records and logs, and two wells of C1 and C2 were cored.

An extensive geological characterization was undertaken to understand the heterogeneous distribution of flow at different scales as confirmed by available flow information. This multi-disciplinary aquifer characterization combines detailed core-log-borehole image analysis and diagenesis study. The borehole logging data indicated that the flowpaths in the Dogger aquifer are mostly concealed within (1) subhorizontal karstic structures and (2) subvertical fractures. All wells that don not intercept these features have very limited pumping capacities. The stratigraphic position of these karstic levels can be identified by cross-referencing in regard to the C1 lithostratigraphic data. The upper (50m) karstic level develops within the granular limestones interbedded with cherty layers in the upper Bajocian. The intermediate (85m) level corresponds to the dolomitized layer in the lower Bajocian, identified from the C1 cores. The lower (115m) karstic level develops within the bioclastic limestones of the upper Aalenian. The vertical interconnectivity between the 3 karstic levels is very likely linked to vertical fracturing.

The pumping test were carried out on most wells with interference data during two campaigns of 2004 and 2005. The studies showed that the data collected during two main campaigns (C2004-C2005) witness non-negligible modifications of the medium due to the drilling of wells and forced flows. Before the C2004 campaign, the site was subjected to a natural non perturbed flow and the C2004 drawdowns obey a logical hierarchy stating that the farther the observation point, the smaller the drawdown and the larger the arrival times of hydraulic stress. In 2005 after the site was stressed by C2004 forced flows, the drawdown curves are almost similar in time and amplitude whatever the distance from the pumped well. This is interpreted as a partial unclogging of preferential karstic flow paths which makes the pressure depletion to propagate very rapidly while keeping a long-time behaviour similar to the draining of a dual medium.

Finally, the Experimental Hydrogeological Site constitutes a very instructive multi-disciplinary data-base to set up consistent methodologies for characterizing the heterogeneity of complex diagenetized reservoirs. The resulting set of interpreted data from this chapter will be integrated into a preliminary geostatistical model that will serve as initial solution for inversion of flow in the EHS. This work is detailed in the next chapters.

CHAPTER 2. Approaches and tools for modelling, simulating and calibrating the hydodynamics of an underground reservoir

2.1. Introduction

The reservoir model is a grid depicted by hydrodynamic properties such as porosity and permeability. The grids values are informed by stochastic porosity or permeability realizations which supposedly should respect local measured values as well as spatial variability inferred from local data. Most often, there is not enough local data to map accurately the reservoir properties. Geostatistics therefore are used to build probable images of reservoirs. Those realizations respect the measured values at static data locations and the spatial variability model inferred from these data.

Furthermore, the reservoir flow model should be consistent with dynamic data as the well tests. This issue is addressed as an inverse problem where flow equations are solved until they provide results (heads) similar to the measured dynamic data. First attempts to solve this problem were initiated by Nelson (1960) and Jacquard and Jain (1965) and then numerous methods have been developed. For a heterogeneous medium mapped by grids with a set of parameters per cell, there is too much unknowns and their number has to be reduced or additional information has to be sought. Because of these difficulties we are interested in the parameterization techniques, especially geostatistical ones. Recently the geostatistical parameterization technique has been proposed to reduce the number of inversion parameters and to ensure that the spatial variability is preserved. One can refer to the pilot point method, the gradual deformation method and finally, the gradual pilot point method.

In this chapter we introduce our step by step modelling approach and their tools as they are implemented.

HERESIM 3D software has been developed by the HERESIM group (gathering a few researchers from Ecole des Mines Paris and IFP). It is an integrated model for building the geostatistical and geological model of a reservoir.

Welgem software package, including the SIMTESTW flow simulator is used for simulating flow and calibrating the petrophysical properties of flow model.

Finally the CONDOR software developed at IFP is used. The general purpose of the CONDOR Software is to constrain reservoir models to fulfil production data. The gradual deformation technique is implemented in CONDOR software.

2.2. The reservoir modelling workflow

Our approach is based on a workflow that consists in building a proper geostatistical-geological model of reservoir and then building a consistent flow model and finally optimizing the model in terms of petrophysical properties and distribution of facies from well test data.

2.2.1. Geostatistical and Geological modelling

The diversity of the geological environments justifies the utility of various types of stochastic models. According to their methods of construction, three types of models can be separated:

- pixel-based models (*e.g.*, models generated by multi-Gaussian simulations);
- object-based models (*e.g.*, the Boolean model);
- process-based (or genetic) models (model based on the sedimentary processes).

The geological modelling of a heterogeneous reservoir is often decomposed into several steps and implies several basic models. Generally continuous Gaussian simulations are used to generate the pixel based models. These models are relatively easy to constrain by quantitative data but they are unable to describe complex geological features, particularly at the field-appraisal stage with few well data. On the contrary, process based models reproduce complex geological features, but they are difficult to constrain by quantitative data. In the cases where geological objects can be clearly identified (fractures, faults, channels and caves), object-based models can be a good alternative between pixel-based and process-based models. The pixel models are based on the discretization of a random function on a grid. This random function characterizes the spatial variability of properties. For this case, one could generate a facies model of the Site through Gaussian simulation. The truncated Gaussian simulation method (Matheron *et al.*, 1987) is often used for describing the lithofacies distribution in a reservoir field. In our approach we use this method for the facies distribution in the reservoir.

Truncated Gaussian simulation

As mentioned above, the truncated Gaussian simulation method (Matheron *et al.*, 1987) is often used for describing the lithofacies distribution in a reservoir field (Ravenne *et al.*, 2002). Let $Y(x)$ ($x \in D$) be a standard random Gaussian function defined over the field D , and $I(x)$ ($x \in D$) an indicator function defined by truncating $Y(x)$ at threshold s :

$$I(x) = \begin{cases} 1 & Y(x) \geq s \\ 0 & Y(x) < s \end{cases} \quad (1)$$

If $Y(x)$ is stationary, then $I(x)$ is also stationary. It can be used to simulate, for instance, the geometry of the spatial distribution of a lithofacies in an oil or water reservoir. This method can be easily extended to the case of several thresholds in order to build models with several lithofacies. In the common practice of this method, each lithofacies corresponds to an interval of the Gaussian variable. The transitions are possible only between the lithofacies whose intervals are contiguous. However, to generate a lithological model with direct transition between two lithofacies, one can use disjoint intervals to define the lithofacies.

This method, however can be generalized to facies that do not follow one another in a fixed order by using two Gaussian stationary random functions, independent or correlated, to define the facies as shown in Figure 2.1 (Truncated plurigaussian simulations: Galli *et al.*, 1994; Le Loc'h and Galli, 1997). Finally, there are adaptations for including connectivity constraints (Chilès and Delfiner, 1999). In this Figure each facies is defined by a domain in the $Y1$ and $Y2$ plane (bounds can be infinite). In these examples $Y1$ has an anisotropic cubic covariance, defining smooth well-marked contours, and $Y2$ has an isotropic spherical covariance defining irregular diffuse contours: (a) facies $F1$ (white) and $F4$ (black) are only in contact for extreme values $Y2$; (b) facies $F1$ and $F4$ are never in contact, and the gray space between them is subdivided into facies $F2$ and $F3$ by variable $Y2$ (Chilès and Delfiner, 1999).

In general, lithofacies indicator along wells can be accounted for in truncated gaussian simulations. This is achieved first by generating truncated Gaussian values along wells using the Gibbs sampler (Geman and Geman, 1984) and then by applying conditioning on the whole Gaussian field (Hu et Le Ravalec, 2004).

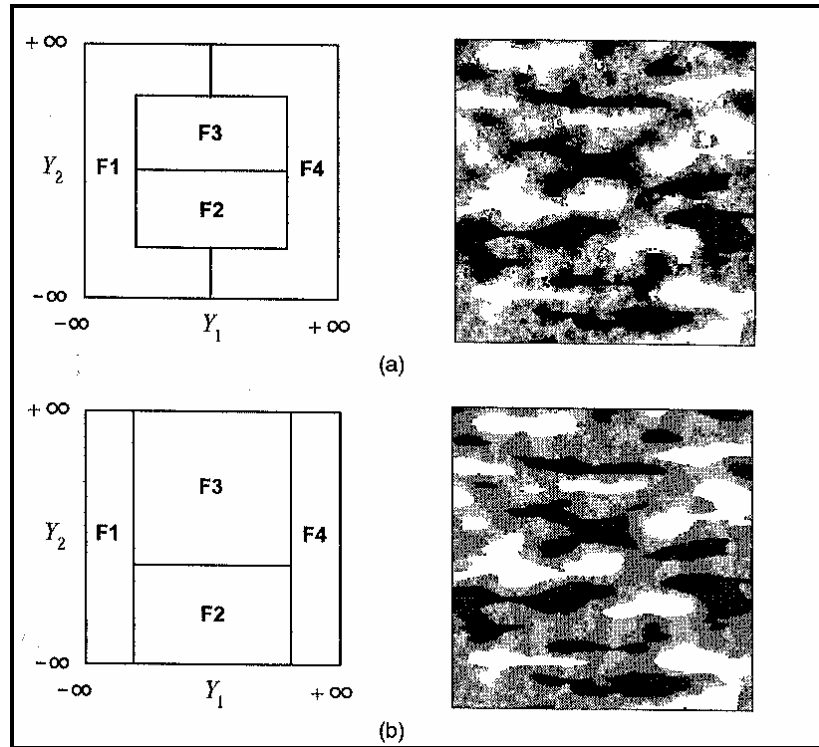


Figure 2.1: Truncated plurigaussian simulations (Chilès and Delfiner, 1999).

2.2.2. Flow modelling

We use numerical methods to solve the governing equations of flow in reservoir. In a numerical simulation, the space region is divided into elements (sub-domains or cells) with each element associated to one or several nodes. The governing equations are then discretized and replaced at these nodes by a system of algebraic equations. The solution of algebraic system provides nodal values of unknown parameters. Several approaches may be used to complete this procedure. Different methods for discretizing the time-space region and for deriving the discretized equations may be used for. Finite Difference Methods (FDM), Finite Element Method (FEM), Boundary Element Methods (BEM), and their variant and hybrids have been extensively applied in ground water modelling during the past two decades. In petroleum industry and hydrology, finite difference methods are used almost universally. The most well-known version is based on gridblock-centred differences and involves gridblock centres and interfaces between adjacent gridblocks (Sun, 1994).

2.2.3. History matching

Conditioning a reservoir to dynamic data, *i.e.*, production data well pressures, water cuts, etc, is called history matching or calibration process which aims at reproducing the flow transfers within the reservoir. This is a nonlinear problem, which may be solved using linearization or optimization (Le Ravalec, 2005). The linearization approach was often preferred in hydrogeology. In the small perturbation method, random variables (permeability, fluid velocity and pressure) are split into two terms: an average term and a perturbation term. Kriging techniques could then be used to incorporate field-measured data. The small perturbation method was suitable for permeability fields that are not too heterogeneous: the variance of the logarithm of permeability is assumed to be much smaller than one.

Nowadays, optimization techniques are preferred, mainly because we have to deal with complex geological environments. The optimization problem requires the definition of an objective function, also called a cost function. This objective function depends on unknown parameters and measurements and expresses the discrepancy between the model of reservoir and the real object. The purpose of optimization is to minimize the objective function by tuning the unknown parameters. The main difficulty lies in the definition of a proper objective function and how to quantify the mismatch between reservoir model and the actual model. Inverse problem theory provides a general framework for incorporating prior information into an objective function (Tarantola, 1987). This theory was developed from Bayes' works. It is therefore often referred to as Bayesian theory.

2.2.3.1. Objective function and formalism

As stated above, the objective function defines the matching criterion and measures the mismatch between the numerical simulation results and the production data. This objective function is minimized by using an optimization algorithm to improve the matching of the production data. The implemented objective function provides a flexible formulation, allowing different terms to be accounted for according to the optimization problem: "weighted" measurements, use of a priori model and inequality constraints. The formulation proposed is based on the Bayesian formalism and allows for a probabilistic interpretation of the matching criterion.

2.2.3.2. Objective function definition

The principle of Bayesian inversion applied to numerical simulation is to modify an initial geological model by constraining it to dynamic data. The goal is to improve the model characterization and reduce uncertainties by integrating static and dynamic data.

The definition of the objective function corresponds to the search for a maximum *a posteriori* probability. Therefore, the criterion to minimize is:

$$F(\theta) = \frac{1}{2} (o - \omega(\theta, t))^T C_o^{-1} (o - \omega(\theta, t)) + \frac{1}{2} (\mu_\theta - \theta)^T C_\theta^{-1} (\mu_\theta - \theta) \quad (2-2)$$
$$F(\theta) = F_o(\theta) + F_a(\theta)$$

o production data

$\omega(\theta, t)$ numerical simulation results

C_o covariance operator

θ a realization of Θ the parameters of the model (“*a priori*” model)

C_θ *a priori* covariance operator

μ_θ *a priori* mean values

The first term, $F_o(\theta)$ quantifies the mismatch between the simulation results, $\omega(\theta, t)$, and the production data o . Therefore, minimizing this term corresponds to the best match of the measurements. The second term, $F_a(\theta)$, includes the “*a priori*” parameter knowledge, through the minimization of the difference between the parameters θ and their *a priori* means μ_θ .

2.2.4. Optimization methods

In the inversion loop, the available optimization algorithms are based on the gradient method (Anterion *et al*, 1989, Bissel, 1994, Roggero and Guérillot, 1996), which significantly increases the inversion performances. Therefore, gradients directly provide a descent direction after each simulation. A numerical approximation of the gradients is computed using a perturbation method if an analytical gradient method is not available in the numerical simulator.

Several optimization algorithms exist in the literature (Chavent *et al.*, 1973, Dennis and Schnabel, 1983, Fletcher, 1987). The methods that are often used in hydrology and petroleum engineering are the Powell (or dog-leg method) method, the Levenberg-Marquardt method, the Gauss-Newton method, the Steepest Descent method and the BFGS method. In our approach, the optimization algorithm will be selected according to the case difficulty, among the methods described below.

2.2.4.1. The steepest-descent method

The basic gradient method is steepest-descent method. The simplest optimization method is the successive descent or ‘steepest descent’ algorithm. This algorithm is based on search for an optimal step in the opposite direction of the objective function gradient. It implies following the ‘line of steepest slope’ on the surface formed by the objective function. In matrix form, the objective function gradient is expressed as:

$$\left[\frac{\partial F}{\partial \theta} \right] = -J^T C_o^{-1} (o - \omega) - C_\theta^{-1} (\mu_\theta - \theta) \quad (2-3)$$

where:

J : Jacobian matrix $\left[\frac{\partial \omega}{\partial \theta} \right]$ (simulation result gradients with respect to the parameters)

The steepest-descent method is well known for its numerical robustness. The convergence of the iterative process is ensured with sufficiently small steps. Therefore, this method is well suited for solving highly non-linear problems or when the initial parameter values are far from the solution. The main drawback of the method is an important performance degradation during the inversion process: the convergence rate of the algorithm significantly decreases near the solution (Roggero and Hu, 1998).

2.2.4.2. The Gauss-Newton method

The Gauss-Newton optimization method is especially designed for minimizing an objective function that has the form of a sum of square differences. This method is commonly used to solve minimization problems. The convergence rate is theoretically quadratic. In general, this method has a better performance than the steepest descent method.

The Gauss-Newton method is obtained with a second-order linearized approximate of the objective function F . This linearized expression Fl can be written in the following form:

$$Fl(\theta + d\theta) = F(\theta) + \left[\frac{\partial F}{\partial \theta} \right] d\theta + \frac{1}{2} d\theta^T \left[\frac{\partial^2 F}{\partial \theta^2} \right] d\theta + O(d\theta^3) \quad (2-4)$$

where:

$d\theta$ is a small variation of the θ parameters vector,

$$\left[\frac{\partial F}{\partial \theta} \right] = -J^T C_o^{-1} (o - \omega) - C_\theta^{-1} (\mu_\theta - \theta) \text{ is the gradient of } F,$$

$$\left[\frac{\partial^2 F}{\partial \theta^2} \right] = J^T C_o^{-1} J - \left[\frac{\partial J}{\partial \theta} \right]^T C_o^{-1} (o - \omega) + C_\theta^{-1} \text{ is the Hessian matrix.}$$

By applying the first order optimality condition to the quadratic approximation of F (Equation 2-4), and by ignoring the third order errors $O(d\theta^3)$, one obtains:

$$\left[\frac{\partial Fl}{\partial \theta} \right] = 0 \quad \text{Thus:} \quad \left[\frac{\partial F}{\partial \theta} \right] + \left[\frac{\partial^2 F}{\partial \theta^2} \right] d\theta = 0$$

The optimal variation δ of θ , which minimizes Fl , is therefore obtained by solving the following linear system:

$$\delta = - \left[\frac{\partial^2 F}{\partial \theta^2} \right]^{-1} \times \left[\frac{\partial F}{\partial \theta} \right] \quad (2-5)$$

Note that the calculation of the Hessian matrix implies, in theory, the calculation of the second order derivatives of the model with respect to the parameters, which form the matrix $[\partial J / \partial \theta]$. These second order derivatives are in general very complex to evaluate. In practice, these terms are often neglected and the gradients are considered constant with respect to the parameters. The algorithm obtained with this assumption is called Gauss-Newton algorithm. Note that neglecting the

second order derivatives is totally licit in the neighbourhood of the optimum, when the norm of the error vector $(o - \omega)$ becomes small.

The Gauss-Newton algorithm is obtained through iterative update of the parameters. At each iteration, an improved estimation of the parameters is computed .

The Gauss-Newton algorithm requires the inversion of the Hessian matrix (more exactly its approximation in the form $J^T C_o^{-1} J$) at each iteration. The Gauss-Newton algorithm is highly efficient in most cases, and allows a quadratic convergence rate to be approached. Unfortunately the method can become unreliable when dealing with a highly non-linear problem or when the initial parameters are too far from the optimal solution. When the case occurs, more sophisticated methods can be implemented. A regularization term can be introduced to avoid the problems associated with singular matrix, which leads to, for example, the Levenberg- Marquardt method. An attempt can be made to combine a descent method with the Gauss Newton method, using the Powell “Dog-Leg” algorithm.

2.2.4.3. The Levenberg-Marquardt method

The method proposed by Levenberg and Marquardt (Marquardt, 1963) is an extension of the Gauss-Newton method. A regularization term is introduced on the diagonal elements of the Hessian matrix in order to obtain a better numerical stability and to avoid the quasi-singular matrix problems. Taking the Gauss-Newton algorithm as a starting point, the following iterative scheme is obtained:

- $d\theta = -\left\{\left[\frac{\partial^2 F}{\partial \theta^2}\right] + \mu I\right\}^{-1} \times \left[\frac{\partial F}{\partial \theta}\right]^n$
- Updating the parameters: $\theta^{n+1} = \theta^n + d\theta$

I being the identity matrix and μ a real positive coefficient

The Marquardt parameter, μ , must be adjusted judiciously during the iterations. Note that the Gauss-Newton method is found for $\mu = 0$. For high values of μ , the solution $d\theta$ tends towards $-1/\mu [\partial F / \partial \theta]$ and therefore has certain similarities with a descent method.

The following method is commonly used to control the Marquardt parameter: when the convergence rate reaches a given criterion (sufficient decrease of the objective function), μ is diminished. Otherwise, a larger value is used which decreases the norm of $d\theta$ and draws it closer to the descent direction.

The Levenberg-Marquardt method has a better numerical behavior for initial parameter values far from the optimum. During iterations, the parameter μ tends to diminish which allows high performances of the Gauss-Newton method to be obtained in the neighborhood of the solution. The main difficulty lies in updating the Marquardt parameter which is often based on more or less empirical criteria.

2.2.4.4. The Powell “Dog-Leg” Method

The Powell “Dog-Leg” method is used as an efficient combination of the advantages of the steepest descent method which is presumed to be stable and robust far from the solution, and the Gauss-Newton method which offers rapid convergence in the neighborhood of the solution (Roggero and Hu, 1998). This method is therefore an improvement of the Levenberg-Marquardt algorithm, based on an interpolation between the steepest descent solution γ and the Gauss-Newton solution.

A trust region, centred in θ and delimited by a norm, ρ , of maximal variation of the parameters, is introduced to control the algorithm. At each iteration, the steepest descent solution γ and the Gauss-Newton solution δ are calculated. These two solutions are compared with the trust region to propose an optimal combination τ using the following scheme:

If the Gauss-Newton solution is inside the trust region, *i.e.*, if $\|\delta\| \leq \rho$, the Gauss-Newton solution is retained:

$$\tau = \delta$$

If the two solutions are outside of the trust region, *i.e.*, if $\|\delta\| > \rho$ and $\|\gamma\| > \rho$, the direction of the steepest descent method, which is reputedly more robust, is used. The solution is renormed to reach the boundary of the confidence region, hence :

$$\tau = \frac{\rho\gamma}{\|\gamma\|}$$

When the Gauss-Newton solution is outside the trust region and the steepest descent solution is inside, *i.e.*, if $\|\delta\| > \rho$ and $\|\gamma\| \leq \rho$, an interpolation is made between these two solutions to reach the boundary of the domain (Figure 2.2)

$$\tau = \alpha \times \gamma + (1 - \alpha) \times \delta$$

α being determined by the relation $\|\tau\| = \rho$

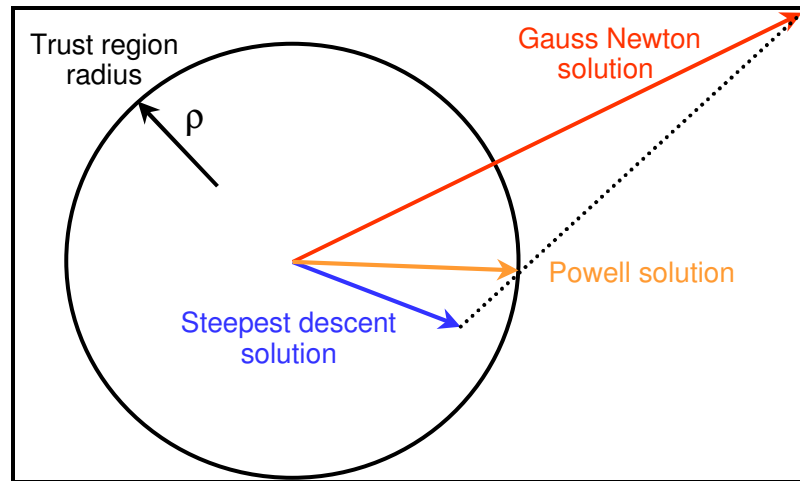


Figure 2.2: The Powell method and the trust region technique (Fornel, 2006).

A schematic representation of this method is given in Figure 2.2. The advantage of the trust region is to adopt a criterion based on a physical understanding of the mechanisms and processes involved. The norm of the maximal variation of the parameters is continually controlled, and the choice combining robustness and efficiency is automatically made.

The extent of the trust region is adjusted during iterations. An upper limit from the data can be prescribed. The radius ρ is increased to this limit or decreased using a linearity criterion of the objective function: the objective function variation forecast by linearization is compared to the variation really obtained. A ratio close to unity indicates a good numerical behaviour and allows a

widening of the trust region. Conversely, a low value of the criterion or an iteration failure results in a smaller radius ρ .

The Powell “Dog-Leg” algorithm can be explained according to the following steps:

- Compute the objective function gradient $G = \left[\frac{\partial F}{\partial \theta} \right]^n$
- Compute the Hessian matrix $H = \left[\frac{\partial^2 F}{\partial \theta^2} \right]^n$
- Compute the Gauss-Newton solution $\delta = -H^{-1} \times G$
- Compute the steepest-descent solution $\gamma = -\mu \times G$
- Test the norms δ and γ with respect to ρ
- Compute the interpolation parameter α
- Compute the new direction: $\tau = \alpha \times \gamma + (1 - \alpha) \times \delta$
- Update the parameters: $\theta^{n+1} = \theta^n + \tau$
- Compute the new numerical simulation $\omega(\theta^{n+1}, t)$ and the gradients
- Update the trust region radius ρ

2.2.5. Parameterization techniques

The early approaches placed the emphasis on providing a good fit only between the simulated and measured dynamic data. Basically, a reservoir model is proposed as the initial estimate and then fluid flow is simulated to mimic production data. In the reservoir model the petrophysical parameters (porosity and permeability) are attributed to the grids while honouring the spatial variability and the static data collected on certain points. For a heterogeneous medium there is a priori as many parameters as the number of cells in the grid multiplied by the number of reservoir properties influencing flow. Of course, it is needed to resort on parameterization (especially here those based on geostatistics) to reduce the number of freedom degrees of the inverse problem.

The geostatistical parameterization techniques reduce the number of parameters. In addition, they ensure that spatial variability is preserved so that the prior constraint can be frequently removed from the objective function. The principal parameterization techniques are the pilot point method (de Marsily, 1978, de Marsily *et al.*, 1984), the gradual deformation (Hu, 2000) and the gradual pilot point method (Le Ravalec and Hu, 2007). An alternative very similar to the gradual deformation method is the probability perturbation method (Caers, 2003).

2.2.5.1. The gradual deformation method

The gradual deformation method is a geostatistical parameterization technique that enables to deform the distribution of facies or parameters. This technique was firstly introduced and implemented by Hu (2000) to continuously modify a gaussian random function. It allows a geostatistical model to be perturbed from a small set of parameters, independently of the number of gridblocks it contains. It speeds up the model calibration to dynamic data while preserving the spatial variability of the model. This method is based on the fact that the sum of two Gaussian random functions is also a Gaussian random function.

Let $Y(x)(x \in D)$ be a stationary (multi-)Gaussian random function of order 2 defined over the field D and assume that $Y(x)$ has a zero mean and unity variance. The random function $Z(x)$ ($x \in D$) is defined as a nondecreasing transformation of $Y(x)$:

$$Z(x) = F^{-1}\{G[Y(x)]\} \quad (2-6)$$

where G is the standard gaussian distribution function and F the distribution function of $Z(x)$. We use $Z(x)$ to model a physical property defined over D . The covariance of $Y(x)$ is determined by $Z(x)$, and the simulation of $Z(x)$ turns out to be that of $Y(x)$. In the following, $Y(x)$ and $Z(x)$ will be simply denoted by Y and Z , respectively. Y and Z may represent a random function in field D or a random vector corresponding to a grid discretizing over D .

Now let $Y(t)$ be a stochastic process whose space of definition is the ensemble of realization of the spatial random function Y . For each t , $Y(t)$ is a Gaussian random function defined over D . In general, the parameter t of the random function $Y(t)$ does not have any physical meaning. Yet, its introduction in the stochastic model allows us to create a dependent transition from one realization to other.

There are many ways of building a spatiotemporal random function $Y(t)$. A convenient way of building a spatiotemporal random function $Y(t)$ consists in combining two independent standard Gaussian random functions Y_1 and Y_2 with identical covariance:

$$Y(t) = Y_1 \cos t + Y_2 \sin t \quad (2-7)$$

It is straightforward that, for each t , $Y(t)$ has zero mean and unit variance since Y_1 and Y_2 obey the same properties and that $Y(t)$ shares the covariances of Y_1 and Y_2 due to their independence. The $\cos t$ and $\sin t$ are simply variance normalization coefficients. Furthermore, for each t , $Y(t)$ is a gaussian random function because it is a linear combination of Gaussian random functions. Given two independent realization y_1 and y_2 of Y_1 and Y_2 , we get a continuous chain of realization $y(t)$:

$$y(t) = y_1 \cos t + y_2 \sin t \quad (2-8)$$

Hence by applying transformation (2-6), we obtain a continuous chain of realization $z(t)$ of random function Z . The basic idea of this method is to calibrate $z(t)$ to nonlinear data by tuning the parameter t .

As stated before, the calibration of a stochastic model to nonlinear data can be formulated as an optimization problem. Let $o^{obs} = (o_1^{obs}, o_2^{obs}, \dots, o_p^{obs})$ be the vector of nonlinear data observed in the physical field and the corresponding vector of the responses of the stochastic model Z . For a given realization a of Z , the value w_1, w_2, \dots, w_p are often obtained through numerical simulation. We define the objective function F as the sum of the weighted quadratic errors between the model simulations and equivalent observed data:

$$F = \frac{1}{2} \sum_{i=1}^p c_i (w_i - o_i^{obs})^2 \quad (2-9)$$

Denote by N the number of components of the vector z . N is often a huge number ($10^4 - 10^7$). Therefore it is highly tedious to optimize the objective function by handling directly the whole vector z . Moreover, in the frame of stochastic optimization, the vector z cannot be arbitrary and it must be a realization of the stochastic model Z .

In order to overcome theses difficulties, it is convenient to transform Z to a Gaussian random function Y and then to apply the gradual deformation algorithm on Y . Starting with an initial realization y_0 of Y and another realization u_1 of Y independent of y_0 , we build a continuous chain of realization $y_1(t)$ by using Equation (2-8) while mixing y_0 and u_1 . Then we minimize the objective function with respect to t . In this way, the N -dimensional optimization problem is reduced to a one-dimensional problem, and moreover, the optimized vector $y_1(t_{opt})$ is actually a realization of Y .

However the above optimization may not reduce sufficiently the value of the objective function. It is then necessary to repeat the above procedure with a new realization chain $y_2(t)$ built by combining $y_1(t_{opt})$ and another independent realization chain built u_2 of Y . More generally, the following iterative optimization procedure can be used. At iteration n , the continuous chain of realization $y_n(t)$, is written:

$$y_n(t) = y_{n-1} \cos t + u_n \sin t \quad (2-10)$$

where $y_{n-1}(t)$ is the optimized realization at iteration $n-1$, and where u_n ($n = 1, 2, \dots$) are a series of independent realizations of Y . Then by minimizing the objective function with respect to parameter t , we get a new realization $y_n(t_{opt})$ that improves (or at least maintains) the calibration to nonlinear data. This iterative procedure is stopped when a satisfactory calibration is reached. Figure 2.3 shows the schematic representation of such a search process. We note that, at each iteration, the objective function F depends only on parameter t . Therefore we deal always with a one-dimensional optimization problem. Note also that, due to the mutual independence of u_n ($n=1, 2, \dots$), the solution space can be explored when n becomes large enough and therefore the procedure converges always to a global minimum (*i.e.* a calibrated realization) (Hu, 2000).

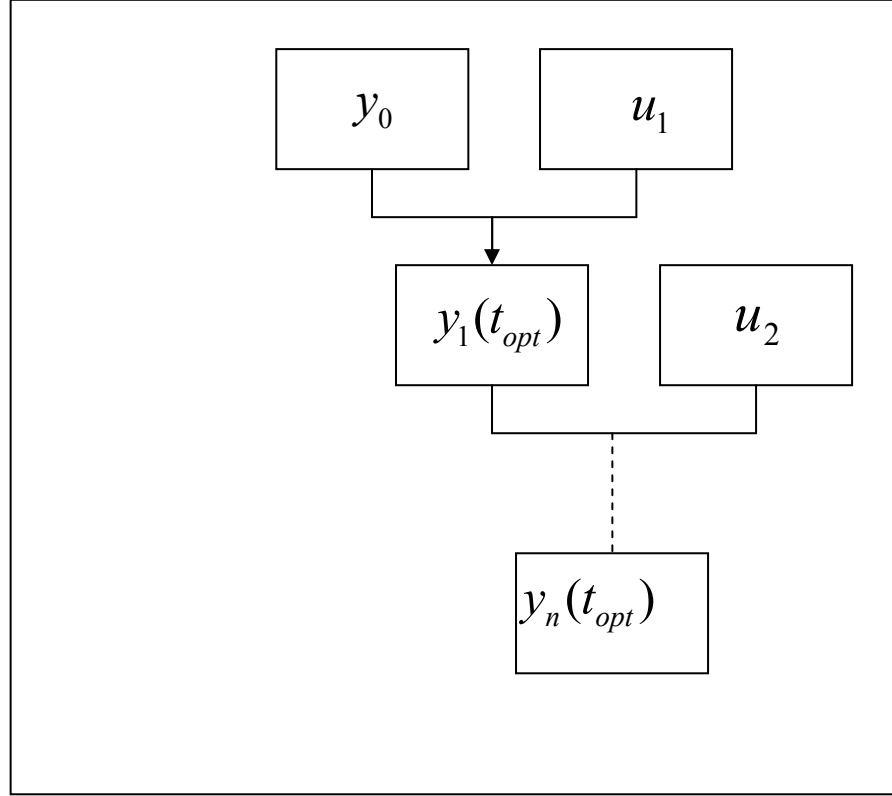


Figure 2.3: Iterative search process involving the gradual deformation of two realizations (one parameter of gradual deformation).

2.2.5.2. Multidimensional gradual deformation

The gradual deformation has been presented as the gradual deformation of two gaussian random functions y_1 and y_2 . The principle of combining random functions was actually extended to any number of gaussian realizations.

Assuming $Y(x)$ is a random gaussian function in the domain D , the multi-dimensional gradual deformation method consists in the construction of a new realization of Y , y , as a linear combination of $N+1$ realizations of Y , y_i , which are independent but have the same covariance γ :

$$y(\rho) = \sum_{i=0}^N \rho_i y_i \quad \text{where } \rho = (\rho_0, \rho_1, \dots, \rho_N)$$

A normality constraint is added to preserve the variance of the random gaussian function:

$$\sum_{i=0}^N \rho_i^2 = 1$$

The new realization of Y can then be presented as the function of N independent gradual deformation parameters, t_1, \dots, t_N :

$$y(t_1, t_2, \dots, t_N) = \prod_{i=1}^N \cos(t_i) y_0 + \sum_{i=1}^{N-1} \sin(t_i) \prod_{j=i+1}^N \cos(t_j) y_i + \sin(t_N) y_N \quad (2-11)$$

Using this equation we solve an optimization problem of N parameters, $t = (t_1, t_2, \dots, t_N)$ to obtain a new realization (Figure 2.4 shows an example of gradual deformation of 4 realizations) that improves the calibration to measured data. That optimization constitutes one step of a whole multi-step optimization process. Actually, if the objective function value resulting from an optimization step is not small enough, a new step is re-initialized with new independent realizations that are combined with the optimal realization of the previous step (Roggero and Hu, 1998, Hu, 2000).

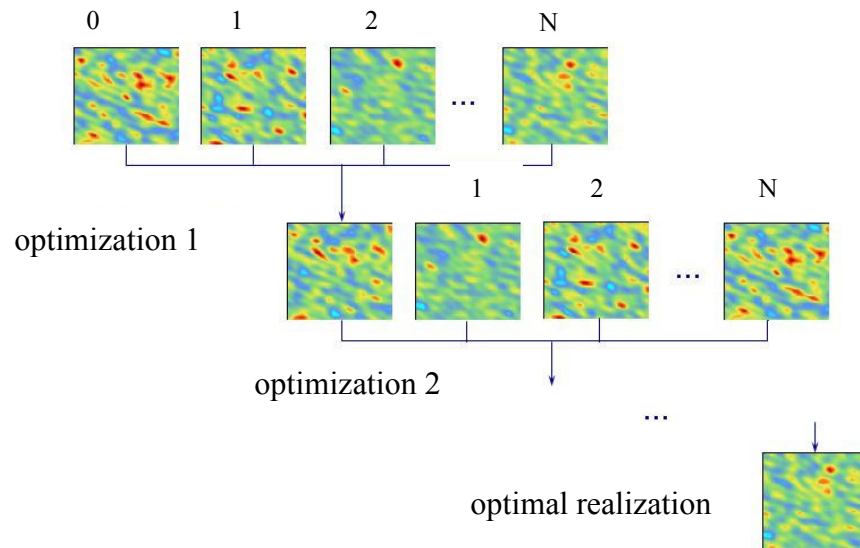


Figure 2.4: Iterative search process involving the gradual deformation of $N+1$ realizations (Fornel, 2006).

2.2.5.3. Gradual deformation with respect to structural parameters

Most stochastic simulation algorithms require at least the specification of the covariance before generating the realization. In order to deform a realization while modifying simultaneously its structural parameters, it is necessary to use an algorithm that separates the generation of random numbers and the imposition of a structure.

Denote by X a standard Gaussian white noise and L the covariance operator, then

$$Y = L[X]$$

is a Gaussian field with imposed covariance. In this form, it is clear that we can gradually deform the Gaussian white noise X by using the above method and modify at the same time the covariance function, as follow:

$$Y(t) = L[X(t)] = L[U \cos t + V \sin t] \quad (2-12)$$

where U and V are two independent standard Gaussian white noises. The covariance operator L is generally made to vary according to factual information which cannot be directly included in the objective function.

There exists several simulation algorithms that separate the generation of random numbers and the imposition of a covariance function. The method based on LU decomposition of the covariance matrix is such a method.

2.2.5.4. Local gradual deformation

When observations are scattered in over different sub-areas of the studied field, calibration using a global deformation may be ineffective, because improving the match in one zone may deteriorate the match in another zone. This limitation can be overcome through the use of a local gradual deformation method (Hu, 2000). Considering a partition of the field into m zones, let X be a Gaussian white noise in the whole field and X_1, X_2, \dots, X_m the partition of X in the m zones. As the X_i are mutually independent, it is then possible to perform their gradual deformation individually. By applying the covariance operator L on these independent white noises, we obtain a consistent correlated Y function:

$$Y(t) = L(X(t)) = L \begin{bmatrix} X_1(t_1) \\ X_2(t_2) \\ \vdots \\ X_m(t_m) \end{bmatrix} = L \begin{bmatrix} U_1 \cos(t_1) + V_1 \sin(t_1) \\ U_2 \cos(t_2) + V_2 \sin(t_2) \\ \vdots \\ U_m \cos(t_m) + V_m \sin(t_m) \end{bmatrix} \quad (2-13)$$

where X_i , $i=1,2,\dots,m$, are mutually independent Gaussian white noises, and $t=(t_1,t_2,\dots,t_m)$, the deformation parameters, with one parameter per zone. For a given set of realizations of U_i and V_i in zone i , we solve an optimization problem with m parameters t_1,t_2,\dots,t_m to obtain a new set of realizations that improves the calibration. Again, this procedure is iterated until a satisfactory calibration is reached in each deformed zone i .

2.3. Workflow tools and methodologies

2.3.1. Geostatistical modelling using HERESIM methodology

HERESIM 3D is an integrated model for computer-aided reservoir description and is designed to help sedimentologists, geostatisticians, reservoir geologists and reservoir engineers to work together. This interactive and graphic software, dedicated particularly to **HE**terogeneities of **RE**servoirs **SIM**ulations, establishes the link between core and log analysis and fluid flow modeling. Stochastic methods are used to generate lithology, porosity and permeability over high resolution grids.

HERESIM Methodology

Truncated Gaussian Models as described previously are used through the HERESIM Group (CG/IFP) in order to describe reservoirs. In this methodology, lithofacies are defined by truncating a Gaussian Random Function. The main interest of such a model is that firstly it ensures a consistent model for both variograms and cross-variograms of indicators describing lithofacies. Secondly the flexibility of this method makes it possible to constrain simulations by geological features such as the evolution of lithofacies proportions in space. Thirdly the current implementation in the software HERESIM 3D is very fast, thus allowing the simulation of huge grids on workstations (Le Loc'h *et al*, 1994).

The truncated Gaussian simulation method in HERESIM may be summarized in three main steps:

- A Computation of 3D lithofacies proportions from well data (or from seismic data)
- B Simulation of Gaussian field of values using the variogram model fitted on the experimental indicator variogram

C Truncation of Gaussian field with thresholds computed from 3D proportions to obtain the facies data

The data available to compute the 3D distribution of facies proportions are the *1D* well data, which provide a very detailed vertical distribution of facies. From these well data, a vertical proportion curve (VPC, see Figure 2.5) is generally computed, which represents the global vertical sequence of facies, in the depositional situation (using a chronostratigraphic marker as reference level and correlation surface). This VPC gives the global proportions of facies at each level, which will be reproduced in the simulation. In a non-stationary case, in case of lateral changes of facies in the unit for example, a 3D Grid of proportions is computed. This 3D grid represents the 3D distribution of proportions of geological facies in the studied area. In practice, each cell of this 3D grid is informed with the local proportion of facies (Doligez *et al*, 2007).

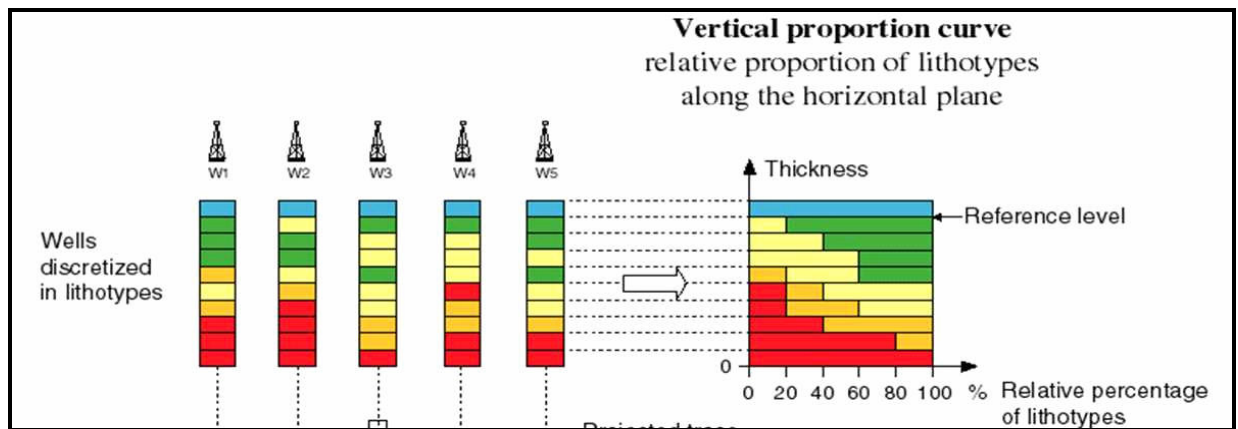


Figure 2.5: Vertical proportion curve computed from the well data (Doligez *et al*, 2007).

The simulation of the underlying Gaussian field needs a variogram model $\rho(h)$ which is obtained from experimental variograms (horizontal and vertical) of facies indicator functions computed from well data. Finally, the spatial distribution of facies is the result of the truncation of Gaussian field simulated using $\rho(h)$, with threshold t_i computed from the previous 3D proportions. The thresholds define a partition of random values into different classes associated with the geological facies.

2.3.2. Flow modelling using SIMTESTW simulator

The SIMTESTW well test numerical simulation program, developed by IFP (Blanc, 1995; Rahon *et al.*, 1996), is used with a conventional finite-difference method. In that code, the pressure behaviour

of a single-phase flow in a 3D reservoir model is formulated by using the well-known conventional equation:

$$\frac{\partial}{\partial x_i} \left(\frac{k}{\mu} \frac{\partial (P + \rho g z)}{\partial x_i} \right) = \phi c_t \frac{\partial P}{\partial t} + q \quad (2-14)$$

where P is the pressure, i is the axis index, x_i are coordinates (x_1, x_2, x_3 , stand respectively for x, y, z), k is the permeability (k_i for a directional permeability), μ is the fluid viscosity, ρ is the fluid density, g is the gravity, ϕ is the porosity, c_t is the total rock-fluid compressibility and q is the production term. This simulator uses a 7-point finite-difference scheme to solve Equation 2-14. Either a single-medium approach or a dual-medium approach can be handled by the software.

2.3.3. Petrophysical inversion using WELGEM methodology

The general purpose of the WELGEM Software is to integrate Well Tests (or more generally Pressure Transients) in the reservoir characterization process. WELGEM allows the inversion of these tests and attempts to determine reservoir and well properties that best fit these tests. WELGEM is based on several underlying assumptions.

2.3.3.1. Implementation with WELGEM software

The main function of the inversion in WELGEM software is to constrain an initial simulation model to dynamic production data with an automatic iterative process. Coupling this inversion process with a numerical fluid flow simulator allows reservoir engineers to calibrate flow models of geologically-complex reservoirs.

The principal data of the optimization loop concern the definition of the initial model and its set of parameters, the prior constraints, the dynamic production data and numerical setting-data. The inversion parameters are typically petrophysical properties (permeability / porosity), fault transmissivity multipliers, well productivity indices, or any kind of reservoir model data usually involved in a classical history matching process.

For example, consider a well test with pressure data, P_o , derivative data, D_o , and two inversion parameters: the reservoir permeability, K , and reservoir porosity Φ . In the absence of *a priori* term, the objective function is:

$$F(K, \Phi) = \frac{1}{2} \sum_{i=1}^{n_o} \left(\frac{P_o^i - P_s(K, \Phi, t^i)}{\sigma_p^i} \right)^2 + \frac{1}{2} \sum_{i=1}^{n_o} \left(\frac{D_o^i - D_s(K, \Phi, t^i)}{\sigma_D^i} \right)^2 \quad (2-15)$$

where:

σ_p^i : standard deviation of the pressure error $(P_o^i - P_s(K, \Phi, t^i))$ at time t^i

σ_D^i : standard deviation of the derivative error $(D_o^i - D_s(K, \Phi, t^i))$ at time t^i

The decrease in the objective function is verified after each simulation. A numerical criterion, constructed by comparing the effective objective function variation with the variation expected by linearization, allows the parameter modifications to be controlled during the iterations.

2.3.3.2. Numerical gradient computation

Among the authors pioneering the techniques to calculate gradients in numerical models, Antérion *et al.* (1989) focused on methods to fit dynamic data. The principle of the method involves calculating the derivative of the flow model equations with respect to the petrophysical parameters that are made to vary.

The WELGEM optimization algorithms are based on the gradient method (Blanc *et al.*, 1996). The gradients are the derivatives of the numerical simulation results with respect to the parameters. The gradient method is implemented in the SIMTESTW numerical simulator, for a limited list of parameters (typically permeability, porosity, fault transmissivity, etc.). In that case, the numerical simulator directly provides analytical gradients to the inversion loop. Otherwise, a numerical approximation of the gradients is computed within the inversion loop by a perturbation method. The numerical approximation of the gradients is computed with a sequential updating technique. This method requires additional numerical simulations in order to initialize the gradient values. These additional simulations correspond to successive perturbations of the model parameters in the vicinity of the initial guess. Moreover, this perturbation process is repeated to update the gradient approximation in case of iteration failure (one iteration is rejected when the objective function increases).

The path of optimization in the parameter space followed by the optimizer and perturbations with additional simulations to compute the gradients is presented in Figure 2.6, for a synthetic example with 2 parameters.

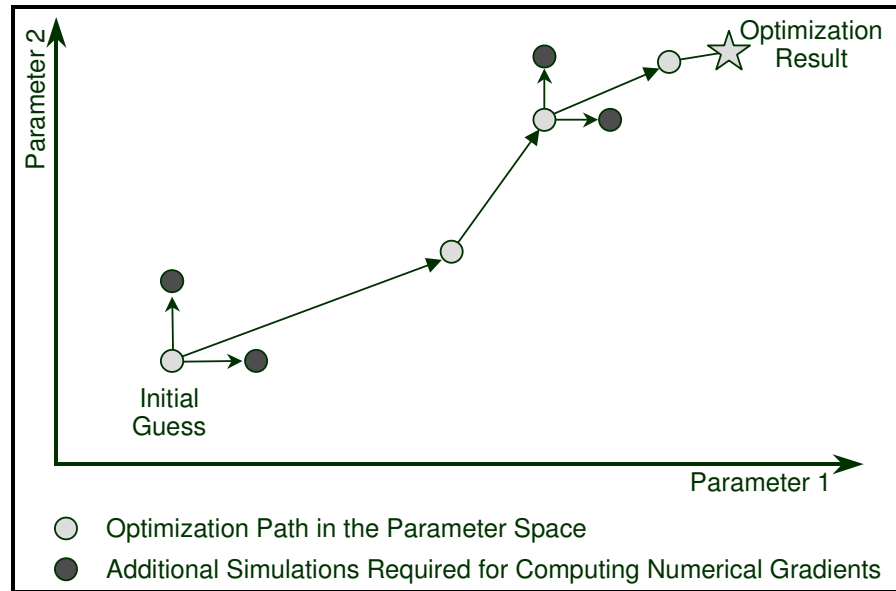


Figure 2.6: Optimization path with numerical gradient computation.

2.3.4. Gradual deformation using CONDOR software package

The general purpose of the CONDOR Software is to constrain reservoir models to fulfil production data. The CONDOR approach is based on an optimization algorithm that derives the modification of reservoir model parameters iteratively in order to minimize an objective function. The easy coupling with any kind of numerical fluid flow simulator allows to select usual reservoir parameters to help history matching. In addition, various parameterization techniques like the gradual deformation and the pilot point methods are implemented in CONDOR to constrain geostatistical models to production data.

The CONDOR Software can manage the forward simulation workflow including the geostatistical simulation of a geological model, the upscaling of that model and fluid flow simulation on the upscaled reservoir model.

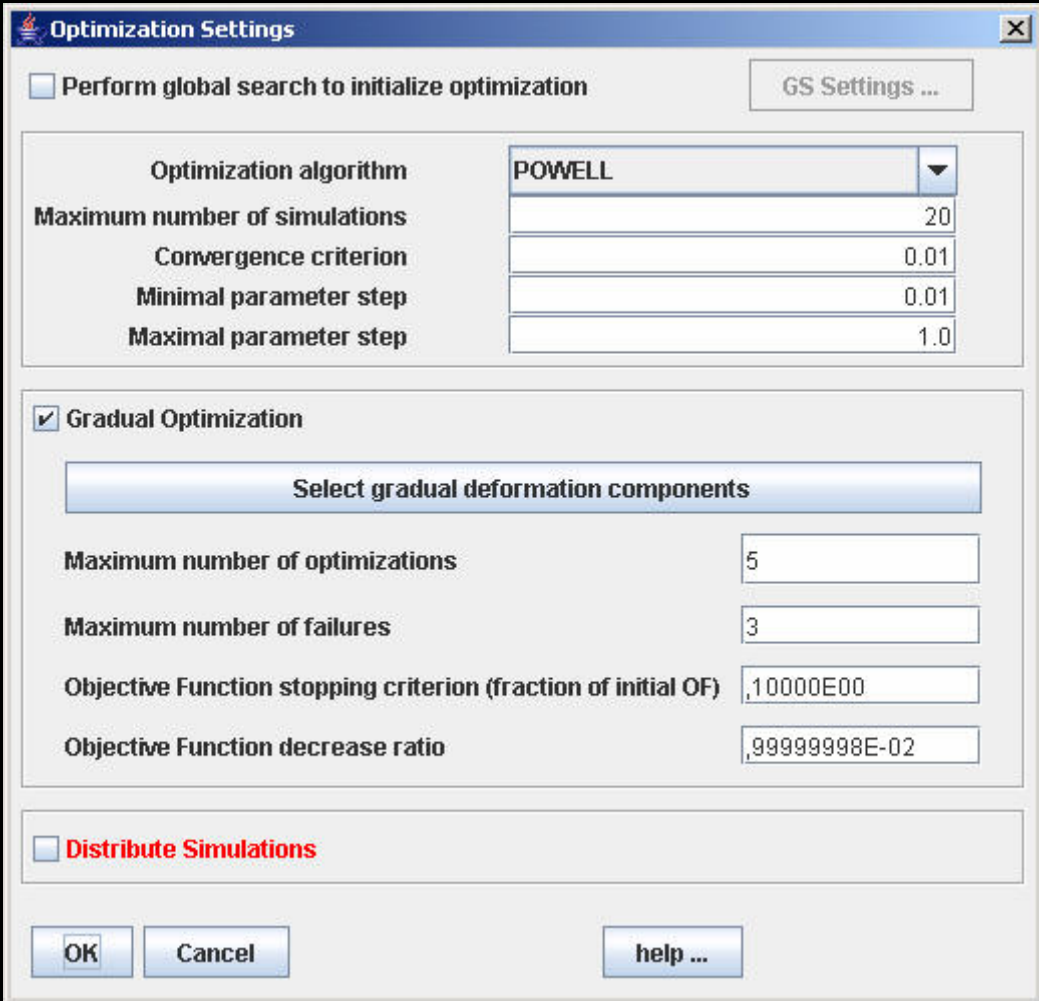
2.3.4.1. Optimization Settings in CONDOR

The following optimization algorithms are available in CONDOR: Powell (or dog-leg method), Levenberg-Marquardt, Gauss-Newton, Steepest Descent, BFGS.

The CONDOR optimization setting editor is illustrated in Figure 2.7. The convergence criterion is a floating point value that determines whether or not the optimization algorithm has converged. For each iteration, a change in the objective function is calculated with respect to the previous iteration (ΔF). This value is then divided by the current value of the objective function (F). If the quantity $\Delta F / F$ is less than the convergence criterion value, the optimization is judged to have converged to a parameter solution and will stop. The minimal parameter step indicates the minimum change in the inversion parameters that is allowed. The maximum parameter step defines the maximum variation allowed to each convergence iteration for the inverted parameters.

In the case of a gradual deformation, the whole process is a sequence of optimizations, the parameters defining each optimization being those introduced above. Each optimization allows for investigating a chain of realizations. The maximal number of optimizations is prescribed (see Figure 2.7, bottom). Some optimizations can lead to a zero improvement of the matching to the data. The objective function stopping criterion is a positive number less than 1, stating that the optimization will stop provided that the ratio between the current value of the objective function and its initial value is less than stopping criterion. The objective function decrease ratio is the same as the convergence criterion described above, but it is now related to a sequence of optimizations instead of a single optimization. If the objective function does not decrease during an optimization, a new optimization can be performed. The maximum number of such restarts is given by the 'Maximum number of failures'.

To close this chapter, a flow chart in Figure 2.8 sums up the main steps of a gradual deformation-based optimization including the main features depicted above.



Optimization Settings

☐ Perform global search to initialize optimization GS Settings ...

Optimization algorithm	POWELL
Maximum number of simulations	20
Convergence criterion	0.01
Minimal parameter step	0.01
Maximal parameter step	1.0

☒ Gradual Optimization

Select gradual deformation components

Maximum number of optimizations	5
Maximum number of failures	3
Objective Function stopping criterion (fraction of initial OF)	,10000E00
Objective Function decrease ratio	,99999998E-02

☐ Distribute Simulations

OK Cancel help ...

Figure 2.7: The optimization settings window. The optimization algorithm and important control parameters for the optimization are selected from this window.

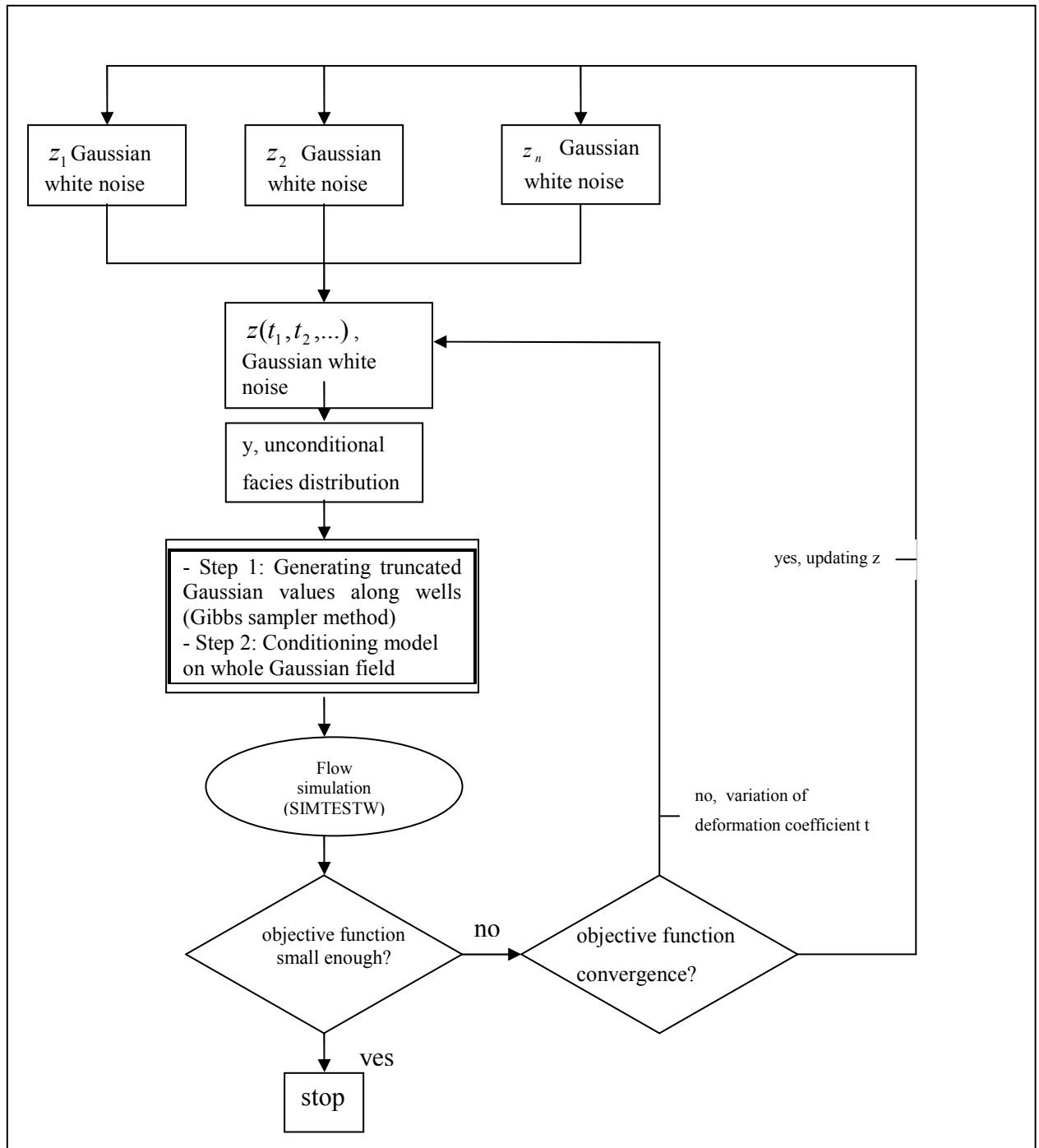


Figure 2.8: Flow chart summing up the main steps of a gradual deformation-based optimization including the main features depicted in this chapter.

CHAPTER 3. Preliminary studies and Geostatistical modelling of the Site

3.1. Introduction

In this chapter as a very preliminary analysis, we estimate an average reservoir permeability from each response of wells to pumping. The idea is to assess the spatial variability of permeability over the Site, considering the aquifer as homogeneous and infinite. As discussed earlier, the drilling records and specific well logs were acquired in most wells, including in particular flowmeter profiles and wellbore images. Moreover the cored samples obtained from cored well C1 and well C2 allow to calculate the petrophysical property of different facies. This valuable information is used to generate the geostatistical model described in this chapter. This model is assumed to be the initial support of a flow model used later for the purpose of inversion based on dynamic data.

3.1.1. Preliminary pumping data analysis

Assuming a steady state radial flow in an homogeneous infinite medium that is fed from infinite distance, the Darcy law gives us a relationship between the flow rate and the imposed pressure gradient as follows:

$$\frac{Q}{A} = \frac{K}{\mu} \cdot \frac{dp}{dr} \quad (3-1)$$

where Q is the pumping rate, A is the flow section, r is the observation distance from the well, K is the permeability, μ is the fluid viscosity and dP/dr is the pressure gradient. Expressing the flow cross-section and pressure gradient versus the drawdown at a distance r from wellbore, Equation 3-1 can be rewritten as follow:

$$Q = - \frac{K(2\pi r)(H - S(r))}{\mu} \rho_w g \frac{dS}{dr} \quad (3-2)$$

where the parameter S is a positive value of drawdown at the distance r from the pumped well. After rearranging Equation (3-2), we can integrate this equation with respect to r and S :

$$\int_{r_d}^r \frac{dr}{r} = - \frac{2\pi \rho_w g K}{\mu Q} \int_0^S (H - S) dS \quad (3)$$

Then we obtain:

$$\ln(r) - \ln(r_d) = -\frac{2\pi\rho_w g K}{\mu Q} \left(HS - \frac{S^2}{2} \right) \quad (3-4)$$

where r_d stands for the drainage radius estimated at 660m. That value was estimated by extrapolating to zero-drawdown axis the semi-logarithmic graph giving the final drawdown in various observation wells versus their distance from the pumped well, for the longest pumping tests. Most tests led to pluri-hectometric drainage radius values (for instance, $r_d=360\text{m}$ for M3, $r_d=250\text{m}$ for M4, $r_d=400\text{m}$ for M5, $r_d=300\text{m}$ for M8, $r_d=1800\text{m}$ for MP4, $r_d=900\text{m}$ for MP5) and an average value was adopted. Although the actual drainage radius value may be underestimated through that procedure, it was considered as valid for the purpose of permeability estimation, inasmuch as a larger value would not much change permeability estimates.

The Formula (3-4) can be re-written as:

$$S \left[1 - \frac{S}{2H} \right] = -Q \cdot \left[\left(\frac{\mu}{\rho_w g} \right) / 2\pi K H \right] \cdot (\ln(r) - \ln(r_d)) \quad (3-5)$$

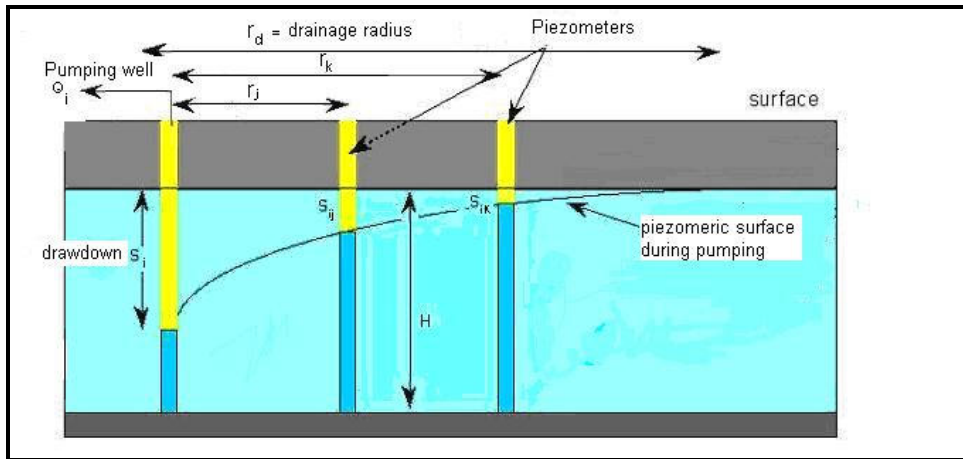


Figure 3.1: Schematic and general illustration of wells for the permeability estimations.

A schematic illustration of wells for the permeability estimations is given in Figure 3.1. Using the general Formula (3-5) and taking into account the final drawdown S_i (for well i) at the end of pumping, the average permeability of the aquifer, K_i (for well i) can be derived as follow :

$$K_i = - \frac{\mu Q (\ln(r_w) - \ln(r_d))}{[2\pi H \rho_w g] S_i \left[1 - \frac{S_i}{2H} \right]} \quad (3-6)$$

Application to EHS :

r_w : Well radius (0.12 m)

H : Thickness of aquifer (estimated 100m)

μ : Viscosity of water (1 cp = 0.001 kg.m⁻¹.s⁻¹)

ρ_w : Water density (1000 kg.m⁻³)

r_d : Drainage radius (660m)

The permeability values calculated with Equation (3-6) are reported in Table 3.1. The measured drawdowns after 24 hours of pumping were taken into account for that permeability estimation because many pumping tests were not pursued beyond 24 hours.

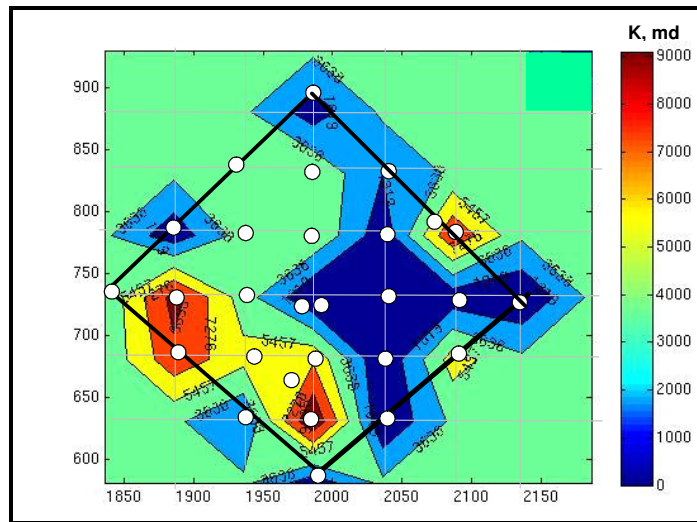


Figure 3.2: Permeability map of the EHS: a thick black line delimits the drilled zone of interest within the Site; wells are shown as white circles; well permeabilities range from around 100 millidarcys to nearly 11 Darcys.

Taking into account the constant drainage radius of 660 meters and assigning sought values of permeability to their respective well location and interpolating between wells, an iso-permeability map is built, as illustrated in Figure 3.2. This map shows contrasted permeability regions over the Site area. Large productivity-permeability differences, in a ratio around 10 are observed between wells. Note the existence of a low-permeability region to the south-east of the Site, with well pumping permeabilities of one to a few hundred millidarcys, *i.e.* about 100 times less than permeability of the west part of the Site. Obviously, the assumption of homogeneity is not valid at

all for this reservoir. Furthermore, the heterogeneity of permeability shown in Figure 3.2 represents a smoothed image of the local distribution of flows which may still be much more contrasted.

Table 3.1: Determination of the permeability at different wells by using drawdowns of quasi-steady state radial flow around pumped wells.

Well	Q(m ³ /h)	Q(m ³ /d)	Time(h)	final drawdown	Permeability(md) using the simple pumping test
C1					
C2					
IM1					
M0					
M01	20	480	24	34.21	230
M02	69.8	1675.2	24.0	5.96	4605
M03	30.6	734.4	24.0	14.81	813
M04	58.4	1401.6	24.0	7.57	3034
M05	57	1368	24.0	5.88	3812
M06	67.4	1617.6	72.0	5.08	5217
M07	63.5	1524	57.0	4.67	5347
M08	15.3	367.2	24.0	10.44	576
M09	7.2	1.0	26.16	26.16	108
M10	5	0.3	23.06	23.06	85
M11	59	1416	78.5	12.82	1810
M12	68.3	1639.2	96.0	2.73	9838
M13	61.4	1473.6	98.5	3.87	6239
M14	-	-	-	-	97
M15	31.3	751.2	75.9	15.68	785
M16	64.5	1548	138.9	2.96	8569
M17	-	-	-	-	97
M18	-	-	-	-	97
M19	64.5	1548	143.7	1.45	17492
M20	62.9	1509.6	90.5	2.79	8866
M21	62.3	1495.2	96.1	3.51	6980
M22	65.5	1572	120.6	2.36	10914
M23	58.4	1401.6	121.6	14.1	1629
M24		0			
MP4	41	984	90.6	26.83	601
MP5	54.8	1315.2	167.0	4.76	4527
MP6	62.8	1507.2	70.3	5.43	4548
MP7	60.7	1456.8	125.5	3.97	6013
P1	27	648	25.0	18.30	580
P2	69.3	1663.2	24.0	6.97	3910
P3	65.5	1572	24.0	20.02	1287

3.1.2. Flowmeter data analysis and interpretation

The wellbore production profiles, derived from flowmeter logs, reveal the presence of few thin water-feeding levels along the wellbore profile, generally only one or two levels per well. The depth of these conductive levels are recorded and will serve later to locate a so-called "water-facies". "Water" facies refers to the conductive karstic medium made up of partly-dissolved/leached carbonate facies, leached sedimentary inter-strata and open/dissolved fracture "planes" that constitute the main flow-paths of that karstic aquifer.

By using the flow rate distribution between these water levels and the average permeability obtained from the pumping tests, the permeability of each water facies level is calculated for each well. These calculations assumes that the total production of the well is ensured only by these conductive levels.

3.1.3. Imaging data

As stated in first chapter, recent borehole images of the EHS wells reveal the presence of a complex partly-collapsed cave system. Typical karstic features, such as caves, sediment fills and fractured-brecciated levels that occur throughout an unfractured host rock are observed on most boreholes optic imaging available at the EHS. Actually, image logs seem to be more reliable indicators of the productive water drains than cores, as core sampling is often incomplete in vuggy or caved wellbore sections. The production logs confirm the effective contribution to flow of these potentially-productive drains. These valuable imaging data are also used to check and detect more precisely the different lithofacies along wells and they will be accounted for when building the geostatistical model of the site.

3.1.4. Core derived petrophysical parameters

These cores derived from well C1 were used to estimate the permeability and porosity of the reservoir facies that can be sampled, *i.e.*, all the constitutive facies except the conductive "Water" facies, whose properties were derived from production profiles and well test data (section 3.1.2.). Because of the low permeability of cores, different methods ought to be tested to estimate their porosities and permeabilities. Regarding permeability, we use the results obtained by a Miniplug method (Table 3.2), *i.e.*, a compressibility technique applied to miniplugs extracted from cores.

Table 3.2 illustrates the permeability and porosity values with the corresponding depth and facies number. Average permeability and porosity values were calculated for the plugs belonging to the same facies as will be assigned to same facies in the geostatistical model. These core-derived petrophysical values could then be used as the initial input of hydraulic parameters of the EHS flow model.

Table 3.2: Petrophysical parameters calculated from cored-well C1 using the Miniplug method

		Miniplugs (MARS 2006)		
C1	C1	C1	C1	
Sample C1	Depth, m	ϕ , %	K, md	Facies number
F05	-123.75	7.3%	0.003	8
F06	-121.80	11.0%	0.009	3
F08	-118.85	17.8%	0.034	4
F10	-116.75	18.7%	218.000	3
F12	-113.60	22.0%	22.000	3
F14	-110.90	15.5%	1.000	3
F17	-106.75	14.1%	0.311	3
F18	-105.25	15.1%	0.171	3
F20	-102.60	14.2%	0.467	3
F25	-95.30	12.6%	0.456	3
F27	-92.10	16.3%	0.491	3
F28B	-90.30	13.7%	13.000	3
F29	-88.05	3.4%	0.007	3
F39	-75.85	13.9%	0.400	3
F43	-70.30	13.9%	0.355	3
F46	-66.80	16.8%	0.713	3
F50	-60.60	12.3%	0.409	3
F51	-59.55	9.0%	0.207	3
F54	-55.45	10.8%	12.000	5
F63	-46.30	15.7%	4.800	4
F66	-42.50	21.7%	80.000	4
F70	-37.50	22.6%	78.000	4
F74	-32.00	18.8%	0.203	5
F77	-28.45	14.4%	5.800	5
F78	-25.10	4.7%	1.500	3
F80	-22.55	19.3%	5.400	3
F87	-11.30	25.3%	22.300	3
F92	-2.90	7.4%	0.250	2

3.2. Building a geostatistical model of the site

As stated before, the first integration of data and the construction of a geostatistical model are carried out by using the HERESIM Software. This model is built from information available at wells. In the present case, the construction resorts on a gamma-ray profile and a drilling report giving the succession of contrasting rock units as well as water arrival events. Well-to-well correlations were attempted combining both stratigraphic surfaces and diagenetic fingerprints. Well-C1 core observations/measurements are used as the reference information to calibrate the correlated units in terms of sedimentary, lithological and petrophysical properties. As discussed before, the wellbore images and production logs recently performed over about half of the site wells provide a refined description of the lithologic column along wellbores, including a more precise location of the water entry points.

3.2.1. Reference 3D grid

The reference grid (Figure 3.3) allows to delimit the working area in the three directions. It is defined by the X,Y,Z coordinates of the reference grid origin O, by the cell dimensions, Dx, Dy, Dz, and the number of cells in each direction of space, Nx, Ny, Nz. The size of cell is very important since it determines the precision in space with which a change between two facies can be delineated. The dimensions of cells are fixed at 10 meters in both X and Y directions. The vertical thickness of cells is one meter since the facies description was initially performed for every one-meter wellbore section.

One can give an angle to the grid. The orientation of model represents the angle between X axis and the East-West axis. The sign of the angle follows the trigonometrical convention, *i.e.*, positive counterclockwise. Finally, the general geometrical properties of the model are as follows:

Original coordinate: X=451670m, Y=2.1478e+06m, Z=-170.89m

Azimuth of the grid: -37°

Number of cells: Nx= 84, Ny= 57, Nz= 172

Elementary size of the cells: Dx=10m, Dy=10m, Dz=1m

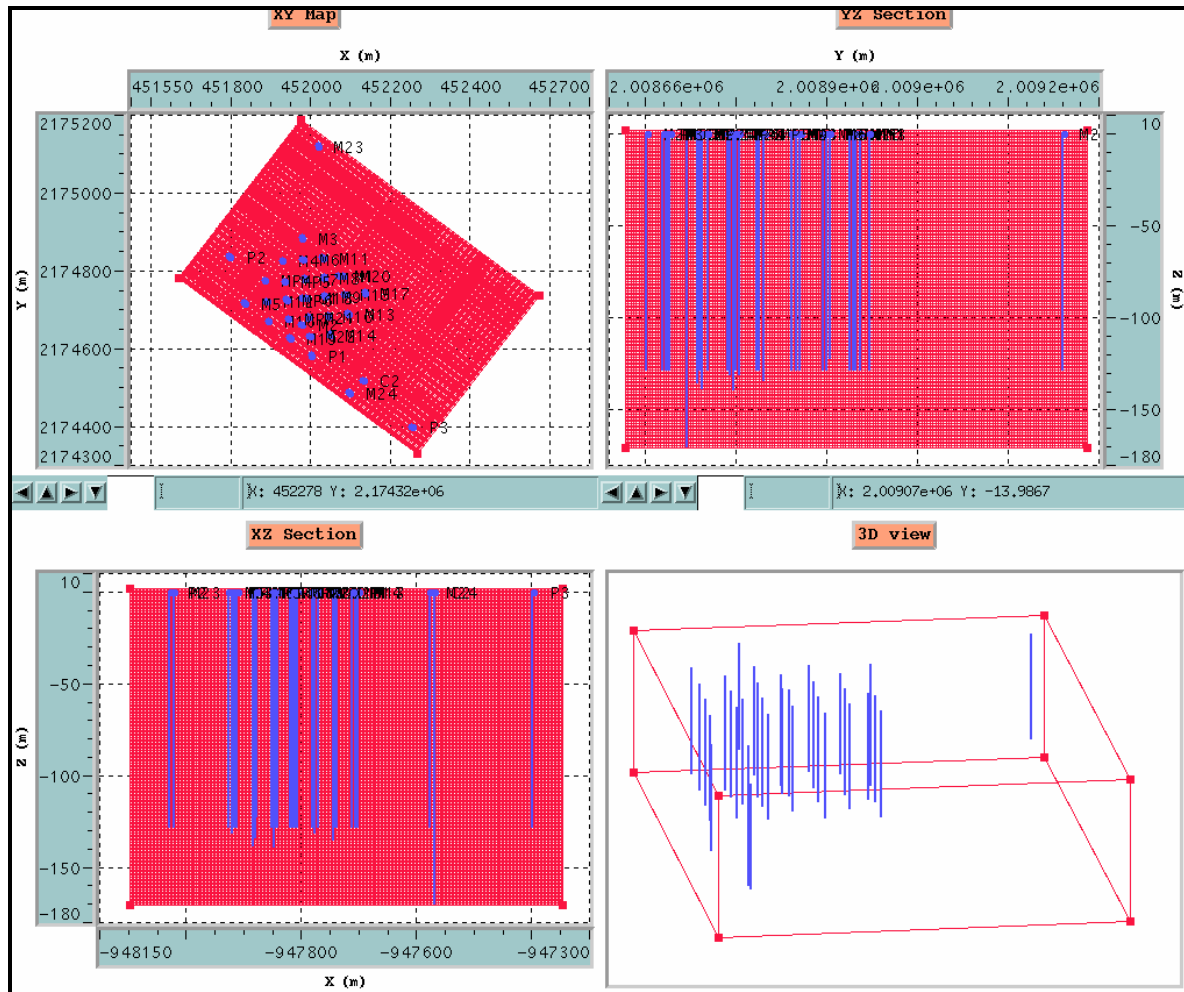


Figure 3.3: Construction of reference grid in HERESIM Software.

3.2.2. Modelling features

The first lithologic coding of facies was done by using core observations. Facies were classified into 21 different geological facies as shown in Table 3.3.

Once the simulation grid was built, for modelling purposes, the various facies defined from core observations were lumped into 8 groups, called lithotypes. These lithotypes take into account both the primary and diagenetic features. Then the referred 21 facies (Table 3.3) have been lumped into 8 lithotypes (Table 3.4) in order to better represent the dominant lithological features in the model. It should be noticed that facies 7, named "water facies", is an important facies since it strongly conditions the flow behaviour in the reservoir. This facies is detailed in next paragraphs.

The three main reservoir lithotypes (Table 3.4, left hand side) are the limestone facies and two diagenetized expressions of this facies that are fractured limestone and cherty limestone. Four other lithotypes represent pure argillaceous or clayey facies: clayey limestone, marl, clay and dark clay. Note that the dark clay, can be considered as a diagenetic facies as it mostly constitutes a fill-in sediment of caves and fractures.

Table 3.3: Facies coding used in well data files in HERESIM

Lithology	HERESIM Code
Clay	1
Limestone clay	2
Limestone	3
Marl	5
Granite	6
Sandy clay	10
Dark clay	11
Red clay	12
Yellow clay	13
Cherty clay	14
White clay	16
Fractured clayey limestone	25
Water arrival (clayey limestone)	27
Dolomite	33
Cherty limestone	34
Fractured limestone	35
Limestone with marly part	36
Water arrival (limestone)	37
Limestone with fractured chert	345
Water arrival (fractured limestone)	357
Water arrival (cherty limestone)	347

The last facies called "Water facies" (facies number 7) represents then the conductive facies levels, as detected in wells during the drilling operations or from the few flow profiles available when the model was built. This "Water" facies is only defined on the basis of its contribution to flow and not according to its lithology or its petrophysical properties. It is found most often within cherty or fractured limestone bodies. In other words this "Water" facies refers to the conductive karstic medium made up of partly-dissolved/leached carbonate facies, leached sedimentary inter-strata and open/dissolved fracture "planes" that constitute the main flow-paths. Although this denomination looks uncommon, we keep that facies name afterwards to underline the flow-property definition basis of that facies.

Table 3.4: Classification of the facies into the different lithological groups (lithotypes).

Lithotype code and name	Facies code and name
1 Clay	1 Clay
	10 Sandy clay
	12 Red clay
	13 Yellow clay
	14 Cherty clay
	16 White clay
2 Clayey limestone	2 Clayey limestone
	22 Clayey limestone pasts to clay
	32 Limestone pasts to clay
3 Limestone	3 Limestone
	33 Dolomite
	36 Limestone past to marl
4 Cherty limestone	34 Cherty limestone
5 Fractured limestone	35 Fractured limestone
	325 Limestone pasts to fractured clay
	345 Limestone with fractured chert
6 Dark clay	11 Dark clay
7 Water	37 Limestone / water arrival
	347 Cherty limestone / water arrival
	357 Fractured limestone / / water arrival
8 Marl	5 Marl

Generally, a matrix of VPC (Vertical Proportion Curves) is used to better constrain the stochastic simulation of facies. The assumption of non-stationary facies distribution over the site was tested by defining 3 regions of Vertical Proportion Curves on the basis of fracture and/or cherts presence criteria. However, the corresponding geostatistical realizations showed unrealistic facies transitions between such regions. Therefore, a single VPC region, *i.e.* a stationary model, was adopted, considering that the high density of wells constitutes a tight deterministic constraint for the geostatistical realization.

Therefore, in our case, only one VPC of all facies (or lithotypes) is determined from all wells together (Figure 3.4) that is, we deal with a stationary truncated gaussian simulation. Facies distribution was modelled by means of a truncated mono-gaussian simulation process, with thresholds determined by the facies proportion curves.

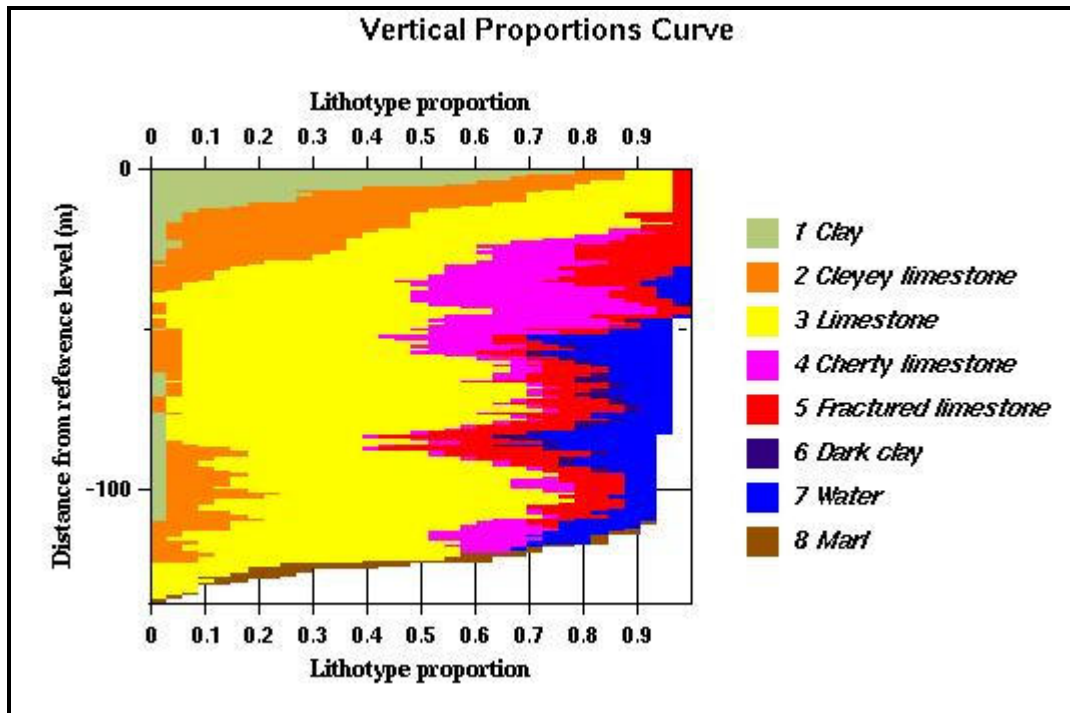


Figure 3.4: Vertical Proportion Curves (VPC) of lithotypes for all wells used for the geostatistical model.

However, that facies distribution could have been modelled using with bi-gaussian simulation process. Theses mono- and bi-gaussian simulation processes are sketched in Figure 3.5. Actually, Figure 3.5 shows how the facies are mutually organized in space, *i.e.* the order in which facies are successively simulated (or realized, or generated), either through a single generation process (on the left : primary sedimentary deposition mechanism) or through two generation processes (deposition and a secondary/late diagenesis process). In the case of two processes, the diagenetized facies, including the conductive one, should clearly form nested bodies or channels within the primary layered deposits, thus yielding a realistic image of flow-impacting heterogeneities in the resulting model.

Although a bi-gaussian model may look more reprehensive of diagenetized facies than a mono-gaussian model, the latter was finally retained for the present study. Actually, a mono gaussian model restitutes the reservoir distribution of facies as well as a bi-gaussian model, probably because of the rather high density of wells providing deterministic constraints for the geostatistical realization.

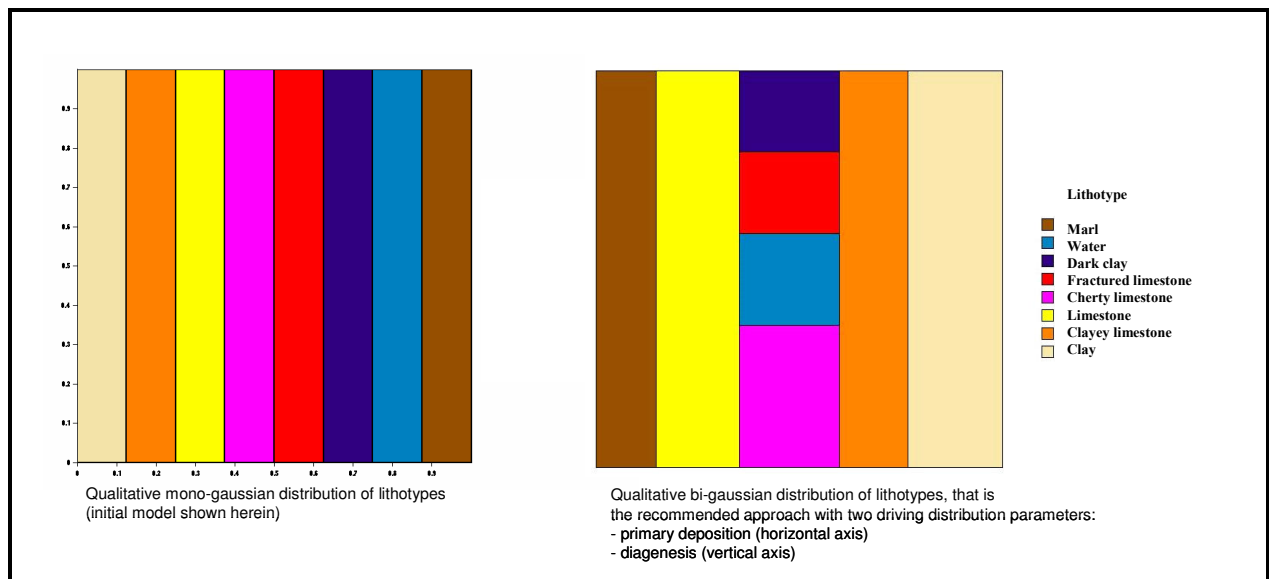


Figure 3.5: Qualitative distribution of facies in the present geostatistical model (left, mono-Gaussian) and in the more advanced model (right, bi-Gaussian/not used here).

3.2.3. Variogram of model

Variograms are built to analyze and quantify the spatial continuity of the previously-defined lithotypes. Experimental vertical variograms *i.e.* established from wellbore facies data, are shown in Figure 3.6. The variogram ranges of the carbonate and/or clayey facies having a primary sedimentary origin cannot be defined as they exceed the hectometric scale of observation. On the opposite, the variogram ranges of the diagenetized facies are much lower, in the order of a few decametres, about 10 meters for the “Water” lithotype and around 30 meters for the cherty limestone. These variogram characteristics are consistent with wellbore observations, that show a very limited vertical extent of conductive bodies, and cherts distributed over pluri-decametric sections in most wellbores.

No meaningful horizontal variogram (X and Y axis) can be defined. Actually, the frequent discontinuity of diagenetized facies between neighbouring wellbores emphasizes the nugget effect. To account for this random continuity or discontinuity of diagenetized facies from a wellbore to the other, the range of the horizontal variogram is estimated to be in the order of the well spacing (50m). Actually, a recent reflection seismic survey over the Site (to be published : *Jean-Luc Mari, Gilles Porel and Bernard Bourbiaux* : "From 3D seismic to 3D reservoir deterministic model thanks to logging data: the case study of a near surface heterogeneous aquifer," submitted to OGST-Revue de l'IFP) tends to confirm the existence of

thin high-(pseudo-)porosity bodies that are mostly-horizontal and may or not connect neighbouring wells. However, it was observed that the wells with high permeability drains were organized along the N175 direction. Therefore an angle of 5° is applied to the simulation grid.

In our approach, only one variogram model is used in the truncated mono-Gaussian method to simulate the Gaussian noise. This model is unique for the whole field and is computed from the covariance models of each indicator function of the facies, and their proportions. In our study, the final characteristics of the variogram model for the underlying Gaussian function are: Gaussian model, range X (50m), range Y (50m) and range Z (10m).

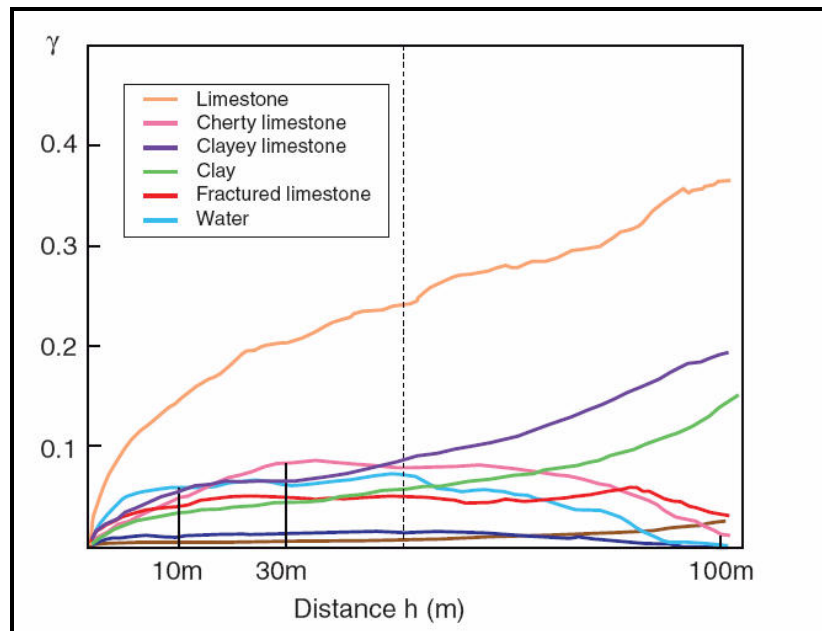


Figure 3.6: Experimental vertical variograms.

3.2.4. The petrophysical modelling

The statistical distribution of porosity and permeability is given for each lithotype according to petrophysical measurements on well-C1 core fragments. However, the permeability of the conductive lithotype, "Water", is given from well production (flowmeter) and pumping test results assuming that the total production of the well is only that of intercepted productive layers.

3.2.5. Resulting Geostatistical model of the EHS

Using the Vertical Proportion Curve of lithotypes and the variogram described above, the distribution of facies is simulated within a 3D grid of the Site. A random truncated gaussian function is used with probability thresholds derived from the proportions of each lithotype at the reservoir location under consideration. These lithotype proportions are read on the Vertical Proportion Curves. In addition, the statistical realization honours both wellbore observations of facies and the calibrated variogram model.

The resulting 3D model including the drilled experimental area is shown in Figure 3.7, with clear evidence of the drains, denoted as the "Water" lithotype, in blue colour. West-East and North-South vertical cross-sections (Figures 3.8 and 3.9) illustrate the vertical connectivity of lithotypes, in particular the conductive "Water" lithotype. The latter is often embedded in fractured or cherty limestone bodies, *i.e.*, diagenetized limestone bodies. Figures 3.10 and 3.11 show the same cross-sections than in Figure 3.8 and 3.9 but expressed in terms of permeability. These permeability cross-sections actually reflect the distribution of the "Water" lithotype, that is the sole very conductive lithotype.

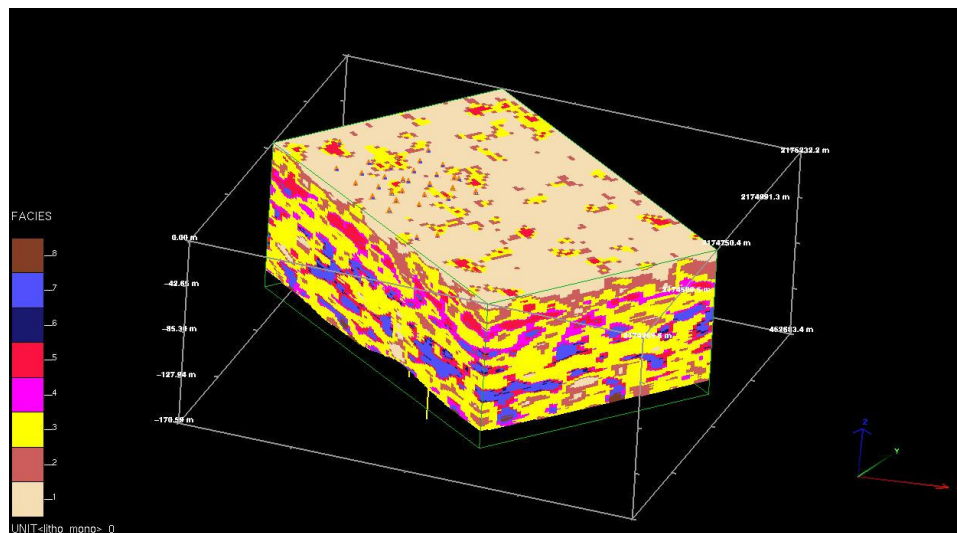


Figure 3.7: 3D geostatistical facies model of the Site (HERESIM software).

The connectivity of the conductive water facies within east-west section and north-south section was also visualized using HERESIM software (Figures 3.12 and 3.13 respectively). Both east-west and north-south sections show 3 independent connected bodies. These sections prove that a vertical connectivity between the conductive channels exists but less important

than the horizontal connectivity. From these connectivity sections, it turns out that the conductive facies can be found as isolated or connected 3D bodies with non-uniform vertical and horizontal connectivity. All these observations are in agreement with the contrasted behaviour of the pumping tests held over the Site.

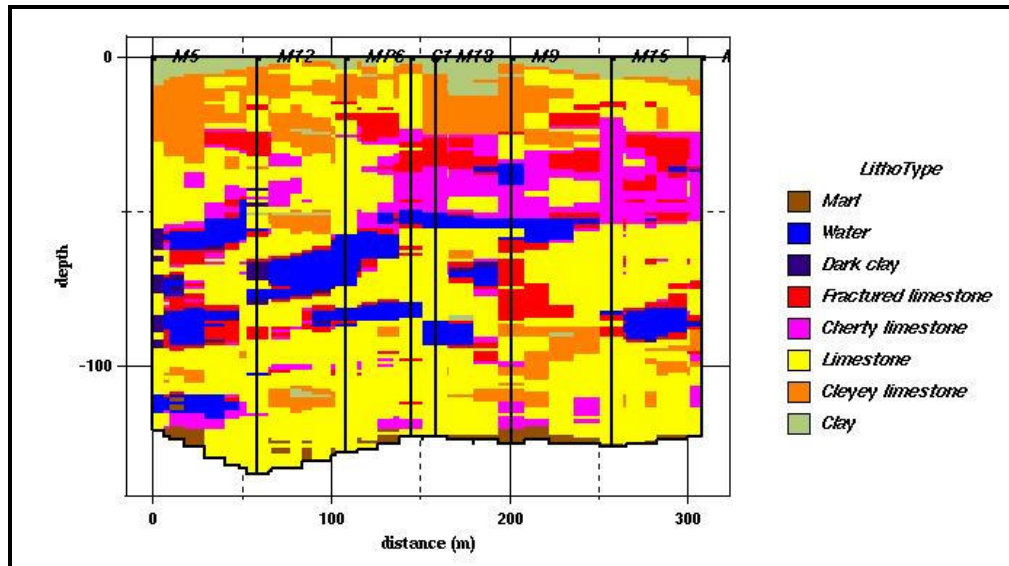


Figure 3.8: West-East facies cross-section of the Site: a poor vertical connectivity of the conductive facies is expected.

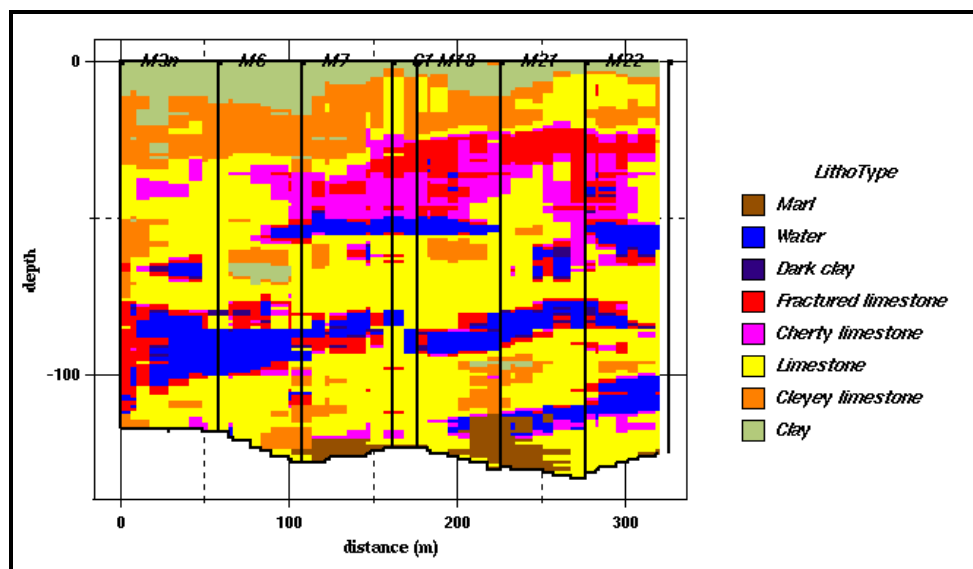


Figure 3.9: North-South facies cross-section of the Site: the conductive lithotype looks here more areally-continuous than in the West-East direction, but no vertical connection is observed between the 50m and 85m productive levels within that section.

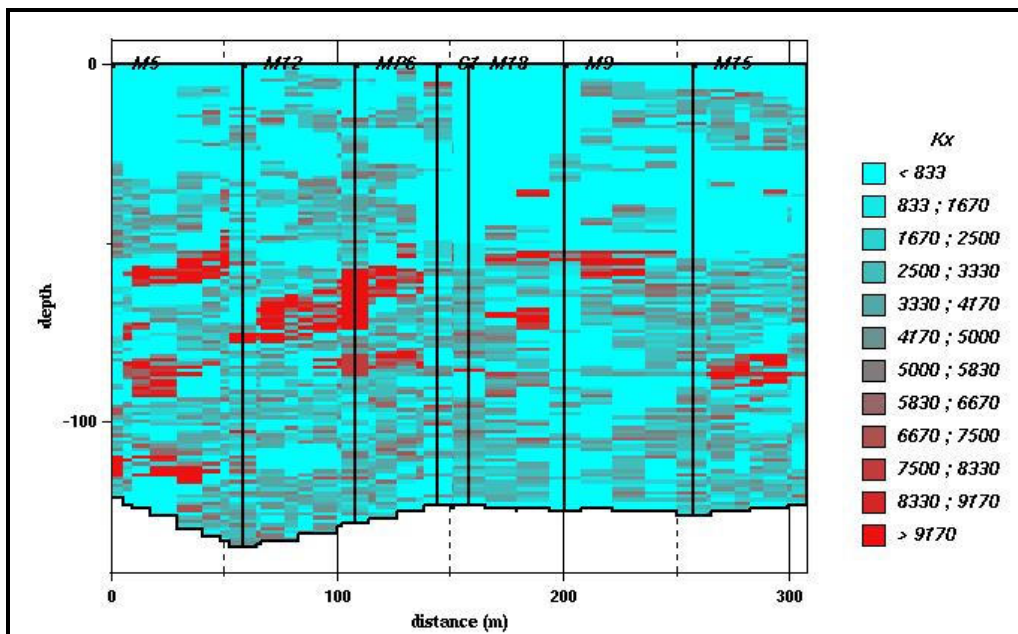


Figure 3.10: West-East permeability cross-section of the Site.

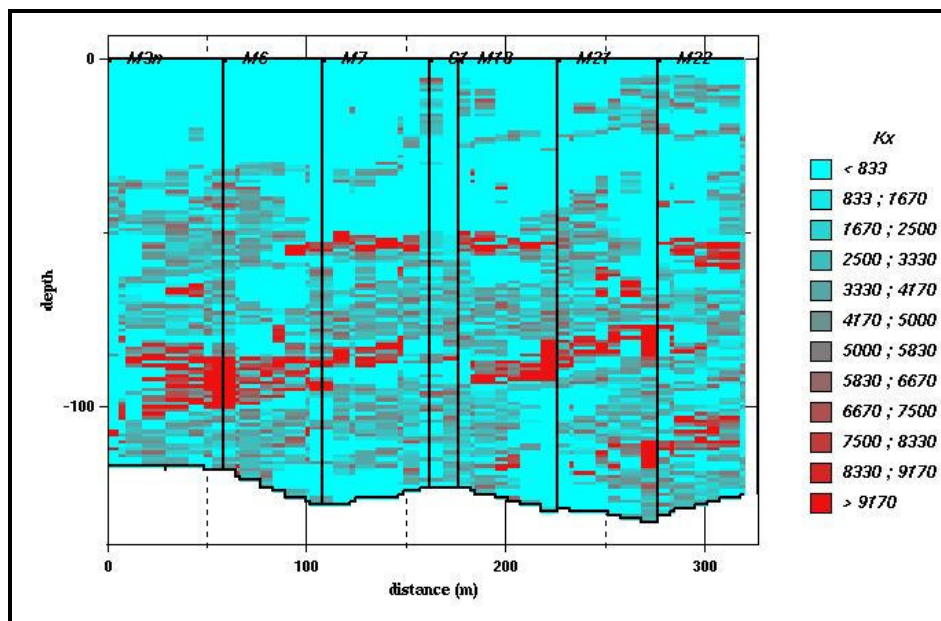


Figure 3.11: North-South permeability cross-section of the Site.

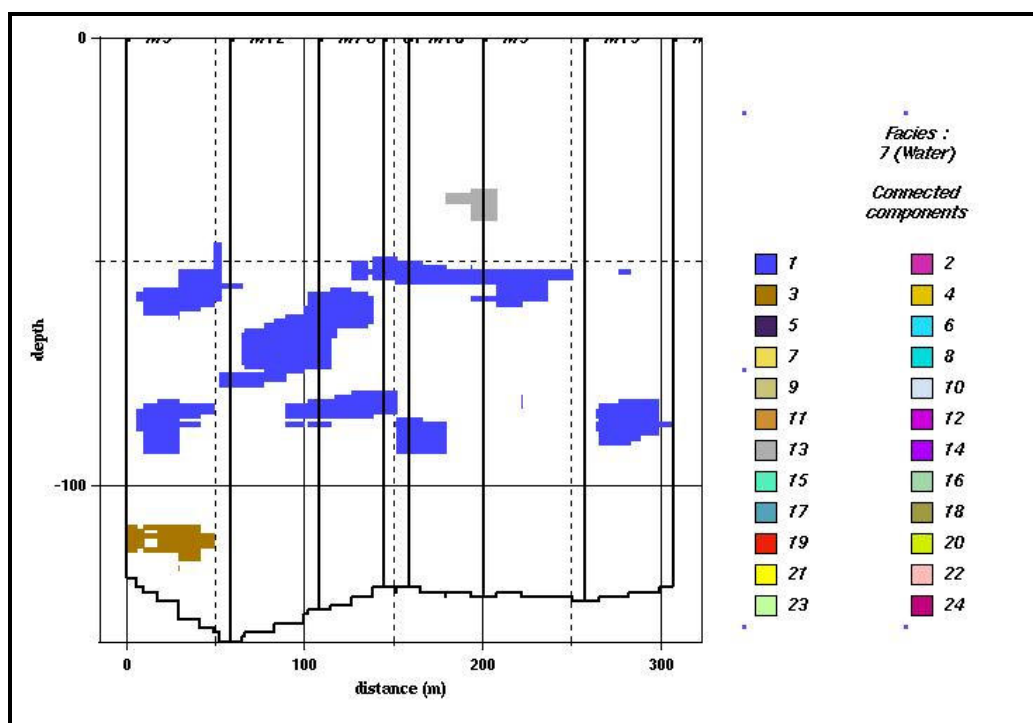


Figure 3.12: West-East connectivity section including 3 groups of connected water facies bodies.

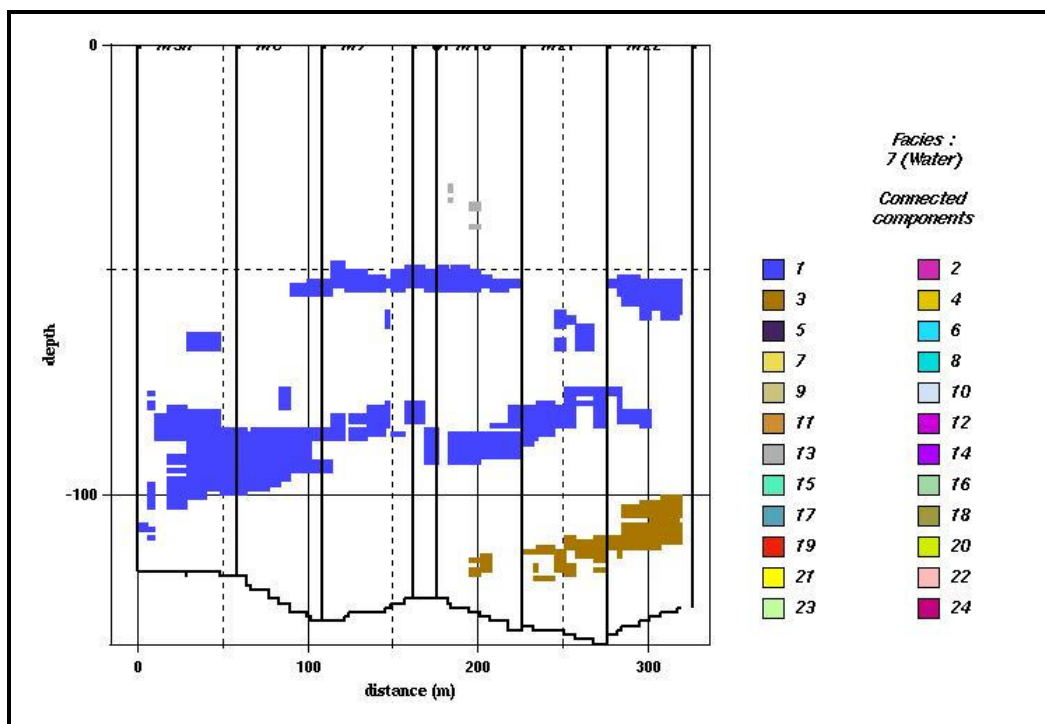


Figure 3.13: North-South connectivity section including 3 groups of connected water facies bodies.

To sum up, the geostatistical model of the EHS aquifer appears as a limestone reservoir within which diagenetized (post-deposition) facies, *i.e.* the cherty limestone and fractured limestone lithotypes, are distributed as complex 3D volume elements that are not uniformly connected both horizontally and vertically. The conductive "Water" lithotype stands itself as isolated or connected 3D bodies of variable size within the previous elements diagenetized limestone. The horizontal connectivity of these conductive bodies looks also non-uniform, even at the two main productive depths around 50-55m and 85 m. A vertical connection between the conductive channels found at these two depths may exist locally but seems much less developed than the horizontal connectivity. Eventually, this distribution pattern of the conductive lithotype explains why neighbouring wells may have similar or contrasted productivity according to the fact that they do or do not cross conductive bodies and these bodies are highly or poorly connected away from the well.

3.3. Conclusion

This preliminary work consisted in a rough evaluation of the spatial variability of permeability from the interpretation in steady-state conditions of the pumping tests carried out over the EHS. An iso-permeability map was then built. Large productivity/permeability differences (a ratio exceeding 10 between largest and smallest values) were observed between wells. Obviously, the assumption of homogeneity is not valid at all for this reservoir.

To build a geostatistical model of the Site, all the different geological facies defined from core observation were regrouped into 8 composite lithotypes. Specific well logs were acquired in most wells, including in particular flowmeter profiles and wellbore images. This valuable additional information was integrated into the geostatistical database considered herein. The "water" facies was defined using a flowing criterion (highly-conductive bodies at the decametric well spacing scale), keeping in mind this flow capability results from the diagenesis of original sedimentary carbonate deposits. The geostatistical model was then built by using a truncated gaussian algorithm. The resulting geostatistical model shows a distribution of facies that is consistent with the conceptual model of paleo-karst assumed for this aquifer.

In the next chapter, the model resulting from the integration of this extensive database will be used as a support for the simulation of well pumping tests and of pressure interferences. This subsequent stage will be determinant to constrain the remaining uncertainties of the aquifer model concerning especially the connectivity of conductive bodies or channels, and perhaps also the role of the rock-matrix as a fluid-feeding source for the long-term supply of wells. To this end, history matching techniques preserving ascertained geological features will be applied.

CHAPTER 4. Design and application of a sequential methodology for calibrating the hydrodynamic model of a highly-heterogeneous reservoir

4.1. Introduction

The purpose of this chapter is to design and implement a sequential calibration methodology for a flow model directly inherited from a geostatistical model taking into account available dynamic data. This methodology uses the available well test data, *i.e.* pumping and interference tests in the present case. The methodology proposed herein maximizes the model consistency with field-measured data, provided that the flow model assumptions and equations are fully representative of the actual field flow behaviour.

4.2. Preliminary tests

At the beginning of this study, very preliminary tests were performed to assess the general behaviour of the EHS aquifer and to understand to which extent the properties of this aquifer would influence the well pressure responses. The inversion tests were done only in terms of petrophysical properties. All calibrations were carried out for the first day of pumping (24 hours), and not for the whole test duration, because a well pumping test investigates rapidly areas distant from the Site

Initially, a total rock compressibility values of 0.0001 bar^{-1} was estimated and assigned to all facies and the petrophysical properties of facies were initialized at values drawn from core samples.

In the first step, the petrophysical properties of the "Water" facies were adjusted alone. The simulations carried out over the first day of pumping, showed a difference between the matched and measured pressure responses. In fact, the adjustment of the properties of "Water" facies alone revealed insufficient to correctly reproduce the whole response of the M7 pumping tests. Therefore, the calibration of the carbonate permeable facies was shown necessary as depicted hereafter.

In the next step, the calibration of the less-conductive porous facies was carried out over the first day of pumping for the pumped well M7 and its interference wells. A satisfactory match was reached, proving that way the necessity of calibrating properties of the porous matrix.

However, at this stage, the solution based on M7 pumping revealed inefficient to mimic without further calibration the other interference tests (with other pumped wells than M7). Moreover, the inverted porosity values did not seem to be realistic (the porosity is too high around 1, for the less-conductive facies and too small, around 0.001, for the conductive water facies). Actually, the remaining discrepancies between simulated drawdowns and data associated with unrealistic values of porosity make think that the compressibility assigned to the lithotypes is not well suited. In fact the real aquifer is much more productive with high capabilities of water supply for relatively small drawdowns.

These preliminary tests revealed that the rock compressibility had a first-order impact on the well responses, both on early- and late-times responses. This parameter should be considered as an adjustment variable in the calibration procedure, in addition to facies porosities and permeabilities. However, that option was not kept for the main practical reason that the software platform did not offer that possibility. Hence, the previously described preliminary simulations and inversion enabled us to set facies compressibility at a value yielding a approximate overall restitution of the pressure responses of pumped wells. This simplification is acceptable however, because fixing the compressibility at a new coarsely-preestimated value is equivalent to take the residual uncertainty on compressibility and lump it onto the porosity. This shortcut remains valid provided that resulting porosity values keep a physical meaning.

Then, facies compressibilities were set up again but at a high value (0.001 bar^{-1}) consistent with previous EHS studies performed by different authors (Delay *et al.*, 2004, Bernard, 2005) as discussed later.

The purpose of these preliminary tests was just to understand the overall hydrodynamic behaviour of EHS and the sensitivity of this aquifer to its parameters.

4.3. Design of a sequential calibration methodology

In this chapter, we propose a calibration methodology applicable to flow models of highly-heterogeneous reservoirs such as the karstic and fractured aquifer depicted in the previous sections and chapters. This practical methodology consists of the following steps:

Firstly we set up an initial consistent model that incorporates all available/measured information collected in the field. In particular, special attention has to be awarded to pore volume compressibilities as they deeply impact well-test pressure responses. The flow model is parameterized with the available petrophysical property values, that are the porosity-permeability measurements performed on the tight matrix facies samples recovered from the cored wells. Compressibilities are fixed at values that are consistent with the overall pressure-drawdown evolution of pumped wells, because compressibility cannot become a calibrated parameter in the code used here. Proper flow boundary conditions also have to be applied to the model. For the present field case, such boundary conditions concern the water recharge of the Site, that is estimated through a (coarse) preliminary petrophysical inversion of a long-term pumping test.

Secondly, the remaining unknown petrophysical facies are calibrated via an inversion of well test data, including pumping and interference pressure data. As will be detailed later on, the calibrated parameters are essentially the porosity and permeability of the conductive facies and, too a less extend, the permeability of hard-rock facies.

Thirdly, once petrophysical parameters are adjusted, a gradual deformation of facies is performed globally to obtain a geostatistical realization of the reservoir that matches up at best the dynamic data while respecting the underlying geostatistical parameters.

The last step consists in capturing local flow heterogeneities through a local gradual deformation method applied to reservoir regions still requiring further tuning to improve the fit to flow data.

Finally, the robustness and predictability of the resulting flow model is evaluated from the forward simulation of another pumping test not used for the calibration purpose of the previous steps.

4.4. Flow model: application to the EHS

The previously-described geostatistical model is used as the facies support of the flow model. Detailed facies properties are shown in Table 4.1.

The facies compressibilities are set at a high value (0.001 bar^{-1}) consistent with previous EHS studies performed by different authors (Delay *et al.*, 2004, Bernard, 2005). This high value accounts for the overall aquifer flow behaviour, *i.e.* high capabilities of water supply for small pressure drawdowns.

An additional fictitious boundary facies, also called "source" facies, was defined in this model. This source facies is represented in the form of very large cells surrounding the region of interest (Figure 4.1 , right and Figure 4.2). Petrophysical-property assignment to this source facies is shortly discussed later.

However, computation efficiency and flow impact considerations justified the initial eight-lithotypes (facies) model to be simplified into an equivalent lumped facies model (Table 4.2 and Figure 4.3, right) with only 2 contrasted facies, a (lumped) matrix facies (re-numbered 1) and the unchanged conductive "water" facies (re-numbered 2), plus the "source" facies (re-numbered 3) in the external boundary cells of the model. The properties of that lumped matrix facies, standing for facies 1 to 6 and 8, were initially set up to average values derived from core measurements of the different facies.

Preliminary flow inversion tests showed that the petrophysical properties of the lumped facies model (if the boundary facies is overlooked) could actually be inverted much more rapidly than the model with 8 facies. Moreover, the lumped model was found to match measured pressure responses as accurately as the detailed model. The comparison of these preliminary tests for lumped model and detailed model is shown in Figure 4.4.

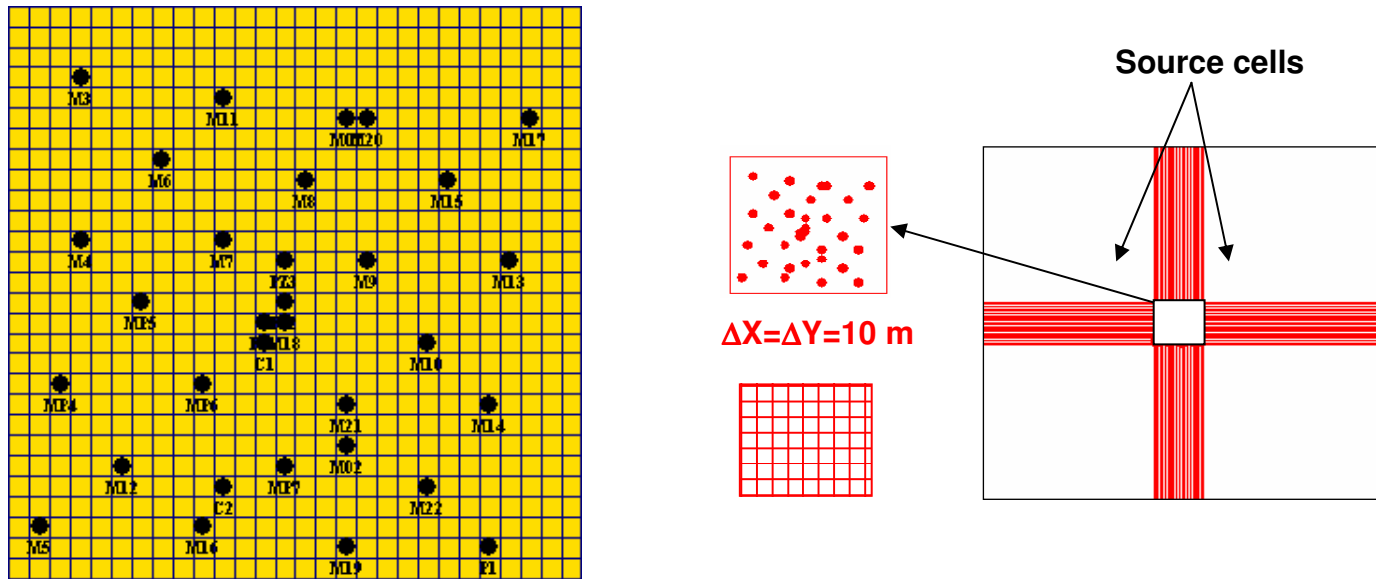


Figure 4.1: Left: Gridded model of the drilled Site area with well locations. Right: Gridded model with surrounding fluid-source cells

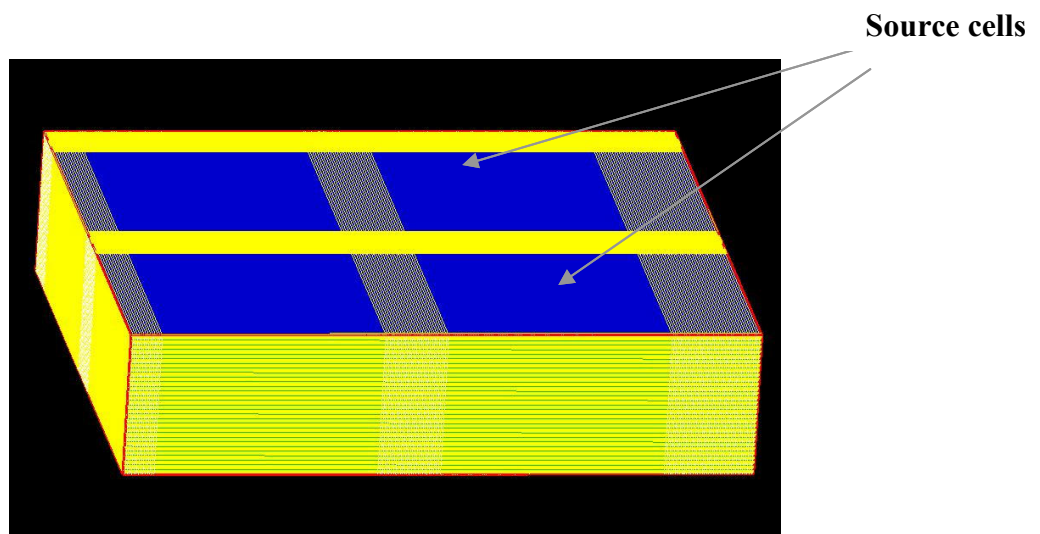


Figure 4.2: The 3D model generated by SIMVIEW IFP software, with the large volume source facies surrounding the Site

Table 4.1: The initial petrophysical parameters assigned to the geostatistical model: porosity-permeability values derived from the core data of well C1; estimated pore compressibility values (from overall pre-calibration) consistently with other dynamic studies.

facies number	facies	Kx(mD)	Kz/Kx	porosity (fraction)	pore compressibility(1/bar)
1	Clay	0.001	1	0.001	0.001
2	Clayey Limestone	0.25	1	0.074	0.001
3	Limestone	3.84	1	0.171	0.001
4	Cherty limestone	40.71	1	0.195	0.001
5	Fractured Limestone	8.9	1	0.144	0.001
6	Dark clay	0.001	1	0.001	0.001
7	Water	-	-	-	0.001
8	Marl	0.003	1	0.001	0.001
9	Source of aquifer		-	-	0.001

Table 4.2: Detailed facies (left) converted to lumped facies (right).

facies numbers	Detailed facies	Lumped facies
1	Clay	
2	Clayey Limestone	
3	Limestone	
4	Cherty limestone	1-tight matrix facies
5	Fractured Limestone	
6	Dark clay	
8	Marl	
7	Water facies	2- Conductive facies
9	Source of aquifer	3- Source facies

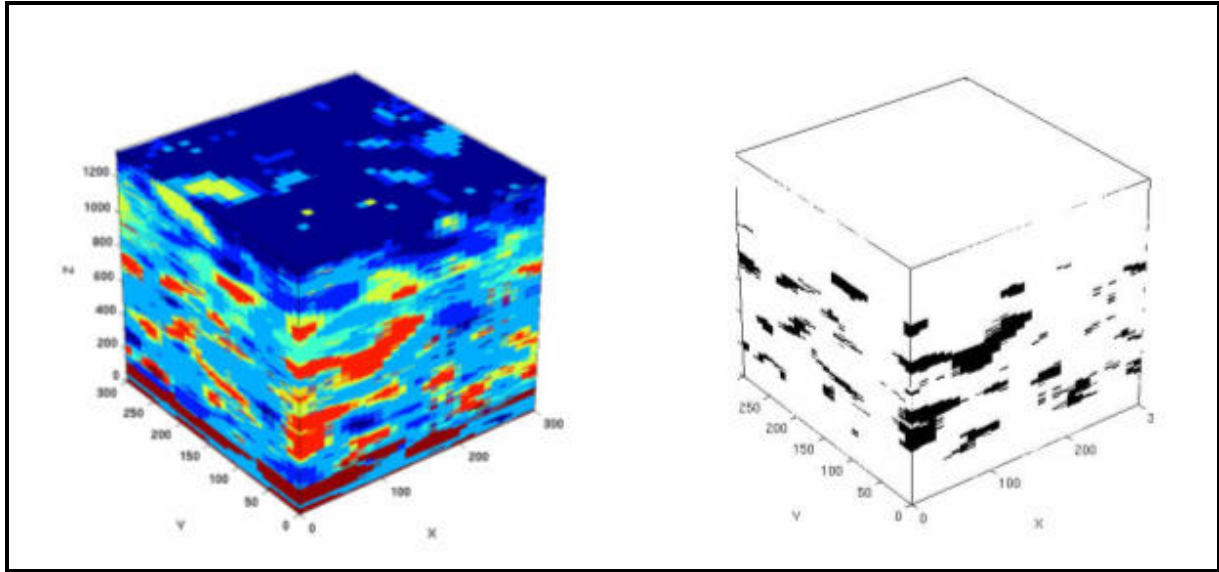


Figure 4.3: Initial detailed facies model (left) converted to an equivalent lumped facies model (right)

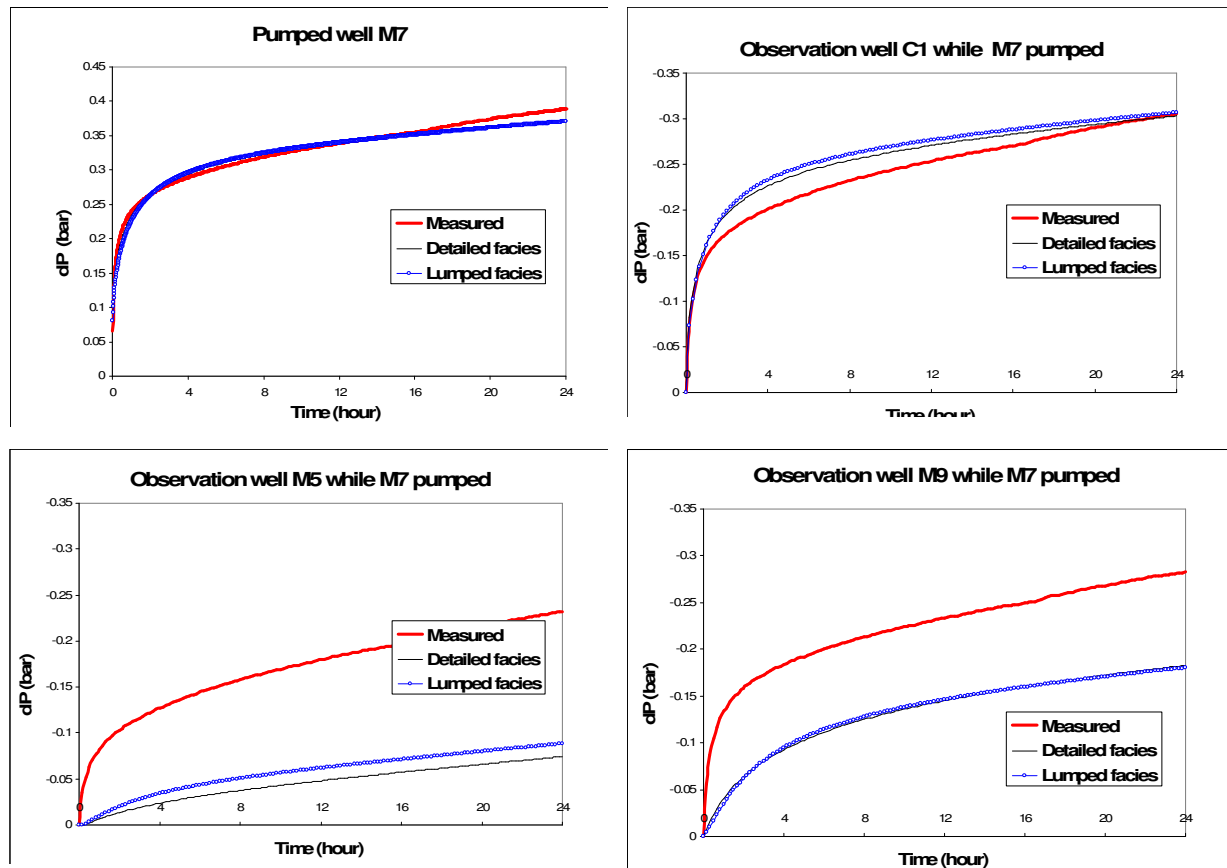


Figure 4.4: Preliminary flow inversion tests: the resulting calibrated lumped model is seemed to match measured pressure responses as accurately as the detailed model. Simulated pressures after petrophysical properties inversion are compared to measured data at the Site: pressure drop (dP , bar) evolution with time (h) for pumped well M7 and 3 selected observation wells during the first 24 hours.

4.5. Selected well data for model calibration

As stated above, several interference tests with a single pumped well were performed on the EHS. Herein, we calibrate the flow model to the field pressures measured while pumping in well M7, including the M7 pressure drawdown evolution and that of 8 observation wells showing significant interference with M7 (Figure 4.5, bottom). Well M7 is selected for its near-central location in the Site and its high productivity, thus providing an instructive set of dynamic data for constraining the flow model. The water level data recorded in wellbores are converted into pressure values using 100 bar as an arbitrary initial reservoir pressure, as shown in Figure 4.5. Even though inversion is performed while accounting for all observation points, for the sake of concision it is only discussed on M7, C1, M9 and M5 drawdowns. These points cover approximately all situations encountered in the whole set of data.

We should note that only the first day of pumping (24 hours) is taken into account for the calibrations. This choice is the consequence of the small size of the monitored area (the size is 210 m on a side) compared with the area influenced by the pumping in M7. This, it is justified to lower the time window to one day so that the transient phenomena taking place within the Site, have more weight than those occurring within the non-monitored area. Note that the influence of the boundary facies (of course, external to the site) is calibrated in a single step by using a complete test including long-time (57 h) drawdowns (see below).

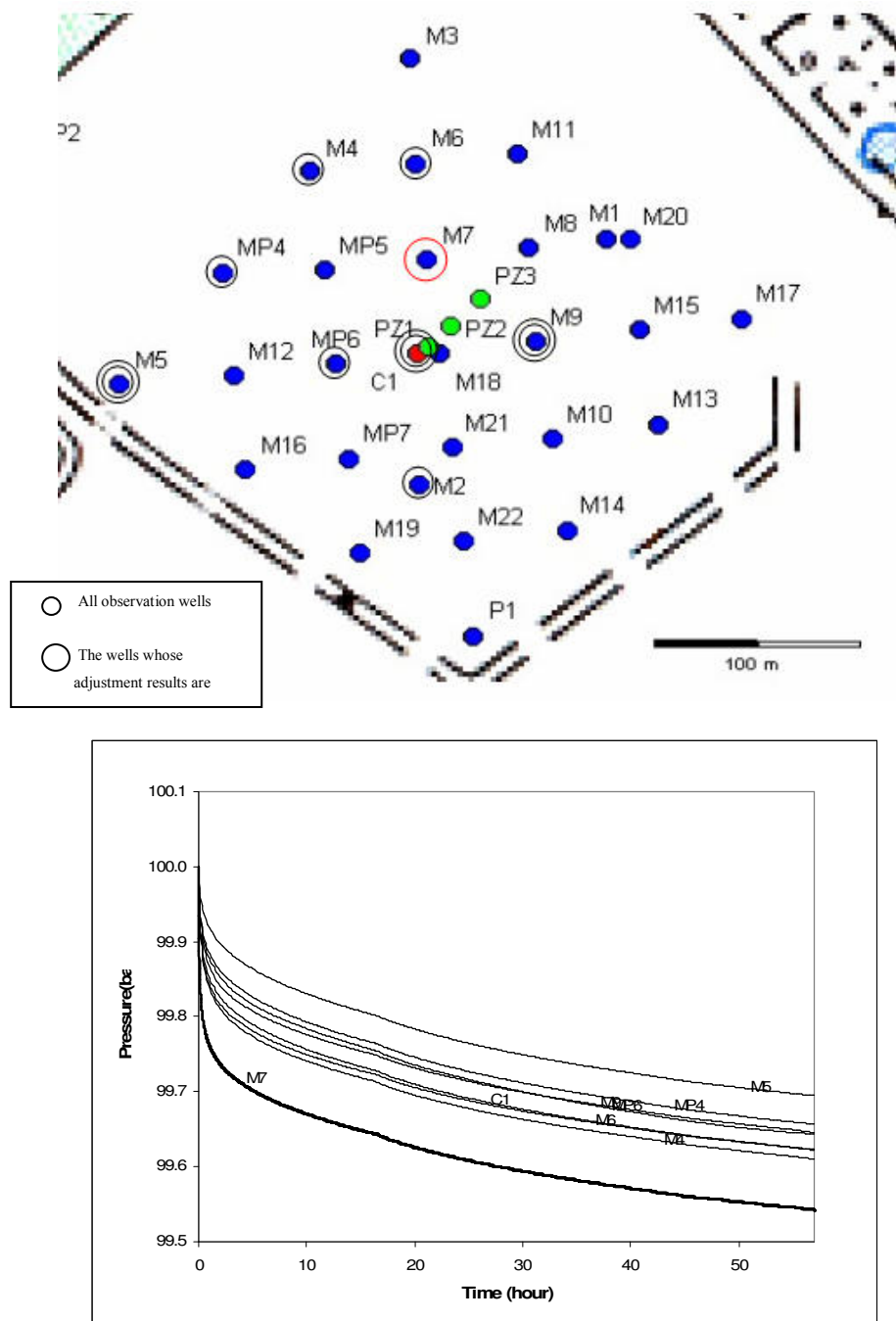


Figure 4.5: Selected data: location (Top) and pressure responses (Bottom) of the selected pumped well, M7, and of the observation wells showing significant pressure interference with M7

4.6. Preliminary calibration of the flow boundary conditions

That calibration is performed through a preliminary petrophysical inversion of the lumped facies model, with the following inversion parameters: the conductive ("Water") and boundary ("Source") facies porosities and permeabilities and only the "Matrix" facies permeability being the 5 calibrated parameters. The porosity of "Matrix" facies is kept constant at core-derived porosity (0.15). The inversion is constrained by the above-selected pressure data over the entire testing period (57 hours) in order to correctly reproduce the overall water recharge of the site during pumping. From now on the gradient-based optimization technique is used which involves deriving the flow model equations with respect to the petrophysical parameters to be adjusted. The Gauss-Newton algorithm is applied to solve the resulting system of equations at each iteration loop.

Inverted permeability and porosity values of respectively 18D and 0.04 are obtained for the "source" facies while permeability and porosity values of respectively 802D and 0.24 are obtained for the conductive ("Water") facies and permeability value of 100mD is obtained for the "Matrix" facies. The high permeability of that "source" facies is related to the presence of highly-conductive (karstic) flow paths establishing rapid communication and recharge of the studied Site of limited area (210m x 210m).

These values are kept unchanged for the rest of study as they characterize the permanent water recharge of the Site area of a vast aquifer.

4.7. Petrophysical inversion

The petrophysical properties of the conductive "water" facies and the tight matrix facies are inverted again, except for the matrix porosity fixed to a reliable average value (0.15) estimated from core data (Table 4.3). As mentioned before, the pumping and interference pressure data recorded during the first 24 hours of pumping in the well-M7 are the dynamic constraints for inverting the lumped facies model associated now with a "source" facies matching up long-term constraints. The inverted petrophysical values of facies 1 and 2 are given in Table 4.4. We observe that the conductive facies has a very high permeability value, around 900D, that characterizes the highly-permeable conduits, cave and flow paths, of the

fractured karstic reservoir. This property of the “Water” facies is also consistent with the production logs that reveal the presence of very few (1, 2 or 3) thin water-feeding levels which do not however hamper the water motion (and incidentally the propagation of the pressure depletion due to pumping).

Table 4.3: Inversion parameters, denoted "?". Porosity value (0.15) for tight facies No. 1 is derived from core data.

facies number	facies	Kx(mD)	Porosity
1	matrix facies	?	0.15
2	conductive facies	?	?

Table 4.4: Inverted values of lumped facies 1 and 2 using the short-term (24 hours) flow data from pumped well M7 and its observation wells as constraints.

facies number	facies	Kx(mD)	Porosity
1	matrix facies	100	0.15
2	conductive facies	895536	0.22

The adjusted pressure drop (dP) evolution versus time (h) for pumped well M7 and selected observation wells are compared with the experimental data in Figure 4.6. The pressure drawdown measured in the pumped well M7 is not yet fully matched. Well C1 is fairly well adjusted, well M9 matching is less satisfactory than for C1 whereas well M5 response is not reproduced at all by the inverted model. Therefore, the calibrated model still fails to represent the flow paths between some pairs of wells. Obviously, the geostatistical facies representation sustaining the flow model remains insufficiently representative of the preferential flow paths within the reservoir, as revealed by interference testing.

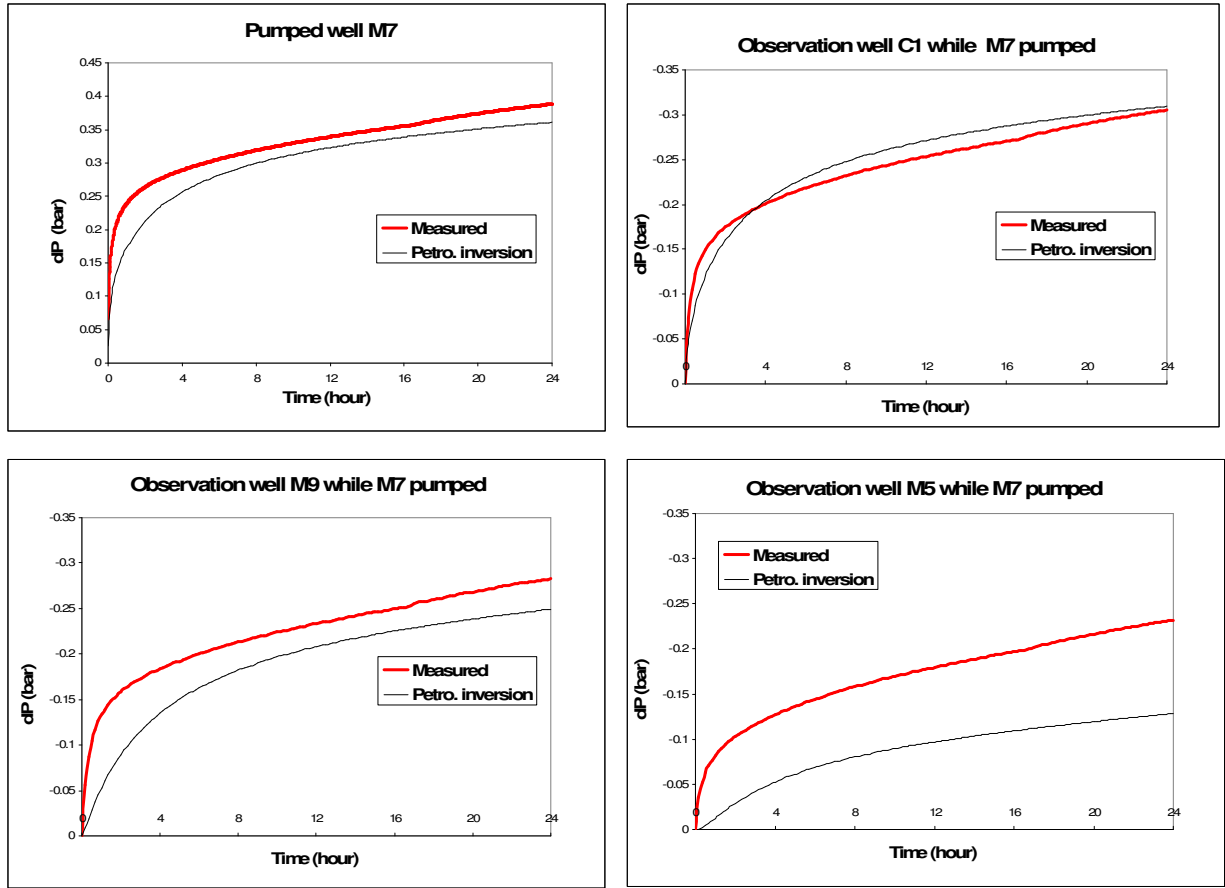


Figure 4.6: Simulated pressures after petrophysical properties inversion are compared to measured data at the Site: pressure drop (dP , bar) evolution with time (h) for pumped well M7 and 3 selected observation wells during the first 24 hours.

4.8. Gradual deformation of facies

Remind that the CONDOR software is designed for the iterative modification by deformation of any geostatistical representation of a reservoir. The easy coupling with any kind of numerical fluid flow simulator allows to select usual reservoir parameters to help history matching. In addition, the advanced parameterization technique of the gradual deformation is particularly well suited to constrain geostatistical models to production data. In our optimization process in CONDOR, the same gradient-based optimization technique is used and the Powell algorithm is applied to solve the resulting system of equations at each iteration loop.

The previously-adjusted model in terms of petrophysical properties is now improved by gradual deformation while keeping the interference data of M7 and observed wells as the

reference in the objective function. As told earlier, an initial geostatistical realization is gradually turned into other realizations through linear combinations of Gaussian random functions, until the objective function is minimized.

Gradual deformation involves here 4 deformation parameters, t_i (chapter 2), and the inversion still concerns the first day of pumping. The evolution of the objective function is shown in Figure 4.7, both for all data and for selected well pressure data. It is obvious that the objective function does not decrease monotonously but shows spurious oscillations. Two reasons may be evoked, one related to the specific flow features of the reservoir, the other to the numerical optimization technique. First, altering the facies distribution from an iteration of deformation to other may establish a new (highly-conductive) flow path between the pumped well and an observation well. It may also disconnect a previous modelled flow paths. In the end, this on/off behavior may yield oscillations in the objective function. Another possible reason to these oscillations is in the gradient-based algorithm version that is used for this work. Actually, numerical gradients are calculated from the simulation results but only for the first iteration of the optimization step. For the subsequent iterations, gradients are estimated from an approximate formula derived from the first iteration. That procedure is not always sufficiently robust to ensure a continuous decrease of the objective function between successive iterations. The adoption of an analytical gradient method would improve the optimization procedure.

The best simulated pressure curves resulting from gradual deformation of facies are compared to that from the previous petrophysical inversion, and to the field data in Figure 4.8. Matching the pressure interference in well M5 is now possible and quite satisfactory with the gradual deformation method whereas this remained impossible by petrophysical inversion. The match of wells C1 and M9 is also improved. The adjustment of pumped well M7 pressure drawdown is unchanged, remaining poor, but at least not deteriorated. Actually, matching the drawdown of a pumped well is a hard task with a classical finite volume code since the latter is often unable to fully depict stiff drawdowns for several reasons, including an inaccurate description of the near-wellbore heterogeneities (conductive paths in the present case). In addition, a non-Darcy flow regime may take place in the vicinity of high-deliverability wells, especially if fed by a limited number of flow paths.

Eventually, the gradual deformation of facies distribution turns out to be very effective to tune the previously-parameterized flow model to field-observed interferences, as such interferences are closely controlled by the continuity of the conductive facies between well pairs. The gradual deformation technique allows to determine rapidly a 3D facies distribution that is the best compromise to fit all well responses driving the deformation process. Obviously, facies deformation is complementary, not an alternative to petrophysical inversion that remains necessary for addressing poorly-defined properties. The deformations of the conductive facies bodies are shown in Figure 4.9 within a selected horizontal section of the 3D model, and in Figure 4.10 for the lateral vertical sections of that model, from the beginning (on the top, left side) to the end (on the bottom, right side) of the tuning process.

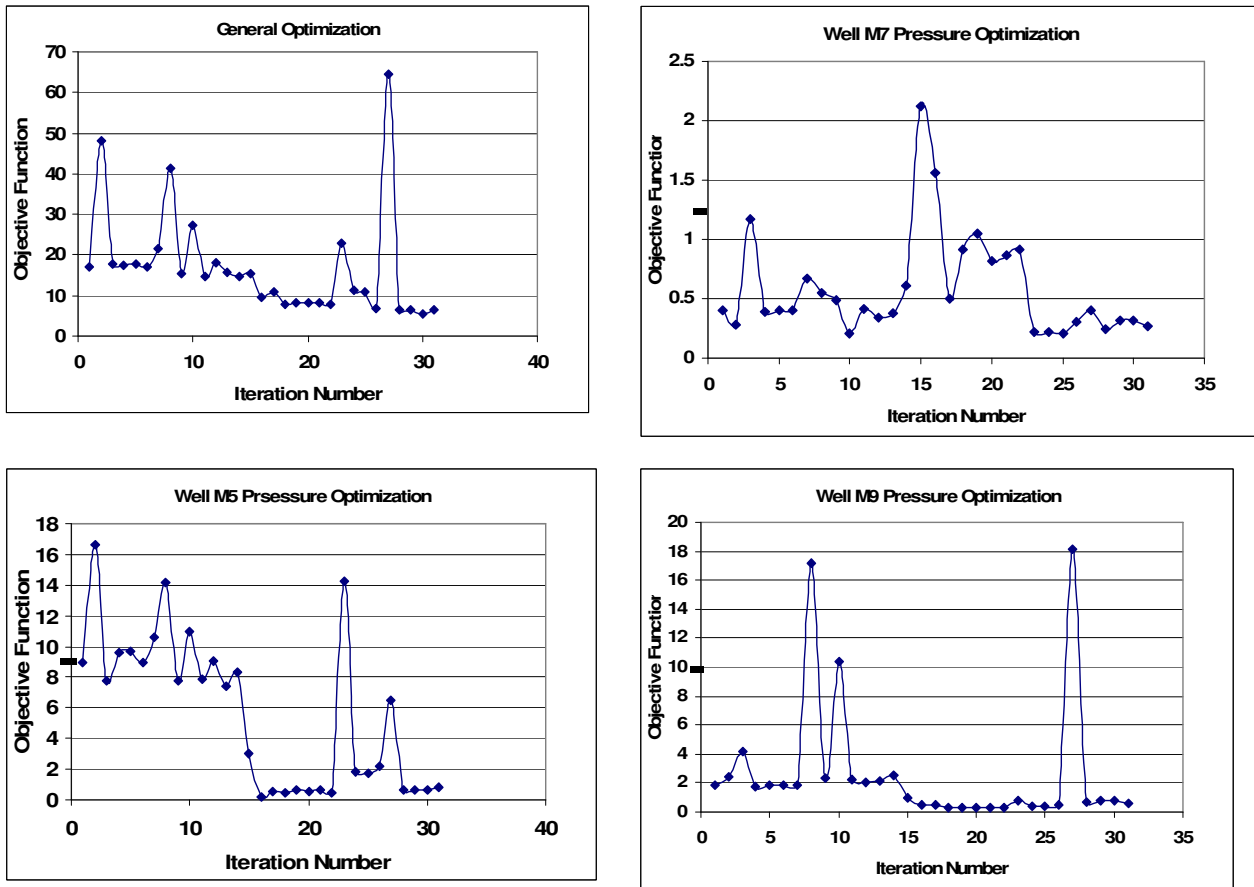


Figure 4.7: Top-left graph (on the top, right): Objective function evolution for the lumped facies model using the gradual deformation method: calibration is done on pumped well M7 and observation wells together. Other plots: Objective function evolution for wells M7, M5 and M9 pressure data. Note that the whole optimization process includes several steps, each step involving the deformation of a given set of geostatistical realizations. A temporary abrupt rise in the objective function may occur during the iterative deformations of such a step. This is due to the highly non-linear relationship between fluid flow results and geostatistical deformation: in that case, the iteration is re-started with a reduced variation of the deformation parameters.

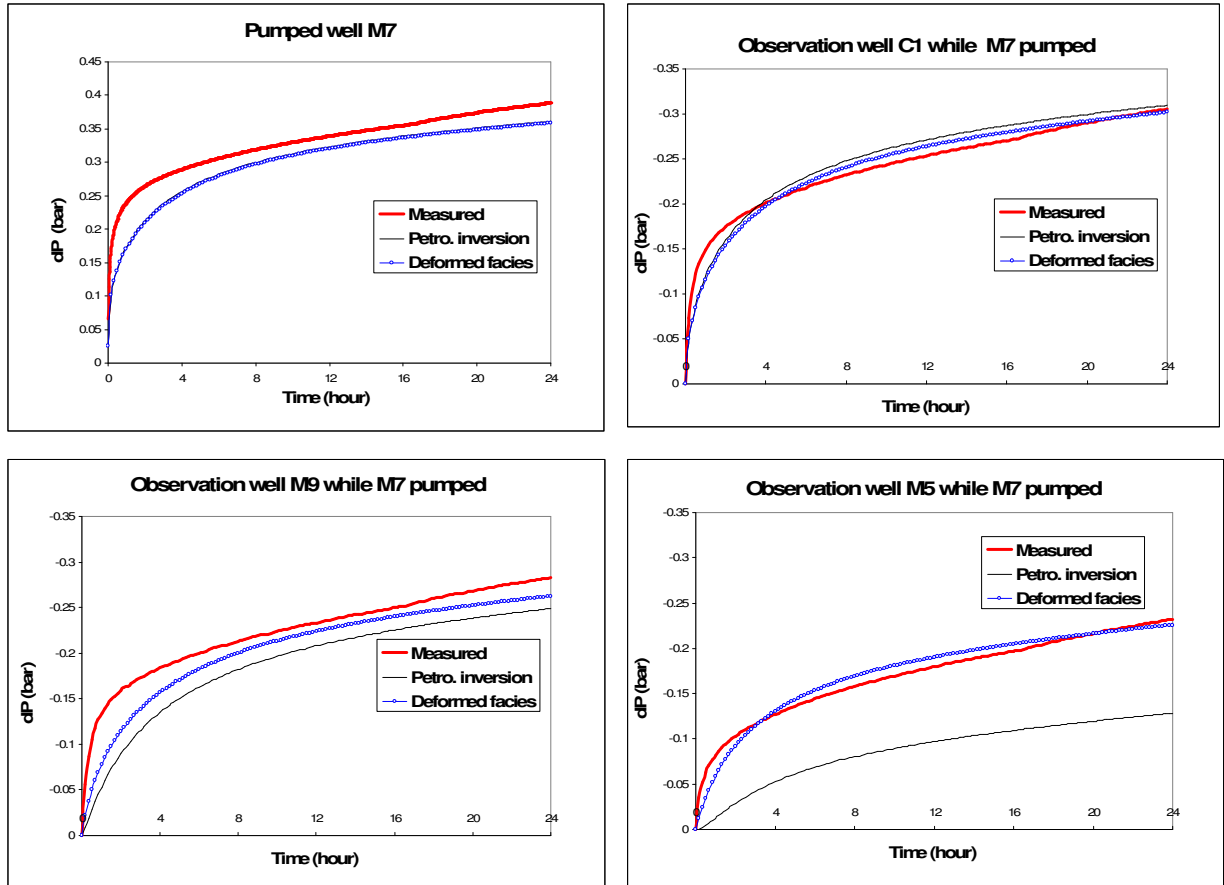


Figure 4.8: Comparison of simulated pressures after petrophysical inversion or gradual deformation of facies, with the field data: evolution of the pressure drop dP (bar) versus time (h) for the pumped well M7 and selected observation wells during the first 24 hours.

4.9. Local gradual deformation of facies

The local gradual deformation is applied to wells M7 and M9, that were not yet fully adjusted after global gradual deformation. To that end, an area including both previous wells is defined (Figure 4.11).

Then, a local gradual deformation of facies is performed on this area alone. Figures 4.11 shows the evolution of the conductive facies distribution within that regions during deformation. The newly-adjusted pressure curves are given in Figure 4.12 showing the comparison with the lastly-adjusted curves resulting from petrophysical inversion and global gradual deformation of facies, and with experimental data. Local gradual deformation actually improves significantly the match of pumped well M7, also that of well M9 to some extent.

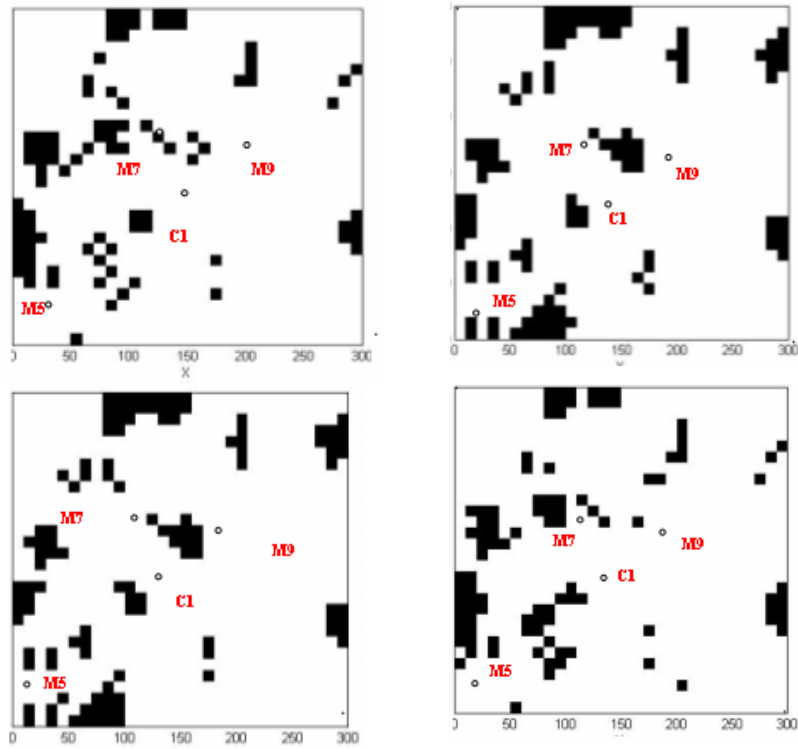


Figure 4.9: Gradual deformation of the EHS model with pumped well M7 and some observation wells as calibration constraints: 2D section of model at the depth of 68 meter (from the initial realization on top on the left, to the optimal one on bottom the right).

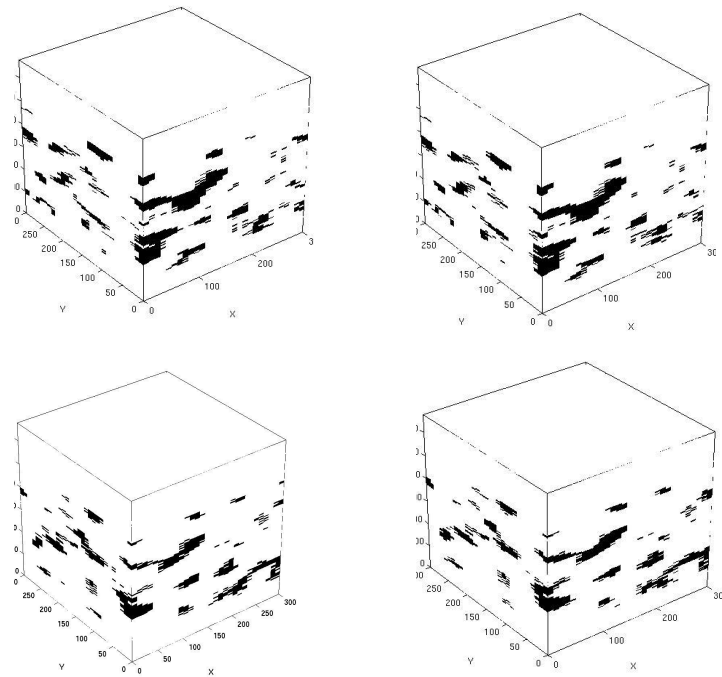


Figure 4.10: Gradual deformation of the EHS model with pumped well M7 and some observation wells as calibration constraints: lateral vertical sections (from the initial realization on top on the left, to the optimal one on bottom the right)

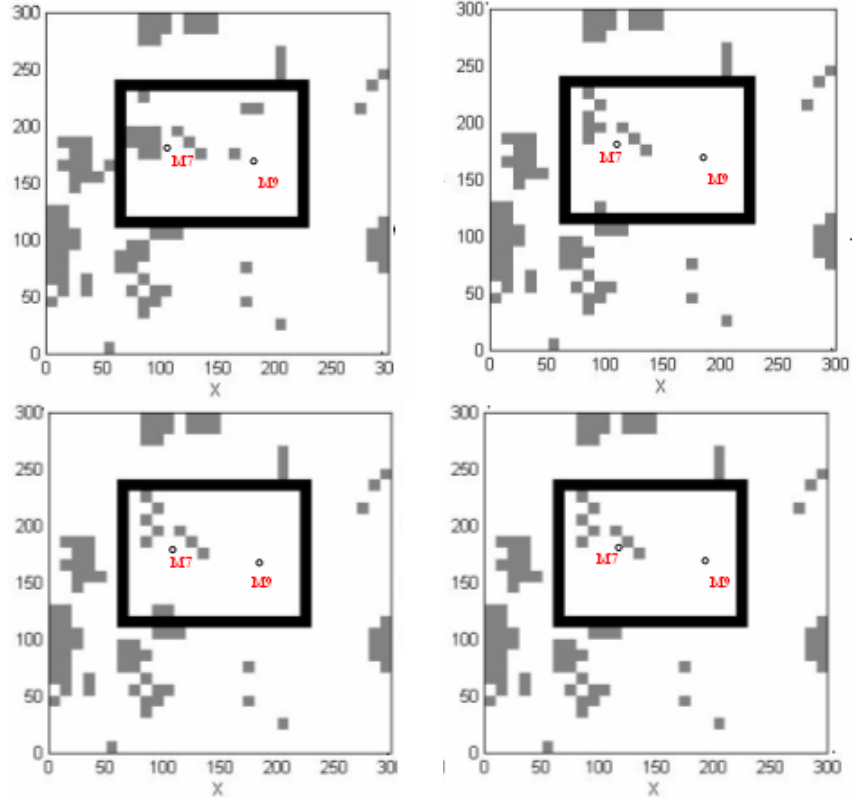


Figure 4.11: Local gradual deformation of the EHS model in a region including wells M7 and M9: horizontal section at the depth of 68m. Only the region of interest is affected by the gradual deformation process (from the initial realization on top on the left, to the optimal one on bottom the right). Note that the bottom images are quite close, because at that stage, the optimization process had nearly converged to the optimal facies distribution.

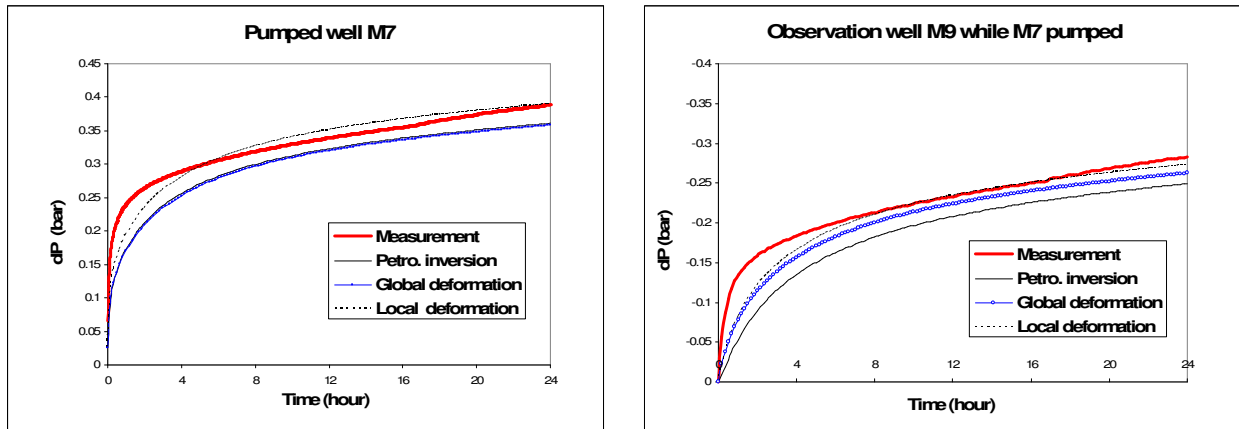


Figure 4.12: Comparison of simulated pressures after petrophysical inversion, global gradual deformation of facies and local gradual deformation of facies, with the field data: evolution of the pressure drop dP (bar) versus time (h) for the pumped well M7 and observation well M9 during the first 24 hours.

4.10. Predictability of the resulting model

Through the above-reported calibrated steps, the poorly-defined petrophysical properties of a geostatistical lumped facies model of the Site were calibrated, then a gradual deformation of facies was applied, to tune all well pressure responses first, and to then refine the pressure match around selected wells. To test the reliability and robustness of that sequential calibration procedure, we use the lastly-calibrated deformed model to simulate several wells responses but for the pumped well in M6 instead of well M7. That blind simulation is assumed to test the model robustness since the interferences with well M6 probably occur via other flow-paths systems than for well M7.

The simulated well responses are compared with experimental data in Figure 4.13. Half of the well responses are fairly well matched. Two interferences should be improved and the poorest match concerns the well M5. Actually, that well remained poorly matched at the end of the calibration process that resulted in the presently-tested simulation model. That is, the calibration procedure looks rather robust and consistent with respect to the degree of calibration refinement.

To sum up, the calibration procedure generates simulations that mimic correctly the magnitude of observed pressure drawdowns. It is worth noticing that the transient pressure evolution at short pumping times (say, less than one our) is not reproduced by the flow model. At that point, it must be reminded that the conductive facies consists of a 3D complex network of connected caves, dissolved bed joints and/or open fractures. The thickness of flow-paths stands far below the metric/deca-metric cell dimensions, 10m x 10m x 1m, of the flow model. The latter model is by construction of an up-scaled representation of the heterogeneous/karstic and porous reservoir. The co-existence in conductive "water" cells of thin highly-conductive flow-paths and of a tight porous medium may then justify the use of a dual-porosity flow model, as tested in the following chapter.

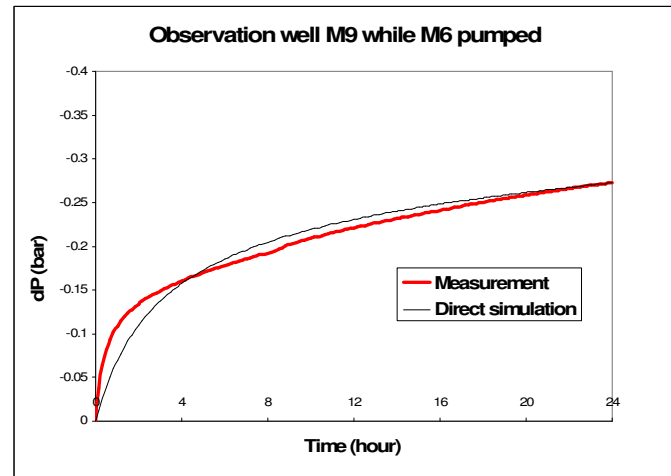
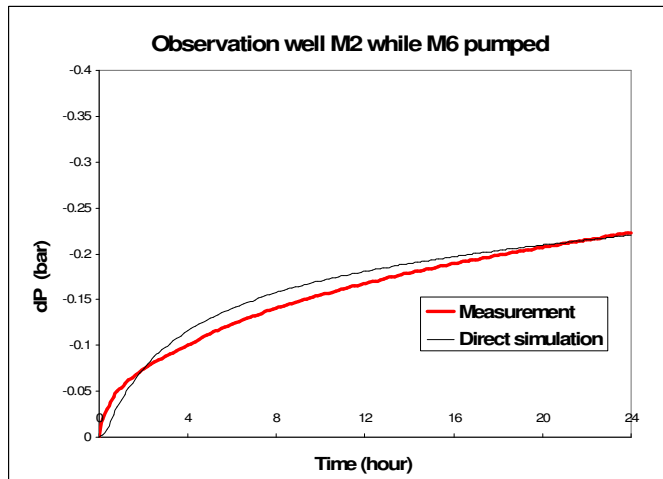
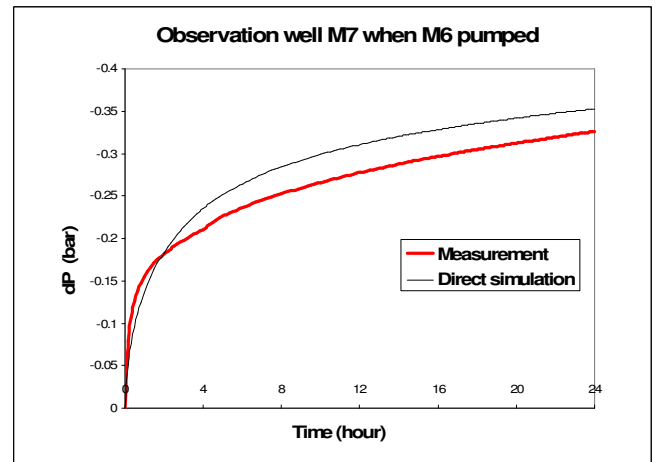
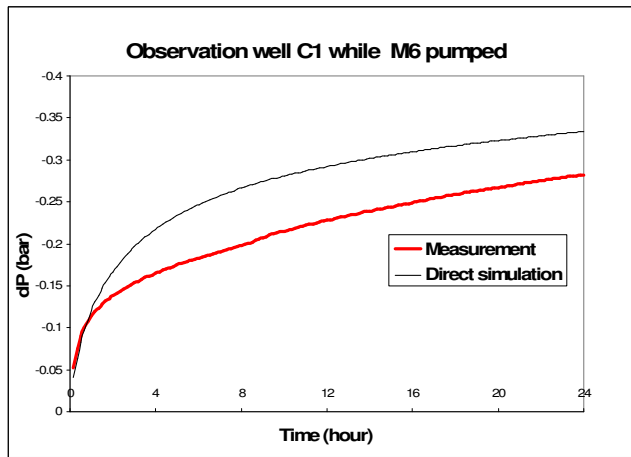
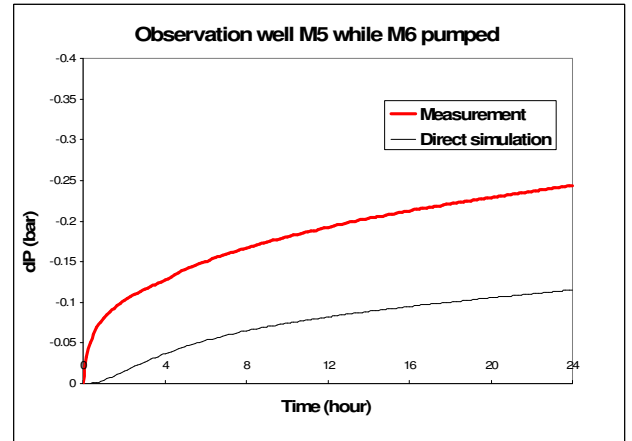
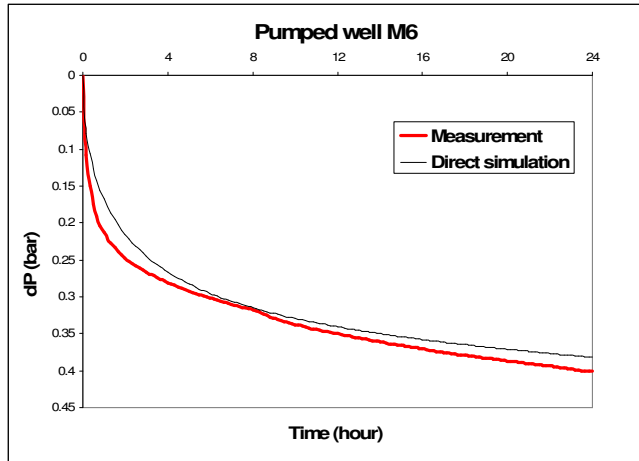


Figure 4.13: Forward/predictive simulation of pumped well M6 and its interferences. Comparison with field data: evolution of well pressure drop dP (bar) with time (h) for pumped well M6 and selected observation wells during the first 24 hours.

4.11. CONCLUSION

The chapter illustrates the efficiency of a sequential inversion methodology to calibrate a flow model of the karstic/fractured Experimental Hydrogeological Site studied herein. The main contribution consists in designing and implementing a sequential calibration methodology for flow in a geostatistical model by accounting for available dynamic data. This methodology uses well test data, *i.e.* pumping and interference tests, as flow constraints. The procedure is sequential as illustrated by the following steps:

- Initializing the flow model

Beside the necessity of incorporating available petrophysical information, derived from core data for instance, special attention has to be awarded to the assignment of representative compressibility values if that parameter cannot be included in the subsequent inversion procedure, as was the case herein. Such a precaution avoids the risk of matching non-physical porosity values.

As a preliminary calibration step, a proper flow boundary condition has also to be defined to mimic the external fluid recharge of such highly-heterogeneous reservoirs as this karstic aquifer. For our Site, this was achieved through the petrophysical tuning of a fictitious and distant "source" facies to a long-term well test, using the subsequent step calibration method.

- Petrophysical calibration. Starting from that consistent initial flow model, the petrophysical properties of the constitutive facies are inverted through an optimization algorithm that minimizes the difference between simulated and measured pressure responses over a time scale that highlights the flowing structures within the studied zone of interest.

- Gradual deformation. Once the flow model is properly calibrated in terms of petrophysical parameters, a gradual deformation technique is applied to improve the geostatistical realization of the reservoir facies distribution, with respect to the same dynamic data as in the previous step.

The gradual deformation is first performed globally to improve the facies image of the reservoir as a whole. Finally, a local gradual deformation may be applied to refine the facies distribution in selected sub-areas where well responses remain poorly-matched.

-Methodology effectiveness.

The reliability and robustness of the resulting model was proven from its fairly-good capability to predict the hydraulic response of other wells than those included as flow constraints in the inversion methodology. Obviously, the more well data constraints are used in the objective function, the more predictive the resulting calibrated model is expected to be, provided that those additional wells actually improve the detection and description of flow heterogeneities.

Finally it must be raised that the reasonable number of iterations required for calibrating or deforming a model ensures the practical applicability of that methodology.

To conclude, the proposed methodology of flow inversion/simulation looks like an effective approach to draw the best of both static/geological and dynamic/flow information for modelling the flow behaviour of hardly-tractable reservoirs as karstic fractured aquifers.

CHAPTER 5. Analysis and Discussion

5.1. Introduction

The purpose of this section is to discuss different aspects of our calibration methodology in terms of practical applications and theoretical features. Moreover, throughout this chapter, we discuss and analyse further studies performed related to the optimization performance.

First of all, the overall sequence of calibration is analyzed and validated. In fact, after the initialization of a consistent flow model (including available core petrophysical data, calibrated source facies properties and calibrated compressibilities), the question is to know whether or not petrophysical calibration has to be performed before the gradual deformation of facies (the option taken up to now). Thus, the new option here is to do the global gradual deformation followed by petrophysical inversion using exactly the same data set and the same initial flow model as described in the previous chapter. Another option is combining (global) gradual deformation and petrophysical inversion in a single calibration step. For each of the 3 options ((i) petrophysical calibration followed by gradual deformation, (ii) gradual deformation followed by petrophysical inversion, (iii) combined (global) gradual deformation and petrophysical inversion), the different inversion data such as the number of iterations, the corresponding evolution of the objective function and the computation times (CPU) are studied and analysed afterwards.

In addition, the sensitivity of calibration to the number of deformation parameters is an important issue that was not studied so far. To this end, by using the same convergence constraints of the optimization function, the global and local gradual deformations are performed again with only 1 deformation parameter instead of 4 initially. The number of gradual deformation steps (involving new realizations) as well as the computation cost of the whole optimization process are compared for both methods.

Finally, we investigate different possible solutions to better capture flow paths, through the choice of another flow model. Three alternatives are considered :

- a dual-medium representation, to account for the fact that cells assigned with conductive-facies stand for the actual rapid flow paths and for the matrix medium representing a large volume fraction of the cell;
- a higher resolution grid to better represent flow paths that are most often planar and horizontal with a thickness often much smaller than the size of the previous meshing;
- an object-based, instead of homogeneous equivalent, model to represent the actual geometry of flow paths.

The first two solutions were tested, while the third one is proposed as a perspective for this PhD work.

5.2. Analysis of inversion as regard the schedule of steps in the sequential calibration

In this section we study the other possible sequence of calibration that could be taken into account in the optimization process. In the previous chapter we examined the case where inversion of petrophysical properties was performed before gradual deformation of facies. Herein, we examine the case where the gradual deformation is performed prior to petrophysical property inversion. Another option is also tested afterwards: the gradual deformation of facies and petrophysical property inversion carried out in a single step. The efficiency and performance of each choice are analysed.

5.2.1. Gradual deformation followed by petrophysical inversion

The gradual deformation method is here performed before adjusting the petrophysical parameters. To do so, the petrophysical values have been kept fixed at the core-derived values during all the gradual deformation sequence. It must be noted that a detailed facies model is used for this test because the initial geostatistical model was generated with eight facies. In other words, in the case where the gradual deformation method has to be performed initially, the software platform is able to generate only the detailed facies model, but without any consequence on the subsequent calibration results since the same petrophysical properties are assigned to the 7 "matrix" facies, thus behaving like a unique "Matrix" facies.

The resulting fitted drawdown curves are compared to field data in Figure 5.1. This calibration sequence, deformation then petrophysics, is unable to match up correctly measured pressures. In particular, the well M5 response cannot be reproduced at all. Figure 5.2 compares the results of this new sequential calibration to that of the firstly designed sequence in chapter 4 (the case handled is that of M7 pumped and M2, M4, M5 and MP6 observed). It shows that this new sequential method does not match the measured pressures if compared to the firstly proposed sequence where petrophysical properties have been adjusted before gradual deformation of facies. Then it seems more efficient to perform the petrophysical inversion before deformation. This is probably because deformation is facing a hard task when it seeks major flow-path for a poorly defined contribution to flow of each facies.

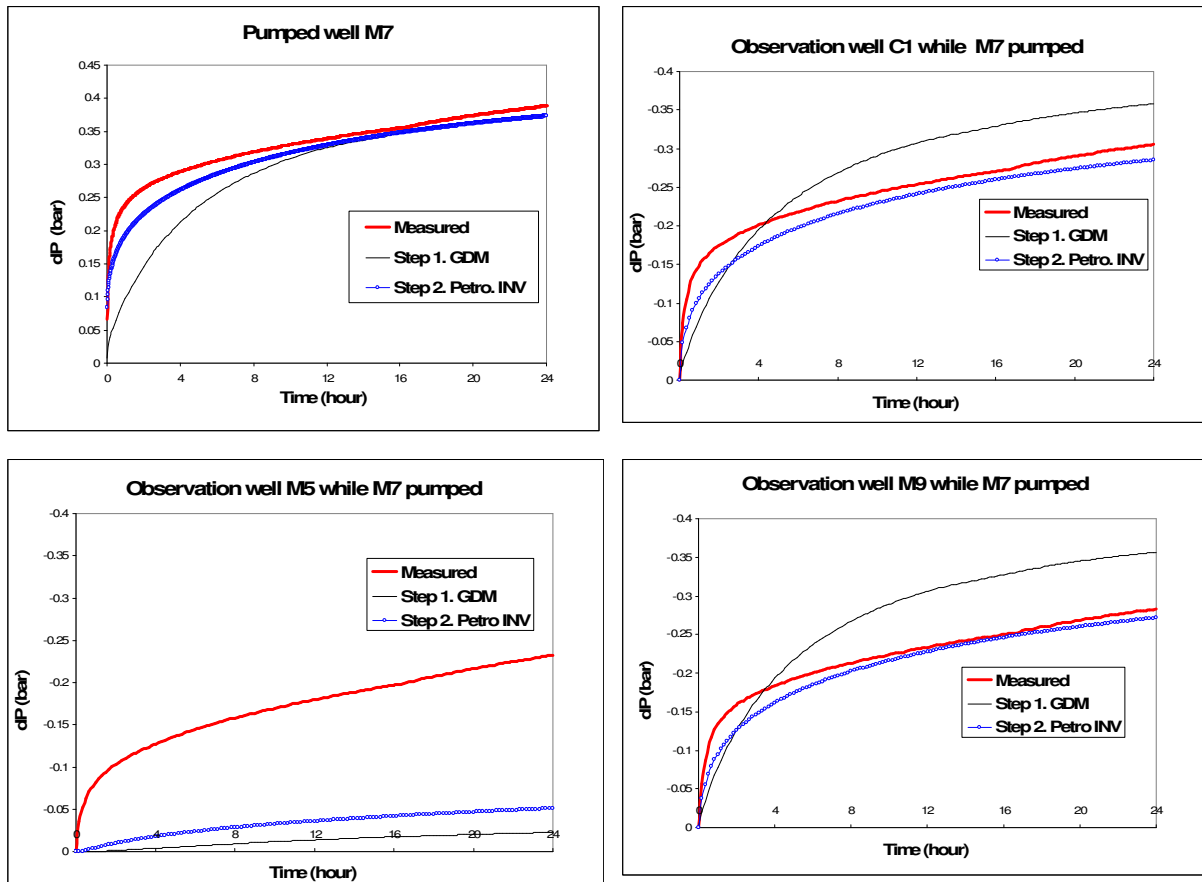


Figure 5.1: Comparison of simulated pressures after petrophysical inversion or gradual deformation of facies, with field data: gradual deformation method has been performed before petrophysical property inversion. Evolution of the pressure drop dP (bar) versus time (h) for the pumped well M7 and selected observation wells during the first 24 hours

The inverted petrophysical values of the new sequence of calibration and those of the firstly-designed methodology are compared in Table 5.1. As shown in Table 5.1 (top), the new sequence finds an average porosity of 0.25 and a permeability of 21.75 mD for the matrix facies whereas the water facies is assigned with 0.25 for porosity and 629 D for permeability. For the firstly-designed method (Table 5.1, bottom), it was obtained a matrix facies porosity of 0.15 and permeability of 100 mD, and a water facies porosity of 0.22 and permeability of 895D.

Although the petrophysical inversion leads to the same order of magnitude of facies porosity and permeability between the two sequential methods, this is not sufficient to obtain a good calibration of wells when deformation is handled before petrophysical inversion.

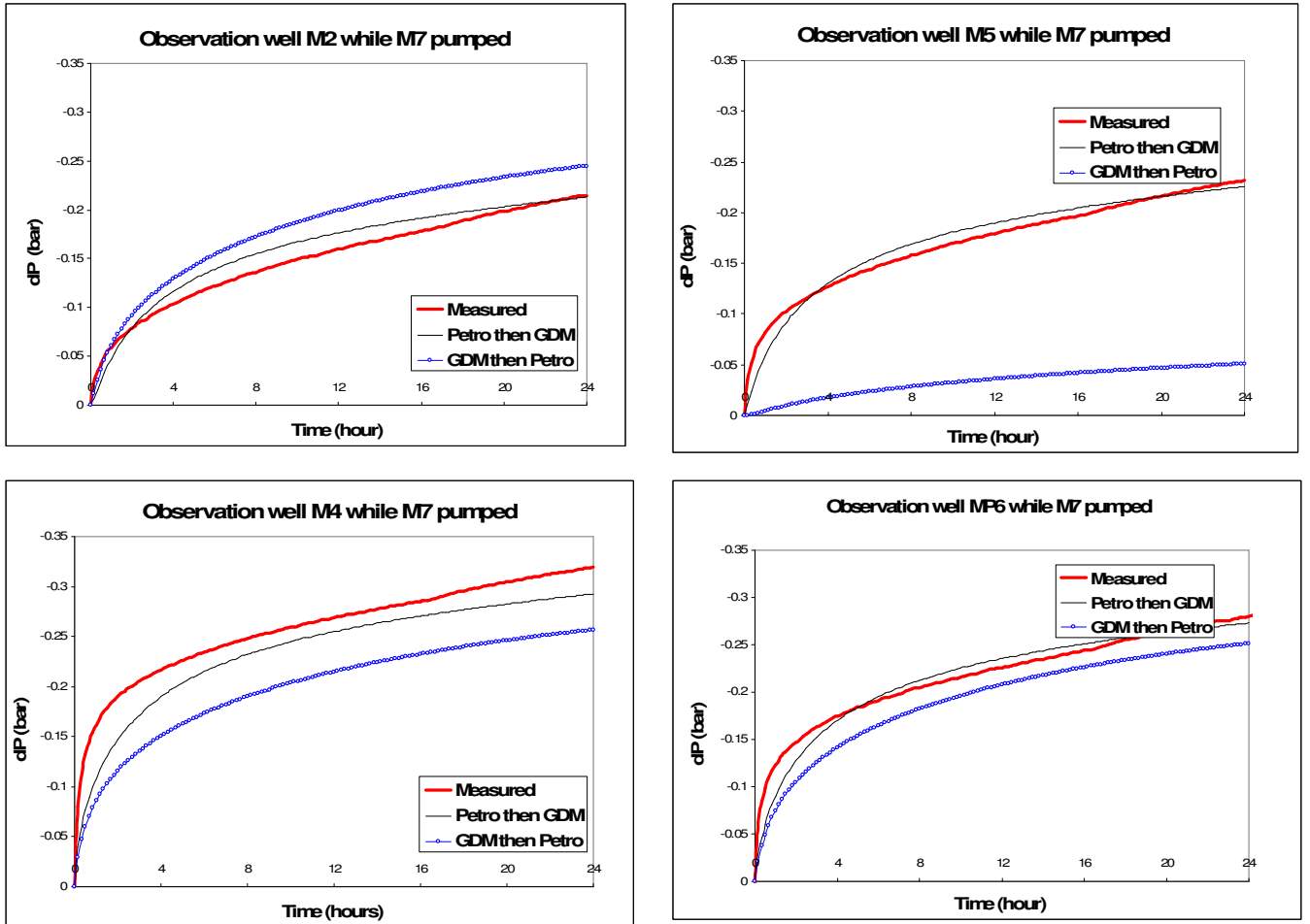


Figure 5.2: Comparison of the second sequential calibration (GDM before Petrophysical inversion) to the previous sequential calibration (Petrophysical inversion before GDM). Wells showing the largest difference in calibration results between the two sequences have been selected here.

Table 5.1: Inverted petrophysical parameters, Top: Results of petrophysical property inversion performed after gradual deformation of facies, Bottom: Results of petrophysical property inversion performed before gradual deformation of facies.

Facies number	Facies name	Kx(mD)	Porosity(fraction)
1	Clay	0.001	0.001
2	Clayey Limestone	3.68	0.45
3	Limestone	146	0.58
4	Cherty limestone	0.88	0.3
5	Fractured Limestone	0.48	0.43
6	Dark clay	0.0005	0.0025
7	Water	629011	0.25
8	Marl	1.24	0.0005

Matrix facies average porosity: 0.25 and permeability 21.75 mD

Water facies porosity 0.25 and permeability 629 D

facies number	facies	Kx(mD)	Porosity
1	matrix facies	100	0.15
2	conductive facies	895536	0.22

5.2.2. Combining (global) gradual deformation and petrophysical inversion in a single calibration phase

As stated earlier, another option is to combine the gradual deformation of facies and petrophysical property inversion into a single step. Again, it must be pointed out that the detailed facies model is used here, because a 8-facies model is generated initially.

The model is initialized by using the core-derived petrophysical property values. Then gradual deformation and inversion of petrophysical properties are performed simultaneously. Results are compared to field data in Figure 5.3 and show that a correct matching between simulations and observations can be reached with the combined (single-phase) procedure of inversion (Deformation mixed with petrophysics). In other words, it seems that using the gradual deformation method and petrophysical property inversion in a combined calibration (single-phase) is efficient enough to reproduce the responses of the pumped and observed wells. In particular, this method can tune well M5 response that was not adjusted at all initially.

To compare the efficiency of this combined (single-phase) calibration method to that of the firstly-designed method (that was done in two steps), the final adjusted-simulated pressures both after combined (single-phase) optimization and after sequential (dual-phase) optimization are compared in Figure 5.4. This Figure shows that the combined (single-phase) optimization is as much efficient as the initially-designed sequential (dual-phase) methodology.

Table 5.2: Inverted petrophysical parameters, Top: Results of the single-step calibration of detailed-facies model, Bottom: Results of dual-step calibration with inversion of petrophysical properties inversion before gradual deformation

Facies number	Facies name	Kx(mD)	Porosity(fraction)
1	Clay	1.84	0.015
2	Clayey Limestone	9.58	0.2
3	Limestone	187	0.407
4	Cherty limestone	169	0.178
5	Fractured Limestone	187	0.03
6	Dark clay	57.12	0.001
7	Water	895820	0.034
8	Marl	4.51	0.094

Matrix facies average porosity: 0.13 and permeability 88 mD

Water facies porosity 0.034 and permeability 895 D

facies number	facies	Kx(mD)	Porosity
1	matrix facies	100	0.15
2	conductive facies	895536	0.22

The inverted parameters, *i.e.* porosity and permeability, of facies from the combined (single-phase) calibration and from the sequential (dual-phase) calibration are shown in Table 5.2 on the top and on the bottom respectively. The average permeability and porosity of matrix facies obtained from single-step optimization are 88 md and 0.13 respectively and those of the firstly-designed method are 100 mD and 0.15. The inverted values of permeability and porosity for the conductive facies (water facies) are 895D, 0.034 respectively for the single-step calibration and 895D and 0.22 for the dual-step calibration. Hence, the inverted petrophysical properties from both optimization techniques appear consistent except for the water facies porosity that differs largely between the two methods. The reason for that low

impact of the water facies porosity lies in the fact that water facies represents a small fraction of the overall reservoir volume of fluid. "Water" facies porosity is much less influential than its permeability and location within the reservoir because that facies ("Water" cells) represents a small fraction of the total reservoir volume, and also a small fraction of the reservoir fluid content or recharge capacity.

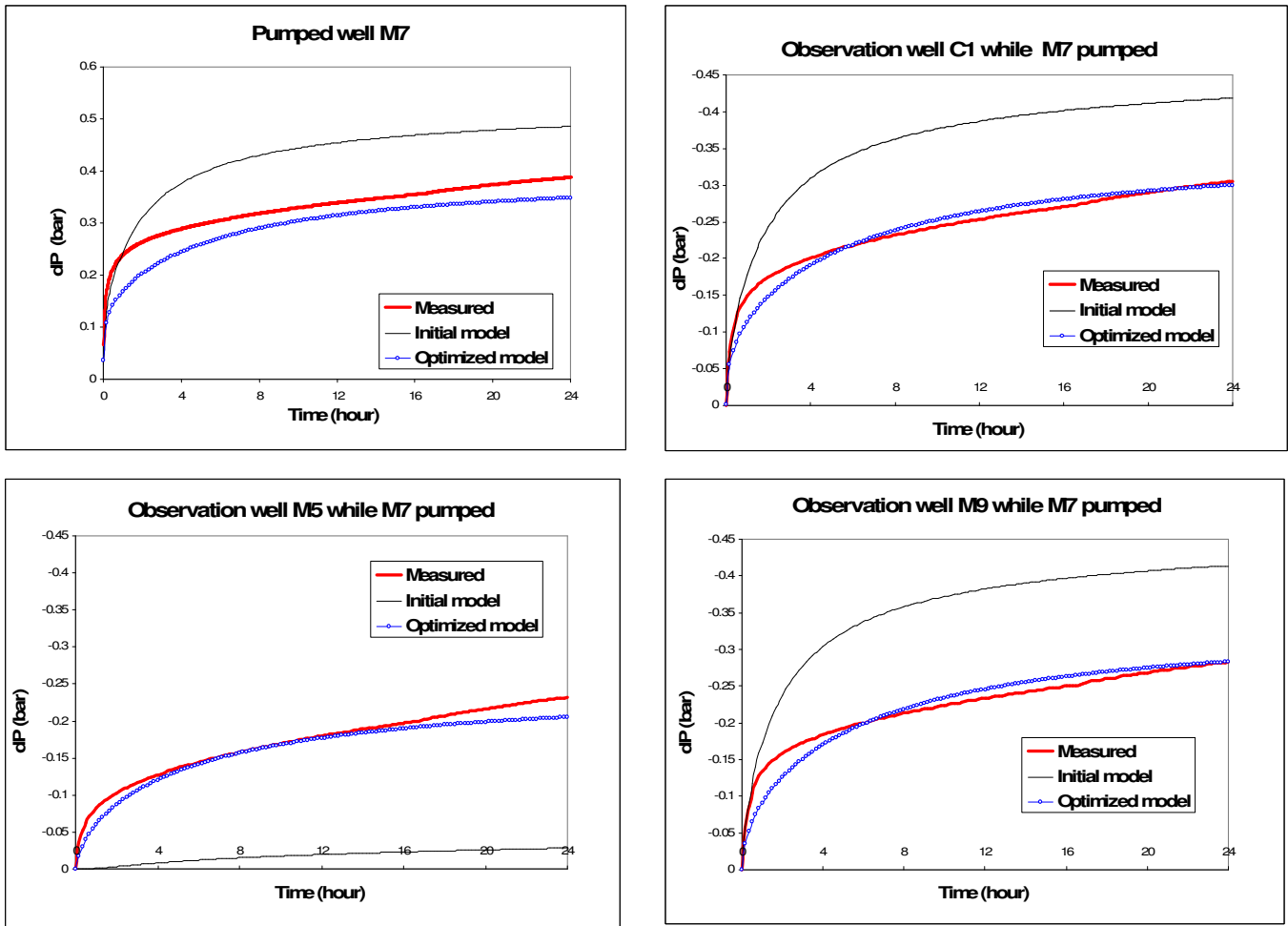


Figure 5.3: Comparison of simulated pressures after petrophysical inversion or gradual deformation of facies, with field data: gradual deformation method and petrophysical property inversion have been performed in a combined calibration process (single-phase calibration). Evolution of the pressure drop dP (bar) versus time (h) for the pumped well M7 and selected observation wells during the first 24 hours

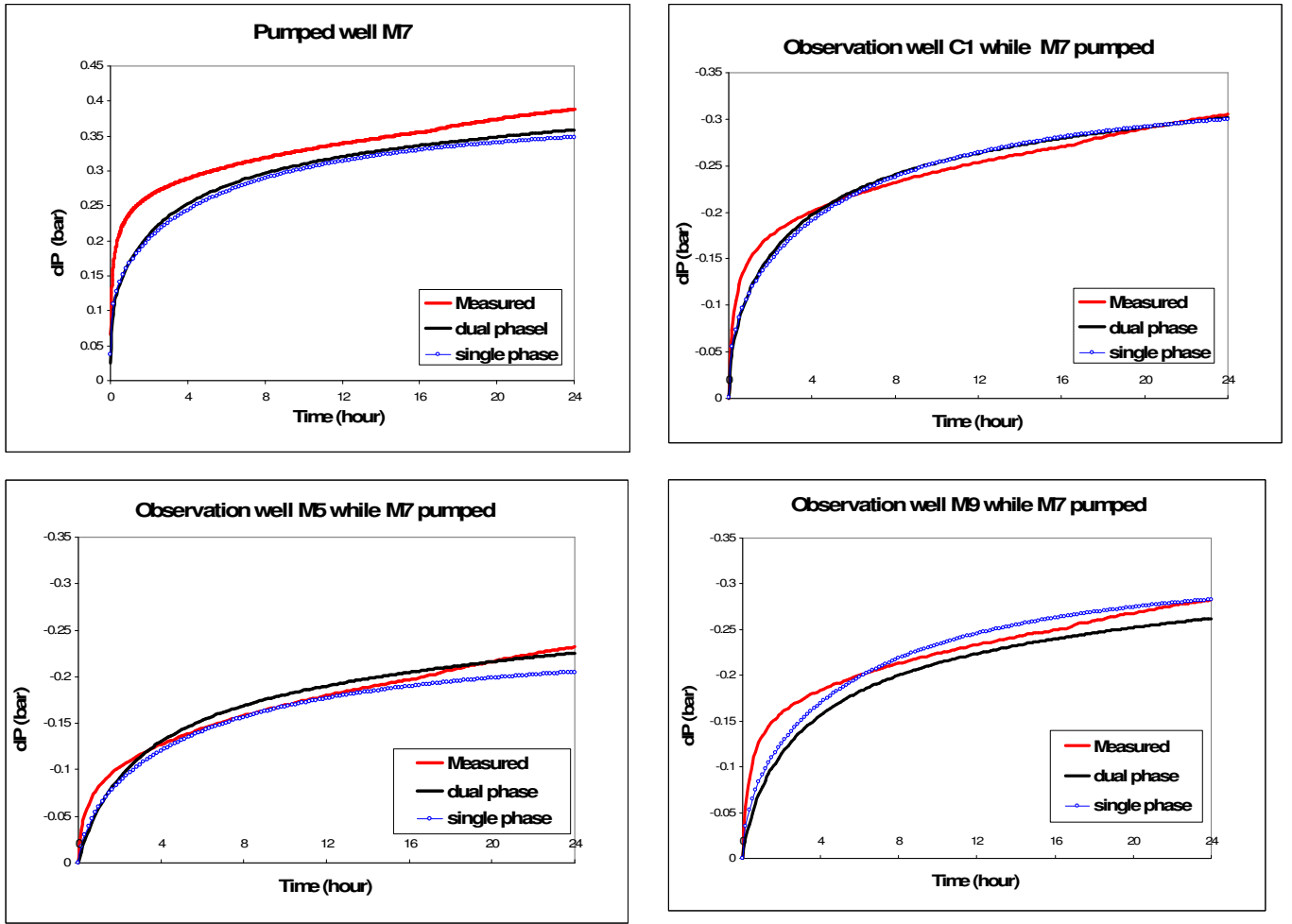


Figure 5.4: Comparison of results of combined (single-phase) calibration (GDM and Petrophysical inversion in a single phase) to the results of firstly-designed calibration method (dual step *i.e.*, Petrophysical inversion and then GDM). Evolution of the pressure drop dP (bar) versus time (h) for the pumped well M7 and selected observation wells during the first 24 hours .

5.3. Impact of the parameterization on the calibration performance

Herein the sensitivity of calibration to the number of deformation parameters is studied in order to analyze and optimize the gradual deformation method. To do so, the same convergence constraints are used and global, forwarded by local gradual deformation steps are performed with only 1 deformation parameter instead of 4 initially. The results and performances are compared between both options.

The initially-calibrated model in terms of petrophysical properties is used again for this step. The gradual deformation method is performed again globally and locally using one parameter of gradual deformation method. The simulated pressure curves after gradual deformation method are compared to those from the initial petrophysical inversion and field data (Figure 5.5). The global gradual deformation with one parameter can reproduce fairly well the field pressure measurements. The adjusted pressure curves of observation wells C1 and M5 can match the measured data satisfactorily, however some small differences remain for pumped well M7 and observation well M9.

Subsequently, the local gradual deformation with one parameter is performed in the same sub-area as previously defined for the deformation with 4 parameters. This area contains pumped well M7 and well M9 that are not fully adjusted by global gradual deformation method. The adjusted pressure curves are also plot in Figure 5.5. The local gradual deformation using only one parameter of gradual deformation does not really improve the matching of these wells.

The global gradual deformation efficiency using one parameter of gradual deformation is compared with that of the global gradual deformation using 4 parameters for 3 previously-selected wells and for 3 other wells (Figure 5.6). The global gradual deformation with one parameter is slightly less efficient than deformation with 4 parameters. Data of wells M4, M9, MP4 and MP6 are more roughly fitted by simulations from deformation with one parameter than with four parameters. However the pumped well M7 is slightly better matched by using one parameter.

The efficiency of local gradual deformation using 1 parameter is now compared to that with 4 parameters in the sub-area of wells M7 and M9 (Figure 5.7). As for global deformation, the local deformation with one parameter is less effective than with 4 parameters.

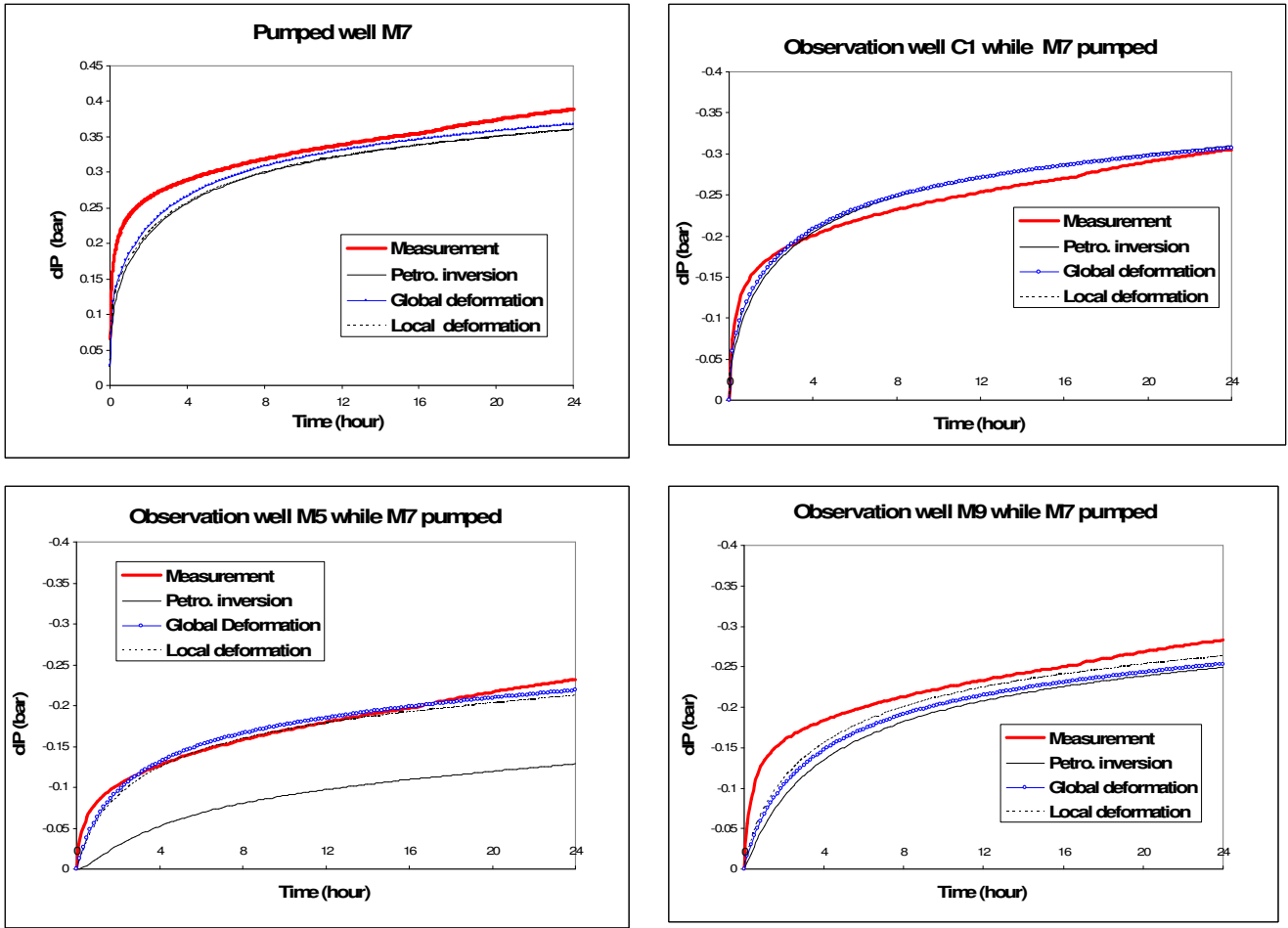


Figure 5.5: Comparison of simulated pressures after petrophysical inversion or gradual deformation of facies, with field data: Global and local gradual deformation are performed with only one parameter. Evolution of the pressure drop dP (bar) versus time (h) for the pumped well M7 and selected observation wells during the first 24 hours.

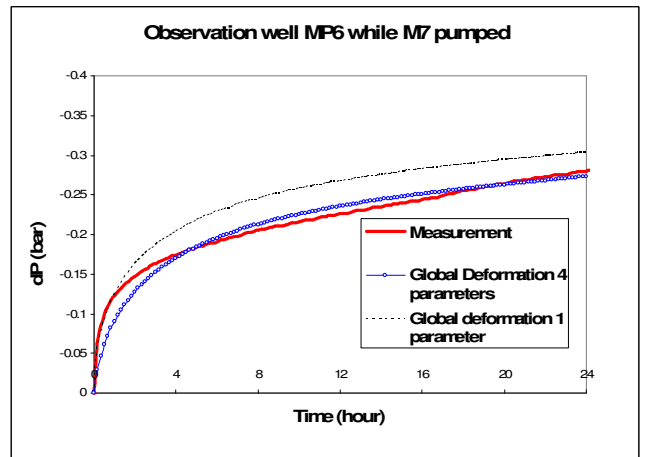
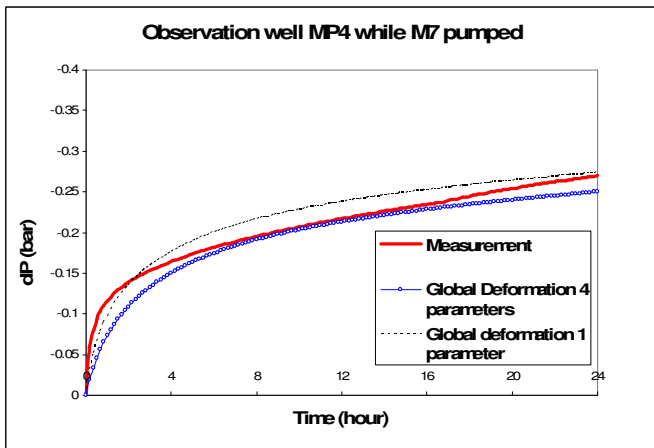
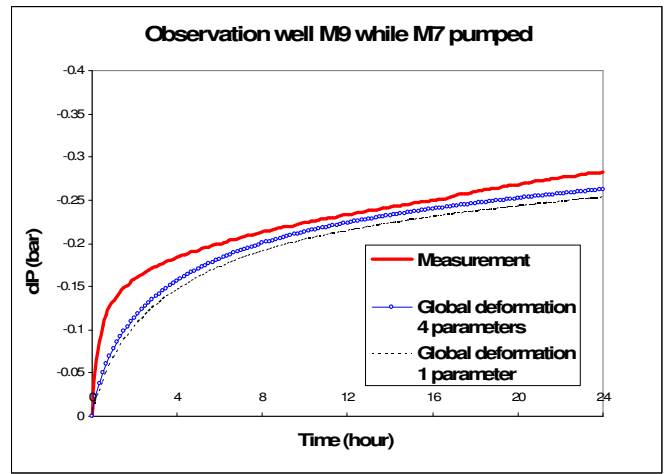
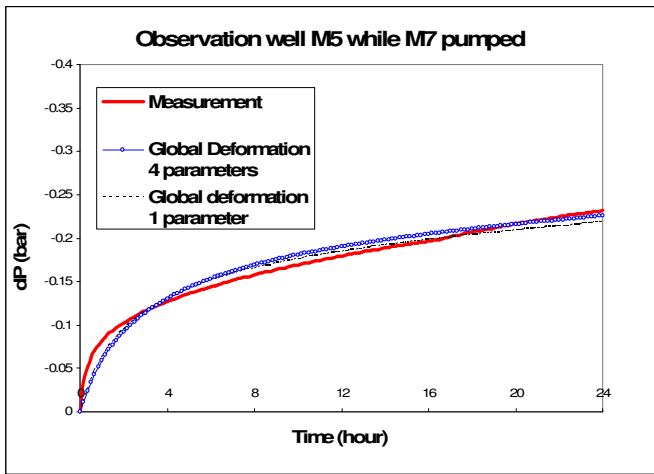
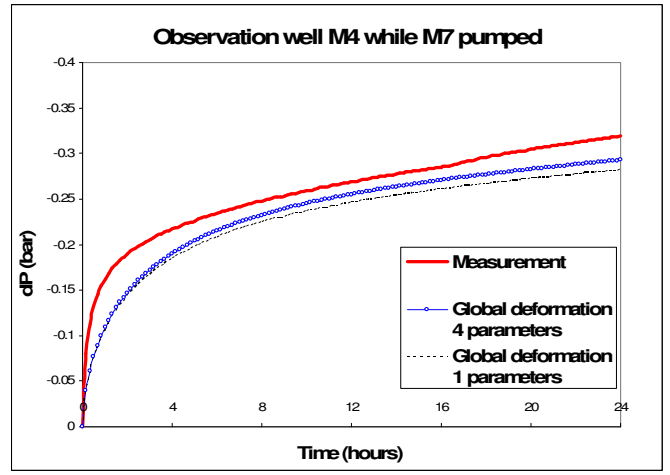
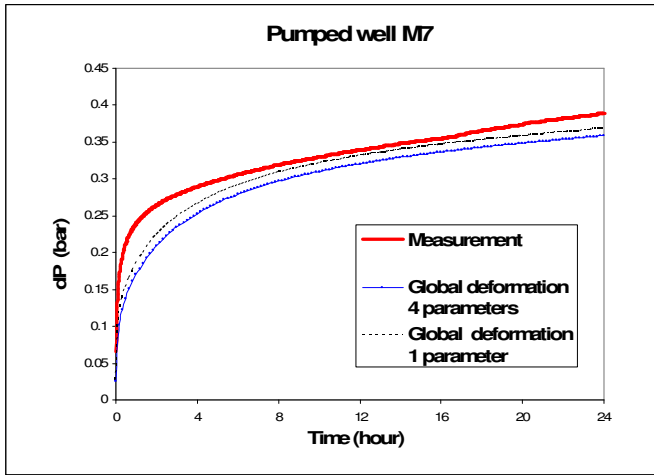


Figure 5.6: Comparison between the results of global gradual deformation with one parameter and that with four parameters. Evolution of the pressure drop dP (bar) versus time (h) for the pumped well M7 and selected observation wells during the first 24 hours.

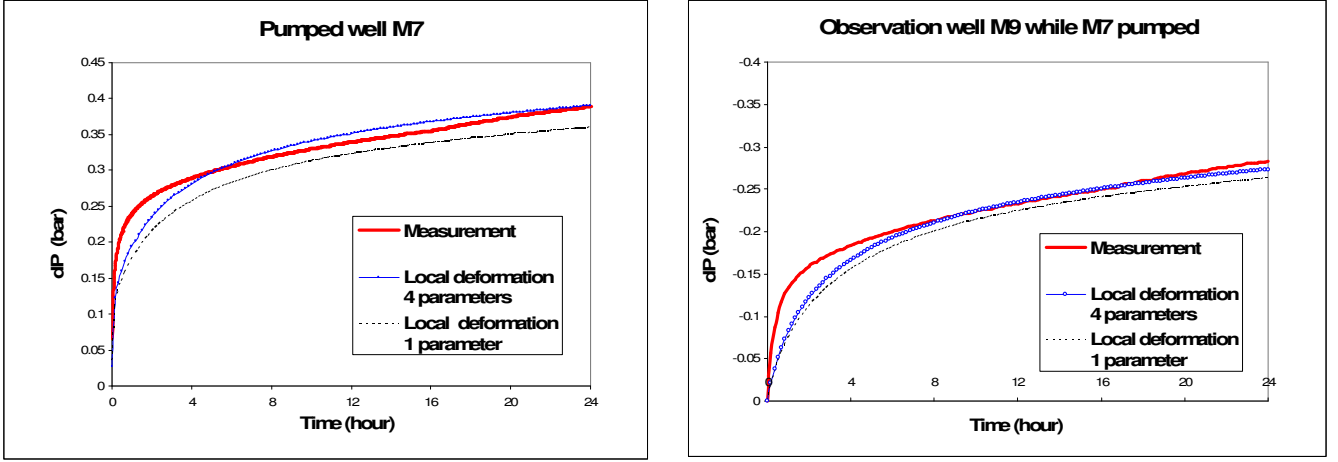


Figure 5.7: Comparison between the results of local gradual deformation with one parameter and that with four parameters. Evolution of the pressure drop dP (bar) versus time (h) for the pumped well M7 and observation well M9 during the first 24 hours.

5.4. Optimization efficiency and computation times

Herein we study the performance of our different calibration techniques. For each of the 3 options ((i) petrophysical calibration followed by gradual deformation, (ii) gradual deformation followed by petrophysical inversion, (iii) combined (global) gradual deformation and petrophysical inversion), the following information is analysed: the number of iterations (including details for the gradual deformation steps: number of flow simulations in each step of gradual deformation, number of steps), the corresponding evolution of the objective function and the computation times (CPU).

5.4.1. Optimization parameters

The convergence criterion, the maximum number of simulations and the selected optimization algorithms for the petrophysical inversion in WELGEM are given in Figure 5.8. The optimization parameters used in CONDOR are also presented in Figure 5.9. This Figure gives specific optimization settings and gradual deformation components. All these components have been extensively described in chapter 2.

Numerical parameters for optimization

Convergence criterion :

Max number of simulations :

Method

☒ G. NEWTON
 ☐ STEEPEST-D
 ☐ F. POWELL
☐ LEVENBERG-MARQUARDT

Figure 5.8: Optimization settings for WELGEM petrophysical inversion .

Optimization Settings

☐ Perform global search to initialize optimization GS Settings ...

Optimization algorithm	POWELL
Maximum number of simulations	20
Convergence criterion	0.01
Minimal parameter step	0.01
Maximal parameter step	1.0

☒ Gradual Optimization

Select gradual deformation components

Maximum number of optimizations	5
Maximum number of failures	3
Objective Function stopping criterion (fraction of initial OF)	,10000E00
Objective Function decrease ratio	,99999998E-02

☐ **Distribute Simulations**

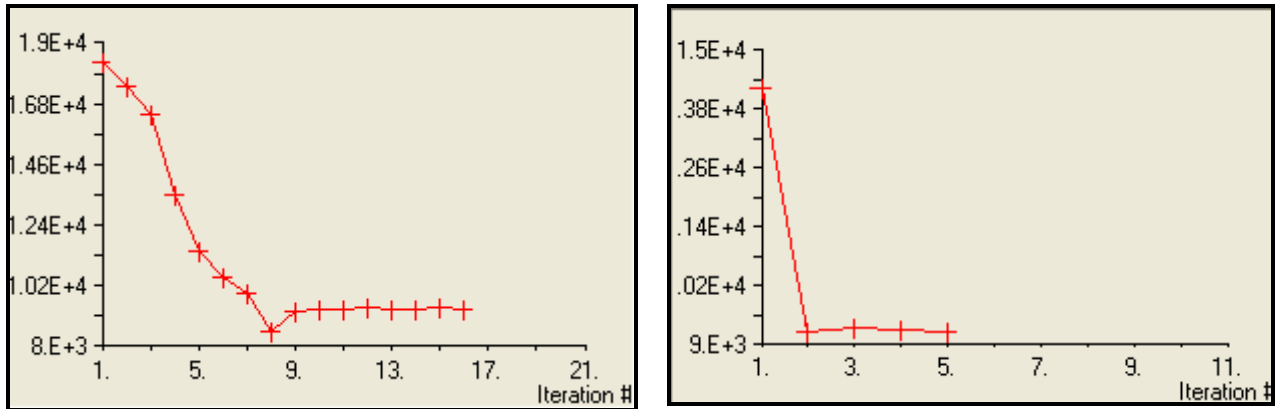
Figure 5.9: Optimization settings for gradual deformation (CONDOR platform).

5.4.2. Performance analysis of the first sequential calibration method

5.4.2.1. Step 1: Petrophysical calibration

Using the first sequentially-designed method, the petrophysical property inversion is performed before gradual deformation of facies .

First, attention is drawn on the fact that detailed facies model is expensive in terms of computation times and CPU requirements. Regarding the initial detailed facies model, the petrophysical property inversion of each facies took more than 48 hours to be performed completely while the lumped facies model could be calibrated to well data much more rapidly (6 hours). The evolution of the objective function with respect to the iteration number is shown in Figure 5.10.



Detailed model inversion, computation time: 48 hours,
number of iterations: 16

Lumped model inversion, computation time: 6 hours,
number of iterations: 5

Figure 5.10: Objective function evolution for petrophysical property inversions: Objective function for detailed facies model inversion to the left and objective function for lumped facies model inversion to the right.

5.4.2.2. Step 2: Global gradual deformation (4 parameters)

The next step is the gradual deformation method using 4 parameters. It is reminded that each gradual deformation optimization is composed of some optimization steps and each is applied to a given set of geostatistical realizations. Each step involves several simulations that are

performed for minimizing the objective function. Initial simulations are performed at the beginning of each step to compute the numerical gradient of the objective function with respect to the deformation parameters. The number of simulations refers to the total number of simulations including those used to compute the numerical gradients of the objective function.

This total number of simulations is representative of computation times and CPU needs. Regarding the optimization process, the number of iterations refers to the number of simulations excluding the initial simulations used for numerical gradient computation. Here, the objective functions are presented with respect to the number of iterations, *i.e.* excluding the initial simulations used for numerical gradient computation.

The evolution of the objective function for gradual deformation with 4 parameters after petrophysical calibration is shown in Figure 5.11 for some selected wells. The gradual deformation is done in five steps (each step is marked by a relaunching of the search of equiprobable realisations from the optimal solution sought at the preceding step (see chapter 2)) including 72 simulations and 32 iterations (effective simulations). The best results are obtained after 69 simulations from a total number of simulations equal to 72. The calibration takes 10 hours to be completed.

Figure 5.12 shows the relative contribution of well data series in the evolution of the objective function. The contribution to the objective function differs from one well to the other and changes also during the whole run. For instance, well M5 contributes much more than the other wells initially while at the end, well M2 contributes more.

5.4.2.3. Step 3: Local gradual deformation (4 parameters)

The local gradual deformation was performed afterwards. This calibration consists of 2 steps performed through 28 simulations including 11 iterations (effective simulations). The best simulation is obtained at the last simulation (simulation number 28). The calibration takes 5 hours to be completed.

Similarly, Figure 5.13 shows the relative contribution of well data series in the evolution of objective function for local gradual deformation of facies with 4 parameters.

5.4.2.4. Gradual deformation with 1 parameter

As discussed before, the gradual deformation was performed again globally and locally by using only one parameter of deformation instead of 4. The global gradual deformation method consists of 19 steps for a total of 111 simulations (best calibration at simulation number 111) and 82 iterations (effective simulations). The calibration process takes 14 hours to be performed completely. The local gradual deformation consists of 14 steps of a total of 91 simulations (best calibration at simulation number 82) and 66 iterations and it takes 10 hours to be completed.

Similarly, the evolution of the objective function with the iteration number is shown in Figure 5.11 and compared to its equivalent with 4 parameters of deformation. As observed earlier, the efficiency of gradual deformation with one parameter appears less satisfactory and also more time consuming than with 4 parameters.

Objective functions relevant to local gradual deformation with one or 4 parameter(s), are shown in Figure 5.14. Again the local gradual deformation with one parameter is less efficient than with four, as it requires much more simulations to reach the assigned convergence criterion value.

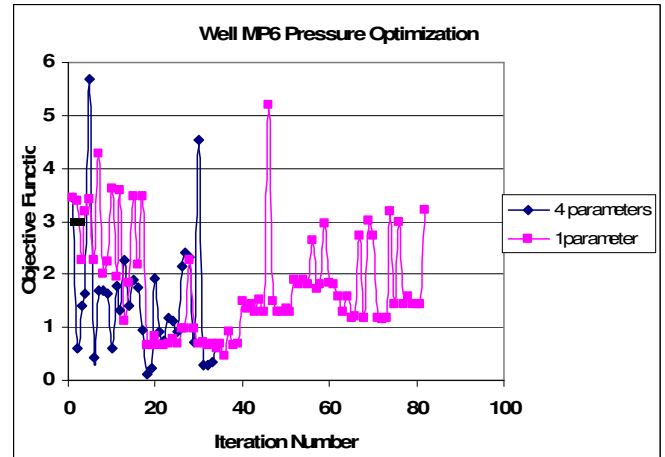
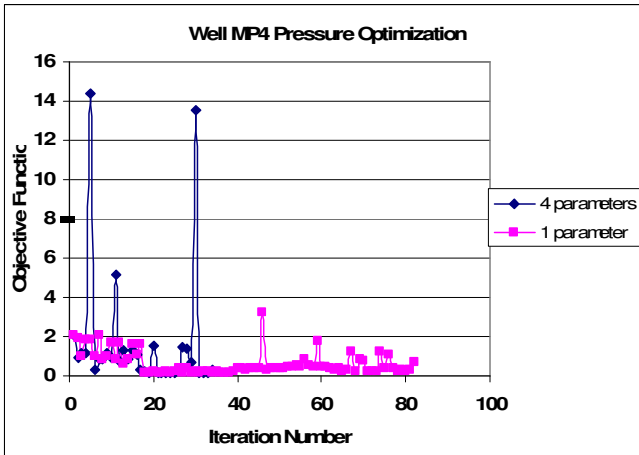
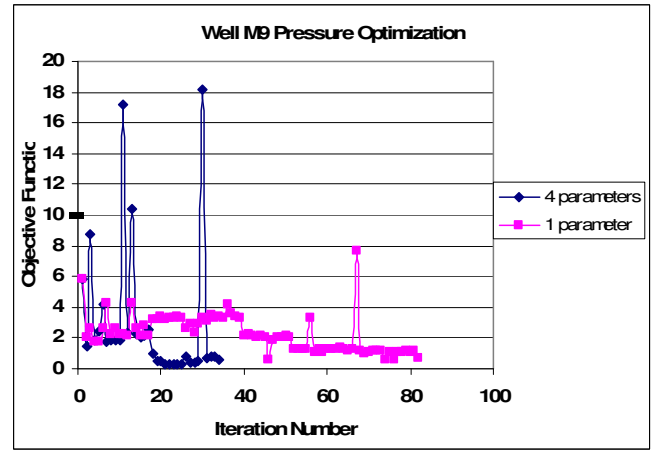
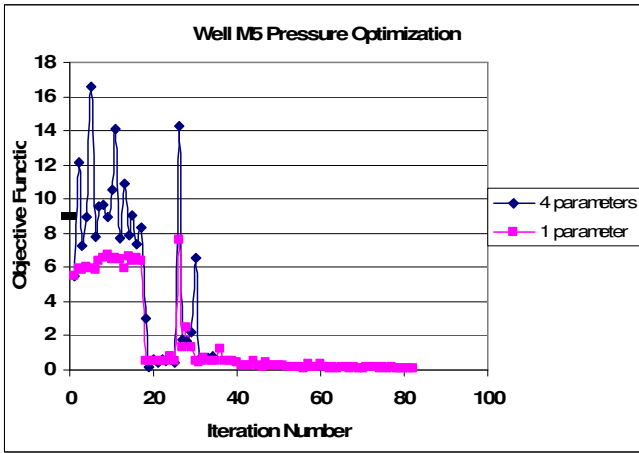
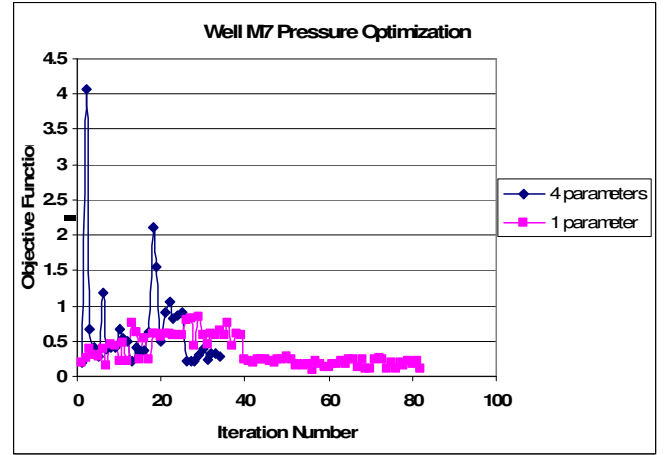
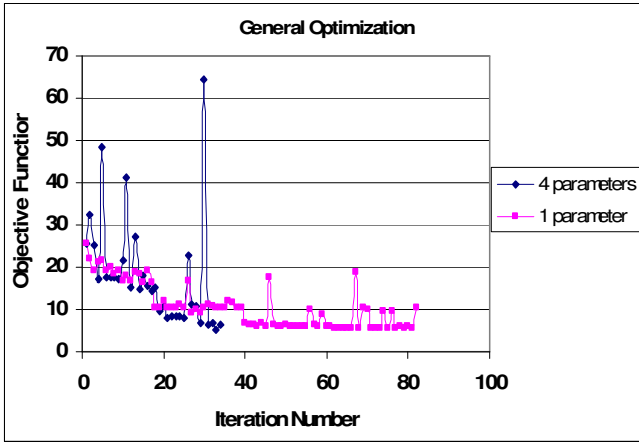


Figure 5.11: Evolution of the objective function for the lumped-facies model during global gradual deformation. Comparison between optimizations with one and four 4 parameter(s) of gradual deformation. Evolution of the objective function with the iteration number for all wells together and for selected observation wells.

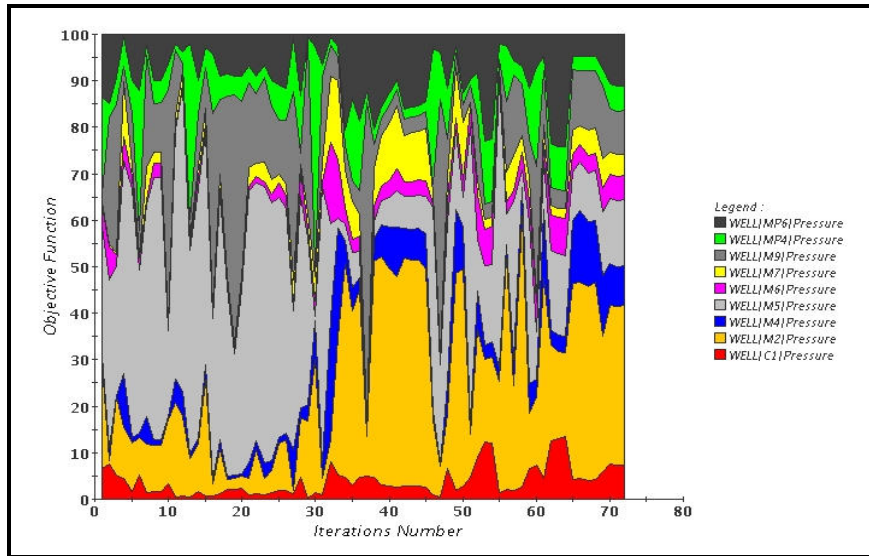


Figure 5.12: Relative contribution of well data series in the objective function evolution for global gradual deformation with 4 parameters.

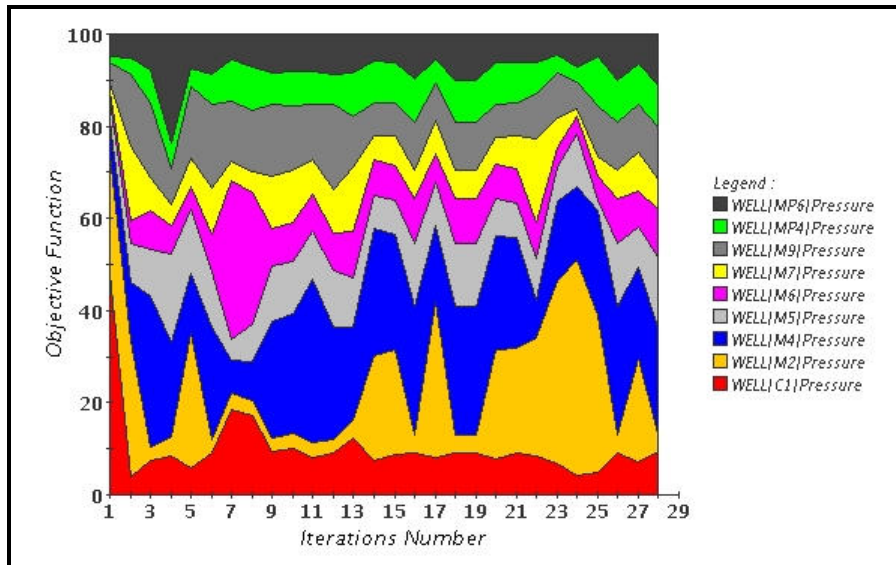


Figure 5.13: Relative contribution of well data series in the objective function evolution for local gradual deformation with 4 parameters.

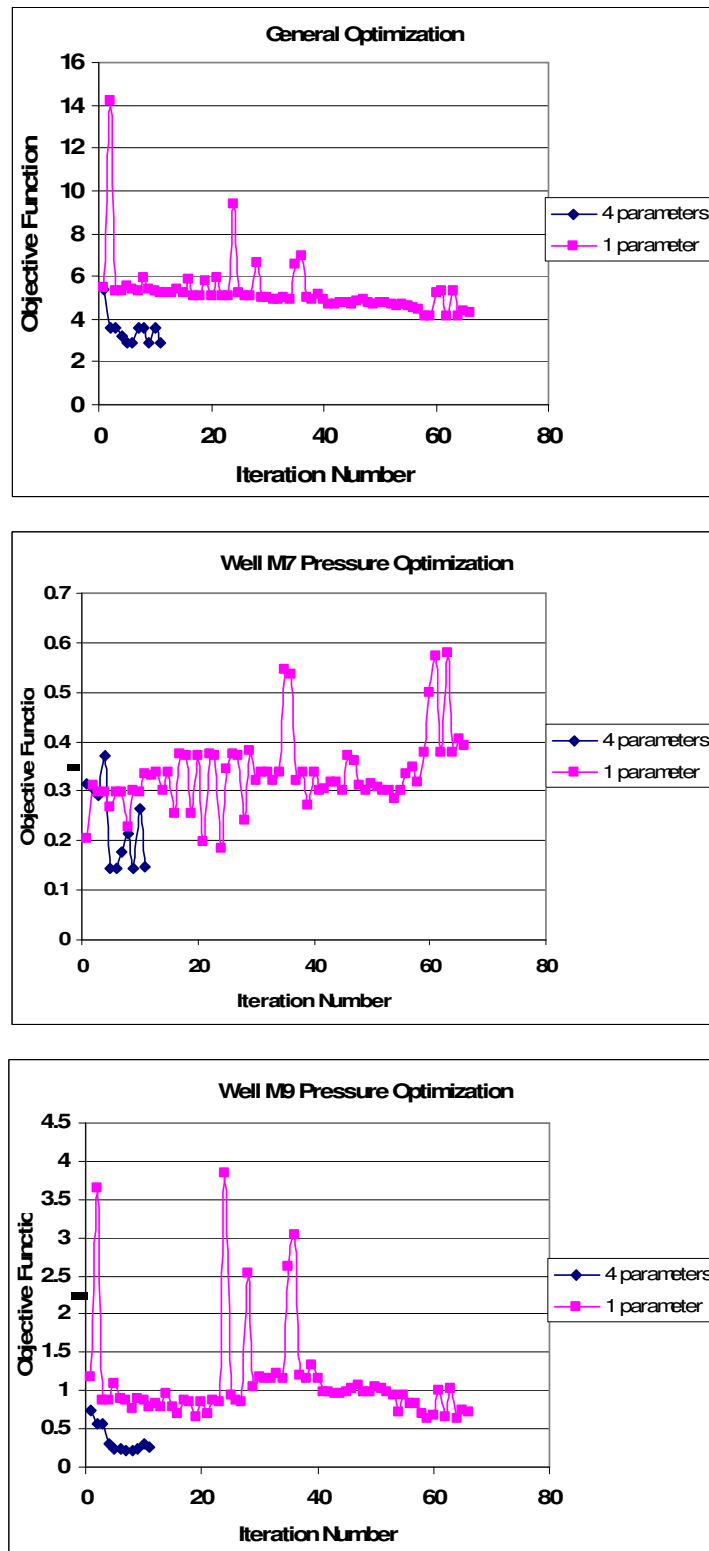


Figure 5.14: Evolution of the objective function for the lumped-facies model during local gradual deformation. Comparison between optimizations with one and four 4 parameter(s) of gradual deformation. Evolution of the objective function with the iteration number for all wells together and for the wells in the deformation area.

5.4.3. Performance analysis of gradual deformation followed by petrophysical inversion

As described before another sequential methodology has been examined, where gradual deformation is done before petrophysical inversion. This gradual deformation was performed using the detailed facies model and consisted of 5 steps including a total of 56 simulations and 27 iterations taking 7 hours to be completed. The evolution of the objective function is shown in Figure 5.15 for the overall optimization and for different wells considered individually. Afterwards, the petrophysical inversion of the lumped model facies was performed through 11 iterations and took 4 hours to be completed. Remind however, this methodology does not lead to acceptable results. Gradual deformation cannot tune the flow paths with "wrong" rock properties. Figure 5.15 shows that the objective function does not decrease sufficiently for several wells.

5.4.4. Performance analysis of combined (global) gradual deformation and petrophysical inversion

As evoked before, combined gradual deformation and petrophysical inversion are here performed simultaneously and not sequentially. This combined (single-phase) calibration is performed on the detailed facies model. Although the calibration of a detailed facies distribution seems expensive, this combined calibration revealed to be satisfactory in terms of efficiency and computation time. The calibration involved 5 steps of deformation including 186 simulations taking 10 hours to be completed. The evolution of the objective function with respect to the simulation number is illustrated in Figure 5.16.

Finally, a summary of performance of all calibration techniques are presented in Table 5.3.

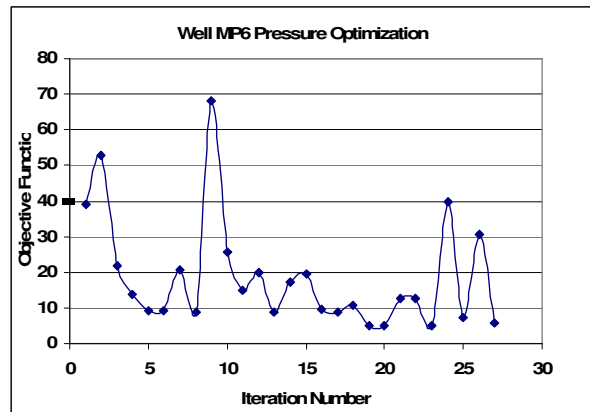
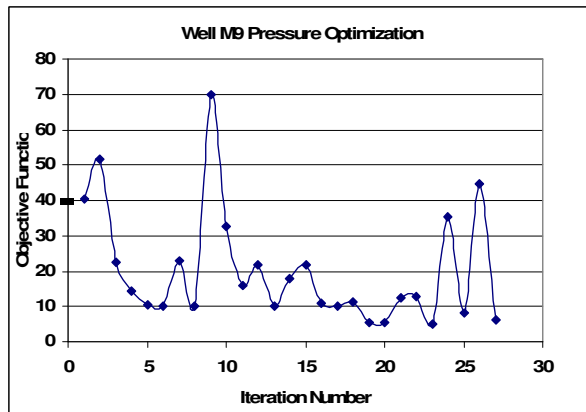
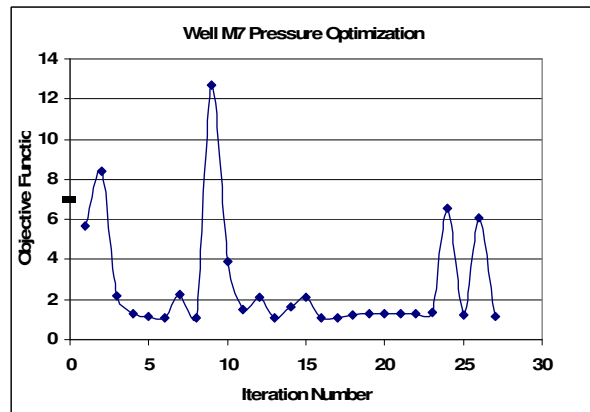
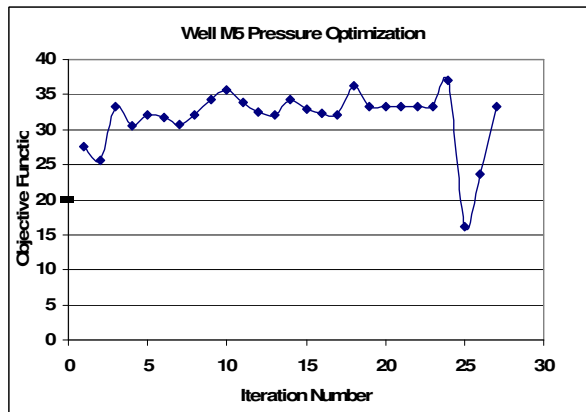
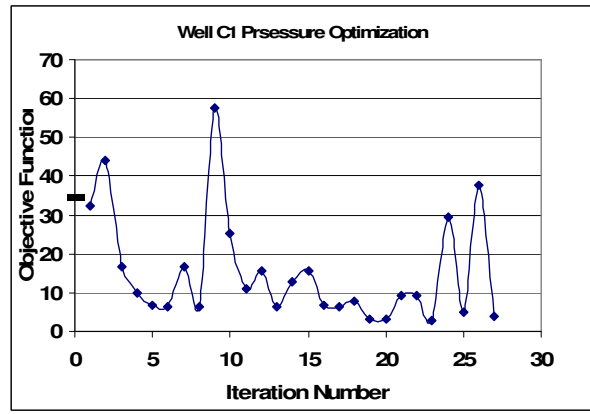
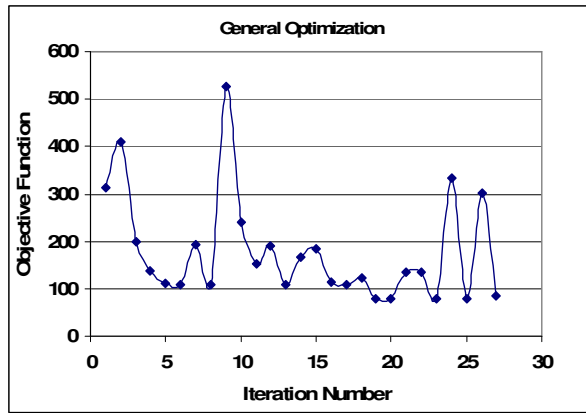


Figure 5.15: Evolution of the objective function when gradual deformation (with 4 parameters) is performed before petrophysical inversion. Evolution of the objective function with the iteration number for all wells together and for selected observation wells.

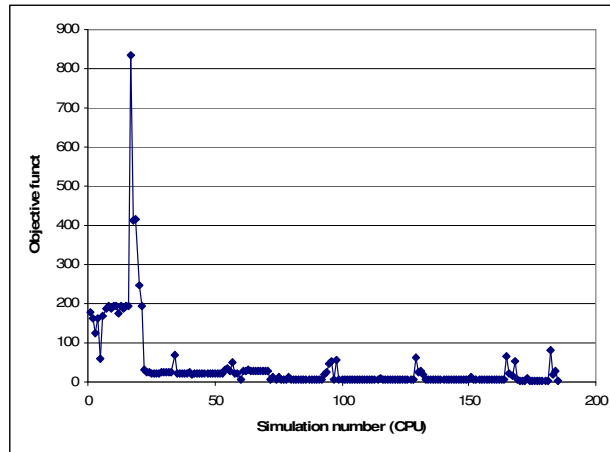


Figure 5.16: Evolution of the objective function for the lumped facies model by using the gradual deformation method and petrophysical inversion mixed together.

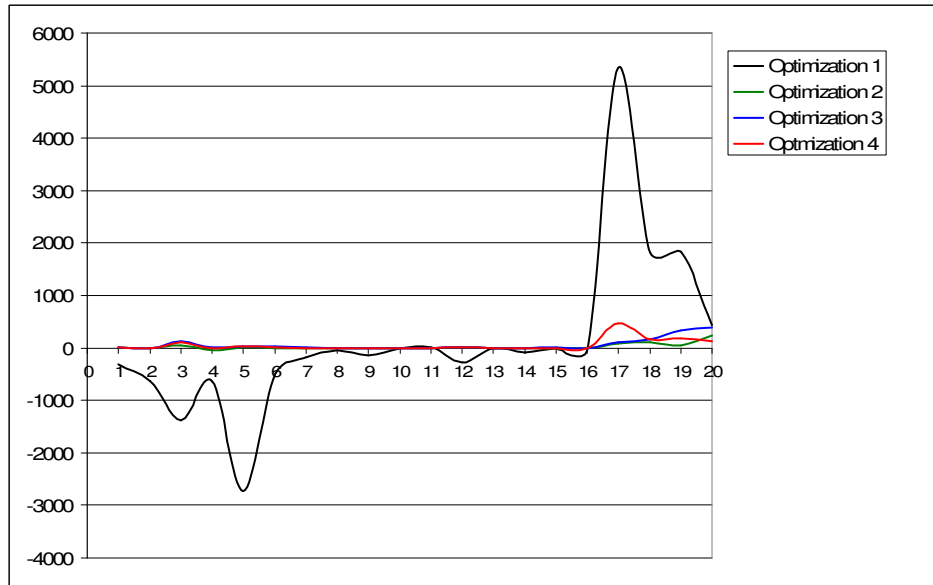
Table 5.3: Summary of performance for all optimization techniques. "Petro. Inv." stands for petrophysical inversion and "GD" stands for gradual deformation

	Petro. Inv.	Global GD	Local GD	Total
Petro. Inv. before GD (4 parameters)	detailed model 16 iterations 48 hours			
	lumped model 5 iterations 6 hours	detailed model 72 simulations 32 iterations 5 optimizations 10 hours	detailed model 28 simulations 11 iterations 2 optimizations 5 hours	105 simulations 47 iterations 7 optimizations (GD) 21 hours
Petro. Inv before GD (1 parameter)	lumped model 5 iterations 6 hours	detailed model 111 simulations 82 iterations 19 optimizations 14 hours	detailed model 91 simulations 66 iterations 14 optimizations 10 hours	207 simulations 148 iterations 33 optimizations (GD) 30 hours

	GD	Petro. Inv.		Total
GD before Petro. Inv. (4 parameters)	detailed model 56 simulations 27 iterations 5 optimizations 7 hours	lumped model 11 iterations 4 hours		67 simulations 38 iterations 5 optimizations (GD) 11 hours
combined (GD-Petro. Inv.) detailed facies (4 parameters)				detailed model 186 simulations 5 optimizations 10 hours

5.4.5. Sensitivity of the objective function to calibration parameters

Hereafter, the combined (single-phase) calibration is considered. The goal is to analyze the evolution of the objective function with respect to each calibration parameters, including petrophysical and gradual deformation parameters. As shown by Figure 5.17, the first optimization reveals a significant sensitivity to permeability and deformation parameters.



1	2	3	4	5	6	7	8	9	10
KX8	KX6	KX5	KX4	KX3	KX2	KX1	PHI4	PHI3	PHI2

11	12	13	14	15	16	17	18	19	20
PHI1	KX7	PHI8	PHI7	PHI6	PHI5	p1	p2	p3	p4

Figure 5.17: Gradient of the objective function with respect to calibration parameters for different steps. The numbers 1 to 20 state for the different calibration parameters. The related parameters are given on the bottom of each number. The p1 to p4 represent the 4 parameters of gradual deformation.

Once the first optimization step ends, the next steps seem to be rather sensitive to the gradual deformation parameters than to the petrophysical parameters. This is consistent with the fact that petrophysical inversion performed before gradual deformation led to a more satisfactory calibration than the reverse sequence (gradual deformation before petrophysical inversion).

5.5. Testing other flow models to better capture flow paths

As shown in the previous chapter, the responses to interference testing in both pumped and observed wells for the first hours of pumping could not be reproduced completely by a single-porosity flow model. The reason evoked is that cells of the numerical flow simulator may enclose both thin conductive layers and rock matrix. When these cells are assigned with the so-called "water" facies, the size of this facies is overestimated and obviously the design in space of this conductive network is much more rough than the real one. Therefore, as a first alternative flow modelling of that Site, it is worthy to test a dual medium approach to see whether or not simulations are improved.

Secondly, according to previous experience of well modelling in fractured reservoirs (Ding *et al.*, 2006), the origin of the early-time discrepancy between model prediction and field measurements could be linked to both the rough geometry of conductive bodies and the specific 3D geometry of radial flow around pumped wells. An accurate simulation of the transient pressure behaviour would require a detailed representation of the thin flow paths feeding the wellbores with high-resolution grids.

A third approach is to build an object-based model. An object-based model of the thin conductive flow-paths in the near-wellbore area would allow to design and then compute a representative relationship between the well rate and the near-wellbore pressure drop. Short-term transient responses could then be taken into account efficiently.

Hereafter, a dual porosity approach and a model with a refined calculation grid are tested.

5.5.1. Testing a dual-porosity representation

As evoked already, the dual-medium approach is based on the superposition of two equivalent media, a "fracture" medium characterized by a high permeability k^f and a low porosity ϕ^f , and a "matrix" medium characterized by a low permeability k^m and but a high porosity ϕ^m . A matrix block size must also be defined to simulate transfers between the two media.

A dual-porosity model of the EHS is directly built from the previously-calibrated-deformed single-porosity model by splitting its single-medium cells into dual-medium cells, with a “matrix” cell standing for the tight facies and a “fracture” cell standing for the conductive “water” facies when present. This conversion assumes that the “water” cells of the previous single-porosity model were standing for both the conductive “water” facies and some porous and tight material. On the opposite, any conductive flow path is still assumed absent from the tight facies (facies 1) cells. With these assumptions, the initial petrophysical values of the dual-medium cells of facies 1 or 2 are derived from the inverted single-medium model as shown in Table 5.4.

With the dual-medium representation it is expected that the flow simulation is able to calculate transient flows occurring locally within small-scale highly-conductive diagenetic features, and between the porous carbonate matrix and those conductive features.

The benefit of this dual-porosity approach is then tested by inverting only the petrophysical properties of the “water” dual-medium cells actually standing for two distinct media. The main unknowns are the actual “fracture” medium properties k_2^f, ϕ_2^f , and the “matrix” block size, a_2 . The other petrophysical properties are kept constant at their predetermined values. Results in terms of parameters are given in Table 5.5. The adjusted pressure curves are compared to those of the single-medium approach in Figure 5.18.

The calibration of a dual-porosity model does not much improve the pressure matching compared with the single-porosity model. The pressure evolution during the first hours of the test is only slightly improved by using a dual-medium representation of the reservoir, and the overall predicted pressure trend by both models remain quite similar. The flow-property contrast between the two facies, 1 and 2, can be simulated by a single-porosity model with a sufficient accuracy, even this model is coarsely discretized compared with the real geometry of conductive bodies and size of the conductive “water”-facies bodies.

The origin of the contrasted short-term transient pressures between the field and models may then be found elsewhere. Actually, the most probable origin of such a difference lies in the complex near-wellbore flow geometry that is not properly accounted for in classical flow simulators. These models use conventional productivity formula (Peaceman, 1978) based on a

radial flow equivalence. However, a recent study (Ding *et al.*, 2006) referring to the simulation of wells in fractured reservoirs showed that 1- high flow simulation errors could result from radial flow equivalence and 2- errors could be greatly reduced by computing near-well flows on the actual/representative discrete fracture network present in the wellbore vicinity. Were it available, it would unfortunately be impossible to represent such a network with a finite-difference model.

Table 5.4: Initialization of the dual-porosity model parameters from the calibrated single-porosity model results.

facies number	fracture permeability (mD)	fracture porosity	matrix permeability (mD)	matrix porosity	matrix block size (m)
1	$k_1^f = k_1^0 = 100$	$\phi_1^f = \phi_1^0 = 0.15$	$k_1^m = k_1^0 = 0$	$\phi_1^m \approx 0$	$a_1 \approx 10^6$
2	$k_2^f = k_2^0 = 895536$ to be inverted	$\phi_2^f = \frac{1}{10} \phi_2^0$ to be inverted	$k_2^m = k_1^0 = 100$	$\phi_2^m = \phi_1^0 = 0.15$	$a_2 \approx 3m$ to be inverted

Table 5.5: Results of the petrophysical property inversion of the dual-porosity model.

facies number	k_2^f (mD)	ϕ_2^f	matrix size(m)	block
1	-	-	-	
2	849984	0.019	3.001	

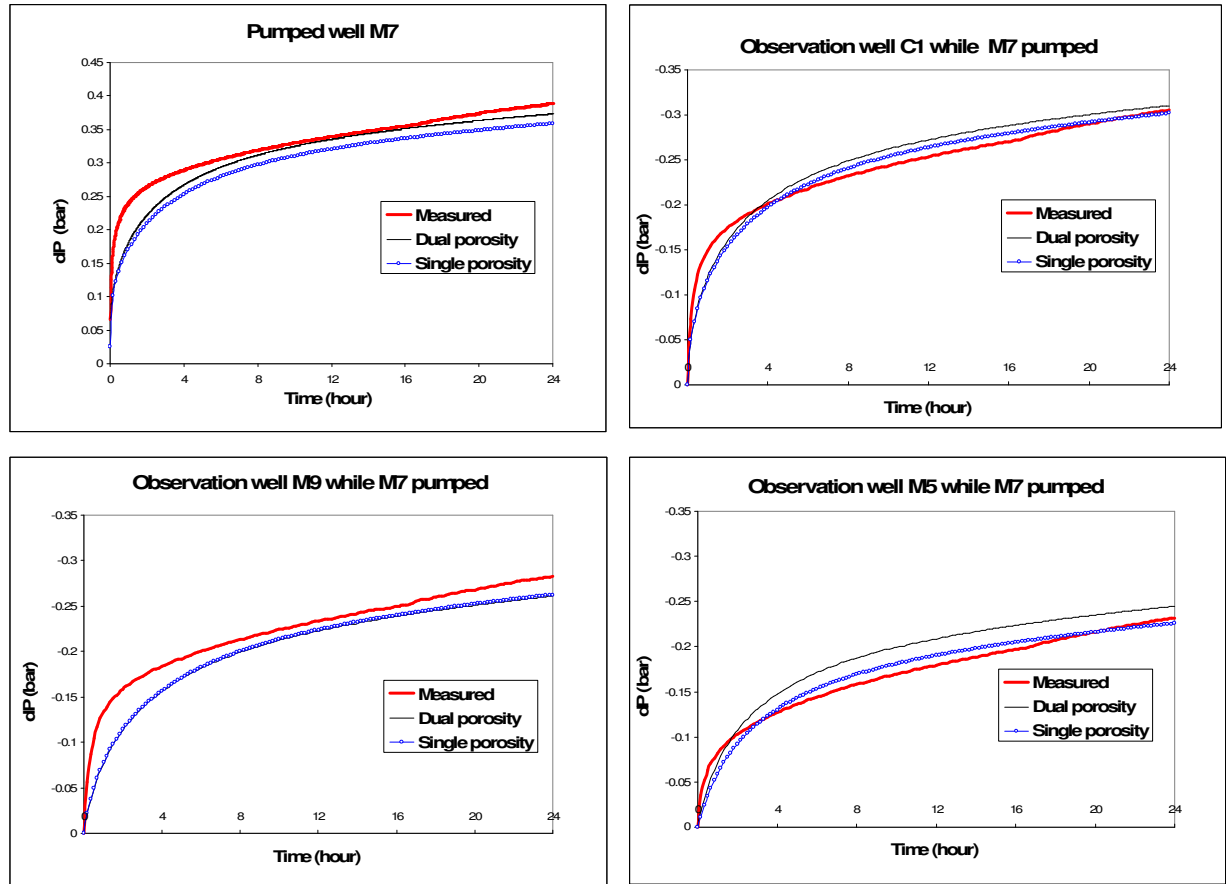


Figure 5.18: Comparison between the inversions of the dual-porosity and the single-porosity models of the Site. Variation of pressure drop (ΔP) versus time (hour) for well M7 and some interference wells; model calibrated to pumped well M7 and some interference wells for short term period (24 hours).

5.5.2. Refined model

In this part, the second alternative dealing with a refined grid is tested. A vertically-refined model is built and the forward-simulated pressure curves are compared with the pressure curves simulated on the initial coarse model. Grid refinement concerns only the vertical direction, because it aims at better tracking the thin conductive bodies that are often sub-horizontal. The calibrated lumped-facies model resulting from the reference methodology (*i.e.* the model resulting from petrophysical inversion followed by global gradual deformation) is used for testing the sensitivity of simulated well responses to grid refinement.

Facies were re-assigned to the cells of the refined-grid model as follows:

- if "water" is present in the original cell (ix, iy,iz) after division of that cell into 3 cells, "water" facies is reassigned to the central cell only (and "matrix" facies to the other two cells)
- if "matrix" is present in the original cell (ix, iy,iz), "matrix" is reassigned to all 3 cells after cell splitting

The corresponding calibrated petrophysical properties are then assigned to cells according to the nature of the facies. Once that finer flow model is built, the forward simulation of pumping and interference tests (M7 pumping test as before) are performed and compared with results from the coarse grid.

Field data, coarse-grid and fine-grid simulated pressures are compared in Figure 5.19. For all wells, the short-term discrepancy between model and field responses is reduced to some extent by using a vertically-refined grid. This proves that the peculiar near-wellbore flow geometry has to be modelled in detail for an accurate simulation of short-time responses.

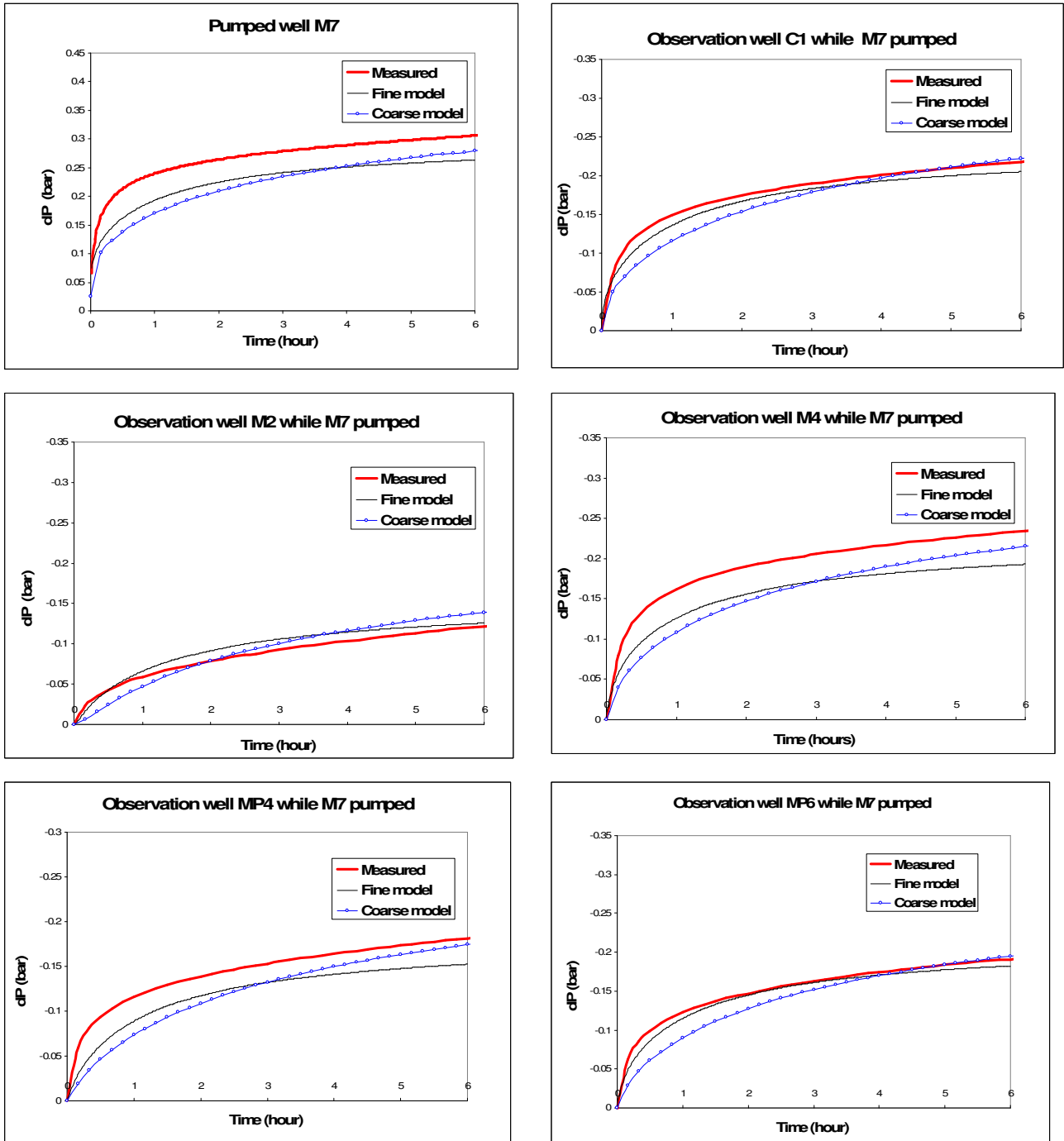


Figure 5.19: Comparison of the simulated pressures from both coarse and refined grids with field data. The fine-grid model is derived from the previously-inversed-deformed coarse model. Evolution of the pressure drop dP (bar) versus time (h) for the pumped well M7 and selected observation wells.

5.6. Conclusion

In this chapter, further studies in terms of methodology effectiveness have been performed. The performance of our optimization techniques has been examined and other modelling aspects have been studied.

An alternate option consisting in a global gradual deformation followed by petrophysical inversion has been examined while using exactly the same data set and the same initial flow model as those of the firstly-designed methodology. The results showed that applying this sequence of calibration could not lead to a good calibration. The point is that the gradual deformation cannot seek the best geometric design of conductive bodies if the latter are not well identified in terms of their hydraulic properties. The availability of a consistent petrophysical model appears essential before performing relevant gradual deformation.

A combined (global) gradual deformation and petrophysical inversion into a single calibration phase has been studied too. Even though this combined calibration was performed using the detailed facies model, the calibration appeared efficient and that combined (single-phase) calibration could reproduce the well responses as well as the firstly-designed method. In other words it could satisfactorily tune both the petrophysical properties and the location of flow paths within the same inversion procedure.

In addition, the sensitivity of calibration to the number of deformation parameters was studied to analyze and optimize the gradual deformation method. The global and local gradual deformation were performed again with only 1 deformation parameter instead of 4 initially. The results showed that the calibration with one parameter is less effective than with four. This single-parameter deformation required more simulations and iterations than a four-parameters deformation.

The performance of different calibration techniques was analysed. For each of the 3 options *i.e.*, petrophysical calibration followed by gradual deformation, gradual deformation followed by petrophysical inversion and combined (global) gradual deformation and petrophysical inversion, quantitative optimization features were reported and compared. The different sequence of calibration by gradual deformation and petrophysical inversion seem to show

analogous performances regardless of the step sequence. However, regarding the minimization of objective function, it is preferable to perform gradual deformation after petrophysical inversion.

A sensitivity study of the objective function to calibration parameters showed that the first optimization is sensitive to both petrophysical properties and gradual deformation parameters. The next optimizations were mainly sensitive to gradual deformation parameters. This is consistent with the conclusion that petrophysical inversion has to be performed before gradual deformation if a sequential calibration procedure is applied.

Eventually, to better capture flow paths and simulate short-time well responses, two alternative flow models were tested, a dual medium approach and a refined-grid model. Adopting a dual-medium flow modelling approach did not change much the simulated pressures. In other words, a single-porosity approach is accurate enough to reproduce satisfactorily the overall/long-term well responses. Then, the conductive facies was modelled more accurately through a vertically refined model. The short-time discrepancy between model and field responses was reduced to some extent, thus showing that the flow geometry around pumped wells had importance for mimicking short-term field data. To improve the knowledge of how flow simulations around wells are improved by an accurate description of conductive bodies, it could be advised to turn toward the implementation of an object-based model. The latter are reputed able to depict complex geometry by "bombing" elementary objects in space.

CHAPTER 6. Conclusion and Perspectives

6.1. Summary of results

A methodology to calibrate the flow model of highly-heterogeneous reservoirs from well test data was designed and tested successfully on data from an actual field Site.

1. **A valuable field data source.** The Experimental Hydrogeological Site (EHS) under consideration constitutes a very instructive multi-disciplinary data-base to set up consistent methodologies for characterizing the hardly-tractable heterogeneity of complex diagenetized reservoirs and for modelling their hydrodynamic behaviour. A geostatistical facies model of this reservoir was generated by integrating all available geological and wellbore core-log data. The numerical representation of the reservoir was done by means of a mono-gaussian distribution of 8 facies related to the deposition of various rock types. An equivalent lumped-facies model made of a tight matrix facies and a conductive facies, was defined from the initial facies distribution. This lumped-model was found to be quite meaningful in terms of fluid flow, considering the channelling effects observed on the Site.

2. **An integrated, specifically-designed flow model calibration methodology.** The main contribution of this work consists in designing and implementing a sequential calibration methodology for a flow model applied to the geostatistical reservoir and by conditioning the model to available dynamic data.

This methodology uses the available well test data, *i.e.* pumping and interference tests for the EHS, as flow constraints and involves the following main steps:

- *Initializing the flow model.* Beside the necessity of incorporating available petrophysical information, derived from core data for instance, special attention has to be awarded to the assignment of realistic values to all other model parameters that are judged unnecessary to be matched or cannot be matched, such as compressibility values in the present application.

As a preliminary calibration step, a proper flow boundary condition has also to be defined to mimic the external fluid recharge. This is all the more important that the reservoir is heterogeneous and the sampled area of small size compared with the influence of hydraulic works providing the data. For the EHS, this was achieved through the petrophysical tuning of a fictitious and distant "source" with parameters calibrated on long-term data of well tests.

Incidentally, the calibration procedure may follow the same methodology as that advocated for fitting the rest of the model.

- *Petrophysical calibration.* Starting from that consistent initial flow model, the petrophysical properties of the constitutive facies are inverted through an optimization algorithm that minimizes the difference between simulated and measured pressure. Generally the responses are analyzed over a time-lag for which the hydraulic test stresses a portion of reservoir consistent with that monitored.

- *Gradual deformation.* Once the flow model is properly calibrated in terms of petrophysical parameters, a gradual deformation technique is applied to improve the geostatistical realization of the reservoir facies distribution, with respect to the same dynamic data as those used for the previous step.

That gradual deformation is first performed globally to improve the facies image of the whole reservoir.

Finally, a local gradual deformation may be applied to refine the facies distribution in selected sub-areas where well responses remain poorly-matched.

3. Methodology effectiveness. The above methodology was robust and effective in calibrating the EHS flow model to the observed pressure responses measured on the Site wells:

- The multiple unknowns of that highly-undetermined flow problem were fixed in a sequence taking into account the main parameters impacting flow, starting with a petrophysical property inversion.
- Applying the gradual facies deformation globally then locally improved the matching of field data that were not fitted correctly by the sole petrophysical calibration.
- The reliability and robustness of the resulting model was proven from its fairly-good capability to predict the hydraulic response of other wells than those serving as constraints to the inversion. Obviously, the more well data constraints are used in the objective function, the more predictive the resulting calibrated model will be, provided that those additional wells actually improve the detection and description of flow heterogeneities.
- The reasonable number of iterations required for calibrating or deforming a model ensures the practical applicability of that methodology.

To conclude on this flow inversion/simulation methodology, it appears as an efficient approach to draw the best of both static/geological and dynamic/flow information for modelling the flow behaviour of hardly-tractable reservoirs as karstic fractured aquifers.

The above methodology was discussed and further analyzed in terms of reliability and numerical performance, in order to assess and enlarge its range of application.

4. Assessment of the sequential calibration methodology.

The *sequence of calibration* starts from a flow model including available core petrophysical data, a calibrated source facies properties and calibrated compressibilities. Several sequences of subsequent steps have been addressed to see whether or not they could improve results from the sequence tested above, *i.e.* petrophysical calibration and then gradual deformation.

- Another option consisting in a global gradual deformation followed by petrophysical inversion has been examined using exactly the same data set and the same initial flow model as that of the firstly-designed methodology. The results showed that applying this sequence of calibration did not yield good calibration. The availability of a consistent petrophysical model before gradual deformation seems to be essential to perform gradual deformation.
- A combined (global) gradual deformation and petrophysical inversion in a single inversion phase has been studied too. Even though this combined calibration was performed using the detailed facies model, the calibration seemed effective and that combined (single-phase) calibration could reproduce the well responses as well as the firstly-designed method.
- A sensitivity study of the objective function with respect to calibration parameters showed that the first optimization is sensitive to both petrophysical properties and gradual deformation parameters. The next optimizations were mainly sensitive to gradual deformation parameters. This result supports the preceding observation stating that petrophysical inversion has to be performed before gradual deformation if a sequential calibration procedure is applied.

Impact of parameterization: the sensitivity of calibration to the number of deformation parameters was also studied. The global and local gradual deformation were performed again with only 1 deformation parameter instead of 4 initially. The results showed that the calibration with one parameter is less efficient than with four. This single-parameter deformation required much more runs than with four parameters.

The ***numerical performance*** of the calibration procedures was analysed. For each of the 3 sequences, the quantitative optimization features were reported and compared. The different sequences of calibration by gradual deformation and petrophysical inversion seem to show analogous performances regardless of the schedule of steps. However, regarding the quality of optimization, it is preferable to perform gradual deformation after petrophysical inversion.

5. Improving the flow model to better capture flow heterogeneities (flow paths) and short-time transient well responses.

a. **Adopting a dual-medium representation of the karstic aquifer.** The dual-medium modelling approach did not change much the simulated pressures. A single-porosity flow modelling approach is accurate enough to reproduce satisfactorily the overall/long-term well responses.

b. **Refining a single-medium representation of the karstic aquifer.** To better capture flow paths, the conductive facies was modelled more accurately by using a vertically-refined grid. This recipe reduced slightly the discrepancies between data and pressure simulations, especially in the close vicinity of the pumped well. This result advocates for the precision required in terms of grid geometry to get relevant results for very transient flow close to stressed wells.

6.2. Perspectives of future developments and research.

1. Object-based modelling. The transient well responses measured during the first hours of pumping and interference tests could not be reproduced by a single-porosity flow model that artificially enlarges the thin discrete conductive flow paths of the reservoir. According to previous experience of well modelling in fractured reservoirs, the origin of such initial

discrepancy between model prediction and field measurements could be associated with the near-wellbore flow geometry roughly accounted for by equivalent/homogenized flow models. An accurate simulation of the transient pressure behaviour would require a detailed representation of the thin flow paths feeding the wellbores, with a discrete, object-based model of flow paths.

2. Object-based gradual deformation. An application of gradual deformation method to the above-suggested object-based model and the design of a similar calibration methodology are recommended. Then, a flow-path network would be deformed instead of a pixel-based facies model as was done here. The wellbore connectivity with the network of conductive objects would also be reproduced more accurately than with a finite-volume modelling approach.

3. Tracer test analysis. At a more advanced stage, once the connected flow network has been identified from well dynamic data, the model calibration to tracer tests could be undertaken to further investigate this network in terms of flow and transport capabilities.

4. Further assessing the predictability of calibrated flow models. Once a flow model of the Site has been calibrated, it is worth testing the capacity of that model to predict various flow tests regarding the choice of wells, and also the tests characteristics and flow regime. A benchmark involving several various flow models is planned for the EHS. In that view, two doublet tests (steady-state injection and production using a given couple of wells) will be performed in the coming months. The simulation results of these two doublets, that concerns (M6, M22) and (M12, M15) couples of wells, are shown in Appendix 2, hoping such predictions will not be invalidated by the field measurements.

References

- Anterion, F., Eymard, R., Karcher, B., 1989. Use of parameter gradients for reservoir history matching. SPE 18433.
- Barenblatt, G.I., Zheltov, I.P., Kochina, I.M., 1960. Basic concepts on the theory of seepage of homogeneous liquids in fissured rocks. *Journal of Applied Mathematics and Mechanics*, 24, pp. 1286-1303.
- Baecher, G.B., 1983. Statistical analysis of rock mass fracturing. *Journal of Mathematical Geology*, 15 (2), pp. 329–347
- Bernard, S., 2005. Caractérisation hydrodynamique des réservoirs carbonatés fracturés. Ph.D. Thesis, University of Poitiers.
- Bernard, S., Delay, F., Porel, G., 2006. A new method of data inversion for the identification of fractal characteristics and homogenization scale from hydraulic pumping tests in fractured aquifers. *Journal of Hydrology*.
- Bissel R., 1994. Calculating optimal parameters for history matching, 4th European Conference on the Mathematics of Oil Recovery, Roros, Norway.
- Blanc, G., 1995. Numerical well test simulations in heterogeneous reservoirs. Poster presented at American Association of Petroleum Geologists Conference, Nice.
- Blanc, G., Guérillot, D., Rahon, D. and Roggero, F., 1996. Building geostatistical models constrained by dynamic data-a Posteriori constraint. SPE 35478, European 3D Reservoir Modeling Conference, Stavanger. Norway, pp. 19-33.
- Blanc, G., 1999. Welgem software, User's guide of the user interface. IFP Internal report.
- Bodin, J., Porel, G., Delay, F., 2003. Simulation of solute transport in discrete fracture networks using the time domain random walk method. *Earth Planetary Science Letters*, 208, pp. 297–304
- Bogdanov, I., Mourzenko, V.V., Thovert, J.F., Adler, P.M., 2003. Two-phase flow through fractured porous media. *Physical Review. E68, Statistical, nonlinear, and soft matter physics*, pp. 26-73
- Bourbiaux, B. Basquet, R., Cacas, M.C., Daniel, J.M., Sarda, S., 2002. An integrated workflow to account for multi-Scale fractures in reservoir simulation models: implementation and benefits. SPE 78489.
- Bourbiaux, B., Callot, J.P., Doligez, B., Fleury, M., Gaumet, F., Guiton, M., Lenormand, R., Mari, J.L., Pourpak, H., 2007. Multi-scale characterization of a heterogeneous aquifer

- through the integration of geological, geophysical and flow Data: A case study. *Oil and Gas Science and Technology, Rev. IFP*, 62 (3), pp. 347-363.
- Caers, J., 2003. History matching under training-image based geological constraints. *SPE* 74716
- Chavent, G., Dupuy, M., Lemonnier, P., 1973. History matching by use of optimal control theory. *SPE* 4627.
- Chiles, J.P. & Delfiner, P., 1999. *Geostatistics: modelling spatial uncertainty*. Wiley, New York, 695 pp.
- Cooper, H.H., Jacob, C.E., 1946. A generalized graphical method for evaluating formation constants and summarizing well field history. *American Geophysical Union*, 27, pp. 526-534.
- Davy, P., Bour, O., Dreuz, J.R., Darcel, C., 2006. Flow in multiscale fractal fracture networks. In: *Fractal Analysis for Natural Hazards*. Geological Society, London, Special Publications.
- Delay, F. and Bodin, J., 2001. Time domain random walk method to simulate transport by advection-dispersion and matrix diffusion in fracture networks. *Geophysical Research Letters*, 28(21), pp. 4051-4054.
- Delay, F., Porel, G., Bernard, S., 2004. Analytical 2D model to invert hydraulic pumping tests in fractured rocks with fractal behavior. *Geophysical Research Letters*, 31(16).
- Delay, F., Kaczmaryk, A., Ackerer, P., 2007. Inversion of interference hydraulic pumping tests in both homogeneous and fractal dual media. *Journal of Advances in Water Resources*, 30(3), pp. 314-334.
- Davies, P.B., Brush, L.H., Mendenhall, F.T., 1991. Assessing the impact of waste generated gas from the degradation of transuranic waste at the Waste Isolation Pilot Plant (WIPP): an overview of strongly coupled chemical, hydrologic, and structural processes. Paper read at Workshop on Gas Generation and Release from Radioactive Waste Repositories. Aix-en-Provence, France.
- Dennis, J.E., Schnabel, R.B., 1983. *Numerical methods for unconstrained optimization and non-linear equation*. Prentice Hall, ISBN: 0136272169.
- Dershowitz, B., Winberg, A., Hermanson, J., Byegård, J., Tullborg, E.L., Andersson, P., Mazurek, M., 2003. Äspö Task Force, Task 6C. A semi-synthetic model of block scale conductive structures at the Äspö Hard Rock laboratory. SKB IPR-03-13, Svensk Kärnbränslehantering AB.

- Ding, Y., Basquet, R., Bourbiaux, B., 2006. Upscaling fracture networks for simulation of horizontal wells using a dual-Porosity reservoir simulator. *SPE Journal of Reservoir Evaluation & Engineering*, 9(4), 513-520.
- Doligez, B., Beucher, H., Lerat, O., Souza, O., 2007. Use of a seismic derived constraint: Different steps and joined uncertainties in the construction of a realistic geological model. *Oil & Gas Science and Technology, Rev. IFP*, 62 (2), pp. 237-248.
- El Albani, A., Porel, G., Meunier, A., Gaumet, F., 2005. Les argiles marqueurs de paléo-circulations dans un réservoir aquifère jurassique. 10ème Congrès Français de Sédimentologie, Abstract Book, ASF Publication, 51, pp. 109.
- Ezzedine, S., 1994. Modélisation des écoulements et du transport dans les milieux fissurés approches continues et discontinues. ENSMP, 198 p.
- Fletcher, R., 1987. Practical methods of optimization. 2nd Ed., John Wiley & Sons, Chichester.
- Fornel, A., 2006. Monitoring de réservoirs: mise à jour du modèle géologique par les données de production et de sismique 4D. PhD thesis, IFP and University of Dauphine.
- Gabilly, J., Cariou, E., 1997. Poitou Vendée Charentes. Guide géologique régional, Masson Editeur, Paris, 223p.
- Galli, A., Beucher, H., Le Loc'h, G., Doligez, B. and Heresim group, 1994. The pros and cons of the Truncated Gaussian Method. In: Armstrong M. and Dowd P.A. eds., *Geostatistical Simulations*, Kluwer Academic Publishers, pp. 217-233.
- Gaumet, F., 2007, EHS Geological report, cores of wells C3-C4: Caves and paleocaves in the EHS: geological synthesis and new evidences from C3-C4 core study.
- Geman, S., Geman, D., 1984. Stochastic relaxation, gibbs distribution and bayesian restoration of images. *IEEE transactions on pattern analysis and machine intelligence*, 6, pp. 721-741.
- Hu, L.Y., 2000. Gradual deformation and iterative calibration of Gaussian-related stochastic models. *Journal of Mathematical Geology*, 32 (1).
- Hu L.Y., Le Ravalec-Dupin M., 2004. Elements for an integrated geostatistical modeling of heterogeneous reservoirs. *Oil and Gas Science and Technology, Rev. IFP*, 59(2), 141-155.
- Jacquard, P., Jain, C., 1965. Permeability distribution from field pressure data. *SPE Journal*, pp. 281-294.
- Jenni, S., Hu, L.Y., Basquet, R., de Marsily, G., Bourbiaux, B., 2004. History matching of stochastic models of field-scale fractures: methodology and case study. Paper SPE

- 90020 presented at the SPE Annual Technical Conference and Exhibition held in Houston, Texas, U.S.A., pp.26–29.
- Jeong, W. C., Bruel, D., Cho, C. H. O., 2006. Numerical experiments of flow and transport in a variable-aperture fracture subject to effective normal stresses. *Journal of Hydraulic Research*, 44, pp. 259-268.
- Jourde, H., Pistre, S., Perrochet, P., Drogue, C., 2002. Origin of fractional flow dimension to a partially penetrating well in previous term stratified fractured reservoirs. New results based on the study of synthetic fracture networks. *Advances in Water Resources*, 25, pp. 371-387.
- Kaczmaryk, A., Delay, F., 2007a. Improving dual-medium approaches to account for karstic flow in a fractured limestone: Application to the automatic inversion of hydraulic interference tests (Hydrogeological Experimental Site, HES - Poitiers - France). *Journal of Hydrology*.
- Kaczmaryk, A., Delay, F., 2007b. Interference pumping tests in a fractured limestone (Poitiers-France): Inversion of data by means of dual-medium approaches. *Journal of Hydrology*, 337, pp. 133-146.
- Kazemi, H., Merrill, L.S., Porterfield, K.L., Zeman, P.R., 1976. Numerical simulation of water-oil flow in naturally fractured reservoirs. *SPE Journal*, pp. 317-326.
- Koudina, N., Gonzales-Garcia, R., Thovert, J.F., Adler, P.M., 1998. Permeability of three-dimensional fracture networks. *Physical Review*, E 57 (4), pp. 4466–4479.
- Le Loc'h G., Galli A., 1997. Truncated plurigaussian method: theoretical and practical points of view. *Proceedings of the Fifth International Geostatistics Congress, Wollongong '96. Australia*, 1, pp. 211-222.
- Le Loc'h G., Beucher H., Galli A., Doligez B., and Heresim Group, 1994. Improvement in the truncated Gaussian method: combining several Gaussian functions. In *Proc. ECMOR IV, Fourth European Conference on the Mathematics of Oil Recovery*, Roros, Norway. 13 p.
- Le Ravalec, M., 2005. Inverse stochastic modelling of flow in porous media: Application to reservoir characterization. *Editions Technip*, ISBN 2-7108-0864-1.
- Le Ravalec, M., Hu, L.Y., 2007. Combining the pilot point and gradual deformation methods for calibrating permeability models to dynamic data. *Oil & Gas Science and Technology, Rev. IFP*, 62 (2), pp. 169-180.

- Loucks, R.G., 1999. Paleocave carbonate reservoirs: origins, burial-depth modifications, spatial complexity, and reservoir implications. *American Association of Petroleum Geologists Bulletin*, 83(11), pp. 1795-1834.
- Loucks, R.G., Mescher, P.K. & McMechan, G.A., 2004. Three-dimensional architecture of a coalesced, collapsed-paleocave system in the Lower Ordovician Ellenburger Group, Central Texas. *American Association of Petroleum Geologists Bulletin*, 88 (5), 545-564.
- Manda, A.K., Gross, M.R., 2006. Identifying and characterizing solution conduits in karst aquifers through geospatial (GIS) analysis of porosity from borehole imagery: an example from the Biscayne aquifer, south Florida (U.S.A.). *Journal of Advances in Water Resources*, 29, p. 383-396.
- Marquardt., D.W., 1963. An algorithm for least squares estimation of non-linear parameters. *Journal of Applied Mathematics*, 11(2), pp. 431-441.
- Marsily, G. de, Lavedan, G., Boucher, M. and Fasanino, G., 1984. Interpretation of interference tests in a well field using geostatistical techniques to fit the permeability distribution in a reservoir model. *Geostatistics for natural resources characterization, Part 2*, pp. 831-849.
- Marsily, G. de, 1978. De l'identification des systèmes hydrologiques, PhD Thesis, University of Paris VI.
- Matheron, G., Beucher, H., de Fouquet, C., Galli, A., Guerillot, D., Ravenne, C. 1987. Conditional simulation of the geometry of fluvio deltaic reservoirs, SPE 62nd Annual Technical Conference and Exhibition, Dallas, Texas, pp. 591-599.
- Mouche, E., Zakharov, P., 2005. Gradual deformation method as a geostatistical based inverse method for the estimation of flow and transport parameters of a heterogeneous aquifer: application to the Waste Isolation Pilot Plant Site (New Mexico, USA). *American Geophysical Union Meeting*, San Francisco, USA.
- Mourier, J.P., Gabilly, J., 1985. Le Lias et le Dogger au sud-est du seuil du Poitou: Tectonique synsédimentaire, paléogéographie. *Géologie de la France*, 3, pp. 293-310.
- Nelson, R. W., 1960. In-place measurement of permeability in heterogeneous media, 1. Theory of a proposed method. *Journal of Geophysical Research*, 65(6), pp.1753-1760.
- Peaceman, D.W., 1978. Interpretation of Well-Block Pressure in Numerical Reservoir Simulation. *SPE Journal*, pp. 183-194.
- Pomar, L., 2001. Types of carbonate platforms : a genetic approach. *Basin Research*. 13, pp. 313-334.

- Rahon, D., Blanc, G., Guérillot, D., 1996. Gradients method constrained by geological bodies for history matching. Proceedings of the 5th European Conference on the Mathematics of Oil Recovery, pp. 283– 293.
- Ravenne, C., Galli, A., Doligez, B., Beucher, H. and Eschard, R., 2002. Quantification of facies relationships via proportion curves. In: Geostatistics Rio 2000, 31st International Geological Congress, Rio de Janeiro, Proceedings 2002, M. Armstrong et al. eds, Kluwer Academic Publishers, pp. 19-39.
- Renault, O., Norie, A., Karnay, G. & Vincent, M., 2002. Cartographie de l'aléa retrait-gonflement des argiles dans le département de la Vienne. BRGM report, RP-51264-FR, 98p.
- Roggero, F., Guérillot, D., 1996. Gradient method and bayesian formalism - application to petrophysical parameter characterization. 5th European Conference on the Mathematics of Oil Recovery, Leoben, Austria.
- Roggero, F. , Hu, L.Y., 1998. Gradual deformation of continuous geostatistical models for history-matching. SPE 49004, Annual Technical Conference and Exhibition, New Orleans., USA.
- Saidi, A. M., 1987. Reservoir engineering of fractured reservoirs: fundamental and practical aspects. Total. Edition Press, Paris.
- Sun. N.Z., 1994. Inverse problems in ground water modelling. Kluwer Academic Publishers, ,337 p.
- Tarantola, A., 1987. Inverse problem theory-methods for fitting and modelling parameters estimations. Elsevier, 613p.
- Warren, J.E. and Root, P. J., 1963. The behaviour of naturally fractured reservoirs. SPE Journal, pp. 245-255.
- Winberg, A., 1996. First TRUE Stage - Tracer retention understanding experiments: Descriptive structural-hydraulic models on block and detailed scales on the TRUE-1 Site. Swedish Nuclear Fuel and Waste Management Company.
- Winberg, A., Andersson, P., Poteri, A., Cvetkovic, V., Dershowitz, W., Hermanson, J., Gomez-Hernandez, J.J, Hautojärvi, A., Billaux, D., Tullborg, E.L., Holton, P., Meier, P., Medina, A., 2003. Final Report of the TRUE Block Scale Project. Report 4, Synthesis of flow, transport and retention in the block scale. Technical Report: Swedish Nuclear Fuel and Waste Management.
- Zerti, S., Vincent, B., Gaumet, F., 2007. Diagenèse d'un aquifère carbonaté hétérogène d'origine karstique (Jurassique moyen, Seuil du Poitou). IFP report, 119p

Appendix 1. Publications

Multi-Scale Characterization of an Heterogeneous Aquifer Through the Integration of Geological, Geophysical and Flow Data: a Case Study

B. Bourbiaux, J-P. Callot, B. Doligez, M. Fleury, F. Gaumet, M. Guiton, R. Lenormand, J-L. Mari and H. Pourpak

Institut français du pétrole, IFP, Direction Ingénierie de réservoir, 1-4, avenue de Bois-Préau, 92852 Rueil-Malmaison Cedex - France
 e-mail: bernard.bourbiaux@ifp.fr - j-paul.callot@ifp.fr - brigitte.doligez@ifp.fr - marc.fleury@ifp.fr - fabrice.gaumet@ifp.fr - martin.guiton@ifp.fr - roland.lenormand@ifp.fr - j-luc.mari@ifp.fr - hamid.pourpak@ifp.fr

Résumé — Caractérisation multi-échelle d'un aquifère hétérogène par intégration de données géologiques, géophysiques et d'écoulement : étude de cas — Cet article présente l'étude de modélisation intégrée d'un Site Expérimental Hydrogéologique (SEH) développé récemment à proximité de Poitiers. Ce site est destiné à la mise au point de méthodologies fiables de simulation des écoulements et transports dans des réservoirs à forte hétérogénéité. Environ 30 puits ont été forés sur cet aquifère captif et peu profond, suivant un maillage carré et centré de 70 mètres de côté. L'ensemble des observations et mesures acquises sur le Site a permis de caractériser la distribution spatiale des hétérogénéités de cet aquifère et d'identifier leur origine probable. En premier lieu, les tests de pompage et les diagraphies de production ont mis en évidence, à l'échelle du Site, le comportement hétérogène à l'écoulement. Une caractérisation statique du réservoir a alors été entreprise à partir de mesures géophysiques et surtout par l'analyse géologique conjointe des carottes et logs, en tenant également compte des mesures d'écoulement. La plupart des informations ainsi acquises se révèlent concordantes vers une origine paléo-karstique de cet aquifère, hypothèse corroborée récemment par des imageries de puits. La première étape de ce projet s'achève par la construction d'un modèle géostatistique qui illustre l'organisation spatiale des principaux drains et leur liaison avec les faciès encaissants. Ce modèle, enrichi grâce aux données récentes, constituera le support de simulation et interprétation des tests de pompage et d'interférence. Cette seconde étape de simulation dynamique du Site sera indispensable pour contraindre la position et la dimension des drains assurant la productivité de chacun des puits et leurs connexions hydrauliques.

Abstract — Multi-Scale Characterization of an Heterogeneous Aquifer Through the Integration of Geological, Geophysical and Flow Data: a Case Study — This paper presents the integrated modelling study of an experimental hydrogeological site recently developed near Poitiers city. The objective assigned to this site is the design of reliable methodologies to simulate flow and transport in highly-heterogeneous reservoirs. Around 30 wells have been drilled on this low-depth captive aquifer, according to a square and centred pattern, with an average well spacing of 70 meters. All the observations and measurements acquired on this Site lead to a characterization of the spatial distribution of the aquifer heterogeneities, and to the recognition of their probable origin. Firstly, pumping tests and production logs revealed the heterogeneous flow behaviour at the Site scale. A static characterization of the reservoir was then undertaken from geophysical surveys and especially from the joint geological analysis of cores

and logs, while taking into account flow measurements. Most information were found to be consistent with a paleo-karstic origin of this aquifer, an assumption that was recently corroborated by wellbore images. The first step of this project ends up with the construction of a geostatistical model that illustrates the spatial organization of the main drains and their link with the background facies. This model, once enriched by recent data, will constitute the support model for simulating and interpreting the pumping and interference tests. This second step, i.e. the dynamic simulation of the Site, will be indispensable to constrain the location and size of the drains that ensure the productivity of each well and their hydraulic connections.

INTRODUCTION

Many underground aquifers were developed as experimental sites during the past decade. These sites are designed for in-situ measurements and calibration of flow, transport and/or reactions in underground reservoirs that are heterogeneous by nature. Some of them are considered as potential repositories for nuclear waste, such as the Yucca Mountain site in the USA (Liu and Sonnenthal, 2003) or for geothermal energy production, such as the Soultz-sous-Forêts project in the Rhine Graben, France (Bruehl, 2002). However, at the present time, they all remain *in situ* research laboratories where experiments are performed to design and test various innovative techniques and methodologies for future industrial applications. Among such applications, one may quote the development of new geophysical methods for the detection of conductive paths in aquifers (Hunt and Worthington, 2000; Hubbard *et al.*, 2001), or remedial methods for contaminated near-surface aquifers taking advantage of the underground microbial natural activity (Nielsen *et al.*, 2006).

The Experimental Hydrogeological Site (EHS) studied in this paper was also developed as a research laboratory aiming at simulating flow and transport in highly-heterogeneous, i.e. fractured and/or karstic, aquifers and also on the design of water quality indicators. The present publication concerns the design of a modelling methodology of flow heterogeneities that starts with the integration of available direct and indirect information from geosciences at various scales. This methodology is to be compared to other research teams approaches, whereby the measured flow data in time and space are directly interpreted with conceptual flow models, that take into account a fractal behaviour of the reservoir for instance (Delay *et al.*, 2004).

The most straightforward industrial applications of the EHS research studies concern the survey and monitoring of heterogeneous drinkable aquifers, and also “field-scale” remedial methods for near-surface aquifer decontamination, from nitrates for instance.

The site under consideration is located on the borderline, named “the Poitou threshold”, between the Paris and the

Aquitaine sedimentary basins. The structural setting consists in a low-depth platform overlying a granitic basement.

This aquifer consists of about 100 meters of tight diagenetized carbonates of Middle Jurassic (Dogger) age, including Aalenian, Bajocian, Bathonian and Callovian stages. It is separated from the granitic basement by 45 m of Liassic marls and lies 20 to 30 meters below a superficial impermeable layer made up of argillaceous and organic-rich weathered deposits. The studied area, denoted as the Experimental Hydrogeological Site (EHS), covers an area of 210 m per 210 m. Well location is shown in Figure 1.

In spite of a minimum well spacing of only 50 meters, the long-duration pumping tests performed after drilling revealed surprisingly-contrasted flow behaviours from one well to another. Indeed, because the carbonate sediments of this water-bearing reservoir were deposited in the shallow marine environment of a platform margin, one does not expect any significant variation of facies or deposits thickness at the Site scale. However, as will be unveiled throughout this paper, this relatively uniform porous carbonate series was transformed into a complex karstified multiple-porosity reservoir. Fractures do not seem to constitute the main direct origin of flow heterogeneity, but probably influenced the development of diagenetic overprints that modified the texture and nature of deposits.

In the following, the heterogeneous distribution of fluid flows over the Site will firstly be illustrated both at the wellbore scale and the Site scale. This flow heterogeneity justified a multi-scale characterization of the reservoir to be undertaken. The corresponding geophysical and geological studies constitute the main section of this paper. Eventually, the resulting set of interpreted data is integrated into a preliminary geostatistical model illustrated in the third section.

1 FLOW OBSERVATIONS AS EXPRESSIONS OF THE RESERVOIR HETEROGENEITY

Evidences of the heterogeneous distribution of flows within the Site are found both at the Site scale from pumping tests and at the local wellbore scale from flow profiles.

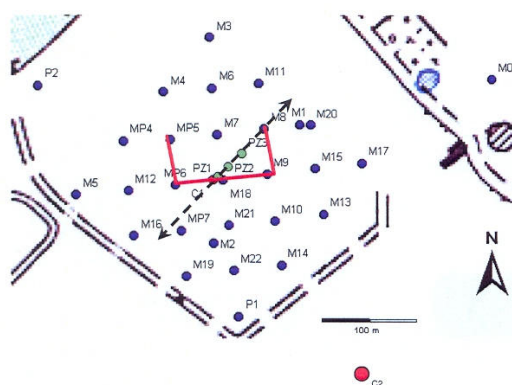


Figure 1

The Experimental Hydrogeological Site - Location of wells: cored wells C1 (reference central well) and C2 are shown in red; the red plain line is a correlation line between wells studied herein; the black dotted line represents the in-line profile of the seismic survey described in the next section of this paper.

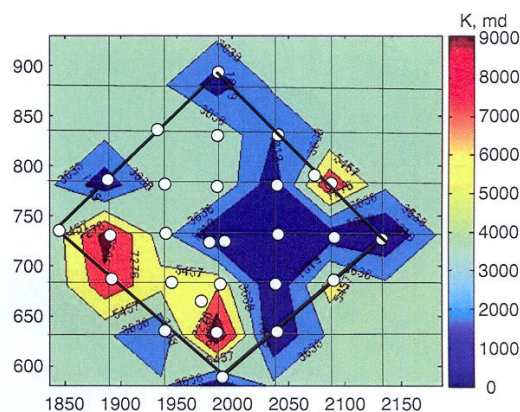


Figure 2

Permeability map of the EHS: a thick black line delimits the drilled zone of interest within the Site; wells are shown as white circles; well permeabilities range from around 100 millidarcys to nearly 11 Darcys.

1.1 Pumping Tests – Overall Permeability Distribution

After drilling, each well was pumped while measuring the pressure interferences in all other wells. Such field-scale measurements constitute a very rich flow data set that will be used to calibrate the hydrodynamical model of the Site.

As a very preliminary analysis, we estimated an average reservoir permeability from each well pumping results, considering the aquifer as homogeneous and infinite. Large productivity/permeability differences, in a ratio exceeding 10, are observed between wells. They are illustrated in Figure 2 showing the iso-permeability regions of the Site. Note the existence of a low-permeability region in the South-Eastern region of the Site, with well pumping permeabilities of one to a few hundred millidarcys, close to 100 times less than in the Western region. Obviously, the assumption of homogeneity is not valid at all for this reservoir. Furthermore, the heterogeneity of permeability shown in Figure 2 represents a smoothed image of the local distribution of flows which may still be much more contrasted.

1.2 Production Logging

As a matter of fact, the flow profiles that were measured along most wellbores revealed that water production was not uniformly distributed along the wellbores but concentrated at very few given depth intervals, generally one or two, more rarely three. The 6 production profiles shown in Figure 3 clearly demonstrate how these flow drains are unpredictable:

- the three wells M2, M21 and M22 are neighbouring wells distant by only 50 or 70 m from one another, however

they produce water from drains located at various depths, around 65 m for M2, 85 m for M21, 115 m and 80 m for M22;

- on the contrary, wells M3 and M5 show very similar flow profiles with a unique water entry point located between 110 and 115 m, although those two wells are far from one another, 210 m apart;
- well M16, located at an intermediate distance between wells M5 and M2, produces via three drains whereas M5 and M2 produce via a single drain.

Therefore, both the location and number of drains feeding wellbores can change considerably within distances less than the minimum well spacing, equal to 50 meters for this Site. The vertical extent of a given drain also seems to be variable, ranging from less than 5 m to 15-20 m.

Considering the 16 wells where a production log was measured, water entry points are encountered at various depths ranging from 115 m to 50 m, with the 80-90 depth interval being the most productive level.

Figure 4 shows the normalized flow profiles along two wellbores, M7 and M3, with a superimposition of the caliper log. The production of these two wells comes from a single major drain found respectively at around 85 m and 110 m. The normalized caliper logs show wellbore enlargements that are due to the presence of large vugs, even caves, at some levels of this limestone reservoir. The well diameter, that is about 22 cm, can increase up to 40 cm at those levels and the vertical extent of such caves, generally decimetric, can reach one meter for the largest ones. It is worthwhile pointing out that a drain is most often associated with the presence of a vuggy/karstified

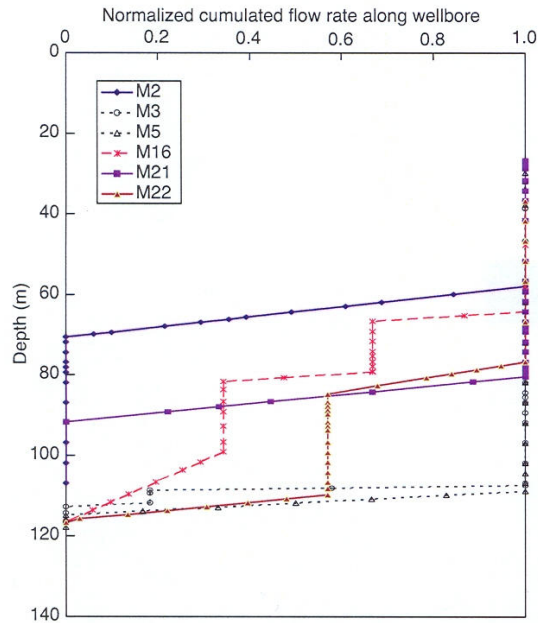


Figure 3

Production logging of various wells of the Site: a few water entry points ensure wells deliverability.

rock but that the reciprocal assertion is not true. For instance, contrary to well M7, the diameter of well M3 shows many enlargements distributed along most of the reservoir interval while water production occurs at only one depth interval, between 115 and 105 m. These observations are valuable indices that will sustain the conceptual

model proposed later on, *i.e.* selective drains crossing the karstic diagenetized layers or bodies found in this limestone reservoir.

The role played by highly-conductive drains is not only suspected from wellbore observations but also from large-scale flow measurements over fairly long time ranges, as briefly illustrated hereafter.

1.3 Interferences

Unexpected interferences were observed in some wells while testing a given well. The water level can actually decrease rapidly and considerably in some wells located far away from the pumped well, contrary to other nearby wells showing delayed and lower responses. For instance, Figure 5 shows that, after pumping in well M7 during 57 hours, a drawdown of less than 2 meters is observed in well M8 located at a distance of 50 m from M7 whereas a higher drawdown, of more than 3 m, is recorded in M5, a well three times as far from M7 as M8.

A preliminary diagnosis of this behaviour can be attempted through a qualitative analysis of transient well responses.

1.4 Transient Flow Behaviour while Pumping

Considering again the same three wells, M7, M5 and M8, the drawdown evolution with logarithmic time (*Fig. 6*) reveals the following indications of a complex hydrodynamics of this aquifer:

- The drawdown curve of pumped well M7 shows two shifted linear segments with a transition zone between them: this kind of observation would indicate the presence

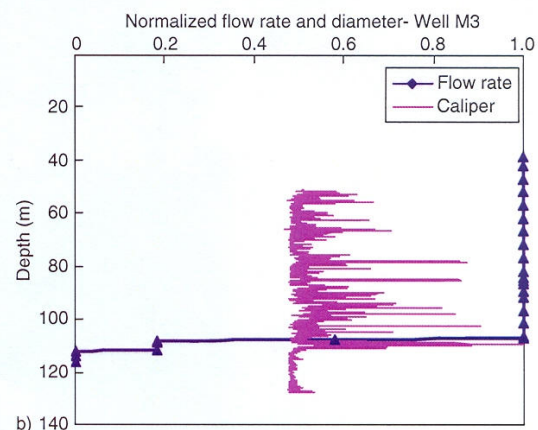
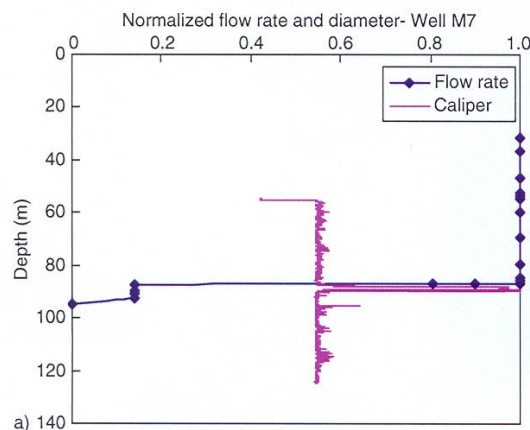


Figure 4

Production and caliper logs of Wells M7 and M3.

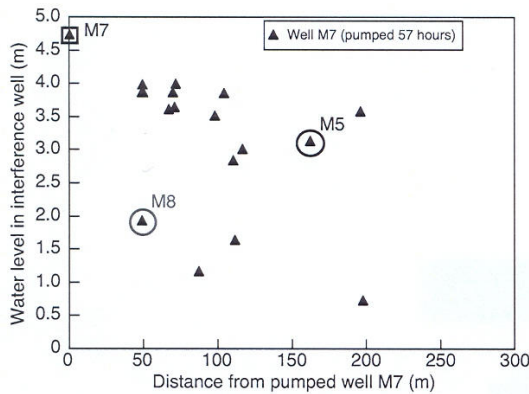


Figure 5

Drawdown measured in all wells after pumping in well M7 at a rate of $63.5 \text{ m}^3/\text{h}$ during 57 hours.

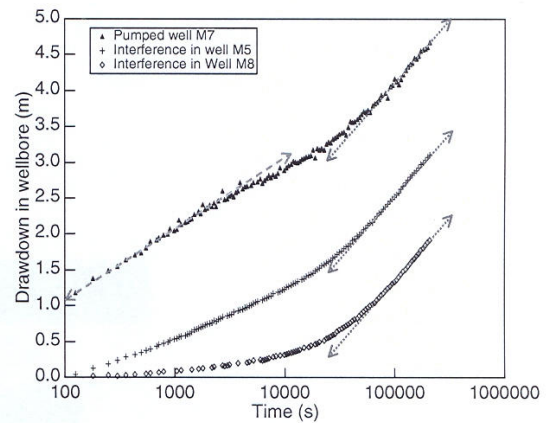


Figure 6

Transient responses of wells M7, M5 and M8 while pumping in well M7 at a rate of $63.5 \text{ m}^3/\text{h}$ during 57 hours.

of two water-feeding media with contrasted properties. However, the slope of these two segments differs contrary to well-differentiated dual-medium systems where only one medium ensures fluid flow at the large scale: in the present case, the late-time period shows a faster drawdown increase than would be observed for a dual medium. This observation can be attributed to the fact that the overall permeability of the draining system decreases with time, *i.e.* when farther regions from the pumped wellbore are sollicitated.

- Interference wells responses differ very much during the initial period of pumping: the interference well M5 shows a quasi-immediate drawdown whereas a significant drawdown is observed much later in well M8 although located much closer from M7 than M5: this observation can be attributed to the presence or absence of highly-conductive flow paths ensuring the hydraulic communication of interference wells with the pumped well.
- Two important observations concern the late-time flow period:
 - first, the drawdown does not show any stabilization with time, even after nearly three days of pumping at a significant rate, that is, a permanent regime of the wells is not yet established, apparently because the pumping goes on sollicitating farther and farther regions from the wellbore;
 - however, at that time, all wells show parallel evolutions of drawdown with logarithmic time: this may result from the fact that all the wells are at that time included in a unique large-scale draining system, which includes the Site but is still expanding with time.

1.5 Conclusion

Available flow information confirm the heterogeneous distribution of flows both at the Site scale and at the local scale along wellbores. An extensive geological characterization of the Site was thus undertaken, combining preliminary geophysical surveys, a detailed core-log analysis of reservoir facies in reference wells and a study of correlations between wells.

2 MULTI-SCALE MULTI-DISCIPLINARY RESERVOIR CHARACTERIZATION

The study of heterogeneity distribution over the Site, still under way, involves a multi-disciplinary approach confronting observations and measurements of different resolution scales. Wellbore data are the main source of information, however they do not constitute sufficient 3D modelling constraints because of the high and hardly-predictable variability in reservoir lithology and properties from one well to another. That is, the inter-well space definitely has to be explored, thus justifying the special effort made to implement the geophysical methods described hereafter.

2.1 Multi-Scale Geophysical Surveys

The seismic and acoustic methods, based on wave propagation, can be used to describe a geological structure, a reservoir zone or an aquifer at different scales. The surface seismic method (reflection survey) has a poor vertical resolution but a huge lateral investigation in comparison with the well-

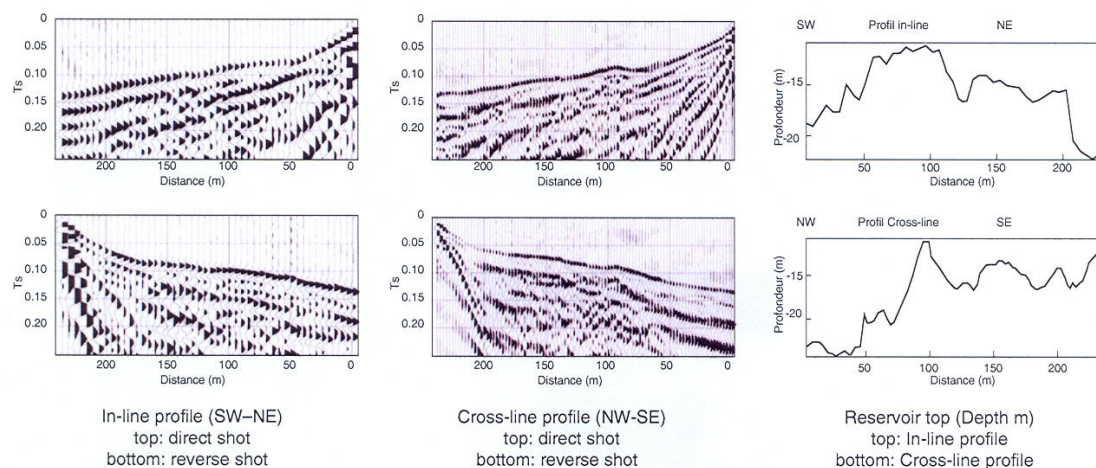


Figure 7

Results of the refraction survey: evidence of an irregular marker above the aquifer.

bore seismic methods. The wellbore methods, *i.e.* Offset or Vertical Seismic Profiles (VSP), have a restricted lateral investigation but a much finer vertical resolution than the surface seismic method. These differences are still enhanced for the acoustic logging that has a very high vertical resolution but a very poor lateral investigation.

The vertical resolution is usually evaluated as the quarter of the dominant wavelength and the lateral resolution as the diameter of the first Fresnel zone. In practice, the full processing sequence, as described hereafter, improves the lateral resolution up to the vertical resolution. As a guide for the application of seismic methods to this low-depth aquifer, the following table summarizes these points:

Method	Band width, Hz	Vertical resolution, m	Lateral investigation, m
Surface seismic	10 - 90	10 - 15	100 - 200
Well seismic	30 - 800	2 - 5	5 - 30
Acoustic logging	3000 - 17 000	0.05 - 0.2	0.05 - 0.2

The acquisition of usable seismic data is particularly difficult for low-depth reservoirs underlying a thick weathered zone, such as the aquifer studied herein. Different surface seismic surveys were however attempted with different acquisition schemes that were implemented in the vicinity of central reference well C1. A refraction survey has been recorded to image in depth the limit between the weathered zone and the unweathered carbonate formation, close to the aquifer upper limit. Some seismic shots have also been recorded to assess reflection seismic as a suitable method to

detect and image reservoir internal markers. However, the geological or petrophysical identification of such markers requires higher resolution methods, *i.e.* well seismic surveys and acoustic logging. These two calibration methods were implemented in well C1 and a few neighbouring wells.

2.1.1 Surface Seismic - Refraction Survey

Two profiles were recorded, a first profile, called the in-line profile, coarsely oriented SW – NE (*Fig. 1*), and a second cross-line profile, orthogonal to the first one. The two profiles are crossing in their middle, in the vicinity of well C1. A detonating impulse source was used. The recording spread consisted of 48 single geophones distant by 5 m from one another in the in-line profile, and 96 single geophones distant by 2.5 m in the cross-line profile. Whatever the profile, two shots (a direct shot and a reverse shot) were fired at the extremities of the recording spread. The time sampling interval was 0.25 ms and the recording length 0.5 s.

The picked times of the refracted arrivals along each profile (*Fig. 7*, left and middle parts) enable to get an image in depth of the low-velocity superficial zone contrasting with the underlying high-velocity carbonates. This rough refraction surface (*Fig. 7*, right part) is a clearly-detectable marker but would not correspond to the aquifer top surface. Actually, the latter was invariably encountered at a depth of -30 m according to the three neighbouring piezometers, PZ1, PZ2 and PZ3, drilled along the in-line profile, whereas the refractor fluctuates within a large depth range, between -10 m and -30 m (*Fig. 7*). One assumption, yet to be confirmed, is that the measured refraction surface would correspond to the bottom limit of a residual paleo-karst locally infiltrating the

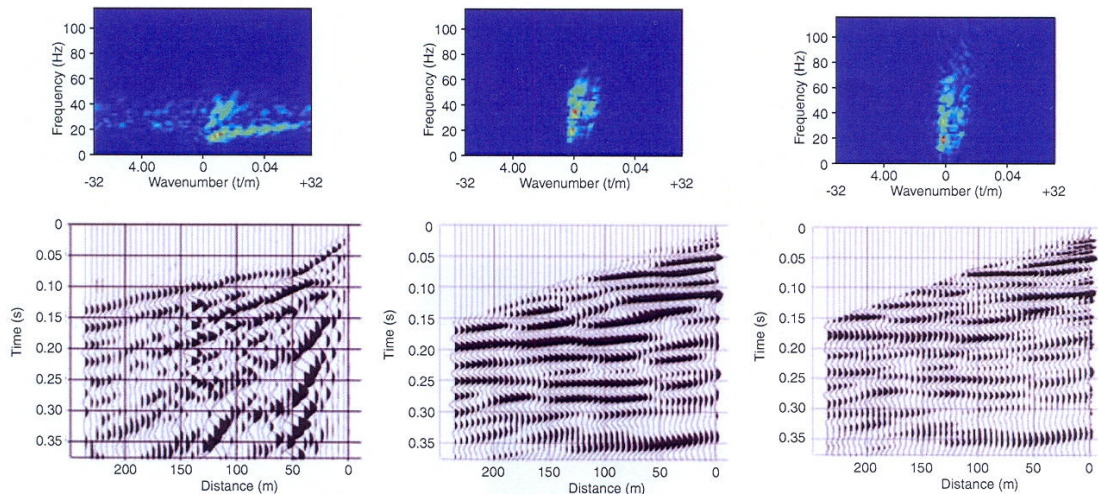


Figure 8

Results of the reflection survey: hardly-detectable reservoir markers as the result of a specific treatment procedure.

limestone aquifer formation via caves or lineaments. During drilling operations, such caves or lineaments were indeed encountered and found to be filled in by clayey surface erosion material.

2.1.2 Surface Seismic - 2D Reflection Survey

Data were recorded on the in-line profile used for the refraction study, with the same recording spread, composed of 48 single geophones. Two sources, either a detonating impulse source or a mini vibrator system, were tested but the latter was discarded because of an insufficient frequency spectrum.

Figure 8 shows a shot point obtained with the impulse source. Data are presented both as frequencies versus wavenumbers and as times versus distances. Undesired energetic wave fields (*Fig. 8*, left section), composed of low and high apparent velocity surface waves and of direct and refracted body waves, mask possibly-recorded waves emanating from reservoir markers. In such a situation, waves had to be separated sequentially thanks to a dedicated procedure involving the selection of suitable filters (Mari, 2006). Although addressed to seismic treatment specialists, this procedure is summarized hereafter, to underline the difficulties of near-surface seismic surveys.

The elimination of an undesired wavefield is performed with the following procedure:

- the extraction of the considered wavefield by a specific filtering method, either in the frequency-wavenumber domain (F-K filtering), or by Singular Value Decomposition coupled with Independent Component Analysis (SVD-ICA filtering);

- the subtraction of the extracted wavefield from the input section to obtain a residual section;
- the residual section becomes the input section for the following step.

For the near-surface objective of our survey, the above separation procedure had to be implemented four times sequentially. The first step consisted in eliminating by a F-K filter the direct wave and the slow (low apparent velocity) near-surface Rayleigh wave. In a second step, the same procedure was applied with a F-K filter to eliminate the fast (high apparent velocity) Rayleigh wave. The residual section shows negative apparent velocity events that are converted refracted waves, which were eliminated by F-K filtering in a third step. The last step consisted in extracting the refracted wave by SVD-ICA filtering. Independent Component Analysis improves the separation of waves obtained by the conventional Single Value Decomposition technique. Details on the SVD-ICA technique can be found in Vrabie *et al.* (2004), with synthetic data set examples.

The residual section thus obtained clearly shows infinite apparent-velocity events which are associated with reflected waves (*Fig. 8*, middle section). Corrections for source-detector offset (Normal Move-Out) and resolution enhancement have finally been applied to this residual section. The seismic section thus obtained is shown in Figure 8 (right part). It shows a few reflected waves in the [0-100] ms time range that investigates the entire reservoir section, in particular a reflected wave at 75 ms.

Then, these reflected waves have to be identified and depth-calibrated by comparison with well data, namely Vertical Seismic Profiles (VSP) and acoustic logs.

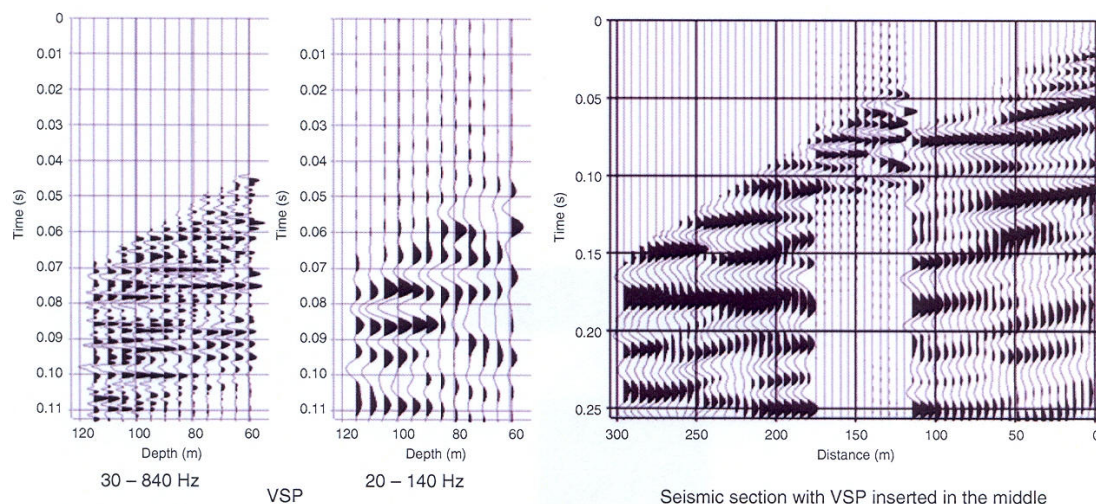


Figure 9

Results of the well seismic survey: calibration of the reflection survey.

2.1.3 Vertical Seismic Profile (VSP)

Vertical and slightly-Offset Seismic Profiles were acquired in the reference well C1 in order to identify major reservoir markers and calibrate the surface seismic sections. The weathered zone obstacle was overcome thanks to buried sources. The frequency bandwidth of received signals was large and reached 800 Hz. Figure 9 (left part) shows the deconvolved upgoing reflected waves of the VSP, both in the entire 30-840 Hz bandwidth and in the limited 20-140 Hz bandwidth of a conventional surface seismic survey. Obviously, the latter delivers an impoverished signature of possible reservoir markers. Figure 9 (right part) shows the VSP data inserted in the surface seismic section of Figure 8 (right-hand section).

VSP data allow the identification of seismic reflectors on the surface seismic section, in particular the event observed at 75 ms. The latter turns out to be a reservoir marker located at a depth of about 110 m, and would then correspond to the Aalenian-Bajocian transition, close to the aquifer bottom limit. Other internal reservoir markers are also observed above, *a priori* within the Bajocian-Bathonian unit.

That is, this well seismic survey validated the surface seismic results and pointed out the interest of carrying out a 3D surface seismic survey to obtain an image of the aquifer. For that purpose, an experimental spread, described hereafter, was tested.

2.1.4 Feasibility of a Full (3D) Seismic Coverage of the Site

Inland 3D seismic surveying generally involves a cross spread, *i.e.* shot lines that are perpendicular to the receiver

lines. In our case, a simple experimental spread was tested. The same recording spread, 48 geophones, as for the refraction study was used on the same in-line profile. A single shot line was also implemented. It was located on the cross line profile used for the refraction study. A single shot has been recorded and processed. For this feasibility study, the source was a light vibrating system. Because the latter generated a strong air wave, the distance between the source point and the receiver line, of 110 m, was chosen in

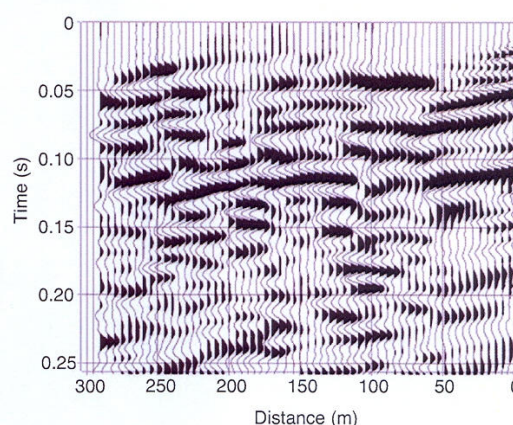


Figure 10

Feasibility study of a 3D seismic survey of the Site: the two seismic sections, shown respectively over [0, 50]m abscissas and over [50, 300]m abscissas, coincide fairly well despite the 55 m lateral shift.

order to avoid the interference between this air wave and the useful body waves. The processing of the 3D shot provided a seismic section parallel with the 2D seismic line described before, but laterally shifted by half the source-receiver line distance, *i.e.* 55 m. Fig. 10 shows a composite section, comprising:

- the 2D section obtained before with the impulse source for distance abscissas ranging from 0 to 50 m,
- the parallel section obtained with the vibrator source for distance abscissas ranging from 50 to 300 m.

Both sets of data correlate well together in spite of the shift between those 2D sections. That is, a 3D seismic reflection survey looks as a feasible alternative to get a 3D image of the aquifer over the Site area, provided however that a low spacing between recording lines is adopted.

To end with, preliminary surface seismic and VSP surveys demonstrated the possibility to identify the aquifer bottom limits as well as the main markers of the aquifer. A surface seismic survey extended to the whole Site is therefore considered in order to correlate seismic markers of major rock heterogeneities possibly playing the role of drains or related to these drains. Assigning such a challenging objective to a 3D surface seismic survey assumes that markers are carefully identified from VSP data, or from acoustic logging data as described hereafter.

2.1.5 Acoustic Logging

Acoustic logs constitute a second and higher-resolution method to calibrate surface seismic surveys. Full waveform acoustic profiles were recorded along wellbore C1 and four neighbouring wells, MP6, MP5, M8 and M9.

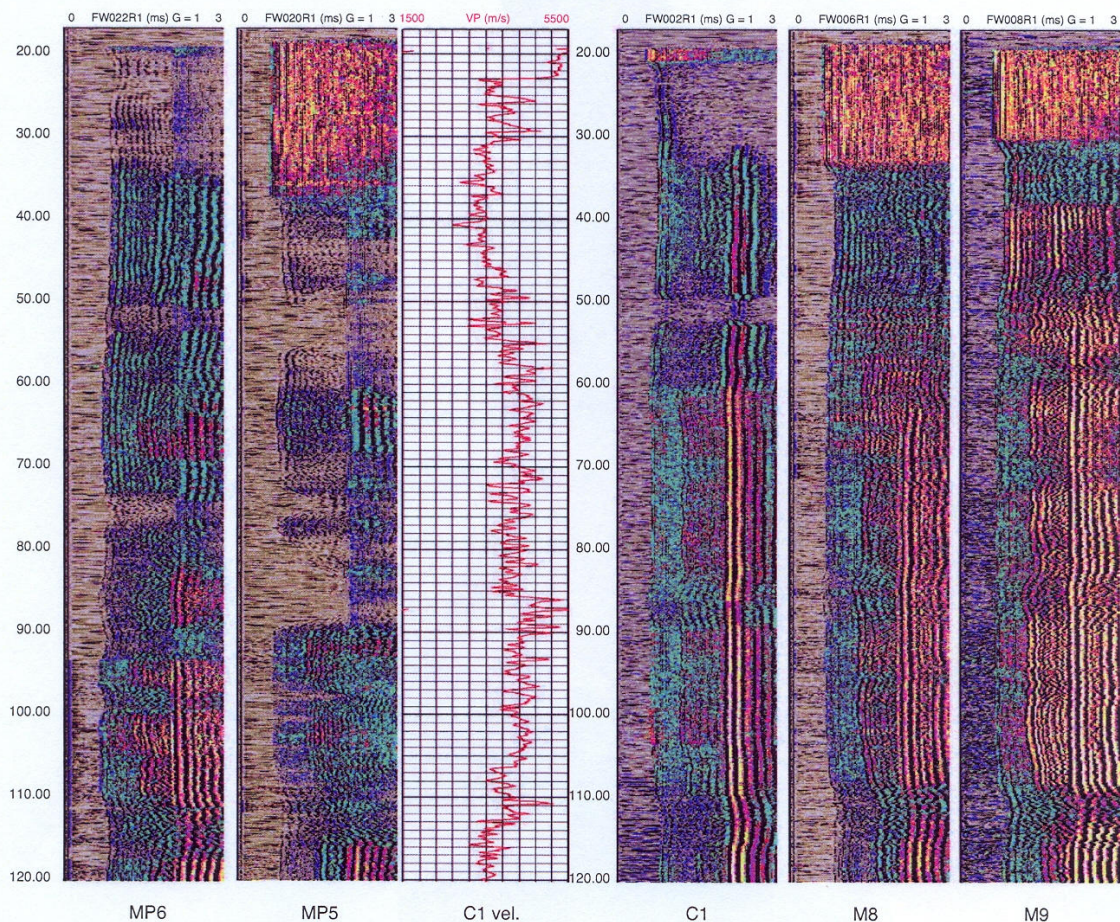


Figure 11

Full waveform acoustic profiles of well C1 and neighbouring wells.

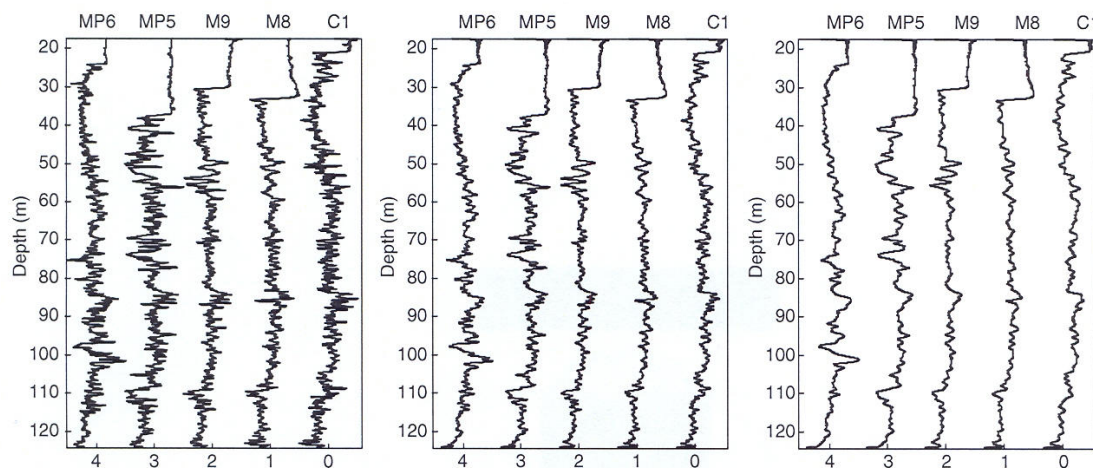


Figure 12

Acoustic velocity profiles of well C1 and neighbouring wells (note that the sharp discontinuity visible in all 5 wells, at a depth varying between 21 m for well C1 and 38 m for well MP5, corresponds to the bottom limit of the steel casing set in the upper section of each borehole).

The acoustic tool was a monopole tool designed and manufactured by S.E.M.M. service company. It includes one transducer and two receivers. The distance between the source and the nearest receiver is 3 m and the distance between the two receivers is 0.25 m. Source and receivers are multidirectional. The transducer generates in the fluid a compressional wavefield which is conveyed in the formation as a compression wave (P wave) and a shear wave (S wave) at the refraction limit angles. More precisely, in a vertical well, such a tool permits the recording of five propagation modes: the refracted P wave, the refracted S wave (only in fast formations – definition below), the fluid wave, and 2 dispersive guided modes (the pseudo-Rayleigh and the Stoneley waves). S waves can be generated only if the formation S-wave velocity is higher than the P-wave velocity in the mud; the formation is then called a fast formation (contrary to the so-called slow formations).

Figure 11 shows a representation versus depth of the recorded waves that are at first the refracted compression wave along the wellbore wall, then the refracted shear wave, and finally the wellbore-conveyed Stoneley waves. The amplitudes of the different waves are coded in different colours.

Such a representation allows to classify the geological entities in acoustic facies. For instance, considering the reference well C1, three main acoustic units could be defined by the following depth intervals: the 32–60 m unit including a discontinuity at 50–52 m, and two heterogeneous units at 60–85 m and 85–110 m that show a fairly similar acoustic facies

and are hardly distinguished from one another. However, the sharp velocity change seen at 85 m on the P-wave velocity log also shown in Figure 11 confirms a major acoustic discontinuity at that depth.

The acoustic profile also gives a qualitative information about the internal heterogeneity of identified units. Whereas wells M8 and M9 show fairly unaltered waves, wells MP5 and MP6 show perturbed and discontinuous acoustic profiles. As a matter of fact, wells MP5 and MP6 reveal themselves as prolific wells contrary to wells M8 and M9 that have a very poor water deliverability.

Furthermore, the Stoneley wave response is strongly related to the state of continuity of the well wall along which it travels. In practice, the disappearance of the Stoneley wave at a given level along the wellbore signs the presence of an open fracture or joint, or of a cavernous layer, as it can be seen here at a depth of about 50–52 m for well C1, and apparently also at depths of 50–53 m and 75 m for well MP6.

Quantitatively, the picking of the arrival times of the different waves gives access to velocity logs. The time shift between the two receivers, distant by 0.25 m from one another, was measured during this acoustic logging. Figure 12 confronts the resulting P-wave velocity logs of the five wells. The raw logs shown on the left side of this Figure have been filtered then smoothed (from left to right). A major velocity perturbation is observed at –85 m and another significant one at –110 m.

To conclude, acoustic logs give a local image of the major reservoir units and of their internal heterogeneity. Moreover, they confirm the presence of major discontinuities, that are in our case related to the presence of vugs and caves. However, such discontinuities may or not reveal themselves as effective water entry points for the well, depending on their connection to the major flow network far from wellbore. In that respect, the production log of well MP6 showed a major water arrival at a depth comprised between 74 and 57 m, which would exclude the 50-53 m discontinuity as a water feeding point for this well, whereas well C1 flow profile confirmed the 50-52 m discontinuity as the single major water entry point for that well.

The main conclusion of this geophysical study is that a preliminary surface seismic survey calibrated from a well seismic survey and logging demonstrated the possibility to identify major markers within the aquifer or limiting it. A 3D surface seismic survey extended to the whole Site is therefore considered along with its calibration from well VSPs and acoustic logs. Expected information is the correlation over the entire Site of major discontinuities or rock heterogeneities possibly playing the role of drains. Due to its limited resolution, hardly less than ten or fifteen meters, one cannot expect that the flow paths be so accurately identified from the surface seismic method as from production logs. Then, the minimum objective assigned to a 3D seismic survey is the detection and 3D visualization of the major caved or vuggy bodies. The assessment of the size and connectivity of such presumably-conductive bodies is essential to build a geostatistical model of the Site, as described later on. In this respect, 3D seismic-derived information may help in defining the variogram parameters and the main reservoir regions reflecting the distribution of those conductive bodies and/or their background facies.

2.2 Geological Characterization of the Site

The reservoir facies were characterized from core observations of two wells, from a limited suite of logs and also drilling reports. Objectives were first to characterize the reservoir facies and understand their origin and genesis, then to establish correlations between wells for the subsequent construction of a 3D model of the Site. In addition to the recognition and correlation of primary sedimentary features, a special attention was devoted to the post-deposition phenomena that altered the lithology, texture and properties of deposits.

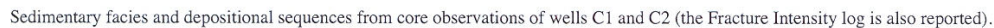
2.2.1 Sedimentary Facies and Depositional Sequences

Reservoir facies as well as depositional sequences, as proposed by Cross (1988) and Van Wagoner *et al.* (1990), were characterized thanks to a thorough analysis of the cores from two wells C1 and C2, distant by 300 m and located respec-

tively at the centre of the Site area and in the South-East. Several stratigraphic markers of Maximum Flooding Surface (MFS) and of sequence boundary were identified on the basis of macro/microfacies observations, with a specific attention to the lithology, the sediment texture and granulometry, the biogenic or detrital origin of figured elements, and also the nature of sedimentary surfaces, either bioturbated or erosive. Except for ammonites found in well-C1 and well-C2 cores at the top of Liassic shales that give a Toarcian age after E. Cariou (*personal communication*), the proposed ages and sequences come from the calibration of cores to regional literature data (Gonnin *et al.*, 1992; Gonnin *et al.*, 1994; Gabilly *et al.*, 1997).

The following vertical succession of sedimentary facies and depositional sequences was thus identified by combining both wells observations (Fig. 13):

- The *granitic basement* was reached in well C2 alone. It was emerged and deeply eroded from the Late Paleozoic time;
- The first sedimentary deposition overlapping this basement consists of 45 meters of *Liassic* marls including:
 - a 8 meter-thick alternation of azoic shales and dolostones, dated Hettangian-Sinemurian in the Vienne district area (after Gabilly *et al.*, 1997), and ending with a strongly-bioturbated surface;
 - mudstones and marls with pelagic and benthic fauna revealing a clear deepening of the depositional setting. Bioclastic marls with common bivalves and belemnites, observed between 150 m and 135 m in well C2, are supposed to be Pliensbachian outer-platform deposits. A Toarcian age of deeper-deposition marls was confirmed and correlated between wells C1 and C2, thanks to ammonites found between 130 m and 127 m in well C1 and between 130 m and 122 m in well C2.
- Overlying Liassic marls, two deposition sequences attributed to the *Aalenian* formation:
 - a 10-meter thick shallowing-up sequence with a clear lithological change from shale to carbonate that is associated with the Aalenian climate change (after Gonnin *et al.*, 1992). The bottom limit of the studied aquifer is assumed to lie within this sequence, *i.e.* at a depth of 120 to 125 m.
 - an upper transgressive-regressive sequence (116-103 m in C1; 110-101 m in C2), with silici-sponges and the first coarse-grained limestones (packstone and grainstone with oncoïds) deposited during the shallowing trend of the sequence.
- The next 3 depositional sequences (103-46 m in C1; 101-46 m in C2) known regionally to be *Bajocian* in age. Each sequence, one to a few tens of meters in thickness, records relative changes of the sea-level of similar magnitude, with associated deposits from open platform to platform margin environments. Each transgressive cycle ends with



highly-bioturbated bioclastic wackstone and packstone rich in skeletal (bivalves, crinoids, sponges, corals, bryozoans), while regressive cycles are underlined by coarser and cleaner facies (packstone to grainstone) that are very rich in non-skeletal grains (peloids, ooids and oncoïds). 3 oncoïd-rich levels (no. 2, 3 and 4) make possible a reliable correlation of the 3 sequence boundaries between the 2 cored wells.

- Between 46 m and 25 m (C1) or 26 m (C2), a fining-up unit attributed to **Bathonian** age. It starts with a non-skeletal, oncoïd-rich grainstone and rudstone that changes vertically to a packstone and then to a skeletal wackstone that reveals a clear deepening event at the end of the deposition unit. A noticeable point however is that the Bathonian unit observed in this well lumps together the five condensed or eroded depositional sequences, named Bt 1 to Bt 5, that are usually reported in adjacent areas for the Bathonian stage (Gonnin *et al.*, 1994). This observation supports the assumption of a karstic origin of this aquifer discussed later on.
- The carbonate column ends with a 20 m-thick, fine-grain, chalky limestone unit assumed to be of Late Bathonian to **Callovian** age. These well-known limestones around Poitiers city have a high microporosity and the fine texture of micro-packstones.
- The last 5-6 meters of Tertiary-Quaternary shaly deposits and soils infiltrate caves that may be locally abundant in the underlying aquifer formations.

In summary, the vertical succession of sedimentary facies and the thickness of deposits are similar in the two cored

wells, C1 and C2. Deposition sequences can be identified and correlated, especially for the Aalenian-Bajocian time interval. That is, the origin of the heterogeneous hydrodynamic behaviour of this aquifer has to be searched for elsewhere, namely in post-depositional phenomena that deeply altered primary reservoir facies. Further investigation of this heterogeneity follows with the observation of structural features and of diagenetic fingerprints.

2.2.2 Structural Features – Fracturing

The Jurassic sediments constituting the reservoir were deposited in a low-depth platform environment located at the threshold of two sedimentary basins, named the Poitou threshold. At that location, sedimentary deposits are thinner than in the Paris and Aquitaine Basins and they overlie a Hercynian granitic basement linking the Vendée and Limousin domains.

The structure of this basement is influenced by N120° to N140° and N060 to N070° tectonic lineaments which have been reactivated during Jurassic, as suggested by the thickness and lithology variations of sediments (see for instance Mourier and Gabilly, 1985).

Following the sedimentation on the post-Hercynian peneplain, several tectonic events, related to distant Pyrenean and Alpine orogenesis of Tertiary age, induced a fracturing of the carbonate deposits. Because of their possible impact on the aquifer flow behaviour, a characterization of these fractures was undertaken on analogue outcrops located near the hydrogeological site, and from the observation of available cores from wells C1 and C2.

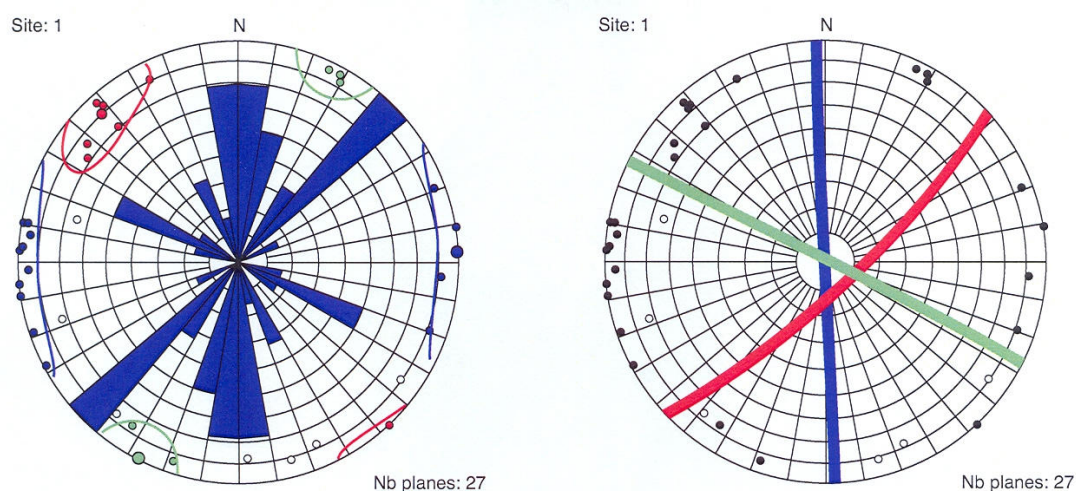


Figure 14

EHS analogue outcrops study - Passelourdin site: (left) the rose diagram of fracture azimuths and poles shows three main clusters, with the corresponding poles shown in red, blue and green colors; (right) cyclographic traces of the mean orientations of those three fracture sets.



Figure 15

Cores from C2 well at about 97 m depth: clay material is filling the upper “damaged” zone (karst residue?); a vertical fracture is observed between two marly (dark) layers in the lower core.

- Analogue outcrops study. Outcrops show that Bajocian and Bathonian limestone formations are mainly crossed by sub-vertical swarms with a high vertical extension rather than bed-controlled diffuse fractures. These fracture swarms are oriented in three directions, N120°, NS and N50° (Fig. 14), with the N120° direction probably influenced by the pre-existing Hercynian lineaments. The spacing of these fracture sets is metric to decametric. The Callovian outcrops show a higher density of fractures, but with clay filling.

- EHS cores study. Regarding the Site, fairly few fractures were observed within the Bajocian-Bathonian sections of the two vertical wells C1 and C2 (Fig. 13). More fractures were found on the Callovian upper sections, but often filled in by a clayey or organic material due to the proximity to the surface. Typical tectonic fractures, *i.e.* high-dip tension and shear fractures, are rare and most often cemented. The few observed fractures, of decimetric size, are often located at the interfaces between cherts and rock matrix or within cherts. Dominant micro-structures are sub-horizontal stylolitic surfaces and compaction bands, apparently associated with burial processes. Some of them are not cemented and may constitute flow conduits. Fluid circulation seems to have influenced the fracturing process and the evolution of fracture properties, as shown by the presence of clay smearing (Fig. 15).

Although distant by only 200 meters, the two wells revealed a high fracture density contrast:

- in well C1, few decimetric-scale fractures are found in the host rock and cherts and are cemented;
- on the contrary, well C2 shows a high fracture intensity, particularly in the 85-95 m and the 55-25 m depth intervals, with more or less connected fractures, associated with vugs and molds. Organic matter and shale are sometimes filling those fractures.

This difference is not yet fully understood. In the absence of any identified large-scale structure near by these wells, such a contrast may be related to the distribution of the diagenetic fingerprints within the reservoir. The greater presence of siliceous nodules in well C1 than in well C2 may be underlined to that respect.

To conclude, typical diffuse tectonic fractures do not seem to constitute the main direct origin of flow heterogeneity. However, horizontal stylolite-associated discontinuities at bed boundaries may constitute preferential flow paths if remained open. In addition, outcrops revealed the existence of fracture corridors at a larger scale. Such discontinuities might influence the flow connectivity between wells at the reservoir scale, either as preferential flow paths or as flow barriers depending on their conductivity. They may also have played a role in the development of the diagenetic features described hereafter.

2.2.3 Diagenetic Fingerprints

Particular attention was given to the detection of the following diagenetic phenomena that deeply altered the porous limestones of this aquifer:

- dolomitization:
 - local dolomitization of vuggy carbonate layers (sucrosic dolomite), in association with stylolithes that may have played the role of conduits for Mg-rich solutions;
 - diffuse dolomitization of the muddy limestone that mainly affected the bioturbation framework;

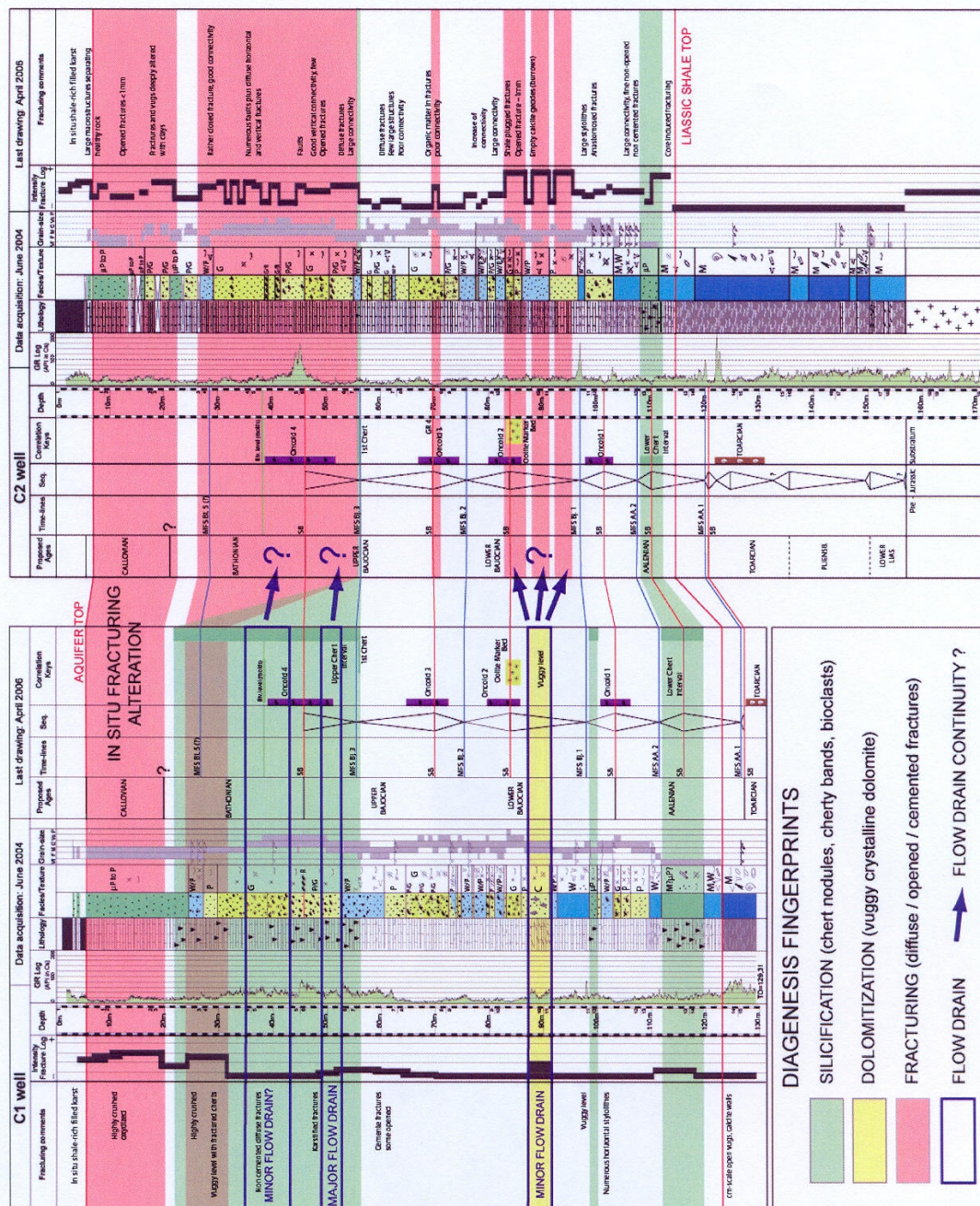


Figure 16

Correlation between wells C1 and C2: evidence of the high spatial variability of diagenetic fingerprints.

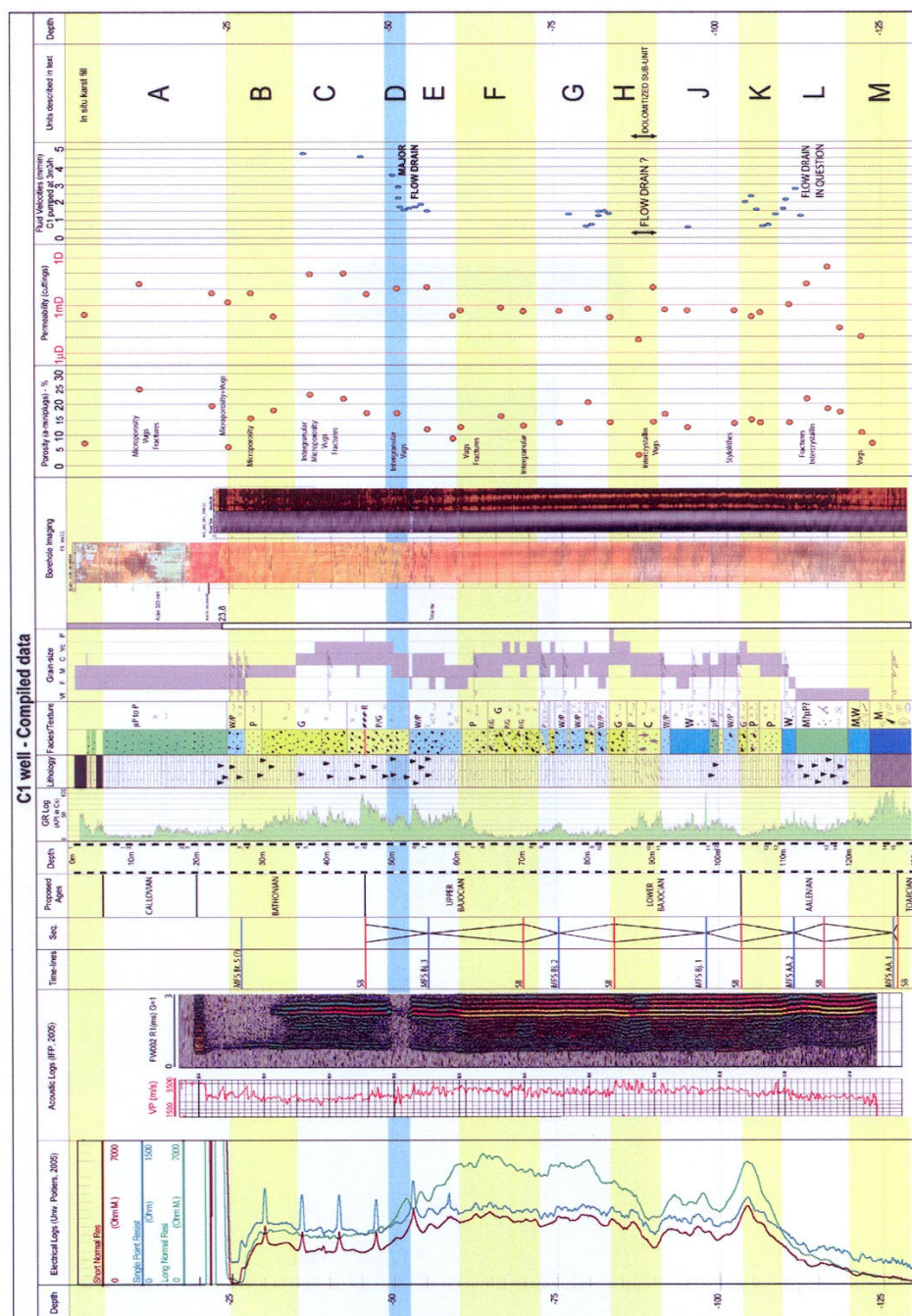


Figure 17

Reference well C1 data integration (fracture observations reported in Figs. 13 and 16).
 Texture codes (underlined): Mudstones, Wackstones, (μ(micro-))Packstones, Grainstones
 Grain sizes (underlined): Very fine, fine, Medium, Coarse, Very coarse, Pebbles
 Presence of cherts shown as black triangles on the lithological column

- silica precipitation: silica is present in the form of cherts grown around calcite biological structures such as burrows or bioclasts, or in the form of cherty bands replacing calcite within formerly-permeable layers;
- argillaceous deposits and clay filling in previously-diagenetized or -dissolved layers and fractures;
- fracturing features;
- and finally also breccia and caves, as a result of extensive dissolution phenomena.

Those diagenetic fingerprints, in particular the presence of silica and dolomite, were identified and characterized in relation with the primary sedimentary features. Hereafter, the core observations from wells C1 and C2 give clear evidences of their spatial variability (Fig. 16):

- Dolomitization: C1 cores reveal the presence of a vuggy re-crystallized dolomitic sub-unit between 91 and 87 m. A similar dolomitized layer is also observed on C2 cores but 1 meter thinner and embedded in a tighter limestone than in well C1. That is, dolomitization does not uniformly affect the aquifer.
- Silicification: well C1 shows cherty limestones over three depth intervals, 120-112 m, 100-98 m and 56-22 m, whereas C2 reveals the presence of only one chert interval between 112 and 108 m, *i.e.* with a reduced thickness compared to the deepest chert interval in well C1. This high variability of chert distribution at the Site scale may contribute to the heterogeneous flow behaviour of the aquifer.
- Stylolithes: they are observed in both wells, more frequently below 60 m. Stylolithes are the result of physico-chemical processes linked to sediment compaction, related to a burial of probably several hundreds of meters for this reservoir.
- Fractures: whereas fracturing is intense over the entire aquifer section of well C2, fractures are only found in the first 30 meters of well C1. Some of these fractures are filled with clays, which were identified as transported clays (El Albani *et al.*, 2005): their assumed origin would be vertisols of Tertiary age and thus, they could constitute the remaining evidence of a paleo-karstic nature of this aquifer.

To conclude, the core observations of wells C1 and C2 reveal that diagenetic fingerprints completely modify the lithology over short distances. Cherty limestones and fractured/karstic units may vanish or pinch out within a distance in the order of the well spacing. Therefore, the main origin of the contrasted well responses at the Site scale may lie in the great variability of diagenetic fingerprints that affected this limestone formation. The confrontation of static and dynamic observations made in reference well C1 further confirms this assumption.

2.2.4 Reference Well C1 Data Integration in Relation with Fluid Flow Behaviour

The central well of the Site, C1, disposes of the most complete dataset among all the Site wells, with detailed core descriptions from the surface down to 129 m in depth, a large set of wireline logs, including gamma-ray, resistivity, acoustic and borehole image logs, petrophysical data, and a flow profile. All these information sources were confronted together to derive possible indicators/drivers of lithological changes and of flow properties along the wellbore.

Figure 17 shows the confrontation of all information sources as well as the proposed units, labelled A to M. Core observations of grain size and rock texture, but also the acoustic, gamma-ray and electrical logs responses, reveal the heterogeneity of Bajocian units. The upper and lower limits of this formation seem to coincide with major resistivity changes. On the contrary, the Bathonian facies look more uniform in terms of texture, except for the presence of numerous cherts.

Regarding fluid flows, the major water arrival observed on the production log is found at a depth of 50 to 52 m and is responsible for about 75% of the well deliverability. This water entry point lies at the base of a cherty limestone unit. As mentioned before, the presence of this drain at that depth is consistent with the full-wave acoustic log showing the disappearance of Stoneley waves in relation with the presence of a fluid-filled discontinuity. According to the recorded flow profile, an entirely-dolomitized vuggy layer at about 90 m and another cherty section, 110 to 120 m deep, may also contribute to fluid flow, however this contribution is not so obvious as for the water-entry point at 50 m.

Petrophysical measurements on well-C1 cores. The matrix porosities and permeabilities were measured on 31 core fragments distributed along the wellbore. Porosity values are ranging from 7 to 25% with an average of 15%, and permeability values from less than 0.01 md to some 200 md. Most Bajocian permeability values are comprised between 0.1 and 1 md, around one order of magnitude less than Bathonian-Callovian values. However, high matrix permeability contrasts, of up to three orders of magnitude, are observed locally within each unit.

The porous structure of these carbonates was characterized from Nuclear Magnetic Resonance measurements. It varies significantly between samples, from unimodal to bimodal pore-size distributions, as illustrated below by the time-T2-NMR-responses of the samples distributed along the wellbore (Fig. 18).

Conclusions regarding the local hydrodynamic behaviour are that:

- water is feeding well C1 via a single entry point, that is a vuggy unit (D) located in a cherty limestone background,

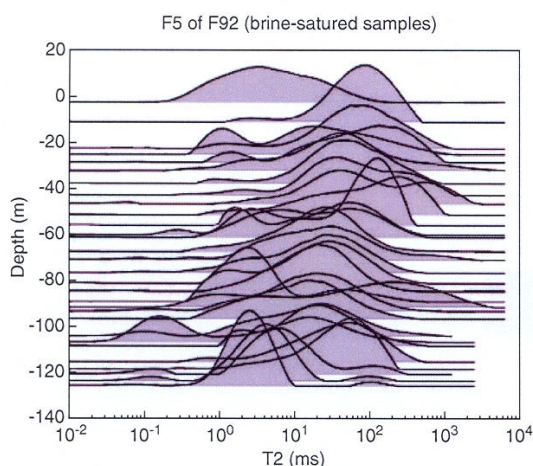


Figure 18

Qualitative pore size distribution of well C1 cores. Time T2 is directly related to the pore size and the signal amplitude is the approximate contribution of a given pore size to the sample porosity: unimodal to bimodal pore size distributions are observed with a very variable spreading from one sample to another.

- other vuggy/dolomitized and/or cherty units (L,H) may also contribute but to a lesser extent to wellbore water deliverability.

However, considering the fairly-high porosities and significant permeabilities measured on some cores, the contribution of the matrix medium to the refilling of the main drains cannot be discarded although it cannot be captured from the observation of the wellbore flow profile.

More generally, the main drains ensuring the well deliverability appear to be embedded in diagenetized units, or found as locally-dolomitized levels within clean limestones: they would then effectively result from post-deposition diagenesis episodes that strongly altered the lithology and petrophysical properties of the original sediments.

2.2.5 Study of Correlations between Wells

Following the advent of the sequence stratigraphy methods in the late seventies and eighties (Vail *et al.*, 1977; Cross, 1988; Galloway, 1989; Van Wagoner *et al.*, 1990), well-to-well correlations were usually based on the wireline log signatures of given time surfaces of stratigraphic sequences, such as Maximum Flooding Surfaces (MFS) and/or Sequence Boundaries (SB). In this study, although wells are very close from one another (50 or 70 m), the correlation of stratigraphic surfaces is unworkable as strong diagenetic fingerprints completely and abruptly modify the lithology, and in consequence the wireline log signatures as well.

At the initial stage of this ongoing project, the only available data for well-to-well correlations were essentially:

- the drilling reports of all wells: they provide useful but only-qualitative information regarding the lithologic changes and water arrivals in wellbore,
- the gamma-ray logs available for all wells.

In addition, acoustic and production logs were also acquired in a limited number of wells. Hereafter, we analyze the well-to-well correlations between the 5 wells located near the Site centre and disposing of acoustic logs, that are MP5, MP6, C1, M9 and M8. This line of wells is drawn in Figure 1 and the results of a tentative correlation between them is shown in Figure 19. For geological interpretation purposes, this correlation study takes also advantage of recently-acquired wellbore images - for C1, M8 and M9 - and of production logs - for C1, MP5, MP6 - as those pieces of information give a more detailed and reliable insight of the reservoir structure and behaviour.

Therefore, the lithology log was built from wellbore images when available, from cores for the reference central well C1, and from the drilling reports in the absence of any core-log information. It involves a limited number of lithotypes that integrates both the sedimentary facies and the diagenetic fingerprints described in the previous section. This lithotype definition is close to the one adopted for the geostatistical model described in the last section.

A few stratigraphic correlations consisting in two Sequence Boundaries could be established between the 5 wells. They constitute the minimum evidence that depositional facies are of similar nature and thickness at the EHS scale. Otherwise, the nature and the sequence of lithotypes are found to change considerably from one well to its neighbour. In particular, cherty and fractured/karstic limestone units may vanish or pinch out within a few tens of meters, as can be observed between wells C1, M9 and M8 that dispose of the most reliable information, derived from cores or borehole images.

The location of drains is reported from available production logs, *i.e.* for wells C1, MP5 and MP6. Obviously, these water drains do neither follow the stratigraphy, nor the lithotype distribution. The only information regarding their distribution is that they are embedded in diagenetized limestone bodies, *i.e.* fractured or cherty limestones, or found as locally-dolomitized levels within clean limestones. In addition, the absence of such drains can be reasonably assumed for M8 and M9 that revealed a poor deliverability from pumping tests.

Eventually, the correlation of the main drains from one well to another turns out to be hazardous as these drains seem to result almost exclusively from local diagenetic phenomena that are not correlated from one well to another. Furthermore, the apparently-random distribution of flow paths within diagenetized units is in favour of a karstic origin of the aquifer drain system. A recent extensive analysis of borehole images did corroborate a paleokarst origin of the aquifer.

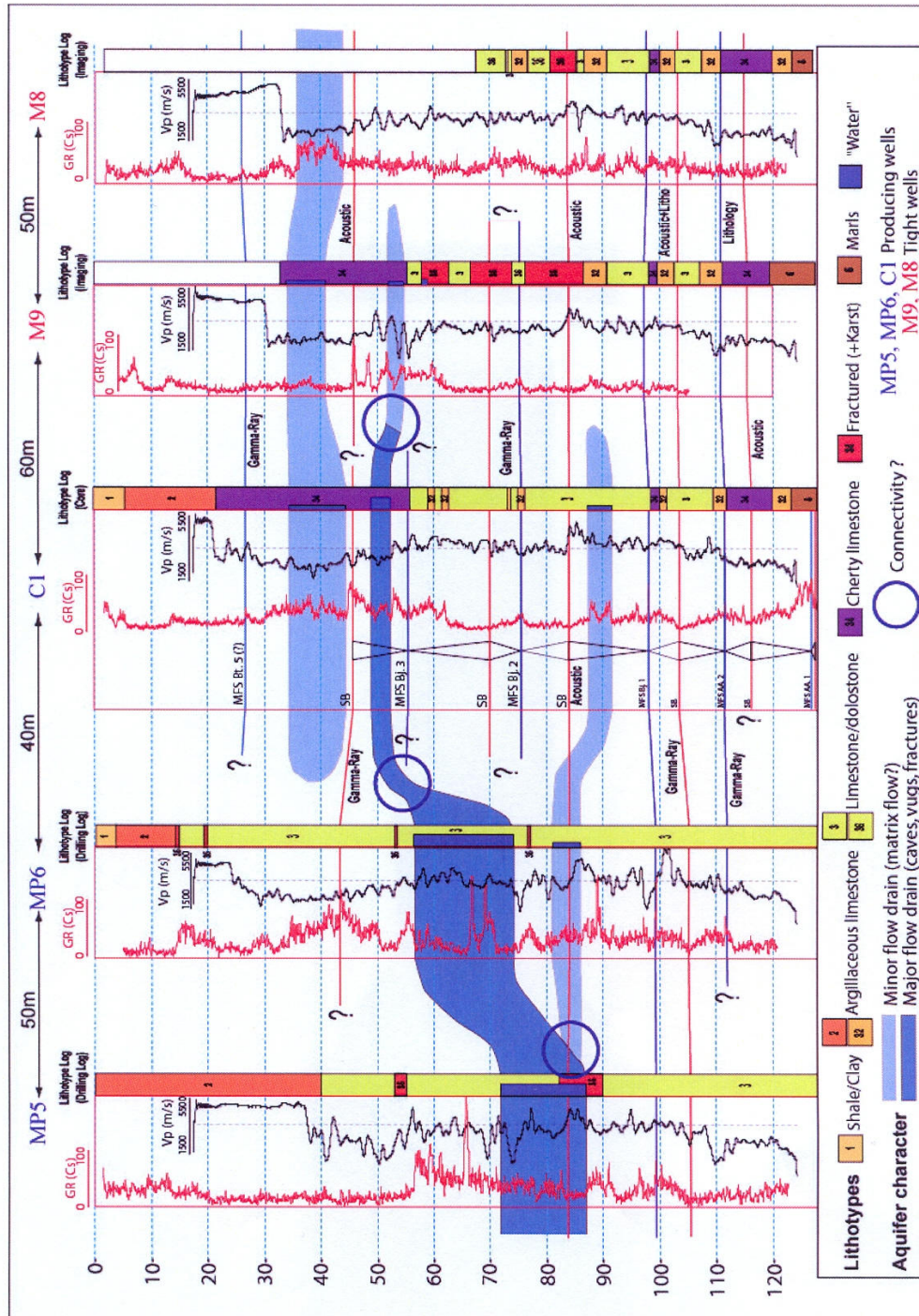


Figure 19

Correlation between wells MP5, MP6, C1, M9 and M8 (red line shown in Fig. 1).

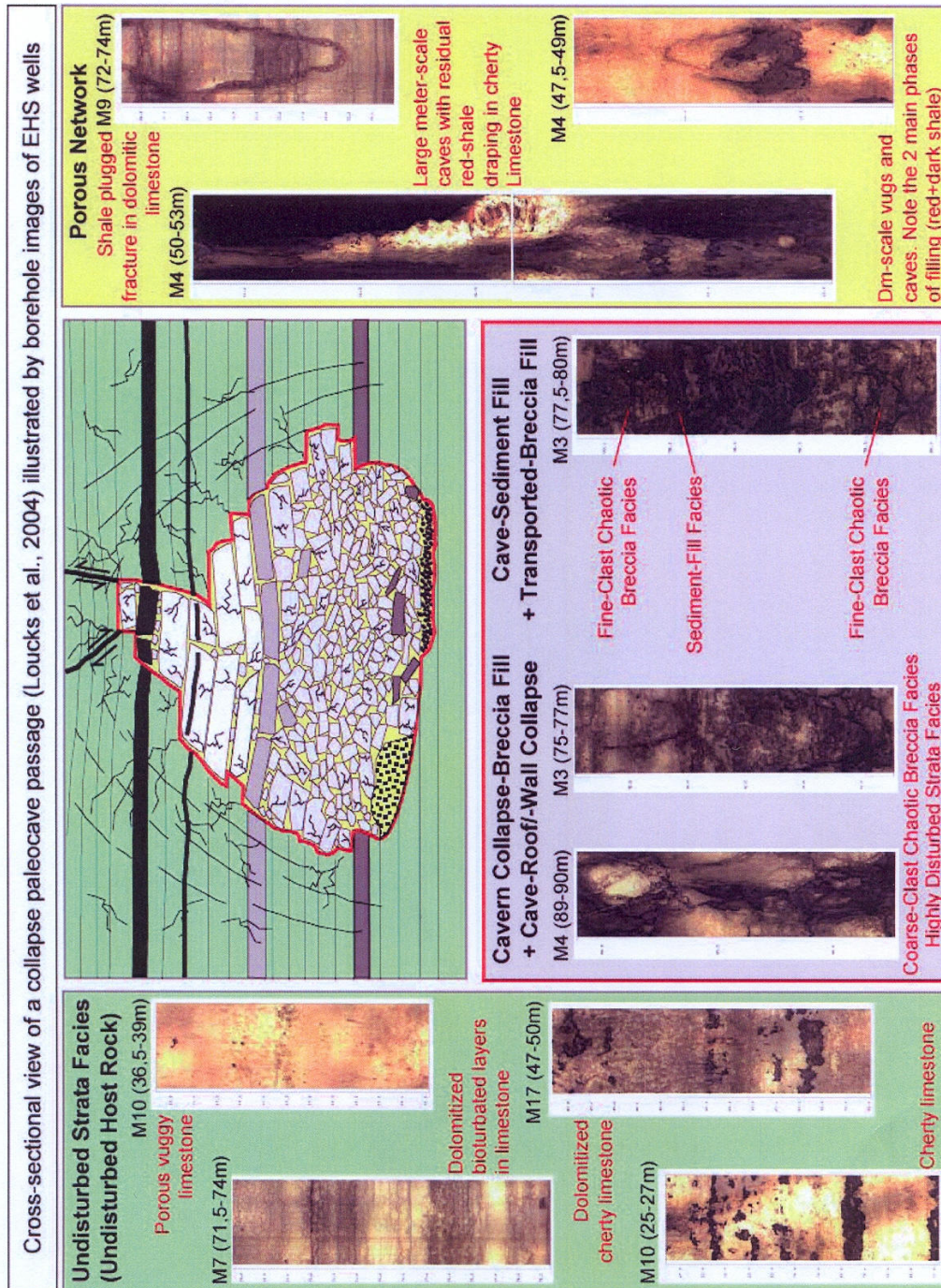


Figure 20

Bore-hole images as evidences of the paleo-karstic origin of the EHS heterogeneities.

2.2.6 The Proposed Conceptual Model of the EHS Aquifer: a Paleo-Karst System

Paleo-karst systems result from a complex history, involving a succession of near-surface karst generation phases and of subsequent sedimentation and burial phases. More precisely, Loucks (1999) proposed the following genesis model:

- first, a long-term exposure of carbonate sediments to the chemically-aggressive conditions of a fluctuating vadose zone leads to the development of a karst made up of superposed near-surface cave systems;
- then, the onset of a new sedimentation phase leads to the burial of this karst and to the collapsing of walls and roofs of superimposed caves, with a concomitant development of breccia and fractures. The result is a paleokarst, *i.e.* a coalesced system of partly-collapsed caves of complex geometry with an apparently-random distribution in space.

Paleo-karst facies are of peculiar nature and distribution. Loucks *et al.* (2004) proposed the following classification:

- undisturbed host rock facies,
- breccia facies, mainly resulting from the collapse of cave walls,
- cave-filling sediments, generally of silici-clastic (clayey) nature.

Regarding our experimental site, recent borehole images of the EHS wells revealed the presence of a complex partly-collapsed cave system. The presence and vertical location of this system change very much and cannot be correlated from one well to another. The various types of facies described above are clearly identified on those images, as shown from left to right in Figure 20:

- the host rock facies, that consist of vuggy limestone, of limestone-dolostone alternations or of cherty limestone with cherts distributed as bands or nodules. Obviously, this host rock underwent several phases of diagenesis.
- breccia facies resulting from the partial collapse of the paleo-caves: they are represented either by a stack of unsorted coarse clasts leaving millimetric to decimetric open vugs or caves between them, or by finer clasts embedded in a shaly matrix.
- cave-filling shales, possibly laminated, that may appear in different colours on borehole images, probably in relation with different episodes of filling.

Whereas the coarse breccia facies has an autochthon origin by cave walls collapsing, the cave-filling facies results from the filling of the karst conduits by allochthon finer sediments of single or multiple origins (El Albani *et al.*, 2005).

Eventually, borehole images bring a direct evidence of the suspected paleo-karstic origin of the major flow network of this aquifer.

Although some questions remain regarding the sequence and dating of the karst generation, burial and re-juvenation phases, a paleo-karstic conceptual model looks consistent

with the paleogeographical evolution of the region. Indeed, the following observations support the assumption that a first karst may have developed during the Bathonian age:

- the shallow marine Bathonian deposits are drastically thinner (between 20 and 40 m) on the Poitou threshold of the Paris Basin than in the central part of this Basin (about 200 m);
- furthermore, the stratigraphic correlations between the central part of Paris Basin and its Southwestern Poitou margin would reveal missing sequences and erosion surfaces during the Middle Bathonian age (P. Houel, *personal communication*).

This initial karst system would then have been buried by the thick marine sediments of Upper Jurassic age, leading to a collapsed paleo-karst. This paleo-karst may then have been rejuvenated during the Lower Cretaceous period following an erosion of the overlying Upper Jurassic cover, before another phase of burial during the Upper Cretaceous period, and other episodes of rejuvenation during the Tertiary-Quaternary eras, finally resulting in the complex filled-in paleo-cave system observed today.

A similar Bathonian paleokarst is known in the Grands Causses area, along the southern margin of the Central Massif (Charcosset *et al.*, 2000).

Beside the geological understanding of the Site, borehole images point out some limitations regarding the detection of the water feeding points of a wellbore. Indeed, image logs turn out to be more reliable indicators of the productive reservoir sections than cores, as core sampling is often incomplete in vuggy or caved wellbore sections. Production logs must then confirm the effective contribution to flow of these potentially-productive sections.

The following section presents a preliminary geostatistical model that attempts to integrate in a consistent way the characterization data described, cross-checked and correlated all through the present section.

3 GEOSTATISTICAL MODELLING OF THE SITE

This model was built at an early stage of the project. At that time, wells disposed of very few pieces of information, essentially a gamma-ray profile and a drilling report giving the succession of contrasting rock units as well as water arrival events. Very few flow profiles and no other borehole images than well-C1 image log were available. This information was used to reconstruct a facies log for each well of the Site. Well-to-well correlations were attempted combining both stratigraphic surfaces and diagenetic fingerprints. Well-C1 core observations/measurements were used as the reference information to calibrate the correlated units in terms of sedimentary, lithological and petrophysical properties.

The resulting set of data and constraints was deemed sufficient to build a preliminary geostatistical model of the site.

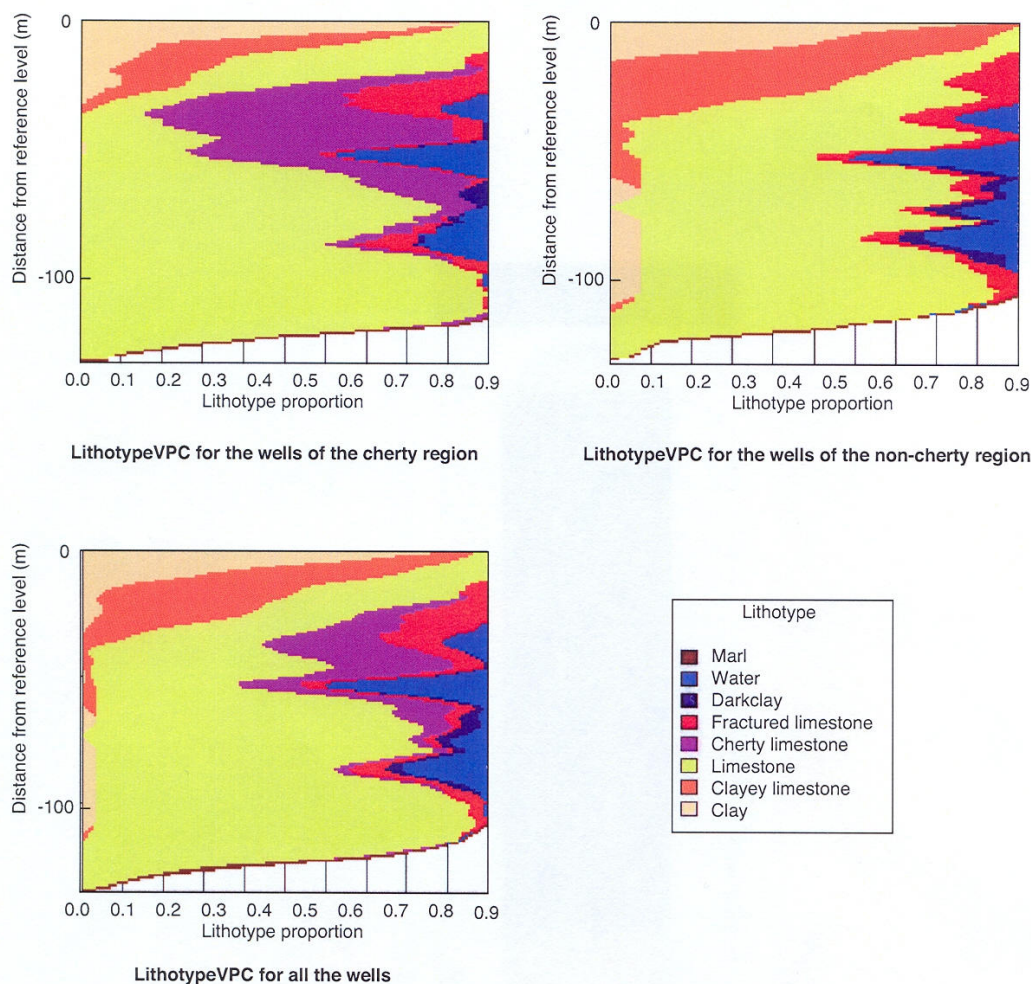


Figure 21

Vertical Proportion Curves (VPC) of lithotypes in the different regions of the geostatistical model (distance is given from a reference level that is the soil surface).

The complex distribution of facies heterogeneities was modelled using the truncated gaussian algorithm, implemented in the 5.2 version of *Heresim* 3D software package. The background of this facies modelling workflow and methodology has been presented in several papers (*e.g.* Matheron *et al.*, 1987; Galli *et al.*, 1993; Doligez *et al.*, 1999; Ravanne *et al.*, 2002). In particular, the method offers a large choice of options to constrain modelling from external geological or seismic-derived information.

3.1 Modelling Features

For modelling purposes, the various facies defined from core observations were lumped into 8 groups, called lithotypes.

These lithotypes take into account both the primary and diagenetic features. The three main reservoir lithotypes are the limestone facies and two diagenetized expressions of this facies that are fractured limestone and cherty limestone.

Four other lithotypes represent pure argillaceous or clayey facies: clayey limestone, marl, clay and dark clay. Note that the latter facies, dark clay, can be considered as a diagenetic facies as it mostly constitutes a fill-in sediment of caves and fractures.

The eighth facies, denoted as “Water”, represents the conductive facies levels, as detected in wells during the drilling operations or from the few flow profiles available at the time of model construction. This “Water” facies is only defined on

the basis of its contribution to flows and not according to its lithology or its petrophysical properties. It is most often found within cherty or fractured limestone bodies.

Wellbore facies data revealed that the presence or absence of cherts was the sole major factor of spatial variability of lithotypes that could be quantified at the Site scale. The vertical distribution of lithotypes was then determined for two groups of wells showing either abundant or scarce cherty levels. Figure 21 shows the Vertical Proportion Curves (VPC) for those two groups of wells and for all the wells together. The probability of presence of the conductive "Water" lithotype at a given depth is clearly correlated to the presence of diagenetic cherty or fractured limestones, themselves embedded in the virgin limestone facies.

The Site was then mapped according to the silicification criterion, with three regions that were "cherty", "non-cherty", or "undefined" in the absence of any wellbore information. Of course, once other logs will be acquired and new wells be drilled, other heterogeneity drivers than the presence of silica might be integrated into the geostatistical model. For the present model, one can state that the delimitation of the Site regions was based on a diagenetic factor, that is the intensity of silicification phenomenon. The latter may have taken place along the main paleo-karst conduits and thus constitute a possible indicator of the present flow paths, but not exclusively as other indicators, such as the presence of a leached or dolomitized facies or more directly the occurrence of caves or fractures, may also explain the flow distribution.

Variograms were built to analyze and quantify the spatial continuity of the previously-defined lithotypes. Vertical variograms are shown in Figure 22. The variogram ranges of the carbonate and/or clayey facies having a primary sedimentary origin cannot be defined as they exceed the hectometric scale of observation. On the opposite, the variogram ranges of the diagenetized facies are much lower, in the order of one or a few decameters, about 10 meters for the "Water" lithotype and around 30 meters for the cherty limestone. These variogram characteristics are consistent with wellbore observations, that show a very limited vertical extent of conductive bodies, and cherts distributed over pluri-decametric sections in most wellbores.

No meaningful horizontal variogram could be defined. Actually, the frequent discontinuity of diagenetized facies between neighbouring wellbores emphasizes the nugget effect. To account for this random continuity or discontinuity of diagenetized facies from one wellbore to another, the range of the horizontal variogram was estimated to be in the order of the well spacing. However, as productivity contrasts between neighbouring wellbores are less often observed in the North-South direction than in the West-East direction (Fig. 2), a higher range value was taken in the North-South direction, *i.e.* 100 m instead of 50 m the East-West direction. These values were used to parameterize a gaussian variogram

model that reflected essentially the spatial distribution of the conductive "Water" lithotype.

Using the regionalized Vertical Proportion Curves of lithotypes and the gaussian variogram described above, the distribution of facies was simulated within a 3D grid of the Site. A random truncated gaussian function was used with probability thresholds derived from the proportions of each lithotype at the reservoir location under consideration. These lithotype proportions are read on the Vertical Proportion Curves. In addition, the statistical realization honours the wellbore observations of facies and the calibrated variogram model.

One last remark on this preliminary geostatistical modelling concerns the adoption of a single gaussian function although several geological processes, *i.e.* primary deposition and multiple subsequent diagenesis phases, determine the nature and distribution of lithotypes and would justify the use of at least two gaussian functions as suggested in the following. The reason for such a choice is the absence of sufficient and reliable data to constrain the spatial distribution of the different lithotypes. Despite such limitations in modelling, the availability of a significant amount of wellbore data and the attention awarded to the "Water" lithotype distribution made possible a realistic modelling of the conductive bodies.

The attribution of petrophysical properties to this model was performed using the statistical distributions of porosity and permeability of each lithotype. The parameters of those distributions were derived from petrophysical measurements on well-C1 core fragments. However, the permeability of the eighth lithotype, "Water", was given for each productive well directly from the pumping test results, taking into account the valid approximation that this facies mostly contributes to the well deliverability.

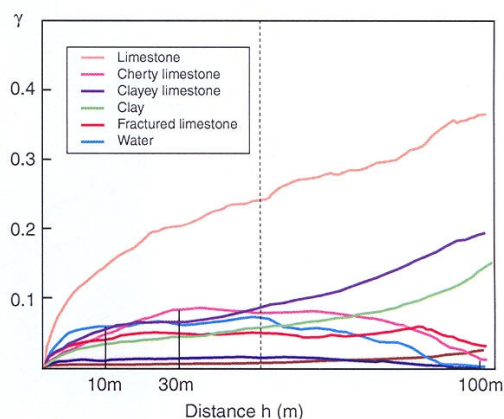


Figure 22
Experimental vertical variograms.

3.2 Result: the Initial EHS Geostatistical Model

The resulting 3D model including the drilled Experimental area is shown in Fig. 23, with clear evidence of the drains, denoted as the “Water” lithotype, in blue colour. Two horizontal cross-cuts of this model at the Site scale (Figs. 24, 25) show clearly the distribution of drains at the 53 and 85 m depths often observed as the major productive levels. West-East and North-South vertical cross-sections (Figs. 26, 27) illustrate the vertical connectivity of lithotypes, in particular the conductive “Water” lithotype. Figures 28 and 29 show the same cross-sections in terms of permeability. Those permeability cross-sections actually reflect the distribution of the “Water” lithotype, that is the sole conductive lithotype.

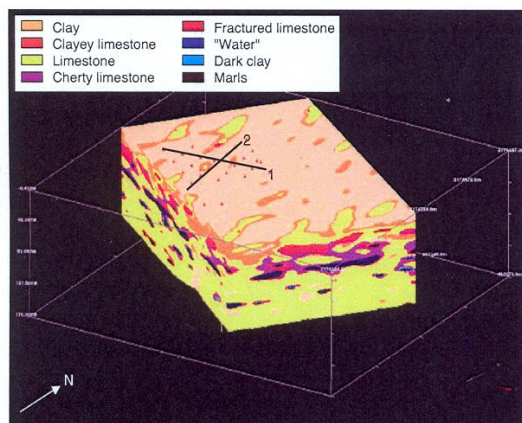


Figure 23

The 3D geostatistical facies model of the Site (cross-sections 1 and 2 shown in Figs. 26-29).

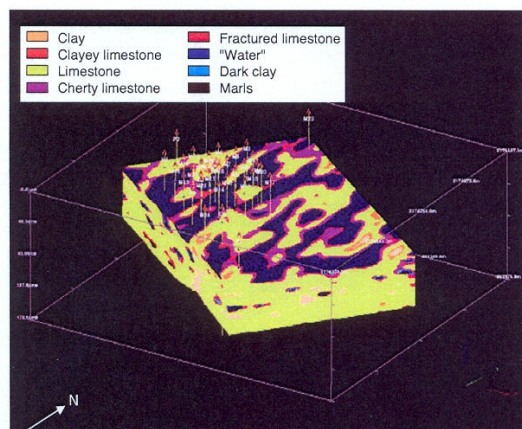


Figure 24

Facies distribution at a depth of 53 m: the blue conductive facies forms a complex network.

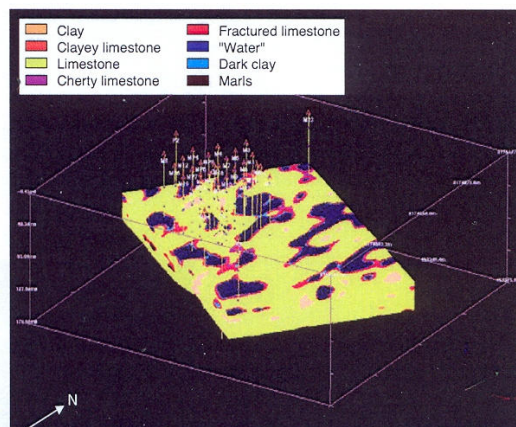


Figure 25

Facies distribution at a depth of 85 m: the blue conductive facies forms a loose network.

According to this geostatistical model, the EHS aquifer appears as a limestone reservoir within which diagenetized (post-deposition) facies, *i.e.* the cherty limestone and fractured limestone lithotypes, are distributed as complex 3D volume elements that may or not be connected both horizontally and vertically. The conductive “Water” lithotype itself is found as isolated or connected 3D bodies of variable size within the previous diagenetized limestone volume elements. The horizontal connectivity of these conductive bodies looks hazardous, even at the two main productive depths around 50-55 m and 85 m. A vertical connection between the conductive channels found at these two depths may exist in some places but looks still much less effective than the areal connectivity.

Eventually, this distribution pattern of the conductive lithotype explains why neighbouring wells have similar or contrasted deliverabilities whether or not they cross conductive bodies and whether or not these bodies are connected away from wellbore.

3.3 Future Improvement of this Model

The wellbore images and production logs recently acquired in about half of the site wells provide a refined description of the lithologic column along wellbores, including a more precise location of the water entry points. Borehole images are particularly adapted to detect the presence of the partly-collapsed cave systems with clay fill-ins. In conjunction with those images, production logs reveal that the flow paths form a sub-domain of the diagenetized limestone bodies without any apparent link with the original sedimentary units. That is, the assumption of a paleo-karst system, probably resulting from several episodes of burial and emersion, is being corroborated.

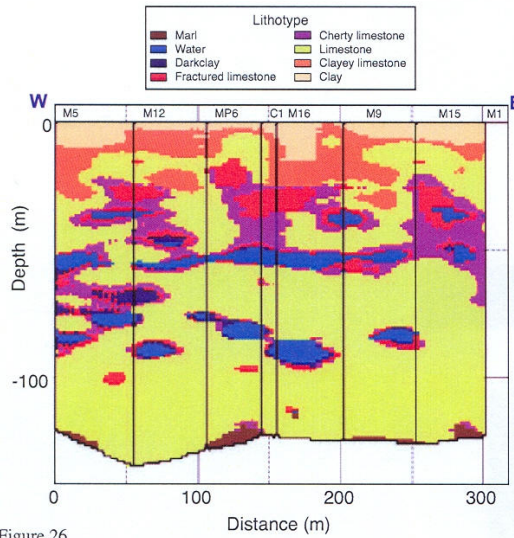


Figure 26

West-East facies cross-section of the Site: a poor connectivity of the conductive facies is expected.

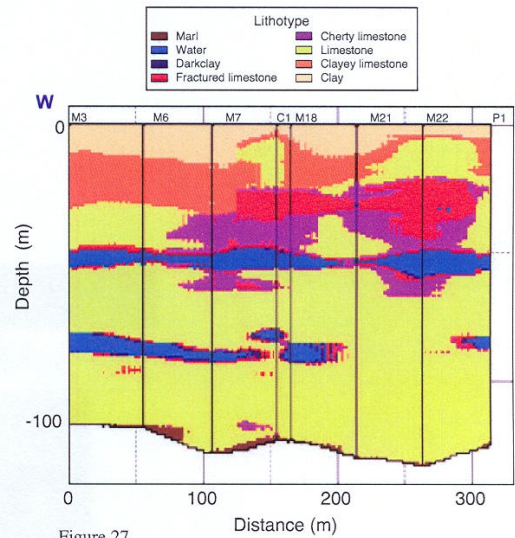


Figure 27

North-South facies cross-section of the Site: the conductive lithotype looks here more areally-continuous than in the West-East direction, but no vertical connection is observed between the 50 m and 85 m productive levels.

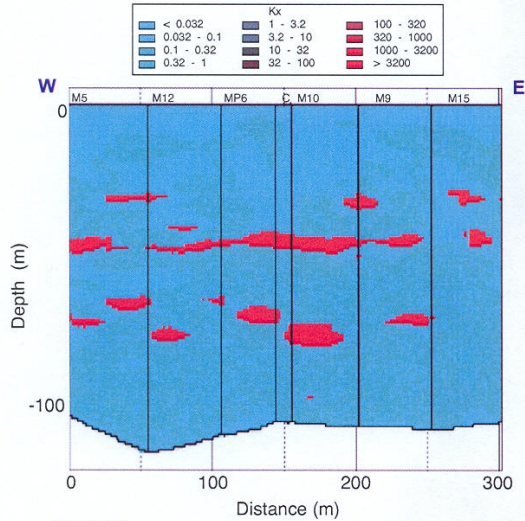


Figure 28

West-East permeability cross-section of the Site.

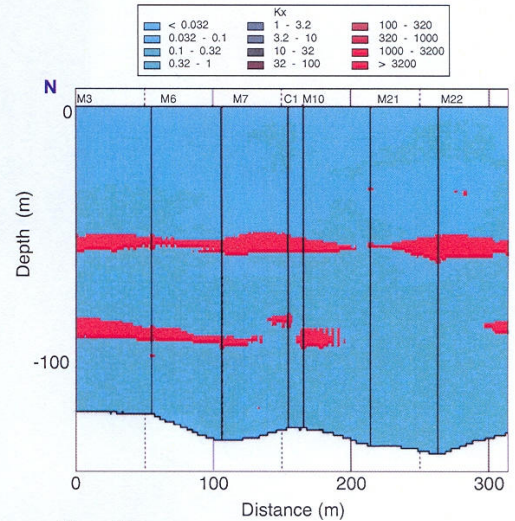


Figure 29

North-South permeability cross-section of the Site.

These images and logs constitute valuable pieces of information to further constrain the geostatistical simulation of facies (or lithotypes) at wellbore locations. In addition, they will give the possibility to build a more realistic model by taking into account two mechanisms driving the distribution of facies instead of one in the preliminary model. These two mechanisms include respectively:

- primary sediment deposition processes, that drive the distribution of all primary facies, essentially limestone, clayey limestone, marl and clay,
- diagenetic processes that control the location of fractured and cherty limestones, of the flow paths (“water” facies), and also of dark clays that mainly constitute a filling sediment of fractures and caves.

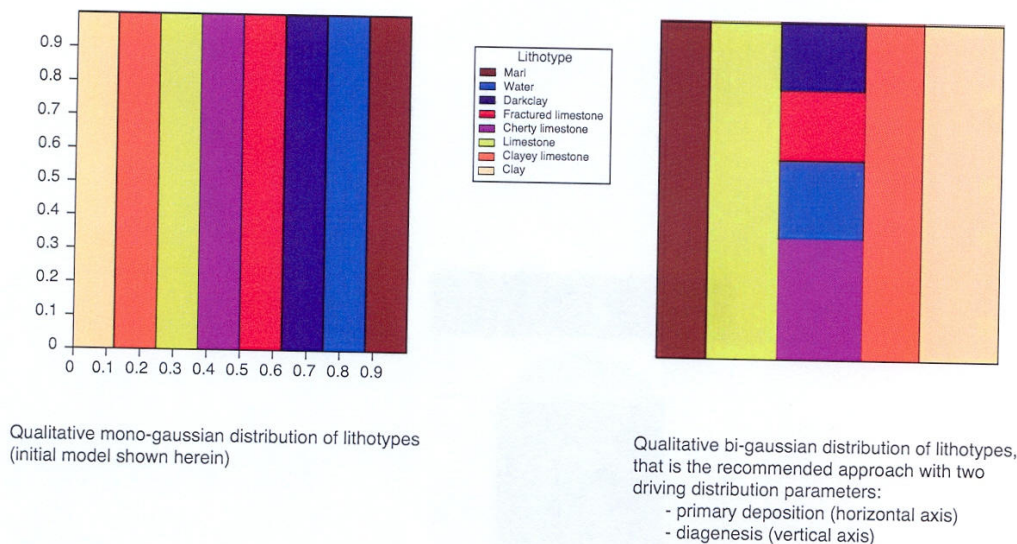


Figure 30

Qualitative distribution of facies in the preliminary geostatistical model (left) and in the updated model under construction (right).

Separate geostatistical parameters will be determined for these two sets of facies, in particular the range of their respective variograms. A long variogram range will characterize the primary-deposition lithotypes, whereas a short range, probably less than the well spacing, will control the geostatistical simulation of embedded diagenetized bodies.

Eventually, the distribution of lithotypes will be simulated using the bi-gaussian distribution qualitatively schematized on the right-hand side of Figure 30, by comparison with the initial distribution shown on the left-hand side. This way, the diagenetized facies, including the conductive one, should clearly form nested bodies or channels within the primary layered deposits, thus yielding a realistic image of flow-impacting heterogeneities in the resulting model.

Nevertheless, the exact location and the detailed size, geometry and connectivity of these heterogeneities are expected to remain incompletely defined as their lateral extension is often less than the well spacing.

CONCLUSION - PERSPECTIVES

This hydrogeological Site constitutes a very instructive multi-disciplinary data base to set up consistent methodologies for characterizing the hardly-tractable heterogeneity of complex diagenetized reservoirs and for modelling their hydrodynamic behaviour.

The static characteristics and the dynamic behaviour of the aquifer were identified and cross-checked from data sources of various nature at different scales:

- flow measurements at the Site scale and at the wellbore scale revealed the heterogeneous dynamic behaviour of this aquifer at all investigated scales;
- preliminary seismic surveys indicated that meaningful markers above and inside the aquifer could be imaged over the Site, following their identification from well seismic or acoustic logging data;
- core observations unveiled the existence of different diagenetic fingerprints strongly modifying the lithology, texture and properties of facies, thus explaining the complexity of most log responses;
- the study of well-to-well correlations confirmed the variability of diagenetic fingerprints over short distances, less than the well spacing.

The geostatistical model resulting from the integration of available data shows a distribution of facies that is consistent with the conceptual model of paleo-karst assumed for this aquifer.

Only the first step of data integration has been undertaken yet. The geostatistical model presented herein will soon be updated thanks to newly-available data, among which well-bore images and flow profiles.

Regarding new data acquisition, the detailed pattern of heterogeneities and flow paths will be further characterized thanks to dedicated seismic surveys and directional drillings that will explore the inter-well space.

Next, the model resulting from the integration of this extensive database will be used as a support for the simulation of well pumping tests and of pressure interferences

within the Site. This subsequent stage will be determinant to constrain the remaining uncertainties of the aquifer model that concern in particular the connectivity of conductive bodies or channels, and maybe also the role of the matrix background as a fluid-feeding source for the long-term deliverability of wells. To that end, history matching techniques that preserve the ascertained geological features will be applied.

At a more advanced stage, once the connected flow network has been identified from well dynamic data, the realization of tracer tests is considered to further investigate this network in terms of flow and transport capabilities.

REFERENCES

- Bruehl, D. (2002) Impact of Induced Thermal Stresses During Circulation Tests in an Engineered Fractured Geothermal Reservoir. Example of the Soultz-sous-Forêts European Hot Fractured Rock Geothermal Project, Rhine Graben, France. *Oil Gas Sci. Technol.*, **57**, 459-470.
- Charcosset, P., Combes, P.-J., Peybernès, B., Ciszak, R., Lopez, M. (2000) Pedogenic and karstic features at the boundaries of Bathonian depositional sequences in the Grands Causses area (southern France): stratigraphic implications. *J. Sediment. Res.*, **70**, 255-264.
- Cross, T.A. (1988) Controls on Coal distribution in Transgressive-Regressive Cycles, Upper Cretaceous, Western Interior, USA. In C.K. Wilgus, B.K. Hastings, H. Posamentier, J. Van Wagoner, C.A. Ross, and C.G. St. C. Kendall, (Eds.), *Sea-Level changes: an integrated approach. SEPM Special Publication*, **42**, 371-380.
- Delay, F., Porel, G. and Bernard, S. (2004) Analytical 2D model to invert hydraulic pumping tests in fractured rocks with fractal behavior. *Geophys. Res. Lett.*, **31**, L16501.
- Doligez B., Beucher H., Geffroy F. and Eschard R. (1999) Integrated reservoir characterization: improvement in heterogeneous stochastic modeling by integration of additional external constraints. In: R. Schatzinger and J. Jordan (Eds.), *Reservoir Characterization Recent Advances, AAPG Memoir*, 333-342.
- El Albani, A., Porel, G., Meunier, A. and Gaumet F. (2005) Les argiles marqueurs de paléo-circulations dans un réservoir aquifère jurassique. 10ème Congrès Français de Sédimentologie, Abstract Book. *ASF Publ.*, **51**, 109.
- Gabilly, J., Cariou, E. et al. (1997) *Poitou Vendée Charentes. Guide Géologique Régional*, Masson Editeur, Paris.
- Galli A., Beucher H., Le Loc'h G., Doligez B. and Heresim group (1993) The Pros and Cons of the Truncated Gaussian Method. In: Armstrong M. and Dowd P.A. (Eds.), *Geostatistical Simulations*, Kluwer Academic Publishers, 217-233.
- Galloway, W.E. (1989) Genetic stratigraphic sequences in basin analysis. I. Architecture and genesis of flooding-surface bounded depositional units. *AAPG Bull.*, **73**, 125-142.
- Gonnin, C., Cariou, E. and Branger, P. (1992) Les facteurs de contrôle de la sédimentation au début du Jurassique moyen sur le seuil du Poitou et ses abords. *C. R. Acad. Sci. Paris Sér. II*, **305**, 853-859.
- Gonnin, C., Cariou, E., Bassoullet, J.-P., Gabilly, J. and Mourier, J.-P. (1994) La stratigraphie séquentielle, outil de datation régional complémentaire de la biostratigraphie: application à la reconstitution de la dynamique sédimentaire des séries bathoniennes de surface du seuil du Poitou (France). *C. R. Acad. Sci. Paris Sér. II*, **318**, 235-241.
- Hubbard, S.S., Chen, J., Peterson, J., Majer, E.L., Williams, K.H., Swift, D.J., Mailloux, B. and Rubin, Y. (2001) Hydrogeological characterization of the South Oyster Bacterial Transport Site using geophysical data. *Water Resour. Res.*, **37**, 2431-2456.
- Hunt, C.W. and Worthington, M.H. (2000) Borehole electrokinetic responses in fracture dominated hydraulically conductive zones. *Geophys. Res. Lett.*, **27**, 1315-1318.
- Liu, J., Sonnenthal, E.L. and Bodvarsson, G.S. (2003) Calibration of Yucca Mountain unsaturated zone flow and transport model using porewater chloride water. *J. Contam. Hydrol.*, **62-63**, 213-235.
- Loucks, R.G. (1999) Paleocave Carbonate Reservoirs: Origins, Burial-Depth Modifications, Spatial Complexity, and reservoir Implications. *AAPG Bull.*, **83**, 1795-1834.
- Loucks, R.G., Mescher, P.K. and McMechan, G.A. (2004) Three-dimensional architecture of a coalesced, collapsed-paleocave system in the Lower Ordovician Ellenburger Group, Central Texas. *AAPG Bull.*, **88**, 545-564.
- Mari, J. L. (2006) Seismic wave separation by SVD and (F-K) combined filters. Presented at the *ISCCSP Conference*, Marrakech, February 2006.
- Matheron G., Beucher H., de Fouquet C., Galli A., Guerillot D. and Ravenne C. (1987) Conditional simulation of the geometry of fluvio deltaic reservoirs, SPE 62nd Ann. Tech. Conf. & Exh., Dallas, Texas, pp. 591-599.
- Mourier, J.P. and Gabilly, J. (1985) Le Lias et le Dogger au sud-est du seuil du Poitou : Tectonique synsédimentaire, paléogéographie. *Géologie de la France*, **3**, 293-310.
- Nielsen, M.E., Fisk, M.R., Istok, J.D. and Pedersen, K. (2006) Microbial nitrate respiration of lactate at *in situ* conditions in ground water from a granitic aquifer situated 450 m underground. *Geobiology*, **4**, 43-52.
- Ravenne C., Galli A., Doligez B., Beucher H. and Eschard R. (2002) Quantification of facies relationships via proportion curves. In: *Geostatistics Rio 2000*, 31st International Geological Congress, Rio de Janeiro, 6-17 August 2000, Proceedings 2002, M. Armstrong et al. (Eds.), Kluwer Academic Publishers, 19-39.
- Vail, P.R., Todd, R.G., Sangree, J.B. (1977). Seismic Stratigraphy - applications to hydrocarbon exploration. C.E. Payton (Ed.), *AAPG Memoir*, **26**.
- Van Wagoner, J.C., Mitchum, R.M., Campion, K.M. and Rahmanian, V.D. (1990) Siliciclastic Sequence Stratigraphy in Well Logs, Cores, and Outcrops: Concepts for High-Resolution Correlation of Time and Facies. *AAPG Methods in Exploration*, **7**.
- Vrabie, V.D., Mars, J.I. and Lacoume, J.L. (2004) Modified Singular Value Decomposition by means of Independent Component Analysis. *Signal Processing*, 645-652.

Final manuscript received in October 2006

Copyright © 2007 Institut français du pétrole

Permission to make digital or hard copies of part or all of this work for personal or classroom use is granted without fee provided that copies are not made or distributed for profit or commercial advantage and that copies bear this notice and the full citation on the first page. Copyrights for components of this work owned by others than IFP must be honored. Abstracting with credit is permitted. To copy otherwise, to republish, to post on servers, or to redistribute to lists, requires prior specific permission and/or a fee: Request permission from Documentation, Institut français du pétrole, fax. +33 1 47 52 70 78, or revueogst@ifp.fr.



SPE-113528-PP

An Integrated Methodology for Calibrating a Heterogeneous/Fractured Reservoir Model From Wellbore Flow Measurements: Case Study

Hamid Pourpak, Bernard Bourbiaux, Frédéric Roggero/Institut Français du Pétrole, Frederick Delay/University of Poitiers

Copyright 2008, Society of Petroleum Engineers

This paper was prepared for presentation at the 2008 SPE Europe/EAGE Annual Conference and Exhibition held in Rome, Italy, 9–12 June 2008.

This paper was selected for presentation by an SPE program committee following review of information contained in an abstract submitted by the author(s). Contents of the paper have not been reviewed by the Society of Petroleum Engineers and are subject to correction by the author(s). The material does not necessarily reflect any position of the Society of Petroleum Engineers, its officers, or members. Electronic reproduction, distribution, or storage of any part of this paper without the written consent of the Society of Petroleum Engineers is prohibited. Permission to reproduce in print is restricted to an abstract of not more than 300 words; illustrations may not be copied. The abstract must contain conspicuous acknowledgment of SPE copyright.

Abstract

Reliable flow modelling of highly-heterogeneous/fractured reservoirs necessarily goes through the calibration of poorly-determined geological and/or petrophysical parameters to field flow measurements. To that end, optimization procedures, based on gradient methods or on gradual deformation techniques, have been developed in the recent years.

This paper proposes a sequential methodology combining those two approaches. The case under consideration is a water-bearing reservoir constituted of heterogeneous, karstic and fractured limestones located near Poitiers city in France. In a preliminary step, drilling, core and log data acquired in about 30 wells were integrated into a geostatistical facies model used as the support for flow simulation.

Firstly, the facies petrophysical properties of this model were calibrated to well pumping and interference responses within a gradient-based inversion loop. Flow responses could be reproduced, except for a few "problematic" observation wells.

Secondly, the gradual deformation method was applied, globally then locally, to improve the distribution of facies while keeping the previously-optimized petrophysical properties. The "problematic" wells responses could be better reproduced without altering the other wells match. Furthermore, that good match of calibration wells was obtained on a simplified geostatistical model involving fewer facies as on the initial model. The gradual deformation method then appears as a robust and effective approach to find a model best matching a set of flow data among equi-probable geostatistical models.

To conclude, the sequential modelling methodology demonstrated herein is an effective way to actually integrate geological and flow data and to link geosciences and reservoir engineering skills, for setting up consistent models of hardly-tractable highly-heterogeneous reservoirs.

Introduction

During the past twenty years, the technique of mathematical modelling has been extensively used in the study of groundwater resources management and aquifer remediation (Sun, 1994). The scientists were always concerned with the water and oil transfer in reservoirs, especially in the heterogeneous and/or fractured reservoirs. The recent years showed conclusive advances in the characterization and modelling of fractured reservoirs (Cacas et al., 2001). However, most often, few direct observations of underground reservoir heterogeneities and fractures, from wells alone, are available. In the presence of fractures or of geological objects similar to fractures, geostatistical pixel-based models or object-based stochastic models can be built. These models must be validated against static and dynamic data like image logs, flow-meters, transient well tests, interference tests or production data, and then be calibrated in terms of hydraulic properties (Sarda et al., 2002). The purpose of this paper is to design and validate a methodology for calibrating the multiple poorly-defined parameters of a flow model of a highly-heterogeneous aquifer to wellbore dynamic data. Firstly, available data from an Experimental Hydrogeological Site were integrated into a geostatistical model, that constituted the geological support of a single-porosity flow model used to simulate the pumping and interference tests carried out on that Site. Then, an inversion of facies petrophysical properties and a gradual deformation of facies were performed according to a sequential methodology extensively described and illustrated throughout that paper. The satisfactory reliability of the resulting model is also demonstrated, and ways of further improvement are also discussed with regard to the use of a dual-porosity model or of a discrete object-based representation.

The Experimental Hydrogeological Site (EHS) : a heterogeneous fractured reservoir

The Experimental Hydrogeological Site (EHS) is located at the threshold between Paris Basin, and Aquitanian Basin, and between the Armorican massif in the north-west and the Central Massif in the south-east. More precisely, it lies 3 kilometers south east of the Poitiers city in the Vienne Department (Figure 1), on a plateau with an average altitude between 100 to 130 m (Gaumet et al., 2005).

The EHS was developed by the University of Poitiers within the framework of the 12th contractual programme supported by the State and the Region (CPER 2000-2006). The objective is to acquire knowledge, experience and data on water resources and flow transfer in porous media.

The studied area covers an area of 210 m per 210 m over a regional low-depth aquifer. That reservoir lies 20 to 30 meters below a superficial impermeable layer of argillaceous and organic-rich weathered deposits. It consists of about 100 meters of tight diagenetized carbonates of Middle Jurassic (Dogger) age, including Aalenian, Bajocian, Bathonian and Callovian stages. It is separated from the granite basement by 45m of Liassic marls. The carbonate sediments of this water-bearing reservoir were deposited in the shallow marine environment of a platform margin, hence no significant variation of facies or deposits thickness would be expected at the hectometric Site scale. However, this relatively uniform porous carbonate series was transformed into a complex karstified multiple-porosity reservoir. Fractures do not seem to constitute the main direct origin of flow heterogeneity, but probably influenced the development of diagenetic fingerprints. Core observations actually showed evidence of intense post-deposition fluid circulation episodes that modified the texture and nature of deposits. Diagenetic features include (a) dolomitization, either diffuse or affecting thin stylolite-associated layers, (b) silica precipitation in the form of cherts or cherty bands replacing calcite within formerly-permeable layers, (c) fracturing features, (d) argillaceous deposits and clay filling in previously-diagenetized or -dissolved layers and fractures, and finally also (e) breccia and caves, as a result of extensive dissolution phenomena. The borehole images, that were acquired in many wells of the EHS Site, revealed the presence of a complex partly-collapsed cave system, thus definitely confirming the karstic and fractured nature of the EHS aquifer (Bourbiaux *et al.*, 2006 and 2007: latter reference accessible via <http://www.crossref.org/> with DOI number: 10.2516/ogst:2007029).

Around 30 wells have been drilled on this Site, according to a NW-SE-oriented five-spot regular pattern, with an average well spacing of 70 meters. Most wells dispose of documented drilling records and logs of various natures, among which gamma-ray, temperature, and acoustic. In addition, two wells were entirely cored, named C1 and C2, the former located at the centre and the latter South-East of the drilled area. Wellbore and surface seismic was also acquired in the vicinity of selected wells. Regarding flow data, pumping tests were performed on most wells of the site with interference recording in all other wells.

Vertical production profiles were also measured along wellbores. Combined with the borehole images and several caliper logs, those profiles confirmed the karstic nature and behaviour of this aquifer with very individualized flow paths related with diagenetized features of sedimentary and/or structural origin.

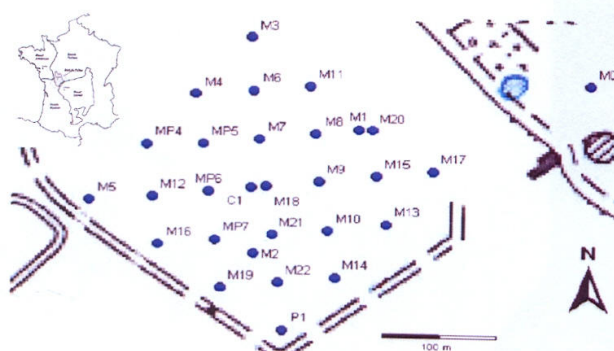


Figure 1: Experimental Hydrogeological Site – Location of wells (Bourbiaux *et al.*, 2007).

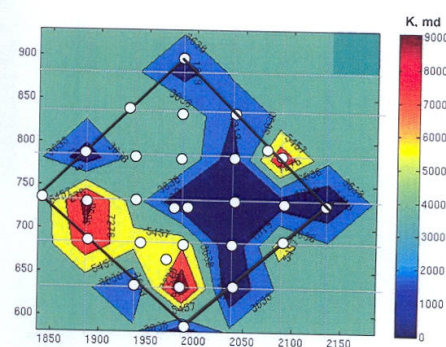


Figure 2: Permeability map of the EHS: a thick black line delimits the drilled zone of interest within the Site; wells are shown as white circles; well permeabilities range from around 100 millidarcys to nearly 11 Darcys (Pourpak *et al.*, 2007).

Preliminary studies of the EHS: multi-disciplinary tests for Site characterization purposes.

Pumping tests and their interferences have been performed for most wells of the Site. The drawdowns of the wells continued to increase even after one week of pumping. These tests revealed contrasted responses, which revealed the heterogeneous character of this aquifer (Bourbiaux *et al.*, 2006). Our preliminary work consisted of the studies of the pumping tests in order to assess the spatial variability of permeabilities and define principal regions of permeability over the Site. To that end, different values of the reservoir permeability were estimated from the pumping results recorded in each well, considering the aquifer as homogeneous and infinite. Large productivity/permeability differences, in a ratio exceeding 10, were actually found between wells. Assigning the permeability values to their respective well location and interpolating between wells, an iso-permeability map was built, as illustrated in Figure 2, showing contrasted permeability regions over the site area. Obviously, the assumption of homogeneity is not valid at all for this reservoir (Pourpak *et al.*, 2007).

The wellbore production profiles, derived from flowmeter logs, revealed the presence of few thin water-feeding levels along the wellbore trajectory, generally only one or two levels per well. We reported the vertical abscissas of those conductive levels and identified them as a facies, referred to as "water" facies later on. "Water" facies refers to the conductive karstic medium made up of

partly-dissolved/leached carbonate facies, leached sedimentary inter-strata and open/dissolved fracture "planes" that constitute the main flow-paths of that so-called karstic aquifer.

Using the flow rate distribution between these water levels and the average permeability obtained from the pumping tests, we calculated the permeability of each water facies level for each well (Pourpak, 2007). That calculation assumed that the total production of the well is ensured only by these conducting levels.

Regarding petrophysical data, well C1 is the only well disposing of core-measured permeability and porosity values. These permeability and porosity values characterize the flow properties of the tight geological facies of that porous carbonate reservoir.

All above data were integrated into a geostatistical model, as described hereafter.

Geostatistical modelling of the EHS

The first integration of data was carried out by Laurianne Dotton (2005) using the information collected in the first wells drilled on the Site at that time. For that initial model, apart from the two cored wells, wellbore facies information remained approximate, mainly inferred from the drilling reports, since the few available logs, among which resistivity logs, were hardly workable because of the diagenetic fingerprints. The initial geostatistical model was then built using an IFP proprietary software formerly developed in partnership with the Centre of Geostatistics of the Paris School of Mines. The different geological facies defined from core observation were lumped into 8 groups called lithotypes (Table 1). These lithotypes, also referred to as facies later on, take into account both the primary and diagenetic features. Three main reservoir facies are the limestone facies and two diagenetized expressions of this facies that are fractured limestone and cherty limestone. As evoked before, the "water" facies is defined using a flowing criterion (highly-conductive bodies at the decametric well spacing scale), keeping in mind that such flow property results from the diagenesis of original sedimentary carbonate deposits. Therefore, the "Water" facies coincides with or is embedded in limestone diagenetized deposits. The 3D distribution of facies within the Site aquifer was modelled using a truncated mono-gaussian algorithm with the realization order schematized in Figure 3, while respecting facies proportion logs and variograms derived from the wellbore facies logs.

The background of this facies modelling workflow and methodology can be found in Matheron *et al.*, (1987), Galli *et al.*, (1993), Doligez *et al.*, (1999) and Ravenne *et al.*, (2002).

Later on, the drilling program of the Site was completed to a total of about 30 wells, and specific well logs were acquired in most wells, including in particular flowmeter profiles and wellbore images. This valuable additional information was used to generate the updated geostatistical model considered herein. For that updating, the adoption of a bi-gaussian distribution of facies was considered and tested in order to account for both sedimentary and diagenesis driving processes, with the facies neighbourhood organization shown in Figure 3 (right side). However, a mono-gaussian facies simulation algorithm was finally retained for that aquifer, because it was found able to simulate as realistic and plausible a distribution of facies as a bi-gaussian algorithm, for two probable reasons, that are the rather high density of wells providing deterministic constraints for the geostatistical realization, and a sufficiently-refined definition of facies that captures the expression of both primary and secondary (diagenetic) processes.

The entire geostatistical model grid, with cell dimensions equal to $\Delta x=10\text{m}$, $\Delta y=10\text{m}$, $\Delta z=1\text{m}$, is shown in Figure 4(a) with well geometries. A 3D perspective of the resulting mono-gaussian facies distribution over the drilled Site area can be examined in Figure 4(b), with the conductive "Water" facies shown in bright red colour.

name of lithotype	Clay	Clayey limestone	Limestone	Cherty limestone	fractured limestone	Dark clay	Water	Marl
code and name of facies	1	2	3	4	5	6	7	8

Table 1. Geological facies (lithotypes) observed on the Site.

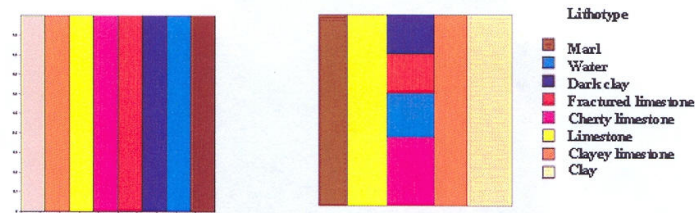


Figure 3: Qualitative lithotype distributions that can be used for geostatistical modelling. Left: mono-gaussian distribution (adopted herein). Right: bi-gaussian distribution of lithotypes (not used herein), with two driving distribution parameters, i.e. primary deposition (horizontal axis) and diagenesis (vertical axis) (Pourpak *et al.*, 2007).

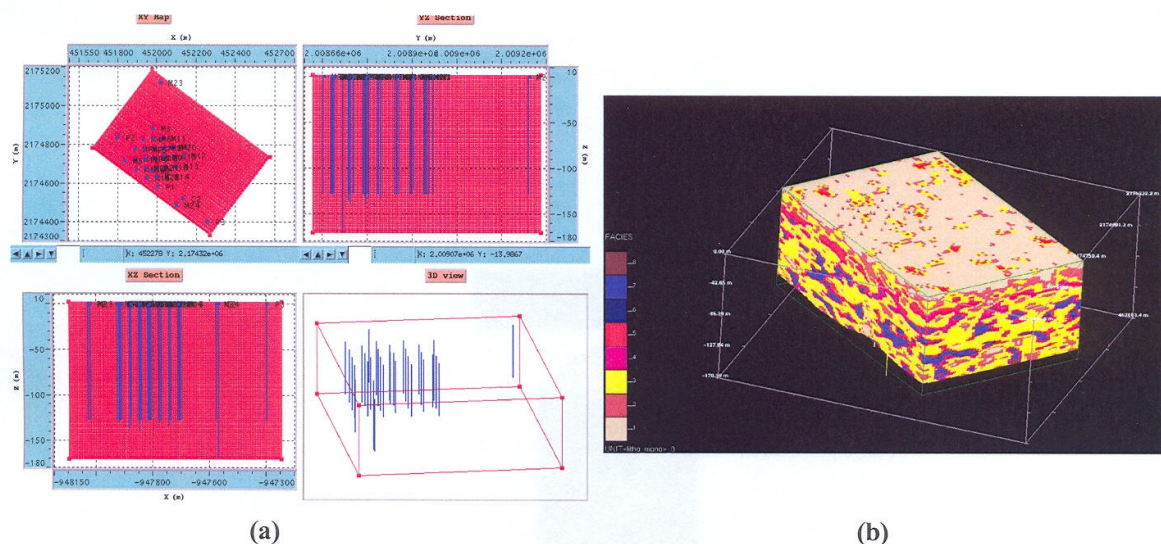


Figure 4: The 3D geostatistical facies model of the Site (Heresim 5.2 software): a) Model grid and well geometries b) 3D view of the mono-gaussian realization of the model (with the same facies colour legend as used in Figure 3).

According to this geostatistical model, the EHS aquifer appears as a limestone reservoir within which diagenetized (post-deposition) facies, i.e. the cherty limestone and fractured limestone lithotypes, are distributed as complex 3D volume elements that may or not be connected both horizontally and vertically. The conductive "Water" lithotype itself is found as isolated or connected 3D bodies of variable size within the previous diagenetized limestone volume elements. The horizontal connectivity of these conductive bodies looks hazardous, even at the two main productive depths around 50-55m and 85 m. A vertical connection between the conductive channels found at these two depths may exist in some places but looks much less effective than the horizontal connectivity (Bourbiaux *et al.*, 2006).

Flow-based calibration methods of fractured/heterogeneous reservoir models

Well test simulation

The previously-described geostatistical model was used as the support for simulating pumping and interference tests. A proprietary well test numerical simulation program, developed by IFP (Blanc, 1995; Rahon *et al.*, 1996), was used with a conventional finite-difference method. In that code, the pressure behaviour of a single-phase flow in a 3D reservoir model is formulated as this well-known conventional equation:

$$\frac{\partial}{\partial x_i} \left(\frac{k}{\mu} \frac{\partial (P + \rho g z)}{\partial x_i} \right) = \phi c_t \frac{\partial P}{\partial t} + q \quad (1)$$

where P is the pressure, i is the axis index, x_i are coordinates (x_1, x_2, x_3 , stand respectively for x, y, z), k is the permeability (k_i for a directional permeability), μ is the fluid viscosity, ρ is the fluid density, g is the gravity, ϕ is the porosity, c_t is the total rock-fluid compressibility and q is the production term. This simulator uses a 7-point finite-difference scheme to solve Equation 1.

Either a single-medium approach or a dual-medium approach can be used in that simulation software.

The dual-medium, or dual-porosity, concept was first proposed by Barenblatt *et al.* in 1960. This concept is based on the superposition of two interacting equivalent media; the fracture medium characterized by a high permeability and a low porosity, and the matrix medium characterized by a low permeability but a high porosity (Kazemi *et al.*, 1976). In order to formulate the fluid transfers taking place between these two continua, Warren and Root (1963) proposed a representation of the fractured medium as parallelepiped blocks surrounded by a connected and uniform network of fractures (sugar-box model).

In this study, we used the single-porosity approach, although a dual-porosity approach was tested at the end of this paper.

Inversion of petrophysical properties - Optimization algorithm

Calibrating realizations of a stochastic model to nonlinear data can be formulated as an optimization problem (*e.g.*, Tarantola, 1987). The calibration of a reservoir model to well test data is performed through an inversion process whereby a set of undefined parameters

driving the simulated pressure response is modified at each iteration until the calculated pressures best match the field data. The quality of the pressure match is measured with the pressure objective function F_p that is defined as follows (Blanc, 1999):

$$F_p = \frac{1}{2} \sum_{i=1}^{nms} \alpha_i (P_{m(i)} - P_{c(i)})^2 \quad (2)$$

with nms the total number of measured pressured records $P_{m(i)}$, α_i the weight applied to the pressure record i , $P_{c(i)}$ the computed pressure. This method, also called least-square minimization, requires an iterative optimization of the flow model to obtain simulated pressures, $P_{c(i)}$, that bestly match the measured pressures, $P_{m(i)}$, thus minimizing F_p . A gradient-based optimization technique is used (Rahon *et al.*, 1996), which involves deriving the flow model equations with respect to the petrophysical parameters the user wishes to adjust. A Gauss-Newton algorithm is applied to solve the resulting system of equations at each iteration loop.

The gradual deformation method

The gradual deformation method is a geostatistical parameterization technique that enables us to deform the distribution of facies. That technique was firstly introduced and implemented by Hu (Hu, 2000) to continuously modify a gaussian random function. It allows a geostatistical model to be perturbed from a small number of parameters, independently of the number of gridblocks it contains. It speeds up the model calibration to dynamic data while preserving the spatial variability of the model. The gradual deformation method is based on the fact that all linear combinations of random gaussian functions remain gaussian functions. Supposing $Y(x)$ as a random gaussian function in the domain D , the gradual deformation method consists in the construction of a new realization of Y , y , as a linear combination of $N+1$ realizations of Y , y_i , which are independent but have the same covariance γ :

$$y(\rho) = \sum_{i=0}^N \rho_i y_i \quad \text{where } \rho = (\rho_0, \rho_1, \dots, \rho_N)$$

A normality constraint is added to preserve the variance of the random gaussian function:

$$\sum_{i=0}^N \rho_i^2 = 1$$

The new realization of Y can then be presented as the function of N independent gradual deformation parameters, t_1, \dots, t_N (Roggero and Hu, 1998):

$$y(t_1, t_2, \dots, t_N) = \prod_{i=1}^N \cos(t_i \pi) y_0 + \sum_{i=1}^{N-1} \sin(t_i \pi) \prod_{j=i+1}^N \cos(t_j \pi) y_i + \sin(t_N \pi) y_N \quad (3)$$

Using this equation we solve an optimization problem of N parameters, $t = (t_1, t_2, \dots, t_N)$, varying between -1 and +1, to obtain a new realization that improves the calibration to measured data, *i.e.* minimizes the objective function. That optimization constitutes one step of a whole multi-step optimization process. Actually, if the objective function value resulting from an optimization step is not yet sufficiently minimized, a new step is re-initialized with new independent realizations that are combined with the optimal realization of the previous step (Roggero and Hu, 1998; Hu, 2000).

That gradual deformation technique was implemented within a proprietary software prototype, that was designed and developed by IFP for constraining reservoir models to full-field production data. That algorithm can be coupled with any kind of numerical fluid flow simulator, such as the well test simulator described before. It allows to select usual poorly-defined reservoir parameters as history matching variables, among which the deformation parameters driving the distribution of facies.

Local gradual deformation

When observations are scattered in different zones of the studied field, calibration using global deformation may be ineffective, because improving the match in one zone may deteriorate the match in another zone. That limitation can be overcome through the use of a local gradual deformation method (Hu, 2000). Considering a partition of the field into m zones, let X be a Gaussian white noise in the whole field and X_1, X_2, \dots, X_m the partition of X in the m zones. As the X_i are mutually independent, it is then possible to perform their gradual deformation individually. By applying the covariance operator L on these independent white noises, we obtain a consistent correlated Y function:

$$Y(t) = L(X(t)) = L \begin{bmatrix} X_1(t_1) \\ X_2(t_2) \\ \vdots \\ X_m(t_m) \end{bmatrix} = L \begin{bmatrix} U_1 \cos(t_1\pi) + V_1 \sin(t_1\pi) \\ U_2 \cos(t_2\pi) + V_2 \sin(t_2\pi) \\ \vdots \\ U_m \cos(t_m\pi) + V_m \sin(t_m\pi) \end{bmatrix} \quad (4)$$

where X_i , $i=1,2,\dots,m$, are mutually independent Gaussian white noises, and $t = (t_1, t_2, \dots, t_m)$ the deformation parameters, with one parameter per field zone. For a given set of realizations of U_i and V_i in field zones i , we solve an optimization problem of m parameters t_1, t_2, \dots, t_m to obtain a new set of realizations that improves (or at least maintains) the calibration to the data. Again, this procedure is iterated until a satisfactory calibration is reached in each deformed zone i .

Design of a sequential calibration methodology

In this paper, we propose a calibration methodology applicable to flow models of highly-heterogeneous reservoirs such as the karstic and fractured aquifer under consideration. This practical methodology consists of the following steps:

Firstly we set up an initial consistent model that incorporates all available/measured information acquired from the field. In particular, special attention has to be awarded to pore volume compressibilities as they greatly impact well-test pressure responses.

In the present study, the flow model was initialized with the available petrophysical property values, that were the porosity-permeability measurements performed on the tight matrix facies samples recovered from the cored wells. Regarding compressibility, because that parameter could not be treated as a matching variable in the subsequent petrophysical inversion step, preliminary simulation and inversion tests were performed to set facies compressibility at a value yielding a coarse overall restitution of the pressure responses of pumped wells.

Proper flow boundary conditions also have to be applied to the model. For the present field case, such boundary conditions concerned the water recharge of the site, that was estimated through a long-term inversion of a pumping test.

Secondly, the remaining unknown petrophysical facies are calibrated via an inversion of well test data, including pumping and interference pressure data. As will be detailed later on, the calibrated parameters are essentially the conductive facies porosity and permeability, and the tight facies permeability to a lesser extent.

Thirdly, once the model petrophysical parameters are adjusted, a gradual deformation of facies is performed globally to obtain a geostatistical realization of the reservoir that best honours the dynamic data while respecting the underlying geostatistical parameters.

The last step consists in capturing local flow heterogeneities through a local gradual deformation method that is applied in reservoir regions still requiring further tuning to measured flow data.

Finally, the robustness and predictability of the resulting flow model can be evaluated from the forward simulation of another flow test whose responses were not used as calibration constraints in the previous steps.

The above methodology maximizes the model consistency with field-measured data, provided that the flow model assumptions and equations are fully representative of the actual field flow behaviour. Otherwise, some discrepancies may subsist between the calibrated model predictions and the measured data. Suspicion of such model inadequacy for our field case justified (i) testing a dual-porosity modelling approach as an alternative to the adopted single-porosity approach, (ii) considering an object-based model instead of a pixel-based facies model as the geological support of our flow model.

Application to the Site

The flow model: a simple "flow-property-based" model directly inherited from the geostatistical model

The previously-described geostatistical model was used as the facies support of the flow model. Detailed facies properties are shown in Table 2. The facies compressibilities were set at a high value (0.001 bar⁻¹) that is consistent with previous EHS studies performed by different authors (Delay *et al.*, 2004, Bernard, 2005). This high value accounts for the overall aquifer flow behaviour, i.e. the high deliverability of productive wells with limited pressure drawdown. An additional fictive boundary facies, also named "source" facies, was defined in this model. This source facies is represented in the form of very large cells surrounding the Site region of interest (Figure 5). Petrophysical-property assignment to this source facies is reported later on.

However, computation efficiency and flow impact considerations justified the initial eight-lithotypes (facies) model to be simplified into an equivalent lumped facies model (Table 3 and Figure 6, right). with 2 contrasted facies, a tight (lumped) matrix facies (re-numbered 1) and the unchanged conductive "water" facies (re-numbered 2), plus the "source" facies (re-numbered 3) in the external boundary cells of the model as before. The properties of the lumped matrix facies, standing for facies 1 to 6 and 8, were initially set at averaged core-derived values.

Preliminary flow inversion tests showed that the petrophysical properties of that lumped facies model could actually be inverted much more rapidly than that of a detailed facies model. Moreover, the resulting calibrated lumped model was found to match measured pressure responses as accurately as the detailed model.

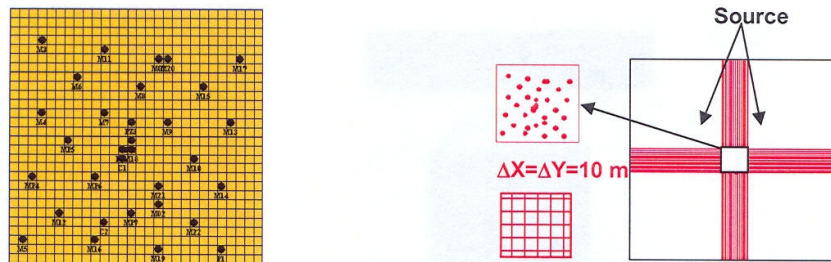


Figure 5: Left: Gridded model of the drilled Site area with well locations. Right: Gridded model with surrounding fluid-source cells.

facies number	facies	Kx(mD)	Kz/Kx	porosity(fraction)	pore compressibility(1/bar)
1	Clay	0.001	1	0.001	0.001
2	Clayey Limestone	0.25	1	0.074	0.001
3	Limestone	3.84	1	0.171	0.001
4	Cherty limestone	40.71	1	0.195	0.001
5	Fractured Limestone	8.9	1	0.144	0.001
6	Dark clay	0.001	1	0.001	0.001
7	Water	-	-	-	0.001
8	Marl	0.003	1	0.001	0.001
9	Source of aquifer	-	-	-	0.001

Table 2. The initial petrophysical parameters assigned to the geostatistical model: porosity-permeability values derived from the core data of well C1 (Bourbiaux et al., 2006); estimated pore compressibility values (from overall pre-calibration) consistently with other dynamic studies of the EHS (Delay et al., 2004, Bernard, 2005).

Facies numbers	Detailed facies	Lumped facies
1	Clay	
2	Clayey Limestone	
3	Limestone	
4	Cherty limestone	1- tight matrix facies
5	Fractured Limestone	
6	Dark clay	
8	Marl	
7	Water facies	2- Conductive facies
9	Source of aquifer	3- Source facies

Table 3. Detailed facies (left) converted to lumped facies (right).

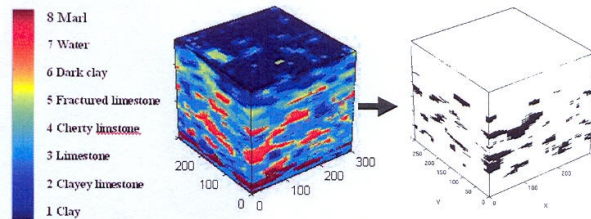


Figure 6. Initial detailed facies model (left, with a different colour legend from that of figure 4(b)) converted to an equivalent lumped facies model (right).

Selected well data for model calibration

As stated above, several single pumping tests were performed on the EHS. Herein, we calibrate the flow model to the field pressures measured while pumping well M7, including the M7 pressure drawdown and the pressure evolution in 8 observation wells showing significant interference with M7 (Figure 7). Well M7 was selected for its near-central location in the Site and its high productivity, thus providing an instructive dynamic data set for constraining the flow model. The water level data recorded in wellbores were converted into pressure values using 100 bar as an arbitrary initial reservoir pressure, as shown in figure 7. Although most well responses showing interference with the pumped well (M7) were included as constraints for inverting the flow model, this paper discusses the pressure match of only 4 wells, including the pumped well M7 and the selected observation wells C1, M9, M5 that cover approximately the range of pressure interference amplitudes observed on the Site.

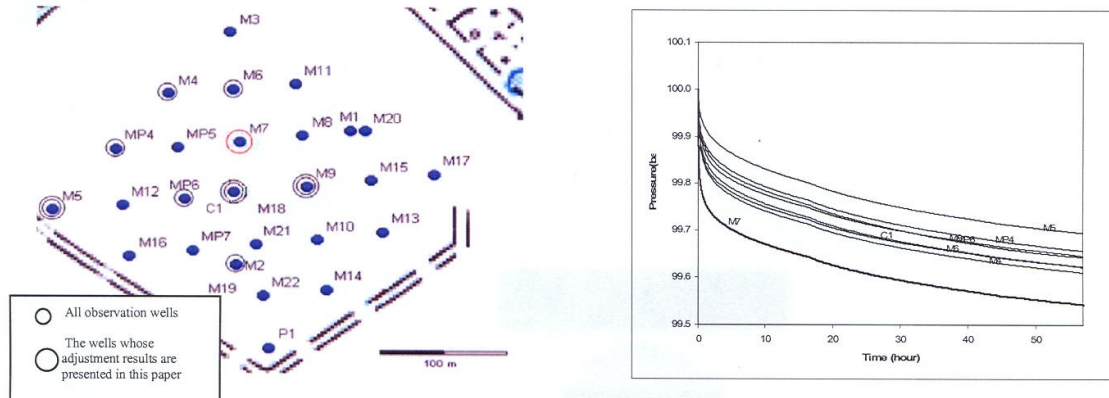


Figure 7: Selected data: location (left side) and pressure responses (right side) of the selected pumped well, M7, and of the observation wells showing significant pressure interference with M7.

Preliminary calibration of the flow boundary conditions

That calibration was performed through a preliminary petrophysical inversion of the porosity and permeability of the 3 lumped-model facies, including the fictive "source" facies under consideration. The inversion was constrained by the above-selected pressure data over the entire testing period (57 hours) in order to correctly reproduce the overall water recharge of the site during pumping. Inverted permeability and porosity values of respectively 18D and 0.04 were obtained for the "source" facies. The high permeability of that "source" facies is related to the presence of highly-conductive (karstic) flow paths establishing rapid communication and recharge of the studied Site of limited area (210m x 210m).

These values were kept unchanged for the rest of study as they characterize the permanent water recharge of the Site area of a vast aquifer.

All subsequent calibrations were carried out for the first day of pumping (24 hours), and not for the whole test duration, because a well pumping test investigates rapidly distant regions from the Site. By adopting that limited time frame, a sufficient weight was given to the transient phenomena taking place within the Site and the impact on calibration of the distant regions from the Site is reduced. Actually, those external regions dispose of very few wellbore modelling constraints hence they can only be taken into account as a source facies calibrated in average over the entire test duration. Eventually, that approach remains of course a compromise that reflects the intrinsic difficulty encountered in the modelling of such karstic reservoirs.

Petrophysical inversion

The petrophysical properties of the conductive "water" facies and the tight matrix facies were inverted again, except for the matrix porosity that was fixed to a reliable average value (0.15) estimated from core data (Table 4). As mentioned before, the pumping and interference pressure data recorded during the first 24 hours of well-M7 pumping were the dynamic constraints for inverting that lumped facies model, now incorporating fixed "source" facies porosity and permeability values equal to the long-term-inverted values of respectively 0.04 and 18355 md. The inverted petrophysical values of facies 1 and 2 are given in Table 5. We observe that the conductive facies has a very high permeability value, around 900D, that characterizes the highly-permeable conduits, cave and flow paths, of this highly-heterogeneous, fractured and karstic reservoir. That extremely-differentiated flow behaviour of the "Water" facies is consistent with the production logs that reveal the presence of very few (1, 2 or 3) thin water-feeding levels along the wellbores.

facies number	facies	Kx(mD)	Porosity
1	matrix facies	?	0.15
2	conductive facies	?	?

Table 4 Inversion parameters, denoted "?". Porosity value (0.15) for tight facies No. 1 is derived from core data.

facies number	facies	Kx(mD)	Porosity
1	matrix facies	100	0.15
2	conductive facies	895536	0.22

Table 5. Inverted values of lumped facies 1 and 2 using the short-term (24 hours) flow data from pumped well M7 and its observation wells as constraints.

The adjusted pressure drop (dP) evolution versus time (h) for pumped well M7 and selected observation wells are compared to the experimental data in Figure 8. The pressure drawdown measured in pumped well M7 is not yet fully matched. Well C1 is fairly well adjusted, well M9 match is less satisfactory than for C1 whereas well M5 response is not reproduced at all by the inverted model. That is, the calibrated model still fails to represent the flow paths between some well pairs of the Site. Obviously, the geostatistical facies model underlying that flow model remains insufficiently representative of the preferential flow paths within the reservoir, as revealed by interference testing.

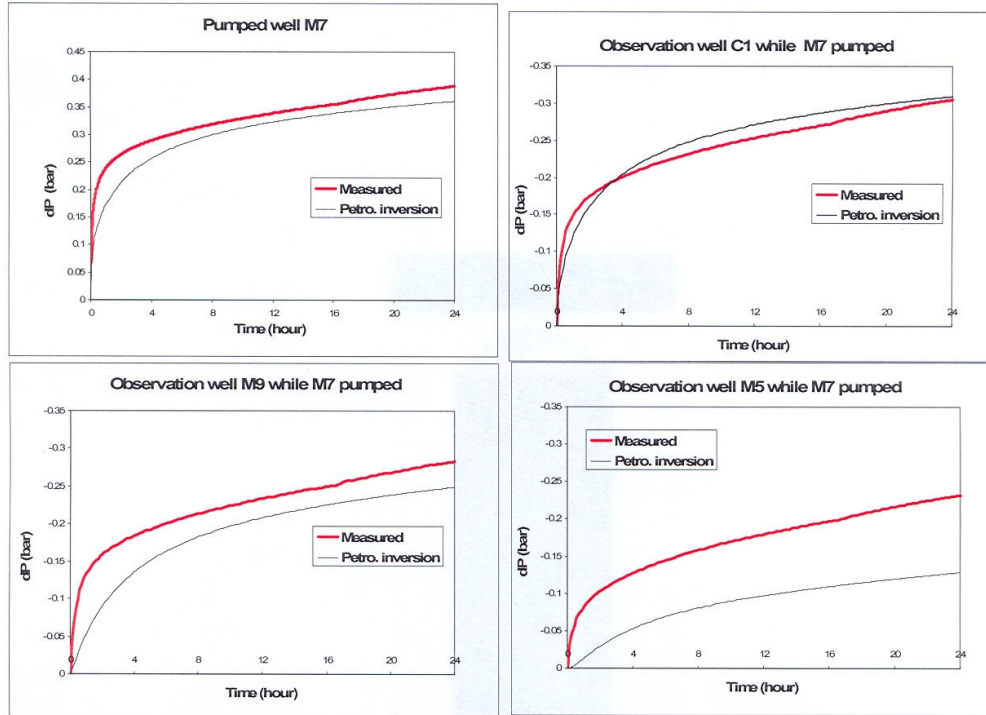


Figure 8. Simulated pressures after petrophysical properties inversion are compared to measured data at the Site: pressure drop (dP , bar) evolution with time (h) for pumped well M7 and 3 selected observation wells during the first 24 hours.

Gradual deformation

The previously-adjusted model in terms of petrophysical properties was calibrated to well M7 and observation wells responses through a gradual deformation of the geostatistical facies distribution. Through that process, an initial geostatistical realization is gradually altered to other realizations through linear combinations of the gaussian random functions used for model generation, until the objective function referring to the selected well responses is minimized. Gradual deformation involved 4 deformation parameters, t_i (Eqn. 3), and the inversion always concerned the first day of pumping. The evolution of the objective function is shown in Figure 9, both for all data and for a selected pressure data set, from well M5. The evolution of that objective function behaviour does not decrease steadily but shows temporary perturbations. Two reasons may be invoked to explain that evolution, one related to the peculiarity of that reservoir, the other to the numerical optimization technique. First, altering the facies distribution from one gradual deformation iteration to another may establish a new (highly-conductive) flow path between the pumped well and an observation well, or on the contrary interrupt a previously-modelled one. Such a switch-on/switch-off behaviour is one probable reason for the observed objective function behaviour. Another possible reason for the objective function perturbations lies in the gradient-based algorithm version that was used for this work. Actually, numerical gradients were calculated from the simulation results but only for the first iteration of the optimization step. For the subsequent iterations, gradients were estimated from an approximate formula derived from the first iteration. That procedure is not always sufficiently robust to ensure a sustained minimization of the objective function between successive iterations. The adoption of an analytical gradient method would improve the optimization to that respect.

The lastly-adjusted pressure curves resulting from gradual deformation of facies are compared to those obtained by the previous petrophysical inversion, and to the field-measured ones in Figure 10. Matching the pressure interference in well M5 is now possible and quite satisfactory with the gradual deformation method whereas it remained impossible by petrophysical inversion. The match of wells C1 and M9 is also improved. The adjustment of pumped well M7 pressure drawdown is unchanged, remaining poor, but at least not deteriorated.

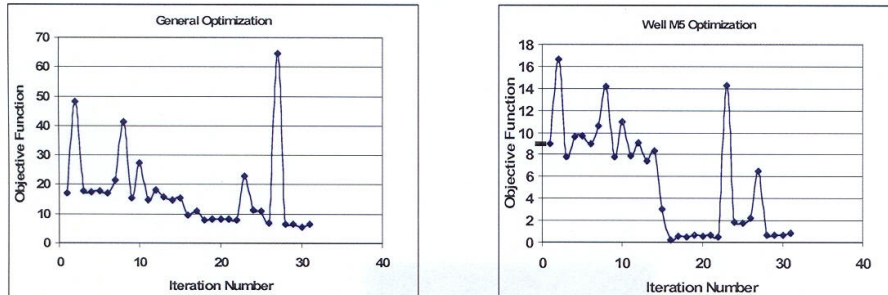


Figure 9. On the left: Objective function evolution for the lumped facies model using the gradual deformation method: calibration is done to pumped well M7 and observation wells together. On the right: Objective function evolution for well M5 pressure data. Note that the whole optimization process includes several steps and that temporary abrupt rise in the objective function may occur during the iterations of a given optimization step. This is due to the highly non-linear relationship between fluid flow results and geostatistical deformation: in that case, the iteration is re-started with a reduced variation of the deformation parameters.

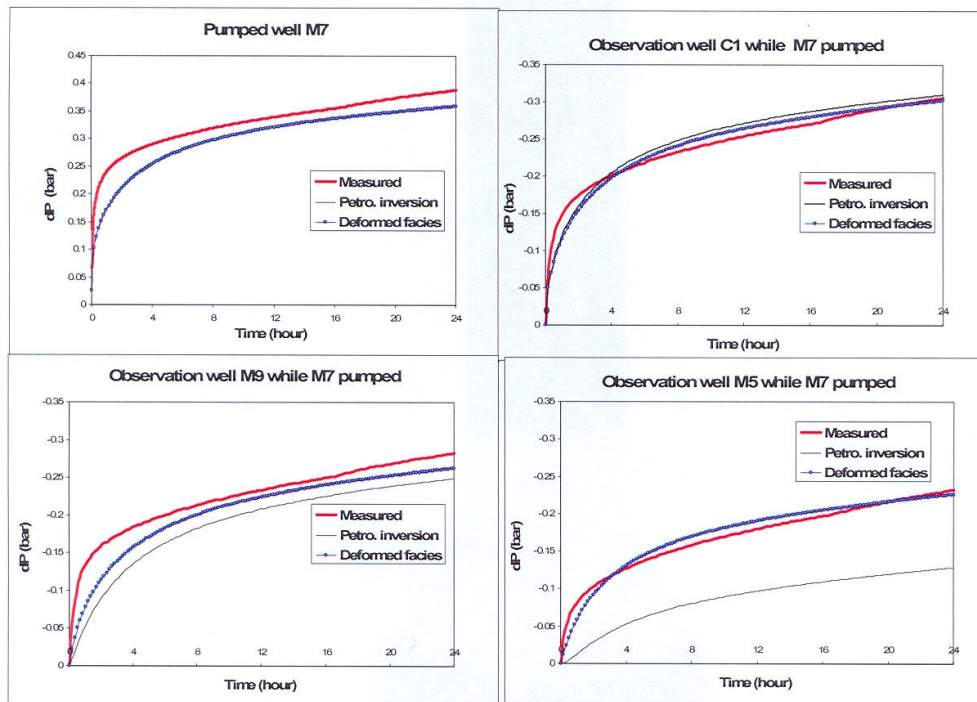


Figure 10. Comparison of simulated pressures after petrophysical inversion or gradual deformation of facies, with the Site-measured pressures: evolution of the pressure drop dP (bar) versus time (h) for the pumped well M7 and selected observation wells during the first 24 hours.

Eventually, the gradual deformation of facies distribution turns out to be very effective to tune the previously-parameterized flow model to field-observed interferences, as such interferences are closely controlled by the continuity of the conductive facies between well pairs. The gradual deformation technique allows one to determine rapidly a 3D facies distribution that fits best with all well responses driving the deformation process. Obviously, facies deformation is complementary, not an alternative to petrophysical inversion that remains necessary for assessing poorly-defined properties.

The deformations of the conductive facies bodies are shown in Figure 11 within a selected 2D section of the model and in Figure 12 for lateral vertical sections of the 3D model, from the beginning (left side of figure) to the end (right side) of the tuning process.

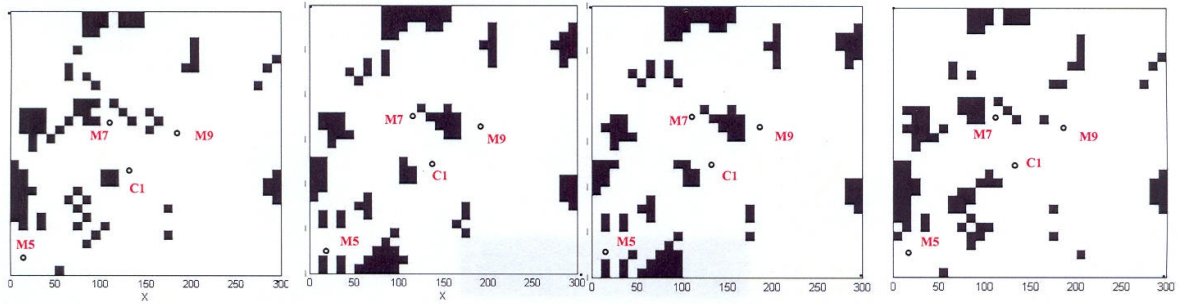


Figure 11. Gradual deformation of the EHS model with pumped well M7 and some observation wells as calibration constraints: 2D section of model at the depth of 68 meter (from the initial realization on the left, to the optimal one on the right).

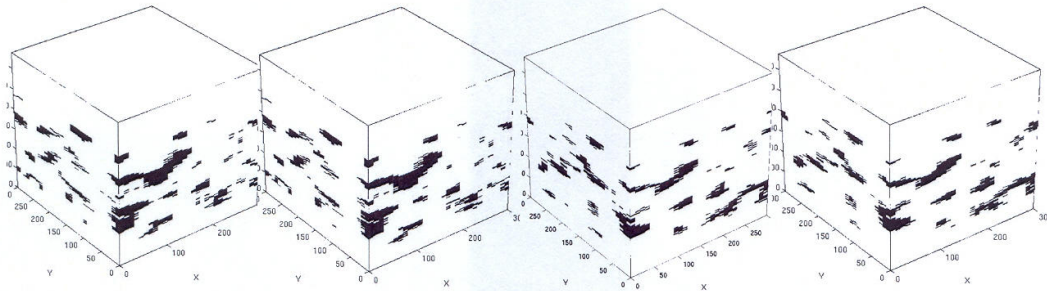


Figure 12. Gradual deformation of the EHS model with pumped well M7 and some observation wells as calibration constraints: lateral vertical sections (from the initial realization on the left, to the optimal one on the right).

Local gradual deformation

The local gradual deformation was applied to wells M7 and M9, that were not yet fully adjusted after global gradual deformation. To that end, an area including both previous wells was defined (Figure 13, left side).

Then, a local gradual deformation of facies was performed on this area alone. Figure 13 shows the evolution of the conductive facies distribution within that region during deformation. The newly-adjusted pressure curves are given in Figure 14 showing the comparison with the lastly-adjusted curves resulting from petrophysical inversion and global gradual deformation of facies, and with experimental data. Local gradual deformation actually improved significantly the match of pumped well M7, also that of well M9 to some extent.

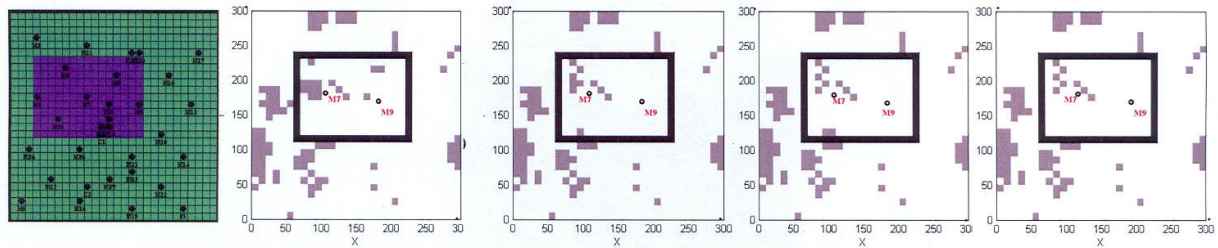


Figure 13. Local gradual deformation of the EHS model in a region including wells M7 and M9: horizontal section at the depth of 68m. Only the region of interest is affected by the gradual deformation process.

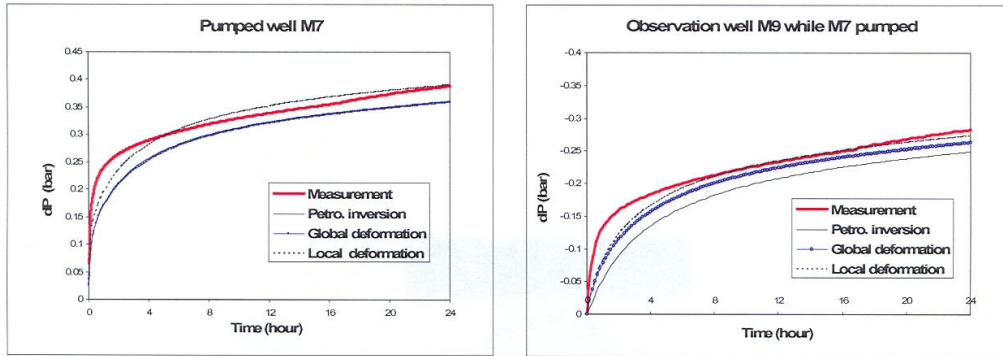


Figure 14. Comparison of simulated pressures after petrophysical inversion, global gradual deformation of facies and local gradual deformation of facies, with the Site-measured pressures: evolution of the pressure drop dP (bar) versus time (h) for the pumped well M7 and observation well M9 during the first 24 hours.

Predictability of the resulting model

Through the above-reported calibrated steps, the poorly-defined petrophysical properties of a geostatistical lumped facies model of the Site were calibrated, then a gradual deformation of facies was applied, to tune all well pressure responses first, and to refine the pressure match around selected wells as the last step. To test the reliability and robustness of that sequential calibration procedure, we used the lastly-calibrated deformed model to simulate several wells responses while pumping well M6 instead of well M7. That blind simulation was considered to test the model robustness to some extent because the interferences with well M6 probably occur via other flow-paths systems than for well M7.

The simulated well responses are compared with experimental data in figure 15. Half of the well responses are fairly well matched. Two interferences should be improved and the poorest match concerns well M5. Actually, that well remained poorly matched at the end of the calibration process that resulted in the presently-tested simulation model. That is, the calibration procedure looks rather robust and consistent with respect to the degree of calibration refinement, through local deformation for instance.

To end with, although respecting the magnitude of well pressure drawdowns and interferences is satisfactory through that calibration procedure, it is worth noticing that the transient pressure evolution during the very short times, i.e. less than around one hour, is not reproduced by the flow model, whatever the well under consideration. At that point, one has to remember that the conductive facies actually consists of a 3D complex network of connected caves, dissolved bed joints and/or open fractures. The thickness of such flow-paths stands far below the metric/deca-metric cell dimensions, 10m x 10m x 1m, of our flow model. That is, our model is necessarily an up-scaled representation of that heterogeneous/karstic and porous reservoir. Co-existence in the conductive "water" cells of thin highly-conductive flow-paths and of a tight porous medium may then justify the use of a dual-porosity flow model, as tested in the following last section.

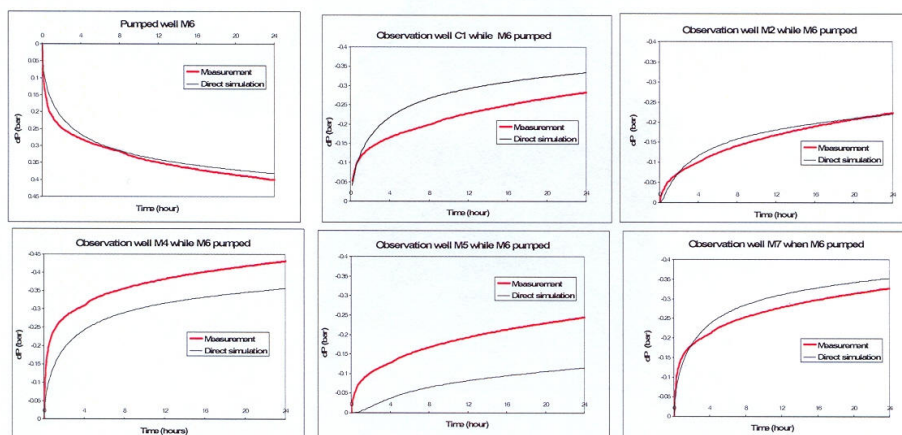


Figure 15. Forward/predictive simulation of pumped well M6 and its interferences and comparison with field-measured: evolution of well pressure drop dP (bar) with time (h) for pumped well M7 and selected observation wells during the first 24 hours.

Testing a dual-porosity representation

As evoked before, the dual-medium approach is based on the superposition of two equivalent media, a “fracture” medium characterized by a high permeability k^f and a low porosity ϕ^f , and a “matrix” medium characterized by a low permeability k^m and but a high porosity ϕ^m . A matrix block size must also be defined to simulate the transfers between the two media. A dual-porosity model of our heterogeneous karstic/fractured reservoir was directly built from the previously-calibrated-deformed single-porosity model by splitting its single-medium cells into dual-medium cells, with a “matrix” cell standing for the tight facies and a “fracture” cell standing for the conductive “water” facies when present. This conversion assumes that the “water” cells of the previous single-porosity model were standing for both the conductive “water” facies and some porous and tight material. On the opposite, any conductive flow path is still assumed absent from the tight facies (facies 1) cells. Taking into account these assumptions, the initial petrophysical values of the dual-medium cells of facies 1 or 2 were derived from the inverted single-medium model as shown in Table 6. Through that dual-medium representation, transient flows occurring locally within small-scale highly-conductive diagenetic features, and between the porous carbonate matrix and those conductive features, can be simulated. The benefit of this dual-porosity simulation approach for calibrating the Site model was then tested by inverting only the petrophysical properties of the “water” dual-medium cells actually standing for two distinct media, the main unknowns being the actual “conductive” medium properties k_2^f, ϕ_2^f , and the “matrix” block size, a_2 . The other petrophysical properties were kept fixed at their predetermined values. Inversion results are given in Table 7. The adjusted pressure curves are compared to those obtained with the single-porosity model in Figure 16. The calibration of a dual-porosity model does not much improve the pressure match by comparison with the single-porosity model. The pressure evolution during the first hours of the test is only slightly improved by using a dual-medium representation of the reservoir, and the overall predicted pressure trend by both single- and dual-medium models remain quite close from one another. The flow-property contrast between the two facies, 1 and 2, can be simulated by a single-porosity model with a sufficient accuracy, even though that model is coarsely gridded with respect to the actual geometry and size of the conductive “water”-facies bodies. The origin of the contrasted short-term transient pressures between the field and models must then be found elsewhere. Actually, the most probable origin of such a difference lies in the complex near-wellbore flow geometry that is not properly taken into account in flow models. Actually, these models use conventional productivity formula (Peaceman, 1978) based on a radial flow equivalence. However, a recent study (Ding *et al.*, 2006) referring to the simulation of wells in fractured reservoirs showed that high flow simulation errors resulted from such a radial flow approximation and that such errors could be greatly reduced by computing near-well flows on the actual/representative discrete fracture network present in the wellbore vicinity. In our situation, an object-based model of the thin conductive flow-paths present in the near-wellbore area should be built and used to compute a representative relationship between the well rate and the near-wellbore pressure drop, if short-term transient responses were to be integrated in the model calibration process.

facies number	fracture permeability (mD)	fracture porosity	matrix permeability (mD)	matrix porosity	matrix block size (m)
1	$k_1^f = k_1^0 = 100$	$\phi_1^f = \phi_1^0 = 0.15$	$k_1^m = k_1^0 = 0$	$\phi_1^m \approx 0$	$a_1 \approx 10^6$
2	$k_2^f = k_2^0 = 895536$ to be inverted	$\phi_2^f = \frac{1}{10} \phi_2^0$ to be inverted	$k_2^m = k_1^0 = 100$	$\phi_2^m = \phi_1^0 = 0.15$	$a_2 \approx 3m$ to be inverted

Table 6. Initialization of the dual-porosity model parameters from the calibrated single-porosity model results.

facies number	k_2^f (mD)	ϕ_2^f	matrix block size(m)
1	-	-	-
2	849984	0.019	3.001

Table 7. Results of the petrophysical property inversion of the dual-porosity model.

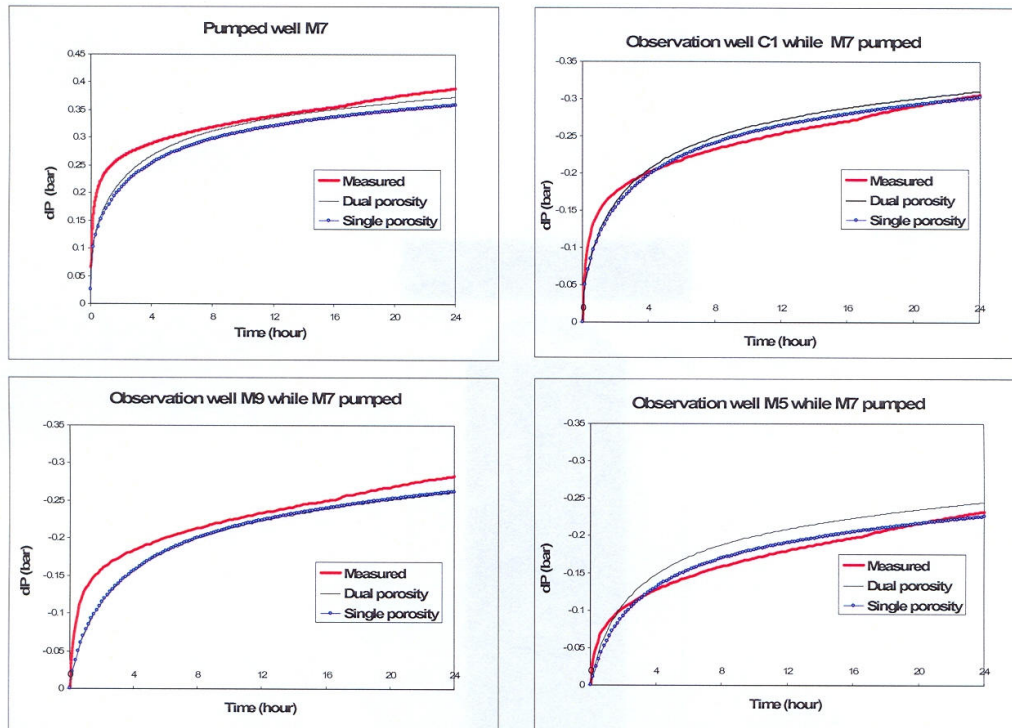


Figure 16. Comparison between the inversions of the dual-porosity and single-porosity models of the Site. Variation of pressure drop (ΔP) versus time (hour) for well M7 and some interference wells; model calibrated to pumped well M7 and some interference wells in short term period (24 hours).

Conclusions

The present paper illustrates the efficiency of a sequential inversion methodology to calibrate a flow model of highly-heterogeneous reservoirs, such as the karstic/fractured Experimental Hydrogeological Site studied herein. The context, approach and main findings are summarized hereafter:

a. **A valuable field data source.** The Experimental Hydrogeological Site under consideration constitutes a very instructive multi-disciplinary data-base to set up consistent methodologies for characterizing the hardly-tractable heterogeneity of complex diagenetized reservoirs and for modelling their hydrodynamic behaviour. Therefore, a geostatistical facies model of this reservoir was generated by integrating all available geological and wellbore core-log data and considering a mono-gaussian distribution of 8 facies related to the deposition of various rock types. An equivalent lumped-facies model with only 2 facies, a tight matrix facies and a conductive facies, was defined from that initial detailed facies model. That model was found to be quite meaningful in terms of fluid flow, considering the extreme flow channelling observed on the Site.

b. **An integrated, specifically-designed flow model calibration methodology.** The main contribution of this work consists in designing and implementing a sequential calibration methodology of a flow model directly inherited from a geostatistical model incorporating available dynamic data.

This methodology uses the available well test data, *i.e.* pumping and interference tests for the present Site, as flow constraints and involves the hereafter-summarized steps:

- Initializing the flow model.

Beside the necessity of incorporating available petrophysical information, derived from core data for instance, special attention has to be awarded to the assignment of representative compressibility values if that parameter cannot be included in the subsequent inversion procedure, as was the case herein.

As a preliminary calibration step, a proper flow boundary condition has also to be defined to mimic the external fluid recharge of such highly-heterogeneous reservoirs as this karstic aquifer. For our Site, this was achieved through the petrophysical tuning of a fictive and distant "source" facies to a long-term well test, using the subsequent step calibration method.

- *Petrophysical calibration.* Starting from that consistent initial flow model, the petrophysical properties of the constitutive facies are inverted through an optimization algorithm that minimizes the difference between simulated and measured pressure responses over a time scale consistent with the reservoir scale of interest.

- *Gradual deformation.* Once the flow model is properly calibrated in terms of petrophysical parameters, a gradual deformation technique is applied to improve the geostatistical realization of the reservoir facies distribution, with respect to the dynamic data measured in wellbores as in the previous step.

That gradual deformation is first performed globally to improve the facies image of the reservoir as a whole.

Finally, a local gradual deformation may be applied to refine the facies distribution in selected reservoir regions where well responses remain poorly-matched.

c. Methodology effectiveness. The above methodology was robust and effective in calibrating the EHS flow model to the observed pressure responses measured on the Site wells:

- The multiple unknowns of that highly-undetermined flow problem were fixed in a sequence taking into account the major flow-impacting parameters, starting with a petrophysical property inversion.

- Applying the gradual facies deformation method globally then locally improved the match of observation wells that had not been correctly calibrated by previous petrophysical property inversion.

- The reliability and robustness of the resulting model was proven from its fairly-good capability to predict the hydraulic response of other wells than those included as flow constraints in the inversion methodology. Obviously, the more well data constraints are used in the objective function, the more predictive the resulting calibrated model will be.

- To end with, the reasonable number of iterations required for calibrating or deforming a model ensures the practical applicability of that methodology.

d. Further improvements. The transient well responses measured during the first hours of pumping and interference tests could not be reproduced by a single-porosity flow model that upscales to some extent the thin discrete conductive flow paths that run through that extremely-heterogeneous reservoir:

- Adopting a dual-medium flow modelling approach did not change much the simulated pressures: that is, a single-porosity flow modelling approach is accurate enough to reproduce satisfactorily the overall/long-term well responses, provided that a sufficiently-fine grid definition is used, as in the present case.

- According to previous experience of well modelling in fractured reservoirs, the origin of such initial discrepancy between model prediction and field measurements is linked to the peculiar near-wellbore flow geometry that is not taken into account by equivalent/homogenized flow models: an accurate simulation of the transient pressure behaviour would require a detailed representation of the thin flow paths feeding the wellbores, either with high-resolution near-wellbore grids or preferably with a discrete, object-based model of those flow paths.

To conclude, the herein-designed flow inversion/simulation methodology looks like an effective approach to draw the best of both static/geological and dynamic/flow information for modelling the flow behaviour of so hardly-tractable reservoirs as karstic fractured aquifers.

Acknowledgements

The authors are grateful to the University of Poitiers (France) for collaborating in this study.

References

- Barenblatt, G.I., Zheltov, Iu.P., Kochina, I.N. (1960) "Basic concepts in the theory of seepage of homogeneous liquids in fissured rocks", *Prikl. Mat. Mekh.*, 24, 852-864.
- Bernard, S. (2005) "Caractérisation hydrodynamique des réservoirs carbonatés fracturés", Ph.D. Thesis, University of Poitiers.
- Blanc, G. (1995) "Numerical Well Test Simulations in Heterogeneous Reservoirs", Poster presented at AAPG Conference, Nice.
- Blanc, G. (1999) "Welgem software, User's guide of the user interface", IFP Internal report.
- Bourbiaux, B., Callot, J.P., Doligez, B., Fleury, M., Gaumet, F., Guiton, M., Lenormand, R., Mari, J.L., Pourpak H. (2006) "Multi-Scale Characterization of an Heterogeneous Aquifer Through the Integration of Geological, Geophysical and Flow Data: A Case Study", *International Conference in Water Resources*, Toulouse.
- Bourbiaux, B., Callot, J.P., Doligez, B., Fleury, M., Gaumet, F., Guiton, M., Lenormand, R., Mari, J.L., Pourpak, H. (2007) "Multi-Scale Characterization of an Heterogeneous Aquifer Through the Integration of Geological, Geophysical and Flow Data: A Case Study " *Oil and Gas Science and Technology, Rev. IFP*, Vol. 62, No. 3, pp. 347-363.
- Cacas, M.C., Daniel, J.M., and Letouzey, J. (2001) "Nested Geological Modeling of Naturally Fractured Reservoirs", *Petroleum Geoscience*, 7, pp. S43-S52.
- Delay, F., Porel, G. and Bernard, S. (2004) "Analytical 2D model to invert hydraulic pumping tests in fractured rocks with fractal behavior", *Geophys. Res. Lett.* Vol. 31.

- Doligez, B., Beucher, H., Geffroy, F. and Eschard, R. (1999) "Integrated reservoir characterization: improvement in heterogeneous stochastic modeling by integration of additional external constraints", In: R. Schatzinger and J. Jordan eds., *Reservoir Characterization Recent Advances*, AAPG Memoir, pp. 333-342.
- Ding, Y., Basquet, R. and Bourbiaux, B. (2006) "Upscaling Fracture Networks for Simulation of Horizontal Wells Using a Dual-Porosity Reservoir Simulator", *SPE Reservoir Evaluation & Engineering*, Vol. 9, No. 4, 513-520.
- Dotton, L. (2005) "Caractérisation des Hétérogénéités d'un Aquifère Carbonaté, Diagénétique, Fracturé et Karstique (Jurassique moyen, seuil du Poitou. Modélisation lithologique et pétrophysique", Rapport de stage de Master, IFP.
- Galli A., Beucher H., Le Loc'h G., Doligez B. and Heresim group (1993) "The Pros and Cons of the Truncated Gaussian Method ", In : Armstrong M. and Dowd P.A. eds., *Geostatistical Simulations*, Kluwer Academic Publishers, pp. 217-233.
- Gaumet, F., Guiton, M., Callot, J.P. (2005) "Hétérogénéité sédimentaire et fracturation dans le Jurassique du Site Expérimental Hydrogéologique de Poitiers", Institut Français du Pétrole, Internal report.
- Hu, L.Y. (2000) "Gradual deformation and iterative calibration of Gaussian-related stochastic models", *Mathematical Geology*, Vol.32, No.1.
- Kazemi, H., Merrill, L.S., Porterfield, K.L. and Zeman, P.R. (1976) "Numerical Simulation of Water-Oil Flow in Naturally Fractured Reservoirs", *SPEJ*, pp. 317-326.
- Matheron G., Beucher H., de Fouquet C., Galli A., Guerillot D. and Ravenne C. (1987) "Conditional simulation of the geometry of fluvio deltaic reservoirs", *SPE 62nd Ann. Tech. Conf. & Exh.*, Dallas, Texas, pp. 591-599.
- Peaceman, D. W. (1978) "Interpretation of Well-Block Pressure in Numerical Reservoir Simulation," *SPE Journal*, pp. 183-194.
- Pourpak, H. (2007) "Méthodologie de déformation graduelle de modèles de réservoir hétérogène fracturé contraints par des mesures d'écoulement aux puits", rapport de thèse à mi-parcours, Institut Français du Pétrole.
- Pourpak, H., Bourbiaux, B., Roggero, F., Doligez, B., Delay F. (2007) "An Inversion Methodology to Calibrate the Model of an Heterogeneous Aquifer from Wellbore flow Measurements: Case study", *EAGE international conference on petroleum geostatistics*, 10-14 sept., Cascais, Portugal.
- Rahon, D., Blanc, G., Guérillot, D., (1996). "Gradients method constrained by geological bodies for history matching", *Proceedings of the 5th European Conference on the Mathematics of Oil Recovery*, pp. 283– 293.
- Ravenne, C., Galli, A., Doligez, B., Beucher, H. and Eschard, R. (2002) "Quantification of facies relationships via proportion curves", In: *Geostatistics Rio 2000, 31st International Geological Congress*, Rio de Janeiro, 6-17 August 2000, *Proceedings 2002*, M. Armstrong et al. eds, Kluwer Academic Publishers, pp. 19-39.
- Roggero, F. and Hu, L.Y. (1998) "Gradual deformation of continuous geostatistical models for history-matching", Paper SPE 49004, *Annual Technical Conference and Exhibition*, New Orleans.
- Sarda, S., Jeannin, L., Basquet, R., Bourbiaux, B. (2002) "Hydraulic characterization of fractured reservoirs: simulation on discrete fracture models", *SPE Reservoir Evaluation & Engineering*, April, pp.154-162.
- Sun, N.Z. (1994) "Inverse problems in ground water modeling", *Kluter Acad Publ. Dordrecht. The Netherlands*, 337 p.
- Tarantola. (1987) "Inverse problem theory-methods for fitting and modeling parameters estimations", Elsevier. 613p
- Warren, J.E. and Root, P. J. (1963) "The Behaviour of Naturally Fractured Reservoirs", *SPEJ* pp. 245-255.

Appendix 2. Forward simulation of two doublet tests on the calibrated EHS model

Forward simulation of two doublet tests on the calibrated EHS model

This Appendix gives the forward simulation results of two doublet tests to be performed in the coming months on the Experimental Site.

The two selected couples of wells are M6-M22 and M12-M15. For each couple, water is pumped in the first well (respectively M6 and M12) at a fixed flow rate of 30m³/h, and reinjected at the same rate in the second well (respectively M22 and M15). Simultaneous pumping and reinjection are carried out during 48 hours.

These two doublet tests were simulated by using SIMTEST on the calibrated lumped-facies model resulting from the reference sequential methodology described in this memory, that is petrophysical inversion followed by global gradual deformation. Note that local gradual deformation was not applied to that model.

For each of the two tests, the simulated well responses are shown hereafter for 6 selected observation wells that are:

- M07, M09, M16, M20, M21, MP6 for M6-M22 doublet test ;
- M04, M07, M09, M14, M21, MP6 for M12-M15 doublet test.

The evolution of drawdown versus time is shown first, then 5 drawdown maps of the Site are shown at successive times of 10, 100, 1000, 10000 and 100000 seconds. Downward (respectively upward) drawdown values are positive (respectively negative). In addition, the permeability map inferred from the pumping tests of each well (Figure 3.2 of the memory) is juxtaposed to these 5 maps to illustrate the coarsely-estimated distribution of permeabilities over the Site. The permeability heterogeneity of the Site explains the drawdown evolution of some wells, that may look unexpected with respect to their distance to the wells of the doublet under consideration. For instance, well M20 drawdown is less than half well M16 drawdown, although their distance to the M6-M22 doublet line is the same.

Note that two observation wells, M9 and M14, of the second doublet test (M12-M15) show negative drawdown values. These two wells are low-deliverability wells and are located on the re-injection side of the Site for that doublet test.

The actual field test results will confirm or not these predictions and thus further indicate to which extent our model of the Site is sufficiently calibrated for flow prediction purposes.

Doublet Test M6 (production)-M22 (injection)

Production/Injection rate: $30 \text{ m}^3/\text{h}$

Test duration: 48 hours

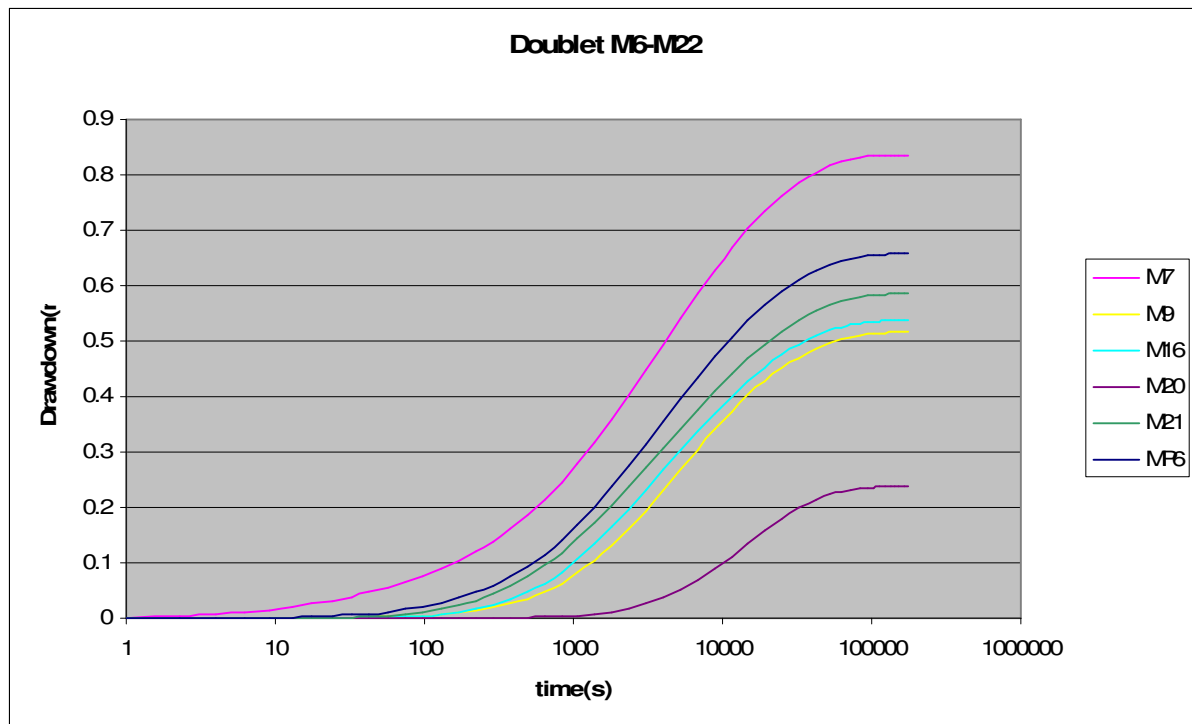


Figure 2.1: Simulated well responses for 6 selected observation wells form doublet test M6 (production)-M22 (injection).

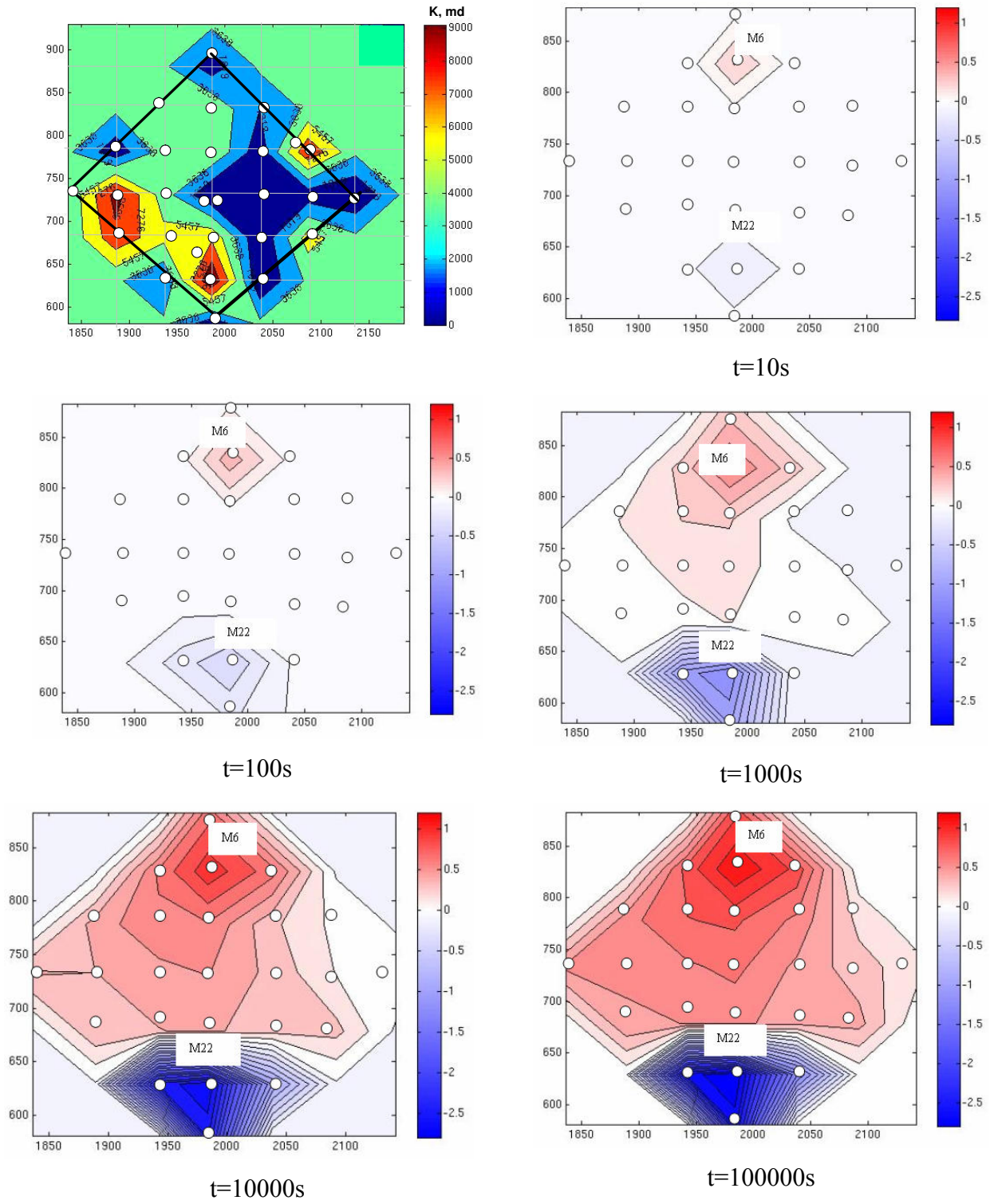


Figure 2.2: Drawdown maps of the Site at successive times of 10, 100, 1000, 10000 and 100000 seconds for doublet test M6 (production)-M22 (injection).

Doublet Test M12 (production)-M15 (injection)

Production/Injection rate: $30 \text{ m}^3/\text{h}$

Test duration: 48 hours

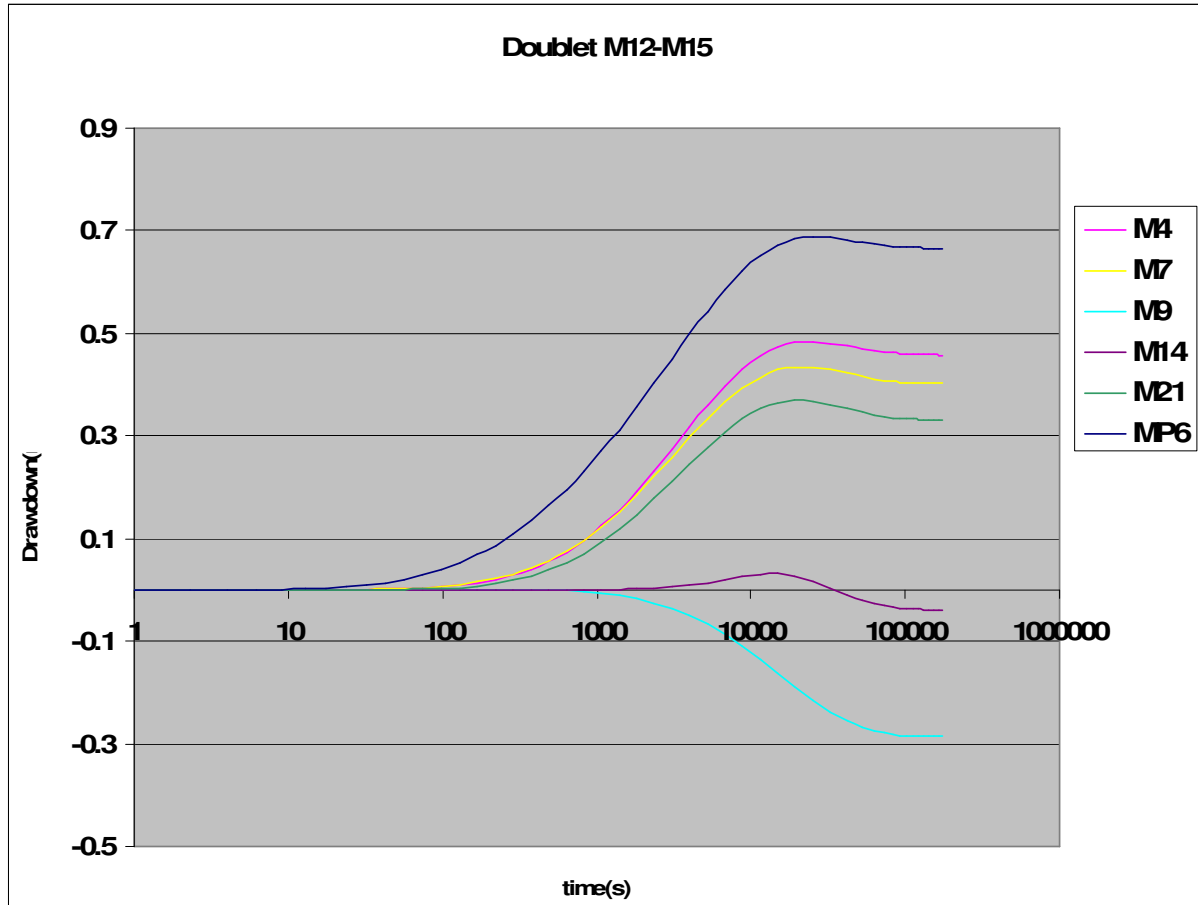


Figure 2.3. Simulated well responses for 6 selected observation wells from doublet test M12 (production)-M15 (injection).

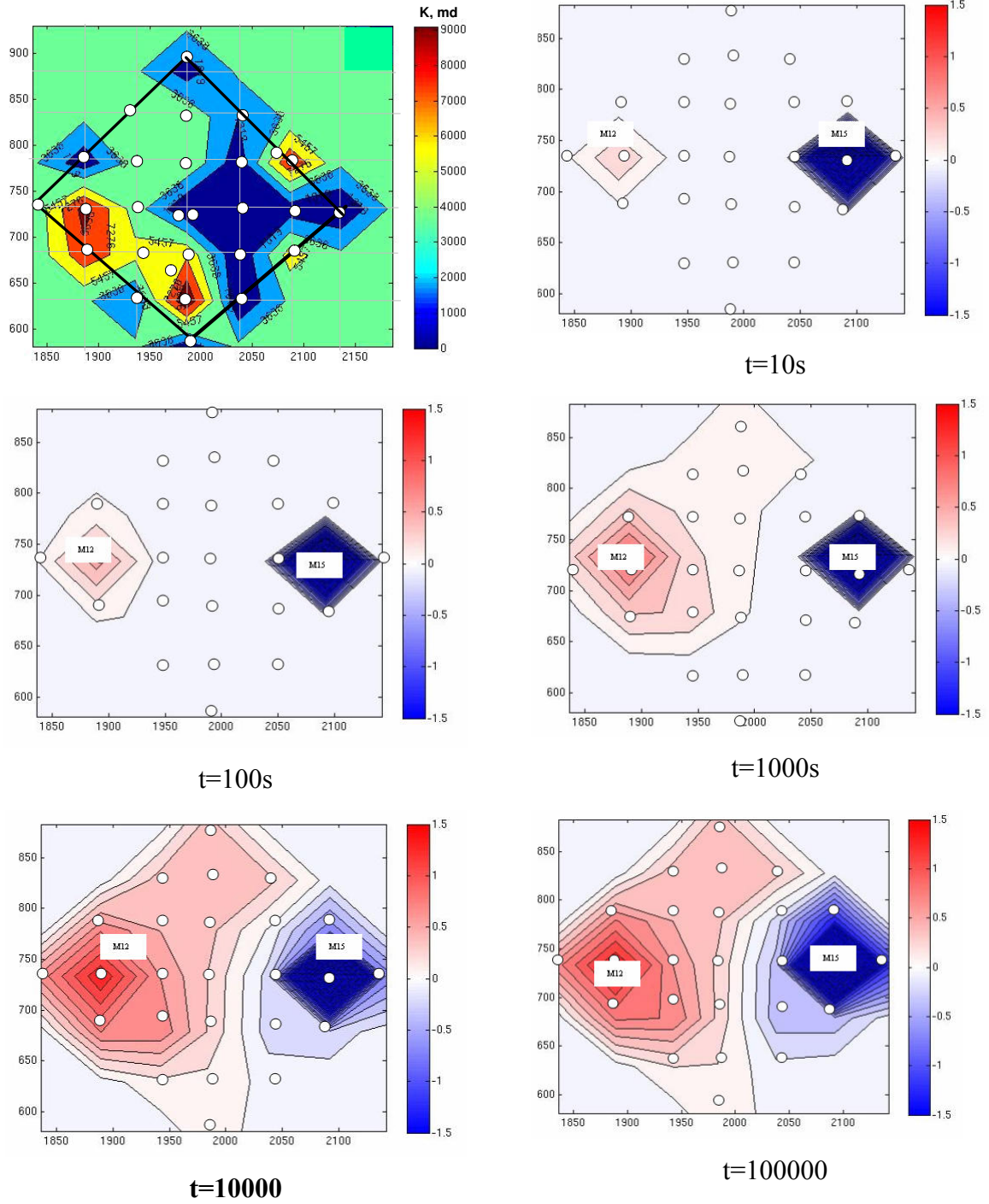


Figure 2.4: Drawdown maps of the Site at successive times of 10, 100, 1000, 10000 and 100000 seconds for doublet test M12 (production)-M15 (injection)

ABSTRACT

This thesis proposes a sequential inversion methodology for calibrating highly-heterogeneous reservoir models on well test data. The design and the application of that methodology are performed on an Experimental Hydrogeological Site settled on a karstic and fractured limestone aquifer located near to Poitiers – France. The flow model is based on a geostatistical distribution of facies. Conditioning information on flow is made of well pumping and interference data. The methodology involves two successive steps that are : - first, the inversion of facies petrophysical properties; - second, the gradual deformation of the facies distribution. By proceeding this way, the gradual deformation method, applied both globally and locally, improves the distribution of facies while keeping the previously-optimized petrophysical properties. The fairly-good capability of the resulting model to predict well responses allows to consider the gradual deformation as an efficient and robust method to find a facies geostatistical realization matching at best flow data constraints.

Alternative implementation of the sequence above are studied, by simply changing the schedule of the calibration steps. A single calibration step combining both petrophysical inversion and gradual deformation reveals as much efficient as the sequence discussed above. On the other hand, a reverse calibration sequence starting with gradual deformation and ending with petrophysical inversion does not yield a satisfactory calibration. Efficiency and numerical performances of the methodology are also assessed by changing the number of gradual deformation parameters, and by analyzing the sensitivity and evolution of the objective function during the entire optimization process.

Finally, it is investigated on the possibility to improve calibration by means of alternative flow modelling approaches. Whereas the adoption of a dual-medium model does not change significantly the simulated pressures, a more accurate modelling of conductive bodies by using a refined grid improves the prediction of short-time well responses. Further works could tentatively address the gradual deformation of object-based models that are reputed relevant for mimicking flow features of karstic and/or fractured heterogeneous reservoirs.

key words: Flow model, Inversion, Gradual deformation, Fractured reservoir, Karstic aquifer, Heterogeneous reservoir, Geostatistics.

RESUME

Cette thèse propose une méthodologie d'inversion séquentielle pour calibrer des modèles de réservoirs très hétérogènes à partir des données de tests de puits. La conception et la démonstration de cette méthodologie sont effectuées sur le Site Expérimental Hydrogéologique d'un aquifère carbonaté karstique et fracturé situé près de Poitiers en France. Le modèle d'écoulement de cet aquifère s'appuie sur une distribution géostatistique des faciès. Les contraintes de simulation des écoulements consistent en des données de tests de pompage et d'interférence. La méthodologie comprend deux étapes successives, en premier lieu l'inversion des propriétés pétrophysiques des faciès, puis la déformation graduelle de la distribution de faciès. La méthode de déformation graduelle, appliquée globalement puis localement, améliore ainsi la distribution des faciès en conservant leurs propriétés pétrophysiques précédemment calibrées. La capacité du modèle résultant à prédire les réponses des puits nous amène à considérer la déformation graduelle comme une méthode efficace et robuste pour trouver une réalisation géostatistique de faciès qui permette d'ajuster au mieux les données d'écoulement.

Des variantes de mise en oeuvre de la méthodologie décrite ci-dessus ont été étudiées, en modifiant l'ordre de la séquence de calibration. Alors qu'une étape de calibration unique, combinant inversion pétrophysique et déformation graduelle, s'avère aussi efficace que la séquence précédente, une séquence inversée commençant par la déformation graduelle et suivie de l'inversion pétrophysique ne conduit pas à un calage satisfaisant. L'efficacité et la performance numérique de la méthodologie sont également évaluées en changeant le nombre de paramètres de déformation graduelle, et en analysant la sensibilité et l'évolution de la fonction objectif au cours de l'ensemble du processus d'optimisation.

Finalement, la possibilité d'améliorer encore l'ajustement aux données de champ est explorée au moyen d'approches alternatives de modélisation des écoulements. Alors que l'adoption d'un modèle double milieu ne modifie pas beaucoup les pressions simulées, une modélisation plus précise des corps conducteurs au moyen d'une grille raffinée améliore la prévision des réponses des puits aux temps courts. Finalement, la déformation graduelle d'un modèle objet de corps conducteurs aux propriétés d'écoulement pré-estimées serait également adaptée à ces cas de réservoir hétérogène karstique et/ou fracturé.

Mots-clés: Modèle d'écoulement, Inversion, Déformation graduelle, Réservoir fracturé, Aquifère karstique, Réservoir hétérogène, Géostatistique.